UNIVERSITY OF CALIFORNIA, SAN DIEGO

Lipidomic Analysis of Eicosanoid Dynamics in Inflammation and Disease

A Dissertation submitted in partial satisfaction of the requirements for the degree

Doctor of Philosophy

in

Chemistry

by

Matthew Wallace Buczynski

Committee in Charge:

Professor Edward A. Dennis, Chair
Professor Daniel Donoghue
Professor Alexander Hoffmann
Professor Douglas Magde
Professor Tony L. Yaksh

2008

The Dissertation of Matthew Wallace Buczynski is approved, and it is acceptable in quality and form for publication on microfilm and electronically:

_____

_____

_____

_____

_____
Chair

University of California, San Diego

2008

For my mom and dad, who instilled in me the importance of an education.

TABLE OF CONTENTS

LIST OF SYMBOLS AND ABBREVIATIONS

1,2-HOPO	1-hydroxypyridine-2(1H)-thione
11-TXBH	11-hydroxythromboxane reductase
15-PGDH	15-prostaglandin dehydrogenase
AA	arachidonic acid
aa	amino acid
CAN	acetonitrile
ActD	actinomycin D
AHA	acetohydroxamic acid
ARK	Aldo-keto reductase
AMPA	p-aminophenylmercuric acetate
B.	*Borrelia*
Bb	*Borrelia burgdorferi*
BAY	BAY 11-7082
C1P	ceramide 1 phosphate
C3H	C3H/HeJ
CBR	Carbonyl reductase
CE	collision energy
cGST	cytosolic glutathione S-transferase
CHX	cycloheximide
CID	collision induced decomposition
COX	cyclooxygenase
cPGES	cytosolic PGE synthase

$cPLA_2$	Group IVA cytosolic PLA_2
CXP	exit cell potential
CYP	cytochrome P450
cysLT	cysteinyl leukotrienes
Δ	trans
d	deoxy
DBA	DBA/2J
dh	13,14-dihydro
DHET	dihydroxytrienoic acid
dhk	13,14-dihydro-15-keto
DiHDoHE	dihydroxy-docosahexaenoic acid
DP	declustering potential
DPA	2,2'-dipyridylamine
EET	epoxyeicosatrienoic acid
ELISA	enzyme-linked immunosorbent assay
Eoxin	EX
EP	entrance potential
ESI	electrospray ionization
EtOH	ethanol
FLAP	5-lipoxygenase activating protein
FSL-1	S-(2,3-bispalmitoyloxypropyl)-Cys-Gly-Asp-Pro-Lys-His-Pro-Ser-Phe
GC	gas chromatography

GPCR	G protein-coupled receptor
HETE	hydroxyeicosatetraenoic acid
HKLM	heat killed *Listeria monocytogenes*
HpETE	hydroperoxyeicosatetraenoic acid
HX	hepoxilin
ID	identity
iNOS	inducible nitric oxide synthase
IPA	isopropyl alcohol
$iPLA_2$	calcium-independent PLA_2
k	keto
LC	high performance liquid chromatography
LC-MS/MS	liquid chromatography-tandem mass spectrometry;
LDH	lactate dehydrogenase
LIPID MAPS	Lipid Metabolites and Pathway Strategy
LOD	limit of detection
LOX	lipoxygenase
$LPLA_2$	lysosomal PLA_2
LPS	lipopolysaccharide
LTAH	leukotriene A hydrolase
LTB_4DH	leukotriene B_4 dehydrogenase
LTCS	leukotriene C synthase
LX	lipoxin
LT,	leukotriene

LTA,	lipoteichoic acid *Staphylococcus aureus*
LTC_4	leukotriene C_4
maltol	3-hydroxy-2-methyl-4H-pyran-4-one
MAPEG	membrane associated proteins in eicosanoid and glutathione
MeOH	methanol
mGST	microsomal glutathione S-transferase
MMP	matrix metalloproteinase
MMPi	MMP inhibitor
mPGES	microsomal PGE synthase
MRM	multiple reaction monitoring
MS	mass spectrometry
MS/MS	tandem mass spectrometry
NF-κB	nuclear factor-κB
NNGH	N-isobutyl-N-(4-methoxyphenylsulfonyl)glycyl hydroxamic acid
ODN1826	synthetic oligodeoxynucleotide 1826
OP	o-phenanthroline
oxoETE	oxo-eicosatetraenoic acid
PA	picolinic acid
PAF	platelet-activating factor
PAF-AH	platelet-activating factor acetylhydrolase
Pam3SCK4	N-palmitoyl-S-[2,3-bis(palmitoyloxy)-(2RS)-propyl]-[R]-Cys-[S]-Ser-[S]-Lys(4) trihydrochloride

PBS	phosphate-buffered saline
p-cPLA$_2$ (S505)	cPLA$_2$ phosphorylated at serine 505
PD	protectin
PG	prostaglandin
PGD2	prostaglandin D$_2$
PGDS	prostaglandin D synthase
PGFS	prostaglandin F synthase
PGIS	prostacyclin synthase
PIP$_2$	phosphatidylinositol 4,5-bisphosphate
PLA$_2$	phospholipase
PM/PGFS	prostamide and prostaglandin F synthase
Poly(I:C)	polyinosine-polycytidylic acid
PPAR	peroxisome proliferators-activated receptor
Rv	resolvin
sEH	soluble epoxide hydrolase
SPE	solid phase extraction
sPLA$_2$	secreted PLA$_2$,
thiomaltol	3-hydroxy-2-methyl-4H-pyran-4-thione
TACE	TNFα converting enzyme
TACN	triazacyclononane
TLR	Toll-like receptor
TLR-4	Toll-like receptor 4
TNFα	tumor necrosis factor α

TX	thomboxane
TXAS	thromboxane synthase
ZBG	zinc-binding group

LIST OF FIGURES

LIST OF TABLES

ACKNOWLEDGEMENTS

I would like to thank my former and current lab mates, who have helped me become the scientist I am today. To Ralph and Ursula, who were the first people to get me to believe in my own ideas and try them out. To Becca and Rick, I owe all my knowledge, understanding and ability to run a mass spectrometer to you. To Daren and Ray, who spent endless time helping me work through the day-to-day difficulties of doing science when I wasn't good enough to do it on my own. To Darren and Tom, who have patiently worked alongside me and helped keep me from being overwhelmed after I bit off a bit more science than I could chew. To Kara, who told me to aim high and do amazing, ground breaking science - because she thought I could. And of course, to Andrej and John, along with my best friends Erin, Faith, and Timmy, who for better or worse, have supported me though my many failures and been there for the less frequent triumphs. I cannot thank these people enough.

I'd also like to thank my amazing collaborators and mentors, whose abilities made this research possible. To Jeff, without your patience, support and infectious enthusiasm I probably would never have ended up in graduate school in the first place. Faith, I enjoyed getting to work with you scientifically; you challenge me in ways I rarely get but push me to be the researcher and person I want to be. True story. To Vicki and Charles, who believed that we could get that crazy infectious disease project off the ground. And to Camilla, whose limitless scientific ability and endless patience with me were probably undeserved but appreciated every day. These people were instrumental in creating the work described herein. Raymond A. Deems, Rebecca Bowers-Gentry, and Richard Harkewicz co-authored work published in *Methods in Enzymology*, and comprises a

significant portion of Chapter 2. Daren L. Stephens, Rebecca Bowers-Gentry, Andrej Grkovich and Raymond A. Deems co-authored a paper published in the *Journal of Biological Chemistry*, described in full in Chapter 3. Faith E. Jacobsen and Seth M. Cohen co-authored work published in *ChemBioChem*, described in full in Chapter 4. Victoria A. Blaho and Charles R. Brown co-authored work currently in submission, described in full in Chapter 5. I feel blessed to have worked with such wonderful people. You guys made science fun.

To my mom and dad, who have supported me in all my endeavors. When as a sophomore in college, I first told my dad I was going to be a chemist. He asked me "How are you going to get a job?" Then I applied to graduate school, which didn't really address that question at all. My mom, who has a passion for genetics, always told me I should become a biologist. I patently refused, "I am not a biologist, I'm a (insert any other type of science here)". In the end, I now have a job studying biology. But no matter what I said or did, they were always proud of me. It means more to me than I can possibly express. I could never have made it here without you two.

Last, but not least, thank you Ed for giving me all these opportunities and experiences. You demonstrated an incredible amount of support and patience, and always believed my projects would work. I hope someday I can be that kind of mentor for my own students.

CURRICULUM VITA

EDUCATION

University of California, San Diego December 2008
Ph.D., Chemistry
Advisor: Professor Edward A. Dennis

University of California, San Diego March 2007
Masters of Science, Chemistry
Advisor: Professor Edward A. Dennis

University of Michigan December 2001
Bachelor of Science in Chemistry
Advisor: Professor Jeffrey F. Horowitz

RESEARCH EXPERIENCE

University of California, San Diego – La Jolla, CA 2002 – Present
Graduate Research Assistant
Advisor: Edward A. Dennis

University of Michigan – Ann Arbor, MI 2000 – 2002
Undergraduate Research Assistant
Advisor: Jeffrey F. Horowitz

AWARDS AND PROFESSIONAL AFFILIATIONS

ASBMB Graduate/Postdoctoral Travel Award 2008
NIH Gastroenterology Pre-doctoral Training Grant 2007 – 2008
San Diego Consortium for Systems Biology Representative 2007 – 2008
Pharmacology Seminar Series Selection Committee Representative 2008

TEACHING EXPERIENCE

University of California, San Diego – La Jolla, CA 2003 – 2004
Teaching Assistant, Department of Chemistry and Biochemistry

Analytical Chemistry Lab (2 quarters)
The Periodic Table (1 quarter)

Point Loma Nazarene University – San Diego, CA
Guest Organic Chemistry Lecturer 2007

PUBLICATIONS

8. **Buczynski MW,** Svensson CI, Jacobsen FE, Dumlao DS, Scherbart T, Yaksh, TL, Dennis EA. Profiling of lipid mediators released spinally in response to peripheral painful inflammation. (2008) *In preparation*.

7. Blaho VA[†], **Buczynski MW**[†], Brown CR, Dennis EA. Lipidomic analysis of eicosanoid dynamics during the development and resolution of Lyme disease-induced arthritis in mice. (2008) *In submission*.

6. Blaho VA, **Buczynski MW**, Dennis EA, Brown CR. Cyclooxygenase-1 regulates IL-6 and IL-17-dependent germinal center development and pathogen-specific antibody production. (2008) *In submission.*

5. Jacobsen FE[†], **Buczynski MW**[†], Dennis EA, Cohen SM. A macrophage cell model for selective metalloprotein inhibitor design. (2008) *ChemBioChem*. *In press*.

4. **Buczynski MW**, Stephens DL, Bowers-Gentry RC, Grkovich A, Deems RA, Dennis EA. TLR and sustained calcium agonists synergistically produce eicosanoids independent of protein synthesis in RAW264.7 cells. (2007) *J. Biol. Chem.* 282, 22834-47.

3. Deems RA, **Buczynski MW**, Bowers-Gentry RC, Harkewicz R, Dennis EA. Detection and quantitation of eicosanoids via high performance liquid chromatography/electrospray ionization mass spectrometry. (2007) *Methods Enzymol.* 432, 59-82.

2. Grkovich A, Johnson CA, **Buczynski MW**, Dennis EA. Lipopolysaccharide-induced cyclooxygenase-2 expression in human U937 macrophages is phosphatidic acid phosphohydrolase-1 pependant. (2006), *J.Biol. Chem.* 281, 32978-87.

1. Raetz CR, Garrett TA, Reynolds CM, Shaw WA, Moore JD, Smith DC Jr, Ribeiro AA, Murphy RC, Ulevitch RJ, Fearns C, Reichart D, Glass CK, Benner C, Subramaniam S, Harkewicz R, Bowers-Gentry RC, **Buczynski MW**, Cooper JA, Deems RA, Dennis EA. Purification and properties of Escherichia coli Kdo2-lipid A, a defined endotoxin that activates macrophages via TLR-4. (2006) *J. Lipid Res.* 47, 1097-1111.

[†]Authors contributed equally to this manuscript.

ORAL PRESENTATIONS

2. Buczynski MW, Blaho VA, Brown, CR, Dennis EA. "Temporal eicosanoid profiling of the inflammatory response to infection by the Lyme disease bacterium" UCSD Department of Pharmacology Research Discussions, San Diego, CA, May 7th, **2008**.
1. Buczynski MW, Blaho VA, Brown, CR, Dennis EA. "Temporal eicosanoid profiling of the inflammatory response to infection by the Lyme disease bacterium" ASBMB, San Diego, CA, April 5th, **2008**.

POSTER PRESENTATIONS

7. Buczynski MW, Blaho VA, Brown, CR, Dennis EA. "Temporal eicosanoid profiling of the inflammatory response to infection by the Lyme disease bacterium" ASBMB, San Diego, CA, April 5th-9th, **2008**.
6. Buczynski MW, Svensson CI, Stephens DL, Yaksh TL, Dennis EA. "Profiling of lipid mediators released spinally in response to peripheral painful inflammation" ASBMB, San Diego, CA, April 5th-9th, **2008**.
5. Buczynski MW, Blaho VA, Dennis EA, Brown CR. "Temporal eicosanoid profiling of the inflammatory response to infection by the Lyme disease bacterium" Keystone Symposia: Eicosanoids and Other Mediators of Chronic Inflammation, Big Sky, MO, January 7th-12th, **2008**.
4. Buczynski MW, Blaho VA, Dennis EA, Brown CR. "Temporal eicosanoid profiling of the inflammatory response to infection by the Lyme disease bacterium" 10th International Conference on Eicosanoids & Other Bioactive Lipids in Cancer, Inflammation, and Related Diseases, Montreal, Canada, September 16th-19th, **2007**.
3. Buczynski MW, Stephens DL, Bowers-Gentry RC, Deems RA, Benner C, Glass CK, Dennis EA. "Multiple Agonist Induced Changes in Eicosanoid Metabolites Correlated with Gene Expression in Macrophages" ASBMB, Washington, DC, April 28th-May 2nd, **2007**.
2. Buczynski MW, Stephens DL, Bowers-Gentry RC, Deems RA, Benner C, Glass CK, Dennis EA. "Multiple Agonist Induced Changes in Eicosanoid Metabolites Correlated with Gene Expression in Macrophages" Keystone Symposia: Bioactive Lipids in the Lipidomics Era, Taos, NM, February 20th-25st, **2007**.
1. Buczynski MW, Harkewicz R, Bowers-Gentry RC, Deems RA, Dennis EA. "LC/MS Lipidomics of Arachidonic Acid Release and Prostaglandin Synthesis in P388D1 Murine Macrophage-like Cells" 9th International Conference on Eicosanoids & Other Bioactive Lipids in Cancer, Inflammation, and Related Diseases, San Francisco, CA, September 11th-14th, **2005**.

ABSTRACT OF THE DISSERTATION

Lipidomic Analysis of Eicosanoid Dynamics in Inflammation and Disease

by

Matthew Wallace Buczynski

Doctor of Philosophy in Chemistry

University of California, San Diego, 2008

Professor Edward A. Dennis, Chair

Eicosanoids begin as a single poly-unsaturated fatty acid, arachidonic acid. Yet from this simple origin, hundreds of bioactive signaling molecules can be created, often within minutes of receiving an initiation signal. Many of these bioactive lipids have a functional partner that generates an opposing effect and helps prevent any one pathway from signaling uncontrollably in the body. For this reason, we have adapted liquid chromatography and tandem mass spectrometry into a lipidomic platform that can be employed to study eicosanoid signaling in a comprehensive manner. The overarching goal of such an approach is to elucidate the role of eicosanoids in physiology and disease at the cellular and organismal level, in hopes of identifying better targets for pharmaceutical intervention.

This thesis first discusses the pathways of eicosanoid biosynthesis and catabolism, as well as the differences between humans and the model organisms commonly used as research surrogates (mouse and rat). Using this background, a mass spectra library of known eicosanoids was generated and used to create high-throughput lipidomic methodology using tandem mass spectrometry that facilitated several different studies. We investigated a number of receptor-mediated eicosanoid activation pathways in the macrophage cell, identifying two distinct pathways that synergistically produce eicosanoids in combination. Using this study, we turned the macrophage model into a tool for developing potent and selective inhibitors of inflammatory metalloproteins. At the organismal level, we developed a model of inflammation in mice infected with Lyme disease that integrates the major eicosanoid pathways, from initial infection to resolution of inflammation.

Chapter 1.

Introduction to Eicosanoid Signaling

1.A Systems biology and eicosanoid lipidomics

Biological processes are comprised of numerous converging signals that concertedly create a coherent effect. Commonly, any one individual signaling element may elicit a physiological response, yet its loss is not fatal to the organism. In fact, a wide range of genetic variation can be observed within individual members of a given species without leading to a dramatic loss of function. As these signals have redundant and emergent properties, it can be difficult to explain how a biological process works using a limited number of molecular indicators. For this reason, systems biology has emerged to address the question of how molecular biology works as an integrated process.

Systems biology has advanced exponentially during the past two decades, producing a wealth of data regarding disease susceptibility and pathology. However, metabolomics has lagged behind its counterpart "omics", genomics and proteomics, hampering the advancement of sequential systems biology as a cohesive approach to disease investigation and drug discovery. The unique challenges faced by metabolomics researchers are evident in the emerging field of lipidomics, the analysis and characterization of the immensely diverse fatty acids and their derivatives. For this reason, the Lipid Metabolites and Pathway Strategy (LIPID MAPS) consortium was created to provide an intellectual infrastructure for the advancement of lipidomics. With the ambitious goal of facilitating the attempts of the international community to bring lipidomics to a level comparable with that of genomics and proteomics, a comprehensive lipid classification system has been established[1], liquid chromatography-tandem mass spectrometry (LC-MS/MS) has been adopted as the consensus methodology for lipid

analysis[2], and a publicly accessible database of lipid mass spectra has been made available online (www.lipidmaps.org).

Eicosanoids comprise a class of bioactive lipid mediators derived from the metabolism of polyunsaturated fatty acids by cyclooxygenases (COX)[3-5], lipoxygenases[3, 6] (LOX), cytochrome P450s (CYP), or non-enzymatic pathways (Figure 1-1). This class of bioactive lipid mediators has been intensely studied because of their contribution to the inflammatory response in diseases such as arthritis and asthma, yet no methodology for comprehensive large-scale eicosanoid quantitation exists. Thus, *in vivo* research has been primarily focused on only a select few eicosanoids for which specific antibodies exish, such as prostaglandin E_2 and leukotriene B_4[7], despite the plethora of other potentially vital lipids produced by the same synthetic pathways. A further challenge is the relatively recent discovery of new anti-inflammatory and pro-resolution lipid mediators such as lipoxins, resolvins, and protectins, which are produced by the same biosynthetic enzymes that produce pro-inflammatory eicosanoids[6].

Although a genomics or proteomics approach would demonstrate the presence of the biosynthetic enzymes, a metabolomics method for quantitatively measuring lipid products is essential to our understanding of many important biological processes. To facilitate a systems biology approach to eicosanoid analysis, the biosynthetic enzymes and metabolic products identified in humans to date have been described here. In many cases, the implications in physiology and disease of a particular eicosanoid have not been thoroughly investigated, and for this reason we have focused this introduction on their general signaling mechanisms. Additionally, since studies of human biology and disease

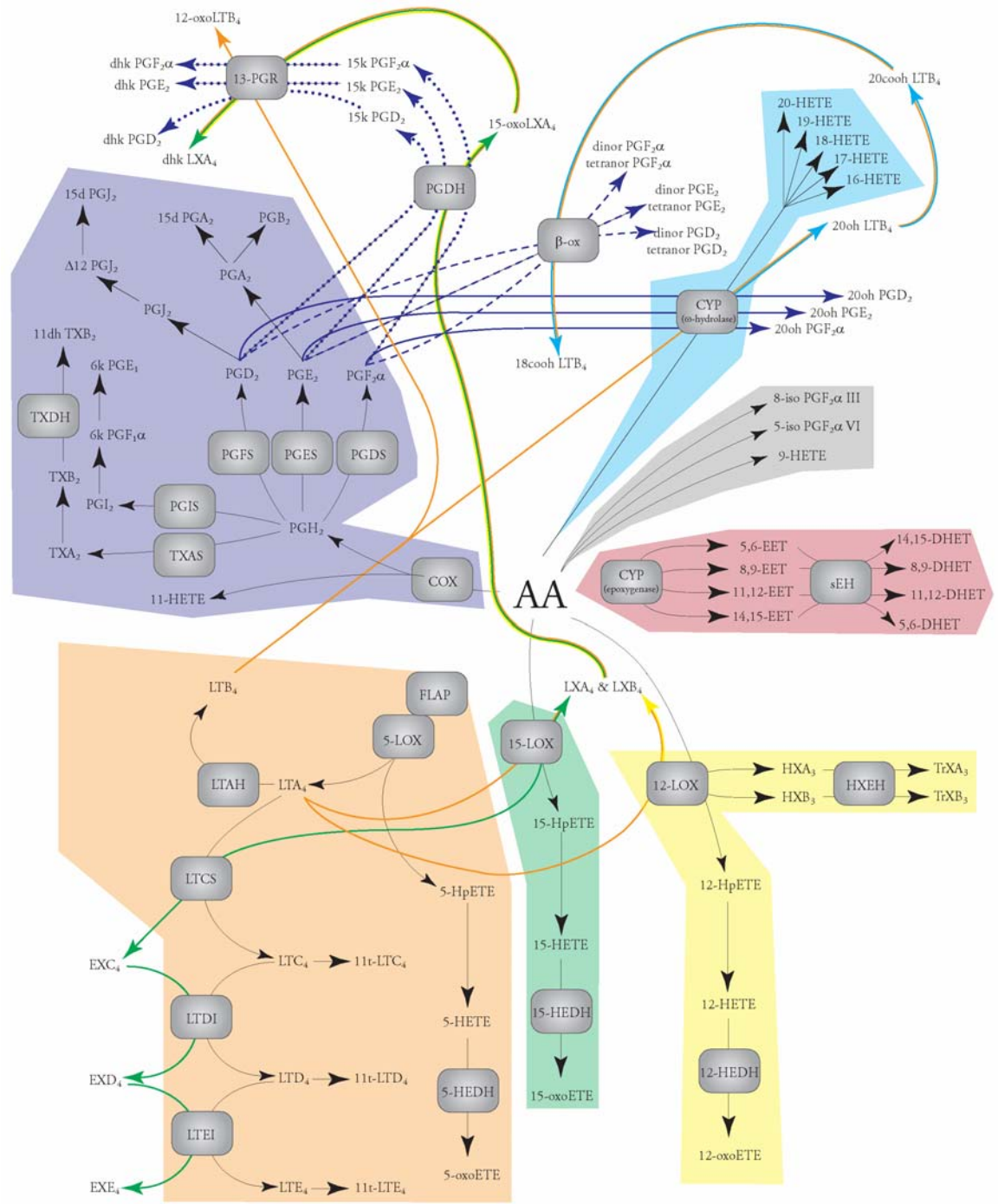

Figure 1-1. Major eicosanoid biosynthetic pathways. The metabolites of the major pathways are indicated in color: COX (blue, 5-LOX (orange), 15-LOX (green), 12-LOX (yellow), CYP epoxygenase (red), CYP ω-hydroxylase (cyan) and non-enzymatic oxidation (grey).

commonly employ mouse or rat models as a surrogate, important differences between these species are highlighted.

1.B Phospholipase A_2 (PLA_2)

Arachidonic acid and other poly-unsaturated fatty acids serve as the metabolic precursors for eicosanoid synthesis[8, 9]. Biologically, these molecules are generally not available in large quantities in the free acid form, but are stored at the *sn-2* position on the glycerol backbone of membrane phospholipids. To be used for the biosynthesis, phospholipase A_2 (PLA_2) liberates fatty acids *sn-2* fatty acids from phospholipids at the membrane interface.

Phospholipase A_2 represents a superfamily of at least 15 groups that have wide-ranging roles in biological processes. These enzymes can be considered as five types: cytosolic PLA_2 ($cPLA_2$), secreted PLA_2, calcium-independent PLA_2 ($iPLA_2$), platelet-activating factor acetylhydrolase (PAF-AH), and lysosomal PLA_2 ($LPLA_2$); their classification and biological functions have been extensively reviewed[8, 9]. Current literature strongly implicates $cPLA_2$, which comprises the group IV PLA_2s, as the chief enzyme involved in poly-unsaturated fatty acid release in eicosanoid biosynthesis. Cytosolic PLA_2s utilizes a catalytic Ser/Asp dyad to hydrolyze fatty acids. With the exception of GIVC, $cPLA_2$s contain a C2 domain which facilitates translocation from the cytosol to the membrane surface where it encounters phospholipid substrate. In contrast, the GIVC association with the membrane is controlled through acylation. To date, six isoforms of group IV PLA_2 have been isolated (Table 1-1). The best characterized is the GIVA, considered the key regulator of free arachidonic acids levels *in vivo* for eicosanoid

Table 1-1. Cytosolic PLA_2s involved in polyunsaturated fatty acid liberation in human, mouse and rat.

		Human				Mouse					Rat				
Pathway	Name	Activity	AA	Gene	Sequence	Activity	AA	Gene	Sequence	%ID	Activity	AA	Gene	Sequence	%ID
cPLA2	GIVA	PLA_2	749	PLA2G4A	NP_077734.1	PLA_2	748	Pla2g4a	NP_032895.1	95	PLA_2	752	Pla2g4a	NP_598235.2	95
	GIVB	PLA_2	781	PLA2G4B	NP_001108105.1	PLA_2	791	Pla2g4b	NP_663353.3	82	PLA_2	791	Pla2g4b	NP_001101234.2	82
	GIVC	PLA_2	541	PLA2G4C	NP_003697.1	PLA_2	597	Pla2g4c	NP_001004762.1	55	PLA_2	687	Pla2g4c	XP_001073384.1	54
	GIVD	PLA_2	818	PLA2G4D	NP_828848.3	PLA_2	825	Pla2g4d	NP_001019308.1	71	PLA_2	842	Pla2g4d	XP_001080051.1	69
	GIVE	PLA_2	839	PLA2G4E	NP_001073959.1	PLA_2	875	Pla2g4e	NP_808513.2	75	PLA_2	915	Pla2g4e	XP_230487.4	76
	GIVF	PLA_2	849	PLA2GIVF	NP_998765.2	PLA_2	855	Pla2g4f	NP_001019316.1	73	PLA_2	861	Pla2g4f	XP_001080057.1	73

production[10]. Gijon *et. al.* have shown that macrophages from GIVA PLA_2 knockout mice were incapable of producing eicosanoids[11]. More recently, Adler *et. al.* identified a patient with inherited GIVA deficiency, and determined that nearly all arachidonic acid utilized for eicosanoid production by platelets and circulating leukocytes was attributable to this enzyme[12]. On the other hand, GIVD, GIVE and GIVF PLA_2 have been less-well characterized. A study of *in vitro* activity of the human GIVD shows a 6-fold preference toward linolenic over arachidonic acid[13], while the murine GIVF appears to prefer phosphatidylethanolamine over phosphatidylcholine substrate[14], differentiating them from other GIV PLA_2s. GIVB and GIVC demonstrate far less specificity for the *sn-2* fatty acid[15, 16], suggesting it is less likely to play an important role in eicosanoid signaling. Overall, $cPLA_2$s have a broad range of homology between human, mouse and rat; while GIVA has 95% identity between species, other $cPLA_2$ show between 54% and 82% identity in these species.

1.C Cyclooxygenase metabolites

1.C.1 Cyclooxygenases (COX)

Prostaglandins (PG) are bioactive signaling molecules derived from cyclooxygenase (COX) and subsequent prostaglandin synthase activity on arachidonic acid[4, 5] (Table 1-2). Cyclooxygenase contains two distinct active sites, a cyclooxygenase and peroxidase site, both of which utilize the same tyrosine radical and heme-iron for catalysis. The cyclooxygenase site incorporates molecular O_2 at the 11- and 15-carbon on arachidonic acid to form PGG_2, which contains the following moieties: a 5-member ring linked at C-8 and C-12, an endoperoxide bridge across C-9 and C-11, and a peroxide at

C-15. The peroxidase site reduces the peroxide to a hydroxyl to form PGH_2, the substrate for the various prostaglandin synthases. In addition to forming PGH_2, arachidonic acid can situate in the active site pocket in a limited number of sub-optimal conformations, leading to incorporation of only a single molecular O_2 and the formation of trace amounts of either 11(R)-HETE or 15(S)-HETE. Cyclooxygenase activity does not exhibit long-term stability, as the catalytic tyrosine radical can be transferred to a nearby tyrosine residue and cause "suicide inactivation" after approximately 300 turnovers. Because the enzyme can perform only a limited number of reactions, it must be constantly re-expressed to generate metabolites. The details of these mechanisms have been reviewed extensively[5].

Cyclooxygenase is encoded by two distinct genes, COX-1 and COX-2. These two isoforms exhibit ~60% identity and have nearly identical active site residues[4]. The most significant structural difference between these enzymes is an isoleucine→valine substitution, which results in a larger COX-2 active site pocket. This allows COX-2 to be more permissive in selecting substrates, and unlike COX-1 it can metabolize dihomo-γ-linoleic and eicosapentanoic acid in addition to AA. Pharmaceutical companies have also taken advantage of larger COX-2 active site, creating isoform selective inhibitors including Celecoxib (Celebrex™). While COX-1 and COX-2 have similar structural and catalytic features, these isozymes exhibit different expression patterns. Cyclooxygenase-1 is constitutively expressed by most cell-types, and has been implicated in a number of homeostatic processes including stomach acidity control, endometrial cycling and renal function. In contrast, COX-2 expression is controlled by the pro-inflammatory

Table 1-2. Cyclooxygenases and related enzymes involved in eicosanoid biosynthesis in human, mouse and rat.

		Human				Mouse					Rat				
Pathway	Name	Activity	AA	Gene	Sequence	Activity	AA	Gene	Sequence	%ID	Activity	AA	Gene	Sequence	%ID
COX	COX-1	cyclooxygenase	599	PTGS1	NP_000953.2	cyclooxygenase	602	Ptgs1	NP_032995.1	89	cyclooxygenase	602	Ptgs1	NP_058739.3	86
	COX-2	cyclooxygenase	604	PTGS2	NP_000954.1	cyclooxygenase	604	Ptgs2	NP_035328.2	87	cyclooxygenase	604	Ptgs2	NP_058928.3	86
PGIS	PGIS	PGI synthase	500	PTGIS	NP_000952.1	PGI synthase	501	Ptgis	NP_032994.1	86	PGI synthase	501	Ptgis	NP_113745.1	84
TXAS	TXAS	TXA synthase	534	TBXAS1	NP_001052.1	TXA synthase	533	Tbxas1	NP_035669.3	81	TXA synthase	533	Tbxas1	NP_036819.1	80
PGFS	PGFS	9,11-endoperoxide reductase (PGH_2), 11-keto reductase (PGD_2)	323	AKR1C3	NP_003730.4	NT	-	-	-	-	NT	324	RGD1564865 _predicted	XP_574074.2	70
	9K-PGR	9-ketoreductase (PGE2)	277	CBR1	NP_001748.1	NT	280	Cbr1	NP_031646.2	87	9-ketoreductase	277	Cbr1	NP_062043.1	86
	PM/PGFS	NT	198	C1orf93	NP_689584.1	Prostamide / PGF synthase	201	2810405K02Rik	NP_079858.2	88	NT	201	RGD1308251 _predicted	NP_001102167.1	87
PGES	mPGES	PGE synthase	152	PTGES	NP_004869.1	PGE synthase	153	Ptges	NP_071860.1	80	PGE synthase	153	Ptges	NP_067594.1	80
	mPGES-2	PGE synthase	377	PTGES2	NP_079348.1	PGE synthase	384	Ptges2	NP_598544.1	83	PGE synthase	384	Ptges2 _predicted	NP_001101302.1	84
	cPGES	PGE synthase	160	PTGES3	NP_006592.3	PGE synthase	160	Ptges3	NP_062740.1	99	PGE synthase	160	Ptges3 _predicted	XP_343136.2	99
PGDS	l-PGDS	PGD synthase	190	PTGDS	NP_000945.3	PGD synthase	189	Ptgds	NP_032989.2	72	PGD synthase	189	Ptgds	NP_037147.1	69
	h-PGDS	PGD synthase	199	PGDS	NP_055300.1	PGD synthase	199	Ptgds2	NP_062328.2	80	PGD synthase	199	Ptgds2	NP_113832.1	81

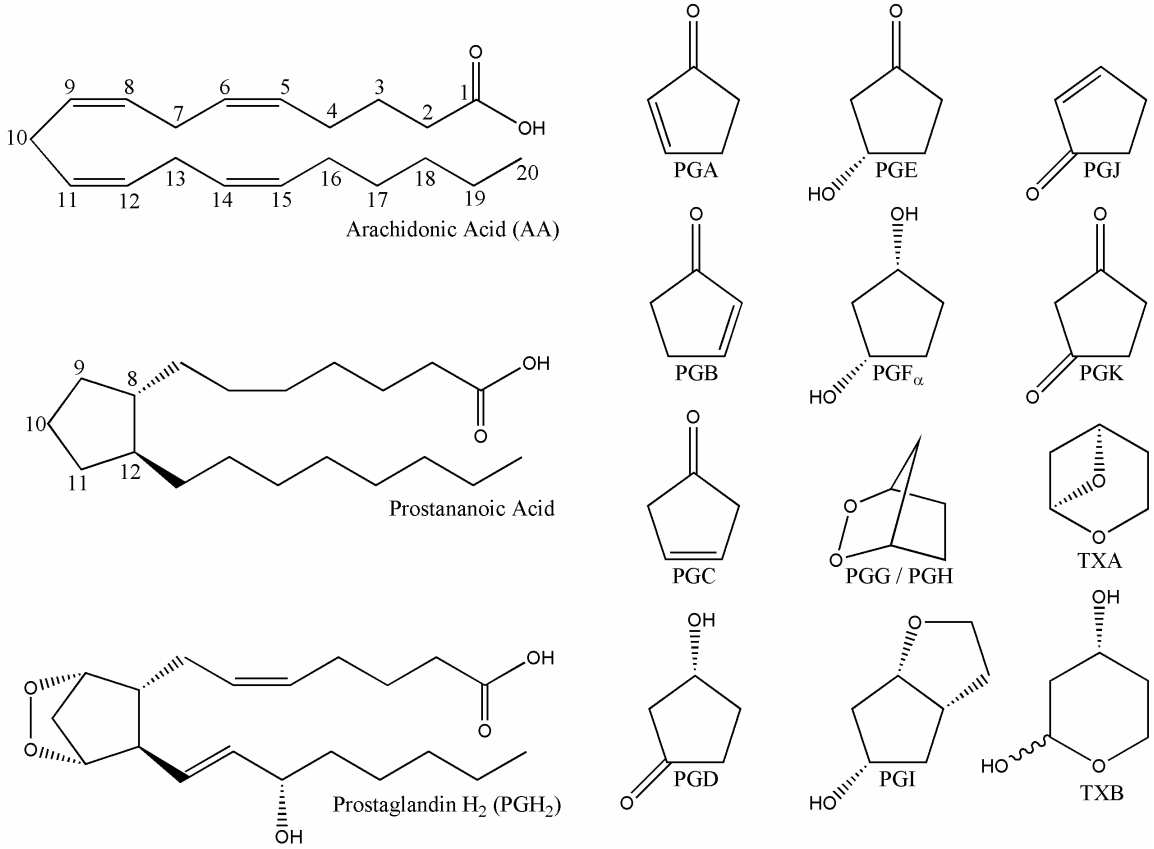

Figure 1-2. Prostaglandin nomenclature and structure. Arachidonic acid carbons are numbered 1-20, starting from the carboxylate. The prostaglandin letter indicate composition of the prostane ring.

transcription factor NF-κB and highly upregulated in response to infection, atherosclerosis and a number of cancers.

1.C.2 Prostaglandins (PG)

Prostaglandin H_2 can form a number of different bioactive products through the action of prostaglandin synthases. This includes a number of important signaling molecules, including prostaglandin I_2 (PGI_2, also known as prostacyclin), thromboxane A_2, prostaglandin E_2 (PGE_2, also known as dinoprostone), prostaglandin D_2 (PGD_2) and

prostaglandin $F_{2\alpha}$ ($PGF_{2\alpha}$). Followings the PG abbreviation (Figure 1-2), the nomenclature highlights two important structural features: the components of the 5-member prostane ring, as denoted by a letter A – K, and the number of double bounds, denoted by a subscript number[17]. The lone exception is thromboxane, which has a 6-member oxane ring, and is abbreviated TX.

1.C.3 Prostaglandin I_2 and thromboxane A_2

Prostaglandin I_2 (PGI_2) was first identified in 1976[18], and is formed by the prostacyclin synthase. Prostacyclin synthase belongs to the cytochrome P450 superfamily[19], but unlike the CYP monooxygenases it facilitates the rearrangement of the PGH_2 endoperoxide bridge[20]. The active site heme-iron interacts with the C-11 oxygen, promoting the hemolytic cleavage of the endoperoxide bond and the formation of an ether linkage between C-9 and C-5. Prostaglandin I_2 is highly labile and the "saturated furan" bond is rapidly hydrated to form the stable but biologically inactive 6-keto $PGF_{1\alpha}$, and because of this PGI_2 and 6-keto $PGF_{1\alpha}$ are often used interchangeably. Prostaglandin I_2 binds the G-coupled protein receptor IP[21, 22], as well as peroxisome proliferators-activated receptor (PPAR) alpha[23], which has a number of important signaling roles.

Identified in 1975[24], thromboxane A_2 (TXA_2) is the physiological lipid counterbalance to PGI_2. Similar to PGI_2, its biosynthesis is catalyzed by a cytochrome P450 superfamily member, thromboxane A synthase[20, 25]. This enzyme facilitates rearrangement of the endoperoxide bridge of PGH_2 in a complimentary mechanism to prostacyclin synthase, interacting with the C-9 oxygen to promote endoperoxide bond cleavage. The C-11 oxygen radical initiates intramolecular rearrangement, resulting in the

formation of TXA_2 containing a stable oxane ring between C-11 and C-12, as well as a labile ether linkage between C-9 and C-11. Thromboxane A_2 has low stability in an aqueous environment, and the C-9 ether linkage is rapidly hydrolyzed *in vivo* to form the biologically inert TXB_2. It also binds a specific G protein-coupled receptor (GPCR), termed the TP receptor, which culminates in increasing intracellular calcium concentrations[25].

1.C.4 Prostaglandin E_2

Prostaglandin E_2 may be the best characterized signaling molecule within the eicosanoid class. A PubMed search for "PGE_2" reveals that, since the identification and isolation of PGE_2 1963 from human seminal plasma[26], well over 27,000 papers have been published studying this molecule. The effects of PGE_2 have been implicated in innumerable biological processes and disease pathologies, including bone formation, parturition, bronchodilation, pain signaling, innate and adaptive immune responses, cancer, arthritis, and atherosclerosis. The wide spectrum of PGE_2 signaling can be partially attributed to differences in expression and function of its four known receptors, $EP_{1\text{-}4}$. The EP receptors are all GPCRs, and their most potent natural ligand is PGE_2. Functionally, EP_1 and EP_3 mediate their responses through calcium signaling, whereas EP_2 and EP_4 do so by increasing cAMP levels. Likewise, PGE_2 synthesis occurs through three unique enzymes, named the cytosolic PGE synthase (cPGES), microsomal PGE synthase-1 (mPGES-1) and synthase-2 (mPGES-2)[27].

Cytosolic PGE_2 synthase was identified by Tanioka *et. al.* in 2000 from rat brain, and determined it to be identical to human p23[28]. Previously, this protein was identified

as a chaperone protein that interacts with heat shock protein-90, which up-regulates cPGES activity *in vitro*. The catalytic activity of cPGES requires glutathione and the conserved Tyr-9 residue for activity, similar to other cytosolic glutathione S-transferases including hematopoietic prostaglandin D synthase[27, 29]. In this case, the glutathione thiol is expected to interact with the C-9 oxygen of PGH_2, facilitating cleavage of the endoperoxide bridge and the formation of PGE_2.

The cloning and characterization of human mPGES-1 was reported by Jakobsson *et. al.* in 1999[30]. As a member of the the membrane associated proteins in eicosanoid and glutathione (MAPEG) superfamily of transmembrane proteins, this enzyme requires glutathione for activity. While mPGES-1 has not yet been crystallized, Huang *et. al.* have examined characterized it using site-directed mutagenesis and computational modeling onto the microsomal glutathione S-transferase (mGST) structure, its nearest subfamily member[31]. They identified Arg-110 and Tyr-114 interactions with the carboxyl-terminus of PGH_2 and determined that the glutathione thiol was positioned to catalyze PGE_2 biosynthesis. The mechanism of PGE_2 formation likely proceeded by a similar mechanism to cPGES and h-PGDS; however, the structural element that activated glutathione remains undetermined. The mPGES-1 enzyme tightly couples metabolically[32], co-regulates its expression and co-localized to the endoplasmic reticulum with COX-2[33]; however, COX-2 resides in the lumen of the ER, whereas the mPGES-1 active site appears to face the cytosol. A thorough examination of mPGES-1 literature has been reviewed by Samuelsson *et. al*[33].

Microsomal PGES-2 activity was first reported by Wantanabe *et. al.* as a distinct PGES from cPGES and m-PGES-1[34]. While it had no specific requirement for

glutathione, its activity was enhanced by the presence of free thiols. The human isoform was cloned in 2002 by Tanikawa *et. al.*[35], and contains a putative C-x-x-C sequence found in glutaredoxin and thioredoxin, but not cPGES and m-PGES-1. Subsequent crystallization by Yamada *et. al.* in 2005[36] confirmed it contained significant structural differences from other PGES. Using molecular modeling, they proposed a mechanism for mPGES-2 catalysis. A hydrogen bonding network between Phe-112, Cys-110, Cys-113, and Tyr-107 lowers the pKa of Cys-110 such that it can donate its thiol hydrogen to the C-11 oxygen. This leads to cleavage of the endoperoxide bridge and the creation of a ketone by the C-9 oxygen, forming PGE_2. The final step is facilitated by free thiols, activated by Tyr-107; however, this does not appear to be necessary for productive catalysis.

1.C.5 Prostaglandin D_2

Prostaglandin D_2 is structural isomer of PGE_2, and early studies of D-series prostaglandins regarded them as side-products of E-series biosynthesis[37]. Whereas the prostane ring on PGE_2 has a 9-keto and 11-hydroxy moiety, the positions of these substituents are reversed on PGD_2. In the late 1970's, prostaglandin D_2 was identified as a major product in rat brain homogenates[38] and activated mast cells[39]. Prostaglandin D_2 is formed by prostaglandin D synthase (PGDS), which describes two evolutionarily distinct but functionally convergent enzymes, the lipocalin-type (l-PGDS) and hematopoietic-type (h-PGDS). One critical difference between the PGDS is the requirement for glutathione; l-PGDS can function without this co-factor, while h-PGDS utilizes it for catalysis. Urade *et. al.* proposed the mechanism for l-PGDS[40], whereby the thiol from

Cys-65 forms a transient bond with the C-11 oxygen of PGH_2, opening the endoperoxide ring. Exogenous sulfhydryl compounds then remove the C-11 hydrogen, culminating in PGD_2 production and release. NMR structural studies and molecular modeling estimated a 5 Å distance between the Cys-65 thiol and the C-11 oxygen, consistent with this model[41]. Following crystallization in 1997, Kanaoka *et. al.* proposed that h-PGDS contains a pocket that binds and activates glutathione via Tyr-8, such that the glutathione thiol functions analogous to Cys-65 of l-PGDS[42].

Prostaglandin D_2 has two known receptors, DP_1 and CRTH2[43]. DP_1 belongs to the family of GPCR that includes IP, TP, $EP_{1\text{-}4}$ and FP, and ligand binding leads to intracellular increases of cAMP. While exhibiting similar PGD_2 binding, CRTH2 shares little homology with DP_1 and appears more closely related to the leukotriene B_4 receptors BLT_1 and BLT_2. CRTH2 activation leads to elevation of intracellular calcium and decreased cAMP levels[44].

1.C.6 Prostaglandin $F_{2\alpha}$

To date, three Prostaglandin $F_{2\alpha}$ biosynthetic enzymes have been cloned and characterized in humans[45]: prostaglandin F synthase (PGFS)[46], prostamide and prostaglandin F synthase (PM/PGFS)[47], and 9-keto prostaglandin reductase (9K-PGR). Prostaglandin $F_{2\alpha}$ was isolated and structurally characterized in 1963 by Samuelsson *et. al.* from human seminal fluid, and demonstrably stimulated smooth muscles from rabbit duodenum[26]. Since then, it has been implicated in a number of physiological processes and disease states[48], including endometrial cycling, embryo development parturition, vasoconstriction, as well as acute inflammation, oxygen-depravation injury and

atherosclerosis. Only one $PGF_{2\alpha}$ specific receptor has been cloned[49], a GPCR termed FP, which upon binding ligand results in an elevation of intracellular calcium.

The human PGFS was cloned in 1999 by Suzuki-Yamamoto *et. al.* and determined to be identical to aldo-keto reductase 1C3 (AKR1C3). Similar to mPGES-2 and hPGDS, PGFS evolved from the thioredoxin protein family and contains the putative C-x-x-C motif. Crystal structures of PGFS were published in 2004[50] and 2006[51] by Komoto *et. al.*, and used to propose a mechanism for $PGF_{2\alpha}$ catalysis. In this model, no specific amino acids coordinate with the PGH_2 endoperoxide; however, the reactive hydrogen of NADPH interacts with the C-9 oxygen of PGH_2. This leads to a hydride shift and cleavage of the endoperoxide bond, whereby the C-11 oxygen can be protonated by H_2O to complete the reaction. Interestingly, PGFS can also take PGD_2 as a substrate. They suggest that His-117 and Tyr-55 form hydrogen bonds with the carbonyl at C-9, promoting an analogous hydride shift from NADPH onto C-9. This forms a stable hydroxyl moiety, and the creation of 11β-$PGF_{2\alpha}$. Structural comparisons show that PGFS is nearly identical to AKR1C1 and AKR1C2, with only seven amino acid differences, and their structures superimposible[50]; however, these substitutions all incorporate smaller amino acids to form a larger active site cavity, and mitigate potential steric hindrance with prostaglandin substrates predicted in AKR1C1 and AKR1C2. An *in vitro* analysis of purified AKR-1C1, AKR-1C2 and AKR-1C4 confirms they have no significant activity toward prostaglandin substrate[52].

Prostamide/Prostaglandin F synthase was identified in mouse and swine brain in 2008[47], recombinant murine protein was expressed and characterized. Like PGFS, PM/PGFS is classified as a thioredoxin protein, and its C-x-x-C motif required for

productive catalysis. It facilitates the reduction of PGH_2 to $PGF_{2\alpha}$ via a similar mechanism to PGFS, involving a hydride transfer from NADPH; in contrast, it does not appear to productively reduce either PGE_2 or PGD_2 but instead takes PGH_2-ethanolamide as a substrate. The mouse gene exhibits a high level of identity with other mammalian sequences, including the human and predicted rat homologs. A comparison of the swine and murine protein demonstrated similar catalytic parameters, and it is expected that its function is well conserved in mammals.

In addition to using PGH_2 and PGD_2 as substrates for the formation of $PGF_{2\alpha}$, it has been shown that PGE_2 can be reduced by 9-keto reductase (9K-PGR) activity to form this molecule[53]. In 2000, Asselin *el. al.* identified AKR1C5 as the putative bovine 9K-PGR, but have yet to definitively identify a functional human homolog. Since proteins in the AKR family often exhibit greater than 80% homology, and previous work has shown that only a few substitutions can radically alter the substrate specificity of these enzymes, homology modeling in absence of *in vitro* data must be viewed with caution.

Carbonyl reductase-1 (CBR-1) has also been demonstrated to reduce a number of exogenous and endogenous metabolic substrates, including 9-keto reductase activity on PGE_2 to form $PGF_{2\alpha}$[54, 55]. Its high k_m value as compared with other substrates indicates PGE_2 may not be an endogenous substrate; however, a number of studies have implicated CBR-1 *in vivo* with lower PGE_2 levels[56] and alterations in the $PGE_2/PGF_{2\alpha}$ ratio[57], warranting more thorough investigation into its role in eicosanoid metabolism.

1.C.7 Cyclopentenone prostaglandins

Cyclopentenone prostaglandins comprise a family of molecules that are formed by dehydration of the cyclopentane ring of PGE_2 and PGD_2[58]. Dehydration of PGE_2 leads to PGA_2, which has been shown to isomerize and form PGC_2 that rapidly undergoes a secondary isomerization, culminating in PGB_2. Prostaglandin A_2 contains an α,β-unsaturated carbonyl which is highly electrophilic, a structural motif found in a number of other cyclopentenones. These electrophilic centers have been shown to react with the thiol moiety on cysteine residues, either on glutathione or cellular proteins. Analogous to PGE_2, PGD_2 dehydration of the prostane ring forms PGJ_2, which also contains an electrophilic center. When PGJ_2 isomerizes to form Δ12-PGJ_2, it promotes secondary dehydration of the C-15 hydroxyl to culminate in 15d-PGJ_2; both Δ12-PGJ_2 and 15d-PGJ_2 contain two electrophilic centers.

Cyclopentenones can exert their effects through both receptor mediated signaling and covalent protein interaction. Dehydration dramatically lowers the affinity of a cyclopentenone for its parent molecule's prostaglandin receptor. However, 15d-PGJ_2 has been identified as a high affinity ligand for the transcription factor peroxisome proliferators-activated receptor-γ (PPARγ), as well as a less potent activator of PPARα and PPARδ. It is unclear whether the levels of 15d-PGJ_2 necessary to activate PPARs are high enough to elicit this response *in vivo*[59]. Evidence suggests that non-receptor mediated effects of cyclopentenones can be attributed to their electrophilic α,β-unsaturated carbonyl centers. Many of these biological actions can be recapitulated by cyclopentenone, while structurally related molecules lacking a reactive center, such as PGB_2, are unable to elicit these effects.

1.D 5-lipoxygenase metabolites

1.D.1 5-lipoxygenase (5-LOX)

Metabolites from the 5-lipoxygenase (5-LOX) pathway were first characterized in 1979, when Murphy *et. al.* identified leukotriene C_4 as the slow-reacting substance of anaphylaxis[60]. Leukotrienes comprise a family of bioactive signaling molecules formed by the activity of 5-lipoxygenase on arachidonic acid (Table 1-3). 5-lipoxgenase contains a non-heme iron bound by three histidine residues, which it uses to catalyze the addition of molecular oxygen into arachidonic acid. 5-lipoxygenase was cloned in 1988[61], but a 3-dimentional structure has not yet been determined. However, attempts have been made to model the human 5-LOX sequence onto the rabbit 15-LOX crystal structure, which has 57% identity. Similar to $cPLA_2$, the 5-LOX has a catalytic domain linked to a C2 domain that facilitates translocation to the membrane surface. Phosphorylation of Ser^{271} and Ser^{663} increase activity, whereas Ser^{523} inactivates this enzyme. 5-LOX also appears to have an ATP binding site that does not require hydrolysis, but instead stabilizes its structure.

1.D.2 5-Lipoxygenase Activating Protein (FLAP)

Unlike other lipoxygenases, 5-LOX requires the presence of 5-lipoxygenase activating protein (FLAP) for productive leukotriene synthesis *in vivo*. FLAP is a member of the MAPEG superfamily, localizing to the nuclear envelope. Recently, a group at Merck Research Laboratories led by Joseph W. Becker succeeded in crystallizing FLAP bound either both MK-886 and MK-591, inhibitors of 5-lipoxygenase metabolism[62]. They suggest FLAP exists as a trimer, creating a 3200 Å binding pocket

that allows arachidonic acid to laterally diffuse from the membrane. The cytosolic loops of FLAP interact with the 5-LOX catalytic domain, and transfer arachidonic acid into the 5-LOX active site. Both 5-LOX and FLAP are highly conserved in these mammalian systems, with the mouse and rat species having greater than 90% identity with their human homologs.

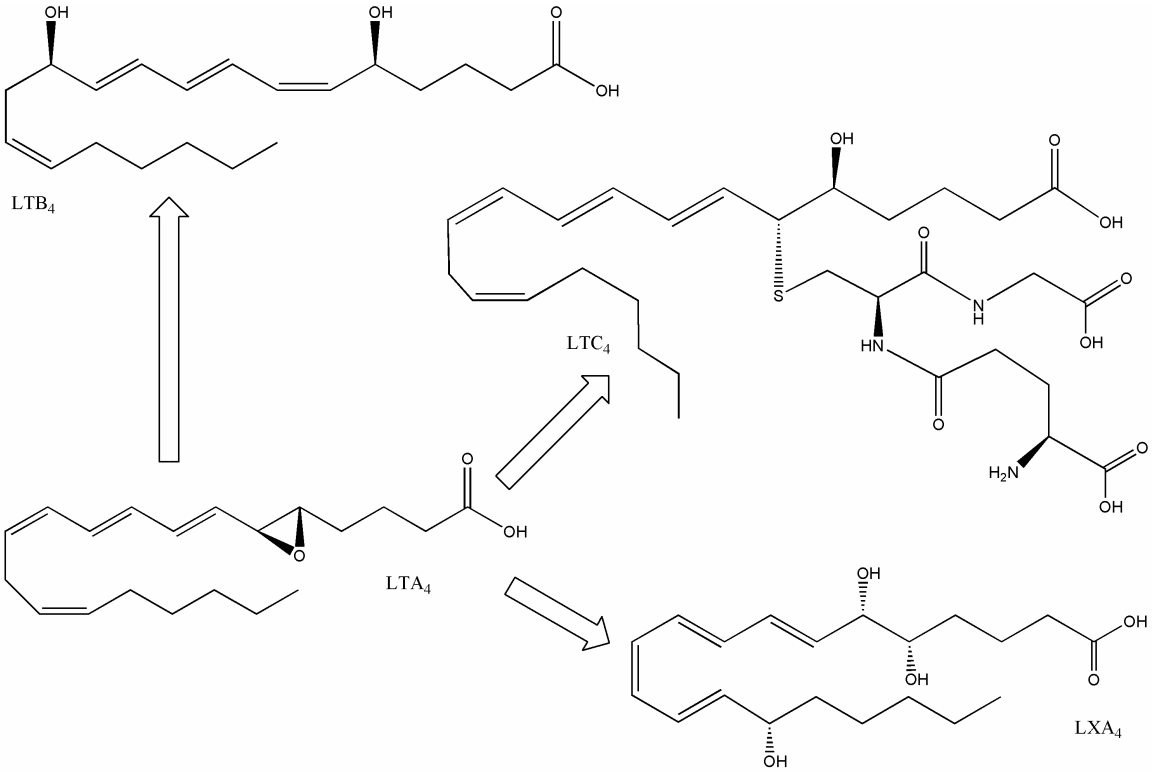

Figure 1-3. Structures of 5-lipoxygenase metabolites. 5-lipoxygenase creates the labile epoxide LTA_4, which can be enzymatically converted into LTB_4, LTC_4 and LXA_4.

Table 1-3. Lipoxygenases, epoxide hydrolases and related enzymes involved in eicosanoid biosynthesis in human, mouse and rat.

		Human				Mouse					Rat				
Pathway	Name	Activity	aa	Gene	Sequence	Activity	aa	Gene	Sequence	%ID	Activity	aa	Gene	Sequence	%ID
5-LOX	5-LOX	5-lipoxygenase, LTA epoxidase	674	ALOX5	NP_000689.1	5-lipoxygenase, LTA epoxidase	674	Alox5	NP_033792.1	93	5-lipoxygenase, LTA epoxidase	670	Alox5	NP_036954.1	92
FLAP	FLAP	FA transfer protein	161	ALOX5AP	NP_001620.2	FA transfer protein	161	Alox5ap	NP_033793.1	92	FA transfer protein	161	Alox5ap	NP_058956.1	92
LTAH	LTAH	LTA hydrolase	611	LTA4H	NP_000886.1	LTA hydrolase	611	Lta4h	NP_032543.2	93	LTA hydrolase	611	Lta4h	NP_001025202.1	98
LTCS	LTCS	LTC syntase	150	LTC4S	NP_665874.1	LTC syntase	150	Ltc4s	NP_032547.1	88	LTC syntase	150	Ltc4s	NP_446091.2	86
	mGST-2	LTC syntase	147	MGST2	NP_002404.1	LTC syntase	147	Mgst2	NP_778160.2	75	LTC syntase	147	Mgst2	NP_001099900.1	79
	mGST-3	LTC syntase	152	MGST3	NP_004519.1	LTC syntase	153	Mgst3	NP_079845.1	86	LTC syntase	221	Mgst3	XP_213943.2	86
GGT	GGT	γ-glutamyl transpeptiase	569	GGT1	NP_001027536.1	γ-glutamyl transpeptiase	568	Ggt1	NP_032142.1	79	γ-glutamyl transpeptiase	568	Ggt1	NP_446292.2	79
	GGL	γ-glutamyl transpeptiase	587	GGT5	NP_001093251.1	γ-glutamyl transpeptiase	573	Ggt5	NP_035950.2	77	NT	572	Ggt5	NP_062108.2	76
MDB	MDB-1	LTD_4 dipeptidase	411	DPEP1	NP_001121613.1	LTD_4 dipeptidase	410	Dpep1	NP_031902.2	72	LTD_4 dipeptidase	410	Dpep1	NP_446043.1	73
	MDB-2	NT	486	DPEP2	NP_071750.1	LTD_4 dipeptidase	578	Dpep2	NP_795887.2	67	NT	481	Dpep2	NP_001011928.1	70
12-LOX	12-LOX-p	12-lipoxygenase	663	ALOX12	NP_000688.2	12-lipoxygenase	663	Alox12	NP_031466.2	86	12-lipoxygenase	662	Alox12_predicted	NP_001099268.1	84
	12-LOX-e	pseudogene	-	ALOX15P	-	12-lipoxygenase	662	Alox12e	NP_663717.1	-	NT	662	Alox12e_predicted	NP_001100484.1	-
	12R-LOX	12(R)-lipoxygenase	701	ALOX12B	NP_001130.1	12(R)-lipoxygenase	701	Alox12b	NP_033789.1	86	NT	701	Alox12b	NP_001034466.1	87
	eLOX3	12(R) hepoxilin synthase	711	ALOXE3	NP_067641.2	12(R) hepoxilin synthase	711	Aloxe3	NP_035916.1	88	12(R) hepoxilin synthase	711	Aloxe3_predicted	NP_001099263.1	88
15-LOX	12/15-LOX-l	12- and 15-lipoxygenase	662	ALOX15	NP_001131.3	12- and 15-lipoxygenase	663	Alox15	NP_033790.3	74	12- and 15-lipoxygenase	663	Alox15	NP_112272.2	75
	8/15-LOX-2	15-lipoxygenase	676	ALOX15B	NP_001132.2	8-lipoxygenase	677	Alox8	NP_033791.1	78	8-lipoxygenase	677	Alox15b	NP_695213.1	81

1.D.3 Leukotrienes (LT)

5-lipoxygenase performs the initial enzymatic step in leukotriene synthesis[63], creating 5-hydroperoxy-eicosatetraenoic acid (5-HpETE) by incorporating one molecular oxygen at the C-5 position of arachidonic acid. Depending on cellular conditions, 5-HpETE has a number of metabolic fates. It can be secreted in its peroxide form, reduced to 5-hydroxy-eicosantetraenoic acid (5-HETE), or isomerize to form LTA_4 in the 5-LOX active site. When produced *in vivo*, LTA_4 can be acted on by LTA_4 hydrolase to generate the stereospecific LTB_4, or used as a substrate by LTC_4 synthase to catalyze the conjugation of the glutathione to form LTC_4. Non-enzymatic hydrolysis of LTA_4 create all four potential steroisomers of LTB_4, including 6-trans LTB_4, 12-epi LTB_4 and 6-trans 12-epi LTB_4. While the enzymes involved in leukotriene metabolism are described here, a thorough review of the subject has been published by Murphy *et. al.*[63]

1.D.4 5-HETE and 5-oxoETE

Currently, 5-HETE itself does not appear to play a significant role in biological signaling. However, it can be further reduced by 5-hydroxy-eicosatetraenoic acid dehydrogenase (5-HEDH) to form 5-oxo-eicosatetraenoic acid (5-oxoETE). While this enzyme has yet to be cloned, its biophysical properties have been well characterized by William Powell's research group[64]. It localizes to the microsomal fraction of a number of cell-types, including neutrophils, monocytes, eosinophils and platelets. It is highly selective for 5-hydroxyl lipids, as HETEs with hydroxyl groups at the 8- through 15-position are not significantly metabolized. It requires $NADP^+$ as a co-factor, which regulates activity levels *in vivo*. When neutrophils activate NADPH oxidase, responsible

for superoxide formation during the respiratory burst, it generated $NADP^+$ and leads to full activity of 5-HEDH *in vivo*. Jones *et. al.* have cloned a human 5-oxoETE receptor[65], previously known as the orphan G-coupled protein receptor R527. Activation of this receptor leads to increased intracellular calcium concentrations and inhibition of cAMP production. It is highly expressed in neutrophils, eosinophils and alveolar macrophages, and appears to plays a role in chemotaxis.

1.D.5 Leukotriene B_4

Leukotriene B_4 was identified as 5-lipoxygenase metabolite produced by polymorphonuclear leukocytes (PMN)[66], and identified as a potent autocrine activator of chemotaxis and aggregation[67]. Leukotriene B_4 has been shown to signal through two GCPR receptors, BLT_1 and BLT_2, and lead to increased intracellular calcium levels[68]. BLT_1 has approximately 20-fold higher affinity for LTB_4 compared with BLT_2, and is highly expressed in leukocytes. Studies using BLT_1 knockout mice have primarily attributed a number of LTB_4-dependant signaling responses to this receptor, including neutrophil chemotaxis[69], neutrophil recruitment *in vivo*[70], and LTB_4 induced leukocyte rolling to firm adhesion[69]. BLT_2 has broader substrate specificity[68], with 12-HETE, 12-HpETE, and 15-HETE demonstrating dose-dependant binding properties; furthermore, it displays a more ubiquitous expression pattern in humans, where in addition to leukocytes it has been detected in the spleen, liver, ovary, pancreas, heart, prostate, lung and colon. In 2008, Okuno *et. al.* demonstrated that 12-HHT showed 10-fold higher affinity for BLT_2 compared with LTB_4[71], leading to reconsideration of LTB_4 binding as this receptors primary function.

LTA_4 hydrolase (LTAH) is zinc-dependant metalloprotein that leads to the stereospecific hydrolysis of the LTA_4 to form the dihydroxy LTB_4[72, 73]. Its activity was characterized from plasma samples in a wide range of mammalian species[74] prior to being sequenced from human lung cDNA libraries in 1987[75]. Homology studies revealed that, in addition to other zinc-hydrolases, this enzyme shares sequence similarity with a number of zinc-dependant aminopeptidases[63]. LTAH exhibits aminopeptidase activity and can be blocked by peptidase inhibitors[73], suggesting a potential evolutionary origin. The first high resolution crystal structure of LTAH was published in 2001[76], and used to propose its catalytic mechanism. The active site zinc ion and Glu-271 coordinate with a free H_2O molecule and position it for deprotonation by the LTA_4 epoxide oxygen. This The delocalized carbocation created between carbon 6 and 12 is attacked by a second H_2O molecule, directed to carbon-12 by Asp-375 in a stereospecific manner forming LTB_4.

1.D.6 Cysteinyl leukotrienes (cysLT)

Cysteinyl leukotrienes LTC_4, LTD_4 and LTE_4 make up the slow-acting substance of anaphylaxis and play an important signaling role in inflammation[77]. They can be synthesized by a number of different cell-types, including mast cells, eosinophils, neutrophils, basophils, and macrophages. Two receptors have been implicated in cysteinyl leukotriene signaling, $cysLT_1$ and $cysLT_2$. The expression of $cysLT_1$ appears to be highest in cell-types that produced these metabolites, whereas $cysLT_2$ is more broadly expressed and can be found in the heart, brain and vasculature[78]. These receptors are both GPCRs that culminates in intracellular calcium mobilization, and have similar binding

affinities; cysLT$_1$ has a rank order of LTD$_4$ > LTC$_4$ >> LTE$_4$, whereas cysLT$_2$ binds LTC$_4$ and LTD$_4$ equipotently.

1.D.7 Leukotriene C$_4$

In 1979, it was demonstrated that LTA$_4$ could be conjugated to glutathione to form leukotriene C$_4$, the first identified component of the slow-reacting substance of anaphylaxis[60]. The enzyme mainly responsible for LTC$_4$ production is leukotriene C$_4$ synthase (LTCS). It was cloned by Lam *et. al.*[79] and Welsch *et. al.*[80] in 1994, and identified as a transmembrane protein from the MAPAG superfamily that includes FLAP and mPGES-1. Other MAPEG enzymes, mGST-2 and mGST-3, also exhibit LTC$_4$ synthase activity and appear to play a role in LTC$_4$ biosynthesis in epithelial cells and the testis[81, 82]. However, LTCS knockout mice demonstrate its role as the primary contributor to LTC$_4$ biosynthesis *in vivo*.

It wasn't until 2007 that Ago *et. al.*[83] and Molina *et. al.*[84] simultaneously solved the LTCS structure using x-ray crystallography, suggesting the following mechanism of catalysis. Leukotriene C$_4$ synthase forms a homotrimer, with each monomer containing four transmembrane alpha-helixes. The LTCS complex forms active site at the interface between two adjacent monomers. One monomer binds glutathione in a U-shaped conformation which then positions the thiol for deprotonation by Arg-104 and subsequent nucleophilic attack of C-6, while the Arg-31 of the second monomer donates a proton to form a hydroxyl group at C-5. The omega-end of LTA$_4$ binds a hydrophobic cavity in the interface that is capped by Trp-116, serving as a molecular "ruler" to facilitate LTCS selectivity for 20-carbon polyunsaturated fatty acids.

1.D.8 Leukotriene D_4

Soon after its discovery, it was recognized that the glutathione amino acids of LTC_4 could be cleaved by endogenous peptidases. The first enzyme identified to work on LTC_4 was γ-glutamyl transpeptidase (GGT)[85], which removes glutamic acid to form LTD_4. In addition to LTC_4, it hydrolyses a broad range of glutathione-containing metabolites proceeding through a modified ping-pong mechanism thought to involve Arg-107 and Asp-423 in the human isoform[86, 87]. GGT resides on the extracellular membrane surface, and its activity can be detected in a number of tissues and fluids, including blood plasma[85, 86].

Interestingly, studies using GGT knockout mice and human subjects deficient in GGT both demonstrated residual activity, suggesting GGT was not solely responsible for LTD_4 production. Using a human cDNA library, Heisterkamp *et. al.* identified related GGT gene, originally termed GGT-rel, with 40% amino acid similarity[88]. This enzyme effectively hydrolyzed LTC_4 while having low activity toward other glutathione substrates for GGT, suggesting it could act specifically on cysteinyl leukotrienes. In the GGT-knockout mouse study, the residual peptidase activity toward LTC_4 was purified from intestinal tissue homogenates[87]. This activity was originally termed γ-glutamyl leukotrienase (GGL) due to its selectivity for LTC_4 as a substrate. Subsequent cloning and sequencing confirmed that murine GGL was a homologue to human GGT-rel gene[89]. Both GGT and GGL play appear to play a functional role in LTC_4 metabolism, as demonstrated by metabolism studies using single and double knockout mice[90].

1.D.9 Leukotriene E_4

Glutathione-derived dipeptides metabolites such as LTD_4 can be further metabolized by dipeptidases. The first such enzyme characterized was membrane-bound dipeptidase-1 (MBD-1)[91], which facilitates the hydrolysis of a broad range of cysteinyl-glycine adducts. MBD-1 is a metalloproteinase that uses active site zinc ion to facilitate the hydrolysis of the amide between dipeptides; in leukotriene biochemistry, it catalyzes the metabolism of LTD_4 to LTE_4. Using an MBD knockout mouse, overall LTE_4 levels decreases, but significant levels of LTE_4 were detectable; furthermore, the changes in activity varied between tissues, with some losing greater than 50% of their activity with others remaining unaffected[92], suggesting the presence of additional genes in LTD_4 metabolism . In 2003, two additional MBD genes, MBD-2 and MBD-3, were identified from a BLAST search of the mouse genome by Habib *et. al.*[93]. Expression of MBD-2 determined it was capable of hydrolyzing LTD_4 into LTE_4, whereas MBD-3 did not demonstrate such a capacity.

1.E Other lipoxygenase metabolites

1.E.1 Lipoxygenases (LOX)

Lipoxygenases are non-heme iron metalloproteins that catalyze the stereoselective insertion of molecular oxygen into arachidonic acid[63, 94]. This leads to the formation of hydroperoxyeicosatetraenoic acids (HpETE) that can be reduced to a corresponding hydroxyl, hydroxyeicosatetraenoic acids (HETE), or isomerize to form hepoxilins (HX). While the 3-dimentional structures of most mammalian lipoxygenases have not been solved, the structure of soybean LOX[95, 96] and rabbit 12/15-LOX-l[97] have been reported

and used as the basis for understanding of other lipoxygenases though homology modeling. The LOX reaction mechanism involves an iron catalyzed hydrogen abstraction from arachidonic acid at C-7, C-10, or C-13, forming a conjugated radical reaching two carbons in either direction[98]. The structure of a given LOX enzyme generally conforms tightly around the fatty acid, and small channels within the protein direct molecular oxygen toward selected carbons, facilitating the formation of the following HpETEs and corresponding HETEs: 8-HETE, 12-HETE and 15-HETE (Table 1-3). With the exception of 12R-LOX, mammalian LOXs typically directs the oxygen to attack the pro-S face of arachidonic acid. The positional specificity by which a LOX incorporates oxygen onto arachidonic acid is determined by how deeply it penetrates the cavity, as well as the orientation, either carboxy-terminus or methyl-terminus as it enters the active site. Work by Jisaka *et. al.* suggested that two amino acids positions opposite of the catalytic Fe ion determine the entry orientation. When a histidine and a bulky aromatic amino acid fill this position, arachidonic acid carboxy-terminus enters the active side and 5-LOX and 8-LOX activity. Substitution of these amino acids with a either glutamine or aspartate alongside an aliphatic residue promotes the entry of the methyl-terminus and facilitates 12-LOX and 15-LOX activity.

1.E.2 Hydroxyeicosatetraenoic acids (HETE)

In mammalian systems, lipoxygenases activities have been implicated in the biosynthesis of 5-HETE (section 4A), 8-HETE, 12-HETE, and 15-HETE[63, 98]. The HETEs have been implicated as potential PPAR ligands, with 8-HETE and 12-HETE binding PPARα[99], 15-HETE binding PPARγ[100], and 8-HETE binding PPARδ[101]. They

exert numerous biological effects including, but are not limited to, MAP kinase signaling[102], monocyte chemoattractant protein-1 (MCP-1) expression[103], angiogenesis[104], cancer growth and metastasis[105, 106], and neuronal apoptosis[107]; however, the precise molecular mechanisms behind these effects remain unclear. Interestingly, 12- and 15-HpETE, but not the corresponding HETEs, have been shown to directly activate the capsaicin-sensitive vanilloid receptor (VR1)[108], which is involved in inflammatory pain signaling.

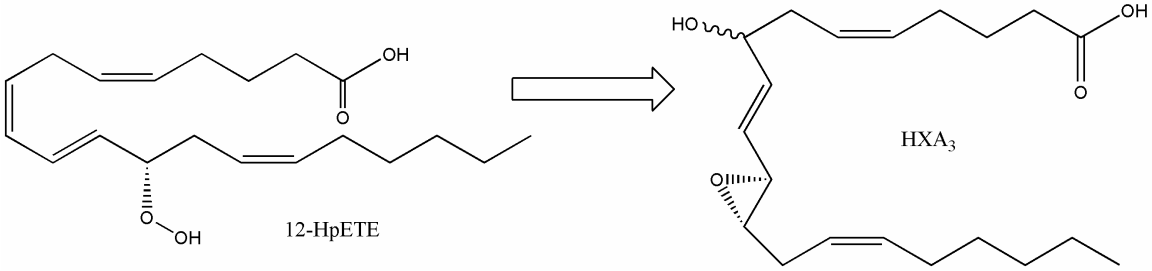

Figure 1-4. Structures of 12-lipoxygenase metabolites. 12-lipoxygenase creates 12-HpETE, which can further isomerize to form HXA_3.

1.E.3 Hepoxilins (HX)

Hepoxilins are biologically relevant signaling molecules produced by certain 12-LOXs[109]. Two hepoxilins have been identified, HXA_3 and HXB_3, both of which incorporate an epoxide across the C-11 and C-12 double bond, as well as an additional hydroxyl moiety[110]; HXA_3 has a C-8 hydroxyl, whereas the HXB_3 hydroxyl occurs at C-10. The epoxy moiety is labile and can be hydrolyzed either by a hepoxilin specific epoxide hydrolase[111] or in acidic aqueous solution to form the corresponding diol metabolites trioxilin A_3 and B_3[110]. Most of the known bioactive effects can be attributed to HXA_3, which include intracellular calcium release[112], neutrophil migration[113], insulin

secretion[114], ichthyosis[115], and modulation of neuronal signaling[116]. Current evidence suggests the existence of a HXA_3 receptor[117], but to date one has not been identified.

1.E.4 Lipoxins (LX)

Early studies of arachidonic acid metabolism demonstrated that multiple lipoxygenases can act on the same substrate to generate a new class of lipid mediators termed lipoxins (LX)[118]. Lipoxins A_4 and B_4, structurally characterized from human neutrophils incubated with 15-HpETE, each contain three hydroxyl moieties and a conjugated tetraene. The third hydroxyl of LXA_4 is positioned at C-6, and of LXB_4 at C-14.

The action of 5-LOX, in concert with a 12-LOX or 15-LOX activity, has been shown to produce lipoxins by three distinct pathways[119], which often occur between heterogeneous transcellular interactions *in vivo*. Neutrophil 5-LOX can produce and secrete LTA_4 that is taken up by platelets, where it is acted upon by 12-LOX-p to form lipoxins[120]. Likewise, 15-LOXs can generate either 15-HpETE or 15-HETE that can be taken up by monocytes and neutrophils, where highly expressed 5-LOX utilizes it to generate lipoxins[118]. Finally, aspirin acetylated COX-2, rendered unable to synthesize prostaglandins, can act as a 15-LOX. This leads to the formation of 15R-HETE and culminates in creation of epi-lipoxins[121], which have altered stereochemistry at the C-15 hydroxyl but similar biological potency.

Lipoxins are the first lipid mediators discovered that demonstrated anti-inflammatory activity as well as the capacity to promote the resolution of inflammation and return to tissue homeostasis[6, 119, 122]. Their biological activity has been shown be

mediated through the lipoxin A_4 receptor (ALX), $cysLT_1$, and the aryl hydrocarbon receptor (AhR), a nuclear transcription factor[122]. The ALX receptor is a GPCR that upon binding ligand can lead to intracellular calcium increases, PLD activation, decreased NF-κB activity. Additionally, ALX cross-talks with vascular endothelial growth factor receptor (VEGFr), connective tissue growth factor receptor (CRGFr), and platelet-derived growth factor receptor (PDGFr) to downregulate their activity. This receptor can also bind a number of small peptides; some dock the LXA_4 binding site, while other others appear to function at a different site and lead to distinct downstream signaling events. LXA_4 binds to recombinant $cysLT_1$ with approximately equal affinity as LTD_4[123], and has been suggested to function as a competitive inhibitor. Lipoxin binding to the AhR transcription factor leads to the expression of suppressor of cytokine signaling-2 (SOCS-2) in dendritic cells[124, 125]. On a pathological level, the lipoxin signaling promotes inhibition of neutrophil migration, the recruitment of non-phlogistic macrophages and increased phagocytosis among the countless documented effects[6, 119]. The complex nature of lipoxin receptor signaling has been reviewed by Chiang et. al. in greater detail[122].

1.E.5 Eoxins (EX)

Analogous to 5-LOX biosynthesis of LTA_4, 12/15-LOX-l can form an epoxide across C-14 and C-15 to form 14,15-LTA_4[126]. Feltenmark *et. al.* demonstrated that eosinophils and mast cells can use 14,15-LTA_4 generate structural analogs of the cysteinyl leukotrienes, which they termed eoxins (EX)[127]. The enzymatic mechanism of eoxin biosynthesis has not been definitively elucidated, but likely occurs by a similar pathway as the cysteinyl leukotrienes. Eoxins had weaker contractile activity on guinea

pig pulmonary parenchyma or ileum[128, 129]; however, in a cell culture model of epithelial barrier function EXC_4, EXD_4, and EXE_4 demonstrably effected epithelial permeability at a lower dose than histamine[127].

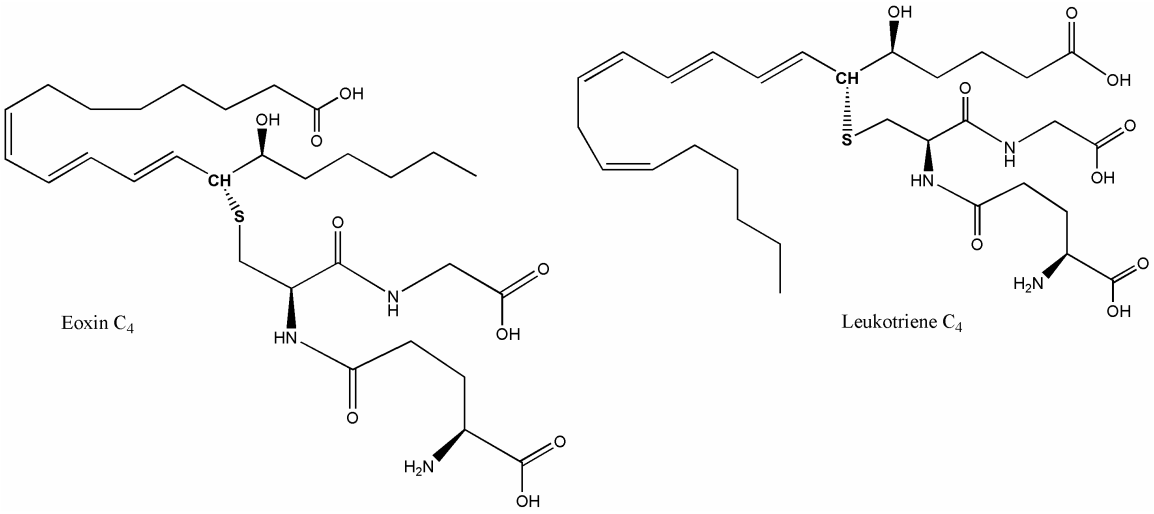

Figure 1-5. Structure of eoxin C_4. Eoxins are the 15-LOX analogues of the cysteinyl leukotrienes, where the thiol attachment occurs at C-15.

1.E.6 Phylogenetic classification of LOX enzymes

Historically, lipoxygenases have been classified according to their activity[94]. This system works well for the 5-LOX, where the human isoform catalyzes 5-HETE formation in a similar manner to the mouse and rat homologs. However, it becomes more confusing when applied to other lipoxygenases, whose the positional specificity are not as clearly defined or tightly conserved between mammalian homologs. For example, the leukocyte 12/15-LOX (12/15-LOX-l) from mouse produces significant amounts of both 12-HETE and 15-HETE[130]. The human isoform of 15-LOX-2 produces 15-HETE, whereas the mouse homolog forms 8-HETE[131]. For these reasons, an alternative classification scheme based on phylogeny has been proposed[94], describing the following 8-LOXs, 12-LOXs and 15-LOXs: platelet-type 12-LOX (12-LOX-p), epidermis-type 12-LOXs (12-LOX-e

and 12R-LOX), leukocyte-type 12/15-LOX (12/15-LOX-l) and 8/15-lipoxygenase (8/15-LOX-2).

1.E.7 Platelet-type 12-LOX (12-LOX-p)

In 1974, Hamburg and Samuelsson described the activity of a lipoxygenases in platelets that converted arachidonic acid into 12-HETE[132]. This enzyme was concurrently cloned by Funk *et. al.*[133] and Isumi *et. al.*[134] in 1990, and due to its high level of expression in these cells has been termed platelet-type 12-lipoxygenase (12-LOX-p). However, it's also abundant in epithelial tissue, and has been demonstrated to provide human skin melanomas with survival signals and promote tumor metastasis[135-137]. Examination of the human 12-LOX-p by *in vivo* and *in vitro* analysis confirmed the native genes positional specificity for producing 12-HETE[133, 138]. In contrast to mutations designed to knock-in 12-LOX activity to the rabbit 12/15-LOX-l that primarily acts as a 15-LOX[139, 140], the reverse mutagenesis experiments failed to convert 12-LOX-p into an effective 15-LOX[138]. Thus, as a lipoxygenase 12-LOX-p functions exclusively as a 12-LOX on arachidonic acid. However, other studies indicate that 12-LOX-p can function as a hepoxilin synthase on 12-HpETE[141], as well as a lipoxin synthase on LTA_4[142].

1.E.8 Epidermal-type 12-LOXs (12-LOX-e, 12R-LOX and e-LOX-3)

The epidermal type 12-lipoxygenase (12-LOX-e) was separately cloned from mice by Funk *et. al.* in 1996[143] and Kinzig *et. al.* in 1997[144]. The gene was the same size as the platelet-type and leukocyte type 12-LOX, and had 60% identity to these enzymes. Expression of the murine 12-LOX-e gene in HEK293 cells confirmed its lipoxygenase

activity, specifically producing 12(S)-HETE[143]. By analogy, 12-LOX-e likely functions by a similar catalytic mechanism as other 12-LOX. Using *in situ* hybridization, 12-LOX-e expression was demonstrated in keratinocytes and targeted areas of the hair follicle. The human isoform of 12-LOX-e was identified as a non-functional pseudogene[145], while in rat its activity has not been investigated.

As early as 1975, scaly lesions caused by psoriasis, an inflammatory disorder that affects the skin and joints, were known to contain increased levels of stereochemically pure 12-HETE[146]. Distinct from other lipoxygenases metabolites, the hydroxyl moiety of 12-HETE found in these lesions was in the R-configuration[147]. In 1998, Boeglin *et. al.* discovered the source of the 12R-HETE originated from 12R-lipoxygenase (12R-LOX)[148], the first known mammalian R-lipoxygenase. Expression of 12R-LOX demonstrated that it produced 12R-HETE to the exclusion of significant amounts of 12S-HETE, as well as 5-HETE, 8-HETE, 9-HETE, 11-HETE and 15-HETE. Using mutants of two R-lipoxygenases (human 12R-LOX and coral 8R-LOX) and two S-lipoxygenases (human and mouse 8/15-LOX-2 isoforms), Coffa *et. al.* identified a conserved amino acid, corresponding with 12R-LOX Gly-441, that confers a substantial amount of stereochemical control two these enzymes[149]. Mutating alanine to a glycine in S-LOXs reversed the chirality of lipid metabolites. However, while mutating the glycine of coral 8R-LOX fully converted it to a 12S-LOX, the 12R-LOX mutant had mixed activity. Meruvu *et. al.* identified Val631 as another important residue in facilitating the positional and stereochemical specificity of this enzyme[150].

Another epidermal-type LOX, e-LOX-3, was cloned from both mouse[151] and human[152]. While it contained the putative lipoxygenases structural features and had

greater than 50% homology with 12R-LOX, gene expression in a number of cell-lines indicated it had no activity toward arachidonic acid[151]. However, mutations in both 12R-LOX and e-LOX-3 were identified in patients afflicted with psorasis[153], and in 2003 Yu *et. al.* identified e-LOX-3 as a hepoxilin synthase that specifically utilized 12R-HpETE as a substrate[154]. This suggests that impairment of hepoxilin production by a 12R-LOX / e-LOX-3 pathway leads to psoriasis in patients.

1.E.9 Leukocyte-type 12/15-LOX (12/15-LOX-l)

The human 12/15-LOX-l was originally cloned as a 15-LOX from a cDNA library in 1988[155], followed by rabbit[156], rat[157], and mouse[158]. The first structural elucidation of a mammalian lipoxygenase was reported using x-ray crystallography on the rabbit 12/15-LOX-l homologue[97]. The substrate binding pocket is lined by hydrophobic residues, and four residues comprise its base: Phe353, Ile418, Met419, and Ile593[140]. These residues are conserved in the human isoform, and considered critical for promoting 15-LOX activity. By comparison, the mouse and rat 12/15-LOX-l have amino acid substitutions at each of these positions that could explain their predilection toward 12-LOX activity. The rat 12/15-LOX-l also has intrinsic hepoxilin synthase activity[141], whereas human homologue does not. Based on the evidence that human 12-LOX-p can synthesize hepoxilins, Nigam *et. al.* surmised that lipoxygenase positional specificity, and not genetic homology, confer an enzyme with hepoxilin synthase activity[109]. This would implicate the mouse 12/15-LOX-l as a hepoxilin synthase, but to date it has not been experimentally examined. The human 12/15-LOX-l exhibits eoxygenase activity that

generates 14,15-LTs[127]; the rabbit[159], pig[126] and sheep[160] homologues also demonstrate this activity, suggesting that mouse and rat enzymes retain this capacity.

From even preliminary investigations[161], 12/15-LOX-l has demonstrated positional promiscuity when oxidizing arachidonic acid, forming 15-HETE, 12-HETE and 8,15-diHETE. The production of 12-HETE by 12/15-LOX-l has been shown to increase expression of monocyte chemoattractant protein-1 (MCP-1), which increases vascular adhesion and the recruitment of macrophages[161]. In addition to action on free arachidonic acid, 12/15-LOX-l can function at the membrane surface and on low-density lipoprotein (LDL) to oxidize phospholipid and cholesterol ester fatty acids, leading to the development of atherosclerosis[162]. In 2008, Harkewicz *et. al.* identified 12/15-LOX-l cholesterol ester peroxides as the active components of minimally oxidized LDL[163]. In contrast to producing pro-inflammatory molecules, 12/15-LOX-l can take LTA_4 as a substrate and produce the anti-inflammatory lipoxins[6, 122]. Using both knockout and overexpression transgenic mouse models, Merched *et. al.* propose that 12/15-LOX-l helps suppress atherosclerosis[164]. Undoubtedly, the capacity of 12/15-LOX-l to make pro-inflammatory as well anti-inflammatory metabolites complicates the study of this enzyme at the whole-animal level, and future research will help elucidate its role in signaling.

1.E.10 8/15-lipoxygenase-2 (8/15-LOX-2)

In 1997, Brash *et. al.* reported the discovery of a second 15-LOX gene in humans[165]. The subsequent identification of the murine homologue[166], however, appeared to have primarily 8-LOX activity. Mutational analyses of these enzymes determined that substitution of Tyr603 and His604 opposite of the catalytic iron are mutated to aspartate

and valine, the corresponding residues in the human isoform, the enzyme has 15-LOX activity[167]. Likewise, mutation of the human enzyme to the murine resides confers 8-LOX activity. Though these enzymes appear to have divergent metabolic output, overexpression of either isoform leads to similar biological consequences in murine keratinocytes[131]. In this model, 8/15-LOX-2 expression, as well as exogenous addition of 15-HETE and 8-HETE, blocked premalignant cell growth in a manner attributed to inhibition of DNA synthesis. Interestingly, both human and murine 8/15-LOX-2 have been shown to produce 8,15-diHETE *in vitro*[168], a more potent agonist of PPARα than 8-HETE. In these studies, the murine enzyme was capable of both reactions and sequentially oxygenates the C-8 and C-15 position. The human homolog could only perform the oxygenation of C-15 but was able to utilize 8-HETE as a substrate. Future investigations may yet elucidate other novel metabolites produced by 8/15-LOX-2 that have other significant bioactivities.

1.F Cytochrome P450 metabolites

1.F.1 Cytochrome P450 (CYP)

Cytochrome P450 (CYP) enzymes comprise a diverse superfamily of enzymes present in bacteria, fungi, prostists, plants and animals[169, 170]. The name was coined in 1962 to describe the first characterized cytochrome P450 based on the unusual absorbance peak of 450 nm by its carbon monoxide-bound form[171]. CYP facilitate the addition of oxygen on a wide range of substrates. To date, 7232 genes in 781 families of have been categorized, and the list constantly growing as more complete genome sequences become available; the generally accepted nomenclature system and current list

of known CYPs is curated by Dr. David R. Nelson (http://drnelson.utmem.edu/CytochromeP450.html). They play an important role in the metabolism of toxins in the liver, as well as signaling throughout the body. In eicosanoid biosynthesis, CYP activities are classified by hydrolase and epoxygenase activities.

Similar to LOXs, CYPs catalyze the hydroxylation and epoxygenation of arachidonic acid. However, whereas LOX utilizes an active non-heme iron to abstract hydrogen directly from arachidonic acid, CYPs contain a heme-iron active site that oxidizes its substrate by a different mechanism[172, 173]. Using NADPH as a co-factor, CYP performs a stepwise reduction of the catalytic iron and molecular oxygen to form a highly reactive oxo-iron species. Depending on the relative position of arachidonic acid, the reactive oxygen can perform an abstraction of an sp^3 hybridized hydrogen, or removal of an electron from an sp^2 hydridized carbon. In both cases, the transfer of oxygen to the unstable arachidonic acid intermediate terminates the reaction by forming HETE or epoxy-eicosatrienoic acid, respectively.

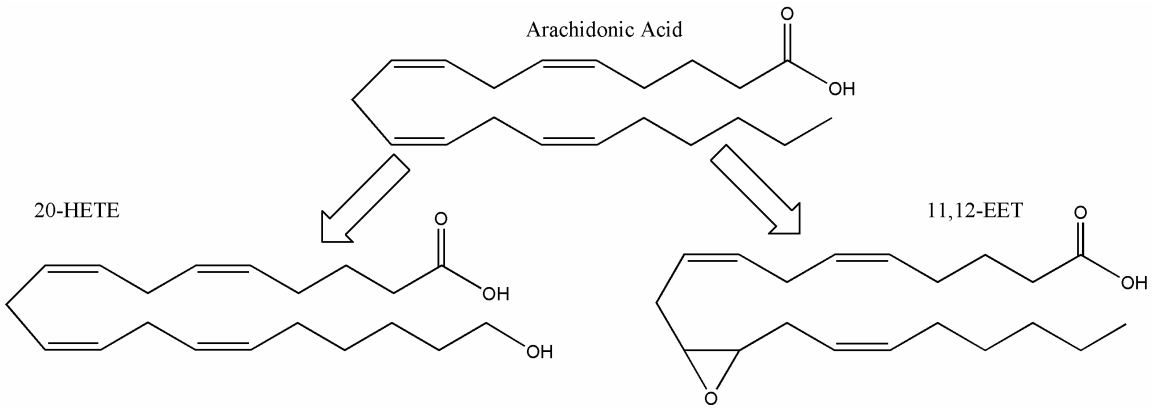

Figure 1-6. Structures of cytochrome P450 metabolites. Cytochrome P450 enzymes can catalyze ω-oxidation (example: 20-HETE) and epoxidation (11,12-EET) reactions.

Each species has its own unique set of CYPs[174]. In 2004, Nelson *et. al.* performed an extensive analysis of the human and mouse genomes, identifying 57 human and 102 mouse functional CYPs[175]. They identified the same CYP families in human and mouse; however, 4 sub-families have been evolutionary discarded in humans, and a significant level of gene cluster size and organization has occurred. These gene expansions and mutations have significant impact on function, with subtle changes in the size and shape of the binding pocket capable of imparting dramatic changes in substrate selectivity and alignment, as well as product formation. In many cases, a single amino acid mutation can drastically alter the function of a CYP. For example, an S473V substitution on CYP2C2 allows a lauric acid hydoxylase to accept the steroid progesterone as a substrate[176]. Thus, CYP homology modeling in the absence of experimental data may inaccurately represent *in vivo* function.

1.F.2 ω-hydrolase HETEs

In addition to hydroxylating arachidonic acid between C-5 and C15 to produce LOX-like HETEs, the CYP enzyme can add a hydroxyl moiety to the sp^3-hybridized ω-carbons to form a unique class of HETEs[170]. Historically, ω-hydrolase activity has been attributed to CYP4A and 4F in mammalian systems, though CYP from other families have demonstrable activity as well (Table 1-4). Of the ω-HETEs, the most well-characterized is 20-HETE, hypothesized to play an important role in hypertension[177]. 20-HETE has been shown promote systemic vasoconstriction by inhibiting K_{Ca} channel activity[178, 179], and in the kidney it blocks sodium reabsorbtion by inhibiting Na^+-K^+-ATPase activity[180]. Other ω-HETEs demonstrate considerable bioactivity that often act in

Table 1-4. Cytochrome P450 ω-hydrolases identified in human, mouse and rat.

Pathway	Species	Gene	AA	Sequence	Activity	REF
CYP (ω-hydrolase)	human	CYP1A1	512	NP_000490.1	HETEs	181, 182
	human	CYP1A2	516	NP_000752.2	HETEs	181, 183
	human	CYP1B1	543	NP_000095.1	HETEs	181
	human	CYP2C8	490	NP_000761.3	8-OH (AA)	184
	human	CYP2C9	490	NP_000762.2	HETEs	183, 184
	human	CYP2C19	490	NP_000760.1	19-OH (AA)	184
	human	CYP2E1	493	NP_000764.1	19-OH (AA), 20-OH (AA)	185
	human	CYP3A4	503	NP_059488.2	7-OH (AA), 10-OH (AA), 13-OH (AA)	183, 184
	human	CYP2U1	544	NP_898898.1	19-OH (AA), 20-OH (AA)	186
	human	CYP2W1	490	NP_060251.2	(20?)-OH (AA)	187
	human	CYP4A11	519	NP_000769.2	20-OH (AA), 19-OH (AA)	188, 189
	human	CYP4F2	520	NP_001073.3	20-OH (AA, EET, LTB_4, HETEs, LXA_4, LXB_4)	188, 189
	human	CYP4F3A	520	NP_000887.2	20-OH (LTB_4)	188, 189
	human	CYP4F3B	520	†	20-OH (AA, EET, HETEs, LXA_4, LXB_4)	188, 189
	human	CYP4F8	520	NP_009184.1	19-OH (AA), isomerizes PGH_2 into PGE_2	188, 189
	human	CYP4F11	524	NP_067010.2	20-OH (AA, LTB_4, 8-HETE, LXA_4)	188, 189
	human	CYP4F12	524	NP_076433.2	17-OH (AA, PGH_2), 18-OH (PGH_2)	188, 189
	mouse	Cyp1b1	543	NP_034124.1	(8?, 12?)-OH (AA), 15-OH (AA)	181
	mouse	Cyp2b19	492	NP_031840.1	11-OH (AA)	190
	mouse	Cyp2c37	490	NP_034131.2	HETEs	191, 192
	mouse	Cyp2c38	490	NP_034132.2	12-OH (AA), 18-OH (AA), 19-OH (AA)	191, 192
	mouse	Cyp2c39	490	NP_034133.1	11-OH (AA), 12-OH (AA), 15-OH (AA)	191, 192
	mouse	Cyp2c40	491	NP_034134.1	16-OH (AA)	191, 192
	mouse	Cyp2c44	494	NP_001001446.2	HETEs	193
	mouse	Cyp2c50	490	NP_598905.1	HETEs	194
	mouse	Cyp2c54	490	NP_996260.1	5-OH (AA), 12-OH (AA), 20-OH (AA)	194
	mouse	Cyp2c55	490	NP_082365.1	19-OH (AA)	194
	mouse	Cyp2j9	502	NP_083255.1	19-OH (AA)	195
	mouse	Cyp4a10	509	NP_034141.2	19-OH (AA), 20-OH (AA)	196
	mouse	Cyp4a12a	508	NP_803125.2	19-OH (AA), 20-OH (AA)	196, 197
	mouse	Cyp4a12b	508	NP_758510.2	18-OH (AA), 19-OH (AA), 20-OH (AA)	196, 197
	mouse	Cyp4f14	524	NP_071879.1	20-OH (LTB_4, HETEs, LXA_4, LXB_4)	188, 197
	mouse	Cyp4f18	524	NP_077764.1	18-OH (LTB_4), 19-OH (LTB_4)	188, 197
	rat	Cyp1a1	524	NP_036672.2	17-OH (AA), 18-OH (AA), 19-OH (AA)	182
	rat	Cyp1a2	513	NP_036673.3	17-OH (AA), 18-OH (AA), 19-OH (AA)	182
	rat	Cyp2e1	493	NP_113731.1	18-OH (AA), 19-OH (AA)	182
	rat	Cyp2j3	502	NP_786942.1	19-OH (AA)	198
	rat	Cyp2j4	501	NP_075414.2	(19?)-OH (AA)	199
	rat	Cyp4a1	509	NP_787031.1	20-OH (AA)	182, 200
	rat	Cyp4a2	504	NP_001038235.1	19-OH (AA), 20-OH (AA)	182, 201
	rat	Cyp4a3	507	NP_786936.1	19-OH (AA), 20-OH (AA)	200, 202
	rat	Cyp4a8	508	NP_113793.2	20-OH (AA, PGA_1)	203
	rat	Cyp4f1	524	NP_062569.2	20-OH (AA, LTB_4, LXA_4, PGs)	188, 204
	rat	Cyp4f4	522	NP_775146.1	20-OH (AA, LTB_4)	188, 197
	rat	Cyp4f5	526	NP_775147.1	18-OH (LTB_4)	188, 197
	rat	Cyp4f6	537	NP_695230.1	18-OH (LTB_4), 19-OH (LTB_4)	188, 197

† Incorrectly annotated on Pubmed, according to accepted CYP nomenclature.

opposition to 20-HETE. For example, 18-HETE and 19-HETE dose-dependently induce vasodilatation by inhibiting the effects of 20-HETE[205]. They also, in addition to 16-HETE and 17-HETE, have been shown induce sodium reuptake in the kidney[205]. More recently, 16-HETE has demonstrated the unique capacity among ω-HETEs to inhibit neutrophil adhesion, suggesting an important role in inflammation[206]. Though it has been suggested that ω-HETEs signal through a putative receptor, the neither the receptor nor its active second-messenger component has be identified[170].

1.F.3 Epoxyeicosatrienoic acids (EET)

The epoxidation of arachidonic acid by CYPs results in the formation of unique bioactive lipid mediators termed epoxyeicosatrienoic acids (EETS). Each double bond has been shown to be susceptible to oxidation, resulting in 5,6-EET, 8,9-EET, 11,12-EET and 14,15-EET. In mammals, the most well documented CYP epoxygenases include the 2C and 2J families, although currently numerous others have been implicated in EET biosynthesis (Table 1-5). The CYP epoxidases display significant promiscuity, with most enzymes making more than one EET, as well as retaining a significant level of ω-hydrolase activity.

EETs have been implicated in a number of important biological processes, including vascular tone, renal function, leukocyte adhesion, neuronal signaling and angiogenesis. However, the effect of specific EET isomers often remains uncertain. In 1999, Node *et. al.* determined that 11,12-EET specifically block the expression of vascular cell adhesion molecule-1 (VCAM-1) by inhibiting NF-κB, an important

Table 1-5. Cytochrome P450 epoxidases identified in human, mouse and rat.

Pathway	Species	Gene	AA	Sequence	Known epoxygenase activity	REF
CYP (epoxygenase)	human	CYP1A2	516	NP_000752.2	5,6-EET, 8,9-EET, 11,12-EET, 14,15-EET	181
	human	CYP2C8	490	NP_000761.3	11,12-EET, 14,15-EET	191, 207, 208
	human	CYP2C9	490	NP_000762.2	11,12-EET, 14,15-EET	191, 208
	human	CYP2C19	490	NP_000760.1	8,9-EET, 11,12-EET, 14,15-EET	184
	human	CYP2J2	502	NP_000766.2	5,6-EET, 8,9-EET, 11,12-EET, 14,15-EET	209
	mouse	Cyp1b1	543	NP_034124.1	5,6-EET, 14,15-EET	181
	mouse	Cyp2b19	492	NP_031840.1	11,12-EET, 14,15-EET	190
	mouse	Cyp2c29	490	NP_031841.3	14,15-EET	191, 192
	mouse	Cyp2c37	490	NP_034131.2	11,12-EET, 14,15-EET	191, 192
	mouse	Cyp2c38	490	NP_034132.2	8,9-EET, 11,12-EET, 14,15-EET	191, 192
	mouse	Cyp2c39	490	NP_034133.1	8,9-EET, 11,12-EET, 14,15-EET	191, 192
	mouse	Cyp2c40	491	NP_034134.1	8,9-EET, 11,12-EET, 14,15-EET	191, 192
	mouse	Cyp2c44	494	NP_001001446.2	8,9-EET, 11,12-EET, 14,15-EET	193
	mouse	Cyp2c50	490	NP_598905.1	5,6-EET, 8,9-EET, 11,12-EET, 14,15-EET	194
	mouse	Cyp2c54	490	NP_996260.1	5,6-EET, 8,9-EET, 11,12-EET, 14,15-EET	194
	mouse	Cyp2c55	490	NP_082365.1	8,9-EET, 11,12-EET, 14,15-EET	194
	mouse	Cyp2j5	501	NP_034137.1	8,9-EET, 11,12-EET, 14,15-EET	210
	mouse	Cyp4a14	507	NP_031848.1	11,12-EET	196
	rat	Cyp1a1	524	NP_036672.2	8,9-EET, 11,12-EET, 14,15-EET	207, 211
	rat	Cyp1a2	513	NP_036673.3	8,9-EET, 11,12-EET, 14,15-EET	207, 211
	rat	Cyp2b1	491	†	8,9-EET, 11,12-EET, 14,15-EET	182, 207
	rat	Cyp2b2	499	†	8,9-EET, 11,12-EET, 14,15-EET	182, 207
	rat	Cyp2b12	492	NP_058852.1	8,9-EET, 11,12-EET	190, 207
	rat	Cyp2c11	500	NP_062057.2	8,9-EET, 11,12-EET, 14,15-EET	182, 212
	rat	Cyp2c23	494	NP_114027.2	8,9-EET, 11,12-EET	182, 207
	rat	Cyp2c24	490	†	8,9-EET, 11,12-EET, 14,15-EET	182
	rat	Cyp2d4v2‡	500	NP_612524.1	11,12-EET, 14,15-EET	213
	rat	Cyp4a2	504	NP_001038235.1	11,12-EET	201, 212
	rat	Cyp4a3	507	NP_786936.1	11,12-EET	212
	rat	Cyp2j3	502	NP_786942.1	8,9-EET, 11,12-EET, 14,15-EET	198, 207
	rat	Cyp2j4	501	NP_075414.2	EETs	199

† Incorrectly annotated on Pubmed, according to accepted CYP nomenclature.
‡ Incorrectly annotated as Cyp2dv1 on Pubmed and Cyp2d18 in citation accepted CYP nomenclature.

mediator of leukocyte recruitment during inflammation[214]. Using a model of vascular laminar flow, Lui *et. al.* suggest NF-κB inhibition can be achieved by any of the four EET stereoisomers[215].

Current evidence suggests that EET signaling occurs through a putative GPCR, though to date it has not been identified. Membranes from human U937 monocyte cell-line were discovered by Wong *et. al.* to contain a high affinity binding site for 11,12-EET and 14,15-EET[216], which has recently been characterized as a GPCR that induces PKA activation and increases in cAMP[217]. The EET-induced GPCR activity leads to the opening of BK_{Ca} channels through the $G_s\alpha$ g-protein[218, 219]. Falck *et. al.* synthesized library of 11,12-EET analogues and, using VCAM-1 expression in human endothelial cells, identified a number of structural elements required for functional recognition by the putative GPCR binding site[220]. An corresponding study measuring BK_{Ca} activity induced by a series of 14,15-EET analogues identified similar structural elements[221], suggesting these two EETs may bind the same receptor *in vivo*.

In addition to GPCR signaling, EETs have been identified as bioactive ligands for cation channels and PPARs. Watanabe *et. al.* identified 5,6-EET, and to a lesser degree 8,9-EET, as an endogenous ligand for the vanilloid type 4 receptor (TRPV4)[222]. When activated, TRPV4 acts as a cation channel to allow the influx of extracellular calcium, and its activity has been implicated in rodent models of inflammatory hyperalgesia[223-225]. Downstream activation of BK_{Ca} channels also result from TRPV4[226]. While these studies implicate EETs in the induction of hyperalgesia, Inceoglu *et. al.* demonstrate that inhibiting soluble epoxide hydrolase, which raises endogenous levels of EETs, blocks inflammatory hyperalgesia in the rat model[227]. Receptor binding assays identified μM

EET affinity for cannabanoid CB_2, neurokinin NK_1 and dopamine D_3 receptors. In rat cardiomyocytes, EETs activate K_{ATP} channels by reducing their sensitivity to endogenous ATP inhibition[228]. Studies have also implicated EETs in the direct activation of transcription factors PPARα and PPARγ[215, 229]. However, the selectivity of these receptors for specific EET regioisomers as well as the downstream biological consequences have remain unclear, and undoubtedly further work will characterize the role that EETs play in biological signaling.[230, 231]

1.F.4 Soluble epoxide hydrolase (sEH) and dihydroxyeicosatrienoic acids (DHET)

The majority of the EETs biological effects are diminished by their hydrolysis to the corresponding dihydroxyeicosatrienoic acids (DHET). In mammals, this process is primarily catalyzed by the enzyme soluble epoxide hydrolase (sEH). The murine and human isoforms have been cloned and structurally characterized by x-ray crystallography[232-234], allowing for a detailed mechanistic description of its catalytic function using the human sequence[235]. The sEH active site forms a deep, L-shaped hydrophobic pocket with a catalytic Asp at the L-turn accessible to both openings. Upon entering the active site, the EET epoxide moiety interacts with Tyr382 and Tyr465. His523 positions and activates Asp334 for nucleophilic attack on an epoxide carbon, opening the ring and facilitating water hydrolysis to the corresponding diol. Unlike other eicosanoid biosynthetic enzymes, sEH does not require any metal cofactor for catalysis. However, its activity can be inhibited by the presence of zinc, suggesting a straightforward mechanism for regulating EET metabolism during inflammation[236]. Due to the loss of EET bioactivity, sEH formation of DHETs has been considered the

metabolic inactivation step of EET signaling. However, recent work has demonstrated that DHETs can retain certain EET signaling capacities, effectively activating BK_{Ca} channels in smooth muscle cells[237], as well as PPARα and PPARγ[215, 238].

1.G Non-enzymatic lipid metabolites (Isoprostanes and 9-HETE)

Free radials generated by oxidative stress have long been believed to participate in the development of a number of neurodegenerative and inflammatory diseases by causing damage to DNA, proteins and lipids[239]. In 1990, Morrow *et. al.* described a class of prostaglandin-like compounds formed *in vitro* by free radical catalyzed peroxidation[240]. Abstraction of hydrogen from C-13 forms a five carbon delocalized radial that can form a prostane ring when followed by the addition of molecular oxygen at the activated C-11. Due to the lack of enzymatic control in the reaction, these $PGF_{2\alpha}$-like compounds comprise series of stereoisomers termed 15-series due to the location of the non-prostane hydroxyl moiety. Furthermore, the reaction can also be initiated at C-7, leading to the 5-series, as well as at C-10, leading to both the 8- and 12-series of isoprostanes. In total, 32 possible isoprostane isomers can be generated by radical initiated perodidation[239]. To date, no specific isoprostane receptors have been identified. However, isoprostanes have demonstrated binding affinity for prostaglandin receptors, including the FP and TP receptor[241, 242].

Lipid peroxidation can also proceed forward in a lipoxygenases-like activity. Following the abstraction of hydrogen, the peroxide formed by oxygenation of the radical can simply be reduced to a corresponding HETE. By this pathway, free radical reactions can produce all the HETEs generated by LOX and CYP. Additionally, non-enzymatic

peroxidation can generate 9-HETE, which has no identifiable biological activity and has been used as a marker of non-enzymatic lipoxygenases-like activity[243]. In practice, both 9-HETE and isoprostanes have been shown to serve as useful biomarkers of oxidative stress *in vivo.* In a recent study of major coronary heart disease[239], plasma levels of isoprostanes and 9-HETE highly correlated with the pathogenesis and may serve as an indicator in clinical assessments of heart disease.

1.H Eicosanoid catabolism

Eicosanoid catabolism plays an important role in the control of bioactive lipid signaling. Not all molecules from the same class break down by the same pathway, which helps further differentiate the functional signaling role of each eicosanoid *in vivo*. In particular, the dysfunction of prostaglandin catabolizing enzymes, reviewed in detail by Tai *et. al.*[244], has been implicated in susceptibility to disease. Generally, the catabolism of eicosanoids leads to diminished bioactive signaling and urinary excretion from the body by facilitating changes that increase their water solubility.

1.H.1 11-hydroxythromboxane B_2 reductase (11-TXBH)

Studies investigating thromboxane clearance indicate that a significant portion undergoes dehydrogenation at C-11 to form 11dh-TXB_2. This degradation metabolite is readily detected in both human blood plasma and urine[245, 246]. The enzyme responsible for catalysis *in vivo* has been termed 11-dehydroxythromboxane B_2 dehydrogenase (11-TXDH), and has two distinct isoforms. Using amino acid composition analysis, the liver-type isoform from swine has been classified as a cytosolic aldehyde dehydrogenase

family member[247]. The second enzyme, the kidney-type 11-TXDH, can catalyze the dehydrogenation but not the reverse reductions, distinguishing it from the liver-type. While the identification of the human, mouse, and rat 11-TXDH enzyme has been cloned, 11dh-TXB_2 has been detected in urine samples from these species. Historically, TXB_2 and 11dh-TXB_2 has been considered biologically inert due to its inability to activate the thromboxane TP receptor[248], but work by Böhm *et. al.* demonstrates that 11dh-TXB_2 is an agonist of the CRTH2 receptor[249].

1.H.2 15-prostaglandin dehydrogenase (15-PGDH)

The catabolism of selected prostaglandins, leukotrienes and HETEs is initiated by oxidation by 15-prostaglandin dehydrogenase (15-PGDH). Two distinct enzymes have been identified with this activity, 15-PGDH-I and 15-PGDH-II; however, the high K_m values of 15-PGDH-II for most prostaglandins suggests that the majority of the *in vivo* activity can be attributed to 15-PGDH-I[244]. The 15-PGDH-I is NAD^+ dependant and metabolizes E-series prostaglandins, lipoxins, 15-HETE, 5,15-diHETE, and 8,15-diHETE, while other prostaglandins appear to be less susceptible substrates[250]. In all likelihood, 15-PGDH can metabolize a larger array of eicosanoids than those which have been tested.

The 15-PGDH-I genes have been cloned in human, mouse and rat, but crystal structure of the enzyme has not been determined. In 2006, Cho *et. al.* used the molecular modeling to develop a three-dimensional structure and propose a catalytic mechanism[251]. Following the sequential binding of NAD^+ and PGE_2, the 15-hydroxyl is coordinated

Table 1-6. Enzymes involved in eicosanoid catabolism in human, mouse and rat.

		Human				Mouse					Rat				
Pathway	Name	Activity	aa	Gene	Sequence	Activity	aa	Gene	Sequence	%ID	Activity	aa	Gene	Sequence	%ID
11-TXDH	11-TXDH	11-TXDH	-	-	-	11-TXDH	-	-	-	-	11-TXDH	-	-	-	-
PGDH	15-PGDH-I	PG dehydrogenase	266	HPGD	NP_000851.2	PG dehydrogenase	269	Hpgd	NP_032304.2	89	PG dehydrogenase	266	Hpgd	NP_077366.2	88
	15-PGDH-II	PG dehydrogenase	277	CBR1	NP_001748.1	NT	280	Cbr1	NP_031646.2	87	PG dehydrogenase	277	Cbr1	NP_062043.1	86
13-PGR	13-PGR-1	PG reductase; LTB_4 12-dehydrogenase	329	PTGR1	NP_036344.1	NT	329	Ptgr1	NP_080244.1	81	NT	329	Ltb4dh	NP_620218.1	82
	13-PGR-2	NT	351	PTGR2	NP_689657.1	PG reductase	351	Ptgr2	NP_084156.2	87	NT	281	Zadh1	NP_001015009.1	68
HEDH	5-HEDH	5-hydroxy dehydrogenase	-	-	-	5-hydroxy dehydrogenase	-	-	-	-	NT	-	-	-	-
HEXH	12-HEDH	12-hydroxy dehydrogenase	-	-	-	12-hydroxy dehydrogenase	-	-	-	-	NT	-	-	-	-
	15-HEDH-I	15-hydroxy dehydrogenase	266	HPGD	NP_000851.2	NT	269	Hpgd	NP_032304.2	89	NT	266	Hpgd	NP_077366.2	88
	15-HEDH-II	15-hydroxy dehydrogenase	277	CBR1	NP_001748.1	NT	280	Cbr1	NP_031646.2	87	NT	277	Cbr1	NP_062043.1	86
	HXEH	Hepoxilin epoxide hydrolase	-	-	-	Hepoxilin epoxide hydrolase	-	-	-	-	Hepoxilin epoxide hydrolase	-	-	-	-
sEH	sEH	EET epoxide hydrolase	555	EPHX2	NP_001970.2	EET epoxide hydrolase	554	Ephx2	NP_031966.2	73	EET epoxide hydrolase	554	Ephx2	NP_075225.1	73

with Tyr151, Ser138 and Gln148. Tyr151 deprotonates the 15-hydroxyl, facilitating a hydride transfer from C-15 and the release of 15k-PGE_2. The reduction to a 15-ketone

The 15-PGDH-I genes have been cloned in human, mouse and rat, but crystal structure of the enzyme has not been determined. In 2006, Cho *et. al.* used the molecular modeling to develop a three-dimensional structure and propose a catalytic mechanism[251]. Following the sequential binding of NAD^+ and PGE_2, the 15-hydroxyl is coordinated with Tyr151, Ser138 and Gln148. Tyr151 deprotonates the 15-hydroxyl, facilitating a hydride transfer from C-15 and the release of 15k-PGE_2. The reduction to a 15-ketone reduces the biological activity of most eicosanoid substrates, and loss of function has been implicated in the development of certain cancers[252]. However, in 2007 Chou *et. al.* identified 15k-PGE_2 as a ligand for PPARγ and an active component of murine 3T3-L1 fibroblast differentiation into adipocytes[253].

1.H.3 13-prostaglandin reductase (13-PGR)

The 13-prostaglandin reductases (13-PGR) metabolize eicosanoids by catalyzing d NADH/NADPH-dependant double bond reduction. The human gene was originally cloned from human and pig sources as Leukotriene B_4 12-hydroxydehydrogenase (LTB_4DH)[254], but later discovered to have dual functionality as a prostaglandin reductase (13-PGR-1)[255]. In addition to reducing prostaglandins, 13-PGR has been shown to utilize lipoxins as substrates[256]. The resulting metabolites from 13-PGR activity show reduced biological activity, and PGE_2 metabolites from this pathway are readily detected in urinary excretion[257].

Structural determinations of 13-PGR-1 in complex with $NADP^+$ and 15k-PGE_2 were solved in 2004, and used to propose the following mechanism of catalysis[258]. 13-PGR-1 forms a homodimer, with an active site pocket formed at the dimer interface. The 2'-hydroxyl group of NADPH forms a hydrogen bond with the C-15 oxygen on PGE_2, promoting the stabilization of an enolate intermediate. The NADPH hydride attacks the carbocation at C-13, followed by ketone formation and the release of the reduced metabolite 13,14-dihydro,15-keto-PGE_2 (dhk-PGE_2). LTB_4 oxidation likely proceeds by a similar mechanism as 15-PGDH, with a conserved tyrosine serving as the catalytic residue. In 2007, Chou *et. al.* reported the discovery of a second prostaglandin reductase gene (13-PGR-2) that they demonstrate works by a similar reductive mechanism on 15k-PGE_2, but have not exhaustively studied its substrate selectivity or potential LTB_4DH activity[253].

1.H.4 Further metabolism for urinary excretion

As part of a Phase I Clinical Trial for LTB_4 administration, Zemski Berry *et. al.* performed an exhaustive study of its catabolism[259]. In this study, urine samples from subjects injected with LTB_4 were analyzed, and 11 different LTB_4 metabolites were identified. Based on the qualitative and quantitative analysis of these metabolites, they proposed a pathway for LTB_4 metabolism that, in addition to LTB_4 specific enzymes, proceeds through three main pathways of catabolism: β-oxidation, CYP ω-hydrolases, and glucuronidation.

1.H.4.a β-oxidation

In addition to working on fatty acids, the β-oxidation metabolic pathway can capably act on the carboxyl moiety of prostaglandins, leukotrienes and HETEs, reviewed in detail by Ulf Diczfalusy[260]. The subsequent losses of two (dinor) or four (tetranor) carbons significantly increases the hydrophilicity of these molecules for urinary excretion. With thromboxane as an exception, the majority of PG metabolites detected in urine have undergone β-oxidation. Pharmacokinetic analysis of first generation lipoxin analogues suggests that this class also undergoes β-oxidation[261]. Following LTB_4 injections in human patients, β-oxidation was not identified at the carboxyl terminus, but instead at the ω-terminus following CYP ω-hydroxylation[259].

1.H.4.b CYP ω-hydrolases

The CYP ω-hydrolase catalyzed hydroxylated metabolites have a number of important bioactivities, described in Section 6B. In addition, they facilitate the catabolism of prostaglandins, leukotrienes, and DHETs for urinary excretion[170]. Hydroxylation of eicosanoids both reduces their bioactivity and increases their water solubility. Following LTB_4 administration, LTB_4 metabolites were found to be hydroxylated at C-17 though C-20; however, the majority of these compounds had undergone further catabolism to form glucuronides at these sites[259].

1.H.4.c Glucuronidation

In addition to action by CYPs, lipophilic molecules are catabolized into water-soluble metabolites though the addition of the sugar glucuronide[262]. In mammals, this

reaction is catalyzed by members of the UDP-glucuronosyltransferase (UGT) enzymes. To date, 15 UDP enzymes have been found in humans, and a study by Turgeon *et. al.* in 2003 using a HEK203 expression system found that most of them were capable of metabolizing LTB_4 and LOX-derived HETEs[263]. Glucuronidation also plays significant role in the catabolism of DHETs in humans, but rats excrete the diol form directly[264]. In the human trials of LTB_4 metabolism, nearly all metabolites with a hydroxyl moiety were found to be glucuronidated, suggesting non-specific catalysis of eicosanoids by UDPs plays a significant role in their removal from the body[259].

1.I Discussion

All eicosanoids begin as a single poly-unsaturated fatty acid, arachidonic acid. Yet from this simple origin, hundreds of bioactive signaling molecules can be created, often within minutes of receiving an initiation signal. They can be classified by their synthetic pathway, catalytic mechanism, structural elements, or receptor-mediated signaling events. Perhaps more importantly, we can organize eicosanoids according to their biological function. Nearly every bioactive eicosanoid discovered to date has functional partners that signal opposing effects and helps prevent any one pathway from signaling uncontrollably. Such is the case with the prototype prostacyclin and thromboxane, which work antagonistically to maintain proper vascular homeostasis[265]. While the use of the selective COX-2 inhibitor rofecoxib (Vioxx™) effectively blocks painful inflammation through the reduction of PGE_2, it also blocks vascular prostacyclin production and tips a delicate vascular balance which may explain its association with increased serious cardiovascular events[266].

In light of this, it seems imperative to begin considering the entire spectrum of eicosanoid production for both understanding inflammatory processes, as well as identifying more subtle consequences stemming from the next-generation of non-steroidal anti-inflammatory drugs. To facilitate this type of analysis, a number of high-throughput procedures were developed using liquid chromatography coupled to tandem mass spectrometry that can quantitatively measure over a hundred unique eicosanoid species (Chapter 2). These techniques were applied in a study of the mechanisms of eicosanoid production in the RAW264.7 murine macrophage cell-line (Chapter 3), which was used as cellular tool for developing more selective inhibitors of metalloenzymes involved in inflammation (Chapter 4), as well as in creating a comprehensive model of inflammation induced by *Borrelia burgdorferi*, the causative agent in Lyme disease (Chapter 5).

Chapter 2.

Detection and Quantitation of Eicosanoids Using Liquid Chromatography and Mass Spectrometry

2.A Abstract

Eicosanoids constitute a large class of biologically active arachidonic acid (AA) metabolites, and in order to completely understand the eicosanoid response of a cell or tissue to a given stimulus, measuring the complete metabolic profile is important. Since the eicosanoids products of AA represent, in the most part, the addition of various oxygen species, the hundreds of eicosanoids have very similar structures, chemistries and physical properties. The identification and quantitation of all eicosanoids in a single biological sample is a challenging task, one that liquid chromatography and tandem mass spectrometry are well suited to handle. Using these techniques, we developed procedures for isolating, identifying, and quantitating a broad spectrum of eicosanoids in a single biological sample. We established an eicosanoid library that includes relative chromatographic retention times and tandem mass spectrometry data for the most common eicosanoids, currently available to the scientific community at www.lipidmaps.org. Our methodology employs stable isotope dilution internal standards to quantitate these specific eicosanoids. We created three different LC-MS/MS procedures for quantitating eicosanoids, each having unique advantages and limitations. The development and evolution of these methods are described in this chapter in detail, and applied to specific biological systems in Chapters 3 – 5.

2.B Historical perspective on eicosanoid quantitation

The eicosanoids comprise a broad class of arachidonic acid (AA) metabolites that mediate a wide variety of important physiological functions. As described in detail in Chapter 1, AA can be metabolized into hundreds of different bioactive lipids, signal through a large number of receptors, illicit potent responses in nearly every tissue, and play a important role in many physiological processes and pathological diseases[3-5, 8, 9, 170, 267, 268]. Eicosanoid biosynthesis is a complex network of interacting pathways and interconnected metabolites. It is quite possible that perturbing one arm of this system could produce changes and compensations in the other arms. In order to fully understand how a given cell or tissue responds to a stimulus or how a drug targeted for one eicosanoid might affect the distribution of the other eicosanoids, one must determine the entire eicosanoid spectrum.

Enzyme-linked immunosorbent assays have long been the primary means of quantitating eicosanoids[269, 270]. This method requires specific antibodies for each eicosanoid to be quantitated; however, relatively few eicosanoids have commercially available antibodies. This significantly limits the number of eicosanoids that can be detected and quantitated. This technique is also expensive and inefficient in that only a single eicosanoid can be determined with each assay. Thus, it is not amenable to analyzing a large number of different eicosanoids. Gas Chromatography/Mass Spectrometry (GC/MS) methods were developed that greatly improved upon these limitations[271] and allowed the simultaneous analysis of multiple eicosanoids. To volatilize the eicosanoids for GC chromatography, they must first be chemically derivatized. A wide variety of derivatization methods are available; however, a single

derivatization method is not suitable for all eicosanoids. Furthermore, Murphy and coworkers have found that some eicosanoids are not suited for GC/MS analysis[272]. These volatilization issues were overcome with the development of electrospray ionization (ESI), which allow the eicosanoids to be analyzed by MS directly from an aqueous sample. The eicosanoid carboxylate moiety readily ionizes in the ESI source.

The similarities in eicosanoid structure and chemical characteristics requires that both high performance liquid chromatography (LC) and collision induced decomposition (CID) be employed, in conjunction with ESI-MS, to isolate and unambiguously identify the individual eicosanoid species. LC isolates the eicosanoids based on their chemical and physical characteristics while CID produces characteristic precursor/product transitions that can be employed in multi-reaction monitoring (MRM) mode on the MS. ESI-MRM was first employed in this field by Issakson and co-workers in 1996 to quantitate 14 eicosanoids directly from a biological sample[273]. In 2002, the resolving power of liquid LC was coupled with the sensitivity of ESI-MRM to study 5 eicosanoids from LPS stimulated synovial cells[274]. Recently, Shimizu and co-workers have developed a high-throughput method for the detection of 18 different eicosanoids from biological samples[275]. Here, we present here three protocols for identifying and quantitating a large number of eicosanoids in a single ESI based LC-MS/MS run without requiring derivatization.

2.C. Eicosanoid mass spectrometry

2.C.1 Fragmentation and the Mass Spectrum Library

Mass spectrometry has played a critical role in the identification of eicosanoids since their initial structural characterization by the seminal work of Sune Bergström and Bengt Samuelsson in the 1960s[276]. Using electrospray ionization and tandem mass spectrometry, nearly every molecular species of eicosanoid has been shown to be amenable to analysis by this technique. In general, the process works as follows: Negative-mode electrospray ionization gently removes a proton from the carboxylate moiety, forming the precursor ion [M-H] and allowing it to enter into the mass spectrometer. Quadrupole 1 can be set to act as a filter, and allow only the [M-H] ion pass through. In quadrupole 2, a small voltage excites the [M-H] ion which, upon impact with a small number of nitrogen molecules introduced, causes colllisionally induced decomposition and the generation of a profile of product ions.

Analogous to the different pathways a chemical reaction can proceed though in solution, precursor ions can fragment in the mass spectrometer through a number of different decomposition pathways. These often occur at positions of the molecule that would be considered structurally reactive in solution. In many cases, decompositions proceed though well-established pathways (described in detail by Murphy *et. al.*[272]), through a number product ions occur by undefined reactions. Under a given set of mass spectrometry conditions, the probability of undergoing one decomposition versus another can be readily reproduced. Thus, the relative identity and intensity of the product ion spectra generates a "metabolic fingerprint" which can be used to identify eicosanoids from a biological sample.

Figure 2-1. Product ion spectra for PGE_2. An example of the MS library available at www.lipidmaps.org.

We have compiled the MS/MS spectra of each of the eicosanoids measured in these studies, and a significant portion of this data is published[277] accessible on the LIPID MAPS web page at www.lipidmaps.org (Figure 2-1). In addition to MS/MS spectra, the web-visitor can obtain chemical structures for standards in both GIF and ChemDraw® formats, specific details regarding MS parameters employed in our analysis, and structures of dominant fragment ions (including literature references, when available, for fragment assignments). Lastly, a web-link to Cayman Chemical provides useful information and references on specific eicosanoids.

2.C.2 Multiple-reaction monitoring

The eicosanoid product ion spectra provides a useful tool for identification, but alone cannot quantify the amount of eicosanoid in solution. By selecting a single precursor→product ion pair that is unique to a given eicosanoid, the intensity of product ion can be measured in a quantitative way. The MS/MS spectra of many eicosanoids contain many product ions, allowing a number of different precursor→product ion pair options. The mass spectrometer can measure a number of different precursor→product ion pairs in nearly simultaneous manner using multiple-reaction monitoring. In MRM mode, the mass spectrometer measures the first precursor→product ion pair for a given period of time (typically 25 msec), then switches to the second pair in the list, and so forth. Upon reaching the end of the list, it restarts at the beginning and repeats the process. Ultimately, combining MRM identification with LC separation (described in Section D) allows the simultaneous identification and quantitation of a large number of eicosanoids in a single analysis.

The ionization parameters for each eicosanoid were optimized for maximal signal using direct infusion mass spectrometry. Solutions containing 100 pg / µl of an individual eicosanoids were prepared in either 100% Solvent A, 100% Solvent B, or a 50% A / 50% B mixture, depending on the LC retention time. Using a 1 ml Hamilton syringe and a syringe pump, sample was injected at a constant rate of 0.208 ml / min. Samples were analyzed in the manual tuning mode by MS to identify the precursor mass [M-H], and by MS/MS to generate a product ion spectrum from which a robust and unique product ion was selected. Using MRM mode, the declustering potential (DP), entrance potential (EP), collision energy (CE), and exit cell potential (CXP) for the selected precursor→product

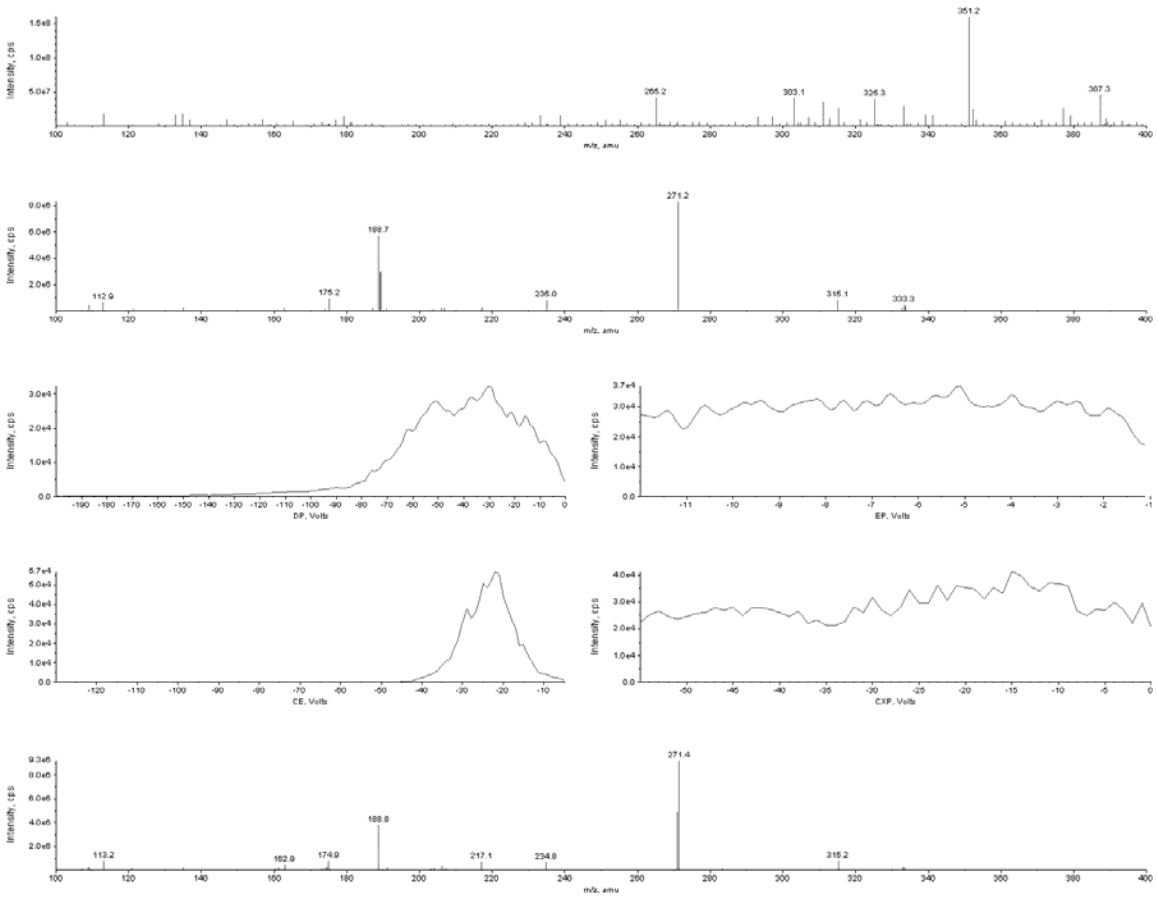

Figure 2-2. Optimization of ionization parameters by direct infusion mass spectrometry. Solution of PGE_2 (100 pg/ul) was analyzed by (A) MS and (B) MS/MS (*m/z* 351). The (C) declustering potential, (D) entrance potential, (E) collision energy, and (F) exit cell potential were optimized to maximize the signal intensity of the selected MRM pair (*m/z* 351→189). Using the optimal parameters, PGE_2 was run in MS/MS (*m/z* 351) to confirm product ion spectra.

ion pair were optimized to maximize signal intensity (Figure 2-2). The product ions employed here for the MRM detection were selected to yield the best discrimination from other eicosanoids that co-elute in the vicinity of the analyte and to yield the highest signal. Balancing LC retention time and product ion selection can successfully distinguish the large majority of the eicosanoids in our library. Different product ions can be selected to obtain greater sensitivity if conflicting eicosanoids are not present in a given set of samples.

2.C.3 Eicosanoid quantitation

Eicosanoid quantitation was performed by the stable isotope dilution method previously described by Hall and Murphy[278]. For each eicosanoid to be quantitated, an internal standard was selected that had a different precursor ion mass than the target analyte but was chemically and structurally as similar to the target analyte as possible. This is ideally achieved by using a deuterated analog of the analyte. We employed these standards whenever they were commercially available. In other cases, we employed a deuterated analog that was the closest to the desired analog in characteristics. For example, (d_4) 15d- PGJ_2 was employed as the internal standard for PGJ_2, 15d PGD_2, and 15d PGJ_2. An aliquot of the internal standard (typically 10 ng std / 100 μl of ethanol in these procedures) was added to biological samples immediately following its isolation. The samples were then processed as detailed above.

The primary standards contained an accurately know amount of each eicosanoid (non-deuterated) to be quantitated and an accurate aliquot of the internal standards. The concentration of the primary standards must be known with high accuracy. This can be accomplished in one of several ways. In some cases, they are commercially available. Cayman Chemicals, for example, offers a "Quanta-PAK" version of many eicosanoids that contains a deuterated internal standard and a vial containing an accurately determined amount of the non-deuterated primary standard. Some of the eicosanoids, e.g. certain HETEs and leukotrienes, have significant UV absorption that can be used to determine the concentration of the standard. The amount of standard can also be determined gravimetrically if a microbalance if available.

A set of primary standards was prepared by adding accurately determined amounts of the given analyte (non-deuterated) to 100 µl of the same internal standard used to spike the samples. A typical standard curve consisted of 0.3, 1, 3, 10, 30 and 100 ng of primary standard per 100 µl of internal standard containing 10 ng of each internal standard. The internal standard and the primary standard samples were run before and after each set of unknown biological samples.

A linear standard curve was generated, where the "eicosanoid ratio" or "MRM ratio", defined here as the ratio of analyte standard intensity to internal standard intensity, was plotted vs. the known amount of primary standard (ng). Figure 2-3 shows examples of three typical standard curves. Linear regression analysis was used to calculate the

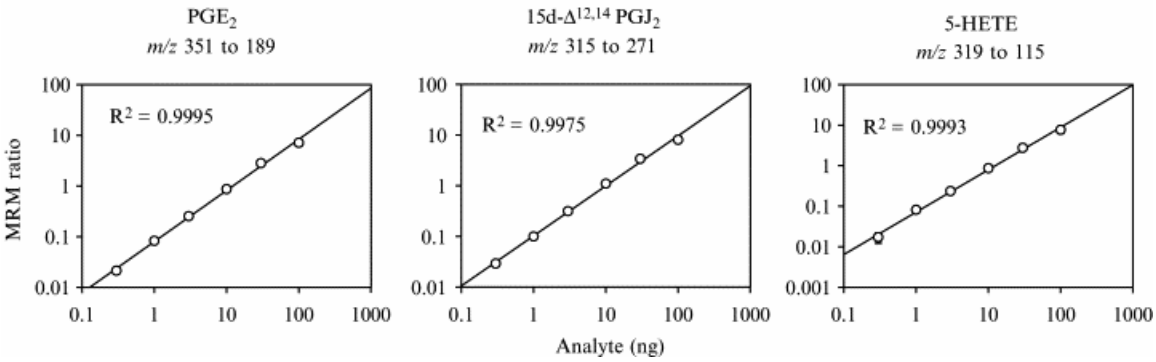

Figure 2-3. Eicosanoid standard curves. Three typical standard curves are shown as described in the text. The solutions contained 10 ng of an internal standard for each analyte and 0.3 to 100 ng of the analyte in 140 µl of which 10 µl were analyzed. The multi-reaction monitoring (MRM) transitions employed to monitor the analytes are listed in the figure. The internal standards and transitions were: (d_4) PGE_2 *m/z* 355→193, (d_4) 15d PGJ_2 *m/z* 319→275, and (d_8) 5-HETE *m/z* 327→116. The data were presented in log scale, but the linear regression analysis to determine parameters was done on the original non-log data.

slope and intercept of the standard curves that were then used to calculate the unknowns. R^2 values for these curves of greater than 0.99 were routinely obtained. The "eicosanoid ratio" in the sample was then compared to the appropriate standard curve to calculate the amount of analyte in the sample. Since, in some cases, the deuterated standards contained a small amount of non-deuterated analyte, the LC-MS/MS of the internal standard was analyzed to determine the amount of non-deuterated analyte present. In this case, the non-deuterated contaminant was subtracted from each analysis either as a part of the standard curve linear regression, or by subtracting an extraction control of internal standard from each sample. The dynamic range is limited on the low end by the amount of non-deuterated analyte in the internal standards and the sensitivity of the mass spectrometer. The upper limit is restricted by ion suppression and detector saturation issues.

In addition to quantitative analysis, in some cases data was expressed as a heat map to identify relative increases and decreases in metabolites over time. Similar to the quantitative analysis, the sample "eicosanoid ratio" was normalized to the corresponding control value (day 0, unstimulated, no inhibitor, etc.). The (1/m) value determined from the quantitative curve cancels out of relative fold calculations; one advantage to eliminating (1/m) is that, for eicosanoids with a limited availability, analysis can be performed in the absence of full quantitation.

2.C.4 Other mass spectrometer parameters

All mass spectral analyses were performed using an Applied Bioscience (Foster City, CA) 4000 QTRAP hybrid triple quadrupole linear ion trap mass spectrometer equipped with a Turbo V ion source and operated in multiple reaction monitoring mode.

For all experiments, the Turbo V ion source was operated in negative electrospray mode and the QTRAP was set as follows: CUR=10 psi, GS1=30 psi, GS2=30psi, IS=-4500 V, CAD=HIGH, TEMP=525°C, ihe=ON. While the entrance and exit cell potentials were optimized for each eicosanoids, these parameters did not affect signal intensity and were set to EP=-10 V and CXP=-10 V for all analyses. The voltage used for collision activated dissociation (-15 to -35 V) and the declustering potentials (-30 to -100 V) varied according to molecular species.

2.D Liquid chromatography

2.D.1 The limitations of multiple-reaction monitoring

While many eicosanoids can be measured using MRM mass spectrometry, as a standalone methodology it has limitations. Direct injection of biological samples that contain large amounts of ionizable compounds can lead to ion suppression and reduce overall sensitivity. Furthermore, a small but important fraction of bioactive eicosanoids have structural differences that cannot be distinguished by mass spectrometry. In most cases, both of these limitations can be overcome using liquid chromatography separation prior to MS analysis.

In many cases, the structural characteristics that cannot be distinguished by mass spectrometry typically affect their LC chromatographic separation. This is clearly demonstrated in the analysis of prostaglandins E_2 and D_2 (Figure 2-4). These compounds have the same precursor ion (m/z = 351) and product ion (m/z = 189) mass, and differ only by the position of the ketone and hydroxyl moiety on the unfragmented prostane ring. While the MS characteristics are nearly identical, LC chromatography can baseline

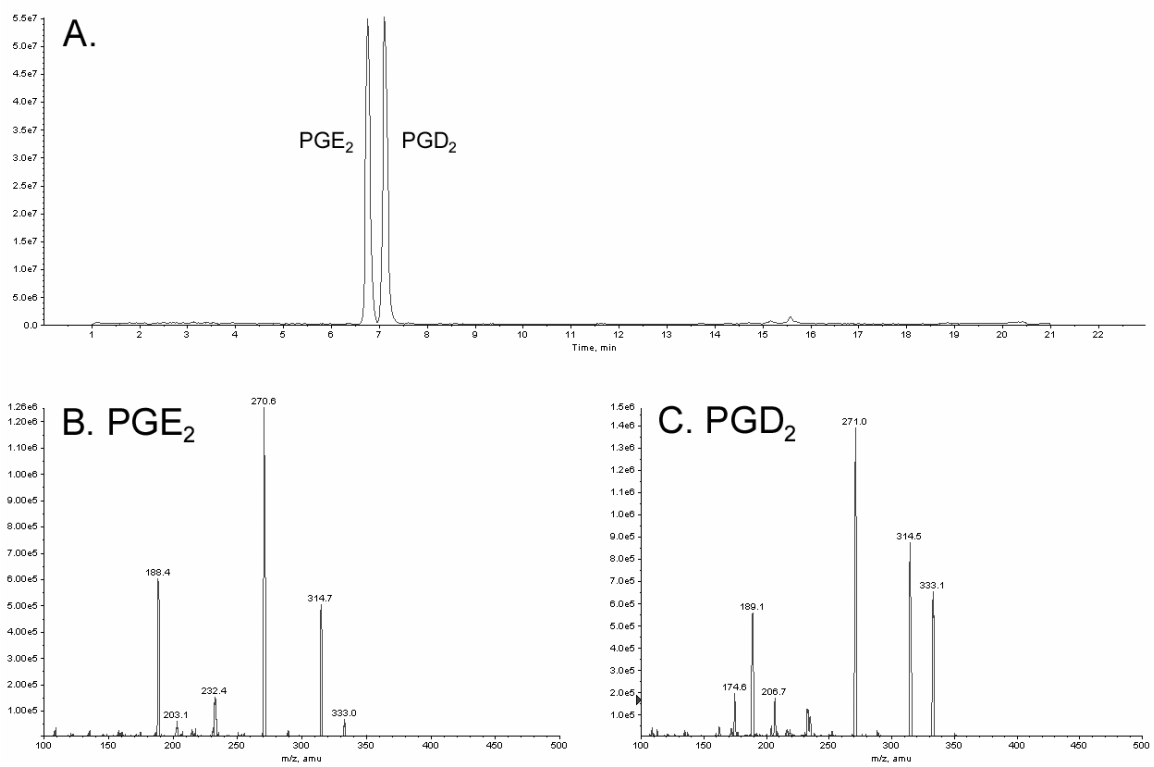

Figure 2-4. LC-MS/MS analysis of PGE_2 and PGD_2. A 1 ng injection of PGE_2 and PGD_2, showing the (A) LC chromatograph of the total ion count of a product ion scan (*m/z* 351), the (B) product ion spectra of PGE_2, and the (B) product ion spectra of PGD_2.

separate these metabolites and easily distinguish them for analysis, highlighting the importance of using LC in conjunction with MS detection.

2.D.2 Analysis of 64 eicosanoids in a 16 min run ("Method 1")

In "Method 1", 64 eicosanoids were separated and analyzed by LC-MS/MS (Table 2-1). Reverse-phase LC was done on a C18 column (2.1 mm x 250 mm, Grace-Vydac) at a flow rate of 300 µl/min at 25°C. All samples were loaded via a Pal auto-sampler (Leap Technologies) that maintained the samples at 4°C to minimize degradation of eicosanoids while queued for analysis. The column was equilibrated in Solvent A, and samples (dissolved in Solvent A) were injected using a 50 µl injection loop and eluted

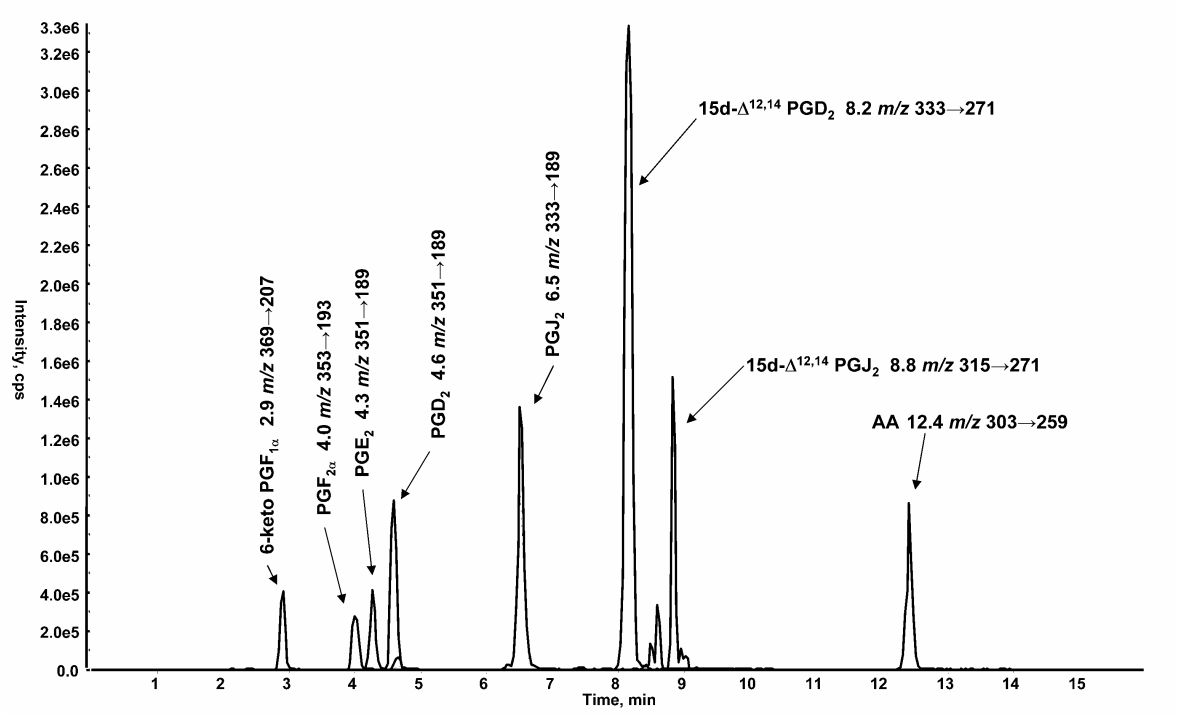

Figure 2-5. Liquid chromatography separation of selected prostaglandins by "Method 1". The individual MRM pairs have been overlaid into a single spectra.

with a linear gradient from 0%-20% solvent B [acetonitrile-isopropyl alcohol (50:50; v/v)] between 0 to 6 min; solvent B was increased to 55% from 6 to 6.5 min and held until 10 min. Solvent B was increased to 100% from 10 to 12 min and held until 13 min; solvent B was dropped to 0% by 13.5 min and held until 16 min.

Figures 2-5 through 2-7 show the chromatograms of a few selected eicosanoids to illustrate several points about this procedure. The sharpest peaks have a width at half height of 6 sec and the baseline peak width on the order of 18 sec. The ABI 4000 QTrap can theoretically handle over hundreds of MRM pairs in a single scan. In this method, the we scan 60 to 70 analytes with a dwell time of 25 msec, producing a duty cycle of 2 sec per scan. This translates to at least 9 data points per peak for the narrowest peaks, which is sufficient to accurately define the peak shape for quantitation but places a practical

limitation on the number of eicosanoids that can be accurately quantitated in a single duty cycle. The ABI software allows the user to break the MRM pairs into sets, and these sets can be run in series during the course of a single analysis, so that only a fraction of the MRM pairs are being scanned during any time period. Running fewer MRM pairs in each scan allows the dwell time to be increased. Although this would not increase the absolute intensity of the peaks, it would increase the time averaging for each data point, thus decreasing the noise levels and increasing the signal to noise ratio.

Figure 2-6 displays the region of the chromatogram that contains the HETEs, diHETEs, EETs, and DHETs. Some prostaglandins and the leukotrienes also elute in this region; however, their molecular ions m/z are different from the hydroxy-eicosanoids so that they do not appear in these scans. Even so, Figure 2-6 clearly indicates that significant care must be taken when assigning the peaks in this region to the correct eicosanoid. While the differences in the retention times of the HETEs are reproducible, for the HETEs that elute between 8- and 12-HETE, the separations are not very large. The absolute value of the retention time for a given eicosanoid fluctuates due to batch variability in the LC solvents, and these shifts can be larger than the differences between the retention times of two neighboring eicosanoids. For this reason, a complete set of standards should be run both before and after each set of unknowns to accurately determine eicosanoid retention times, especially when assigning peak identities. If these HETEs are present in the samples, the gradient in this region of the chromatogram can be altered to spread out this region and improve the resolution.

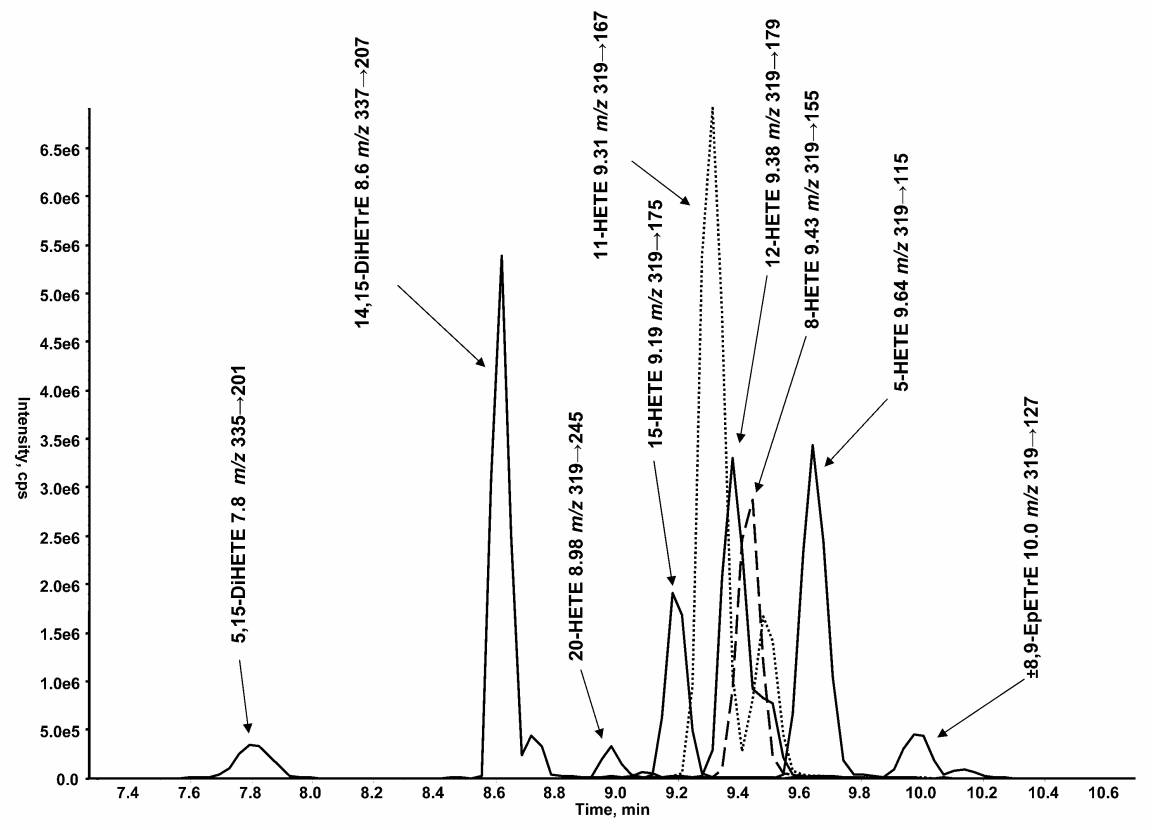

Figure 2-6. Liquid chromatography separation of selected HETEs, diHETEs, EETs and DHETs by "Method 1". The individual MRM pairs have been overlaid into a single spectra.

Figure 2-7 shows the chromatograms of LTB_4, LTC_4, Δ11-trans LTC_4, LTE_4, and Δ11-trans LTE_4, and demonstrates one of the significant powers of the MRM method. Examination of Figures 2-5 and 2-6 clearly show that the region from 8 to 11 min is very crowded, and that a significant number of eicosanoids elute in this region. Yet when the MRM transitions are different, the chromatograms are very clean and the assignments are easily made. However, it also highlights an important precaution that must be considered when using MRM. While the chromatogram of a particular analyte may appear to be very clean, as no other compounds exhibit the same MRM transition, a tremendous amount of material co-elute but go undetected. Such material can still cause significant ion

suppression of the analyte being examined. For example, we have found that PGE_2 and PGD_2 appear to co-elute with material co-extracted from DMEM cell culture media, significantly diminishing the MS sensitivity of these eicosanoids (see Section 2. F. 4.). The proper use of internal standards can compensate for many of these issues during quantitation.

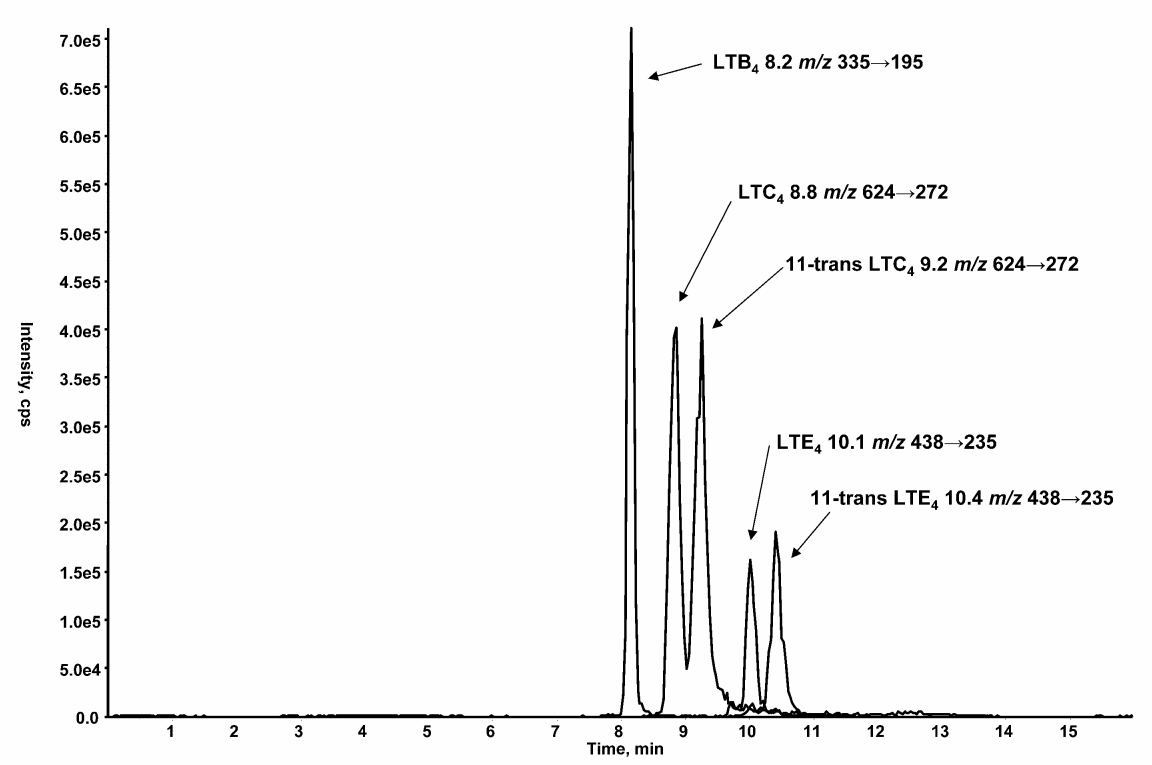

Figure 2-7. Liquid chromatography separation of selected leukotrienes by "Method 1". The individual MRM pairs have been overlaid into a single spectra.

2.D.3 Analysis of 104 eicosanoids in a 23 min run ("Method 2")

The number of compounds that can be simultaneously analyzed by this technique is mainly limited by the duty cycle of the mass spectrometer. Previously described "Method 1" generated a 2 second duty cycle, which corresponded to between 8-12 points across the LC peak (near the minimum necessary for quantitative analysis) and imposed a practical upper limit on further expansion of the method. Moreover, it decreases the time averaging of the noise creating a gap between the limit of detection and the limit of quantitation low signal metabolites. To address these issues, a second procedure was created, termed "Method 2". In total, over 100 MRM pairs were separated into 7 periods (the final period elutes fatty acids, and was not used in these studies) based on their relative LC retention times (Table 2-2); the duty cycles of these periods ranged from 390 to 840 ms, with an average time of 565 ms. This method was used in the analysis of murine tibiotarsal joints in Chapter 5.

In "Method 2", eicosanoids were separated by reverse-phase LC on a Synergy C18 column (2.1 mm x 250 mm, 4u) preceded by a C18 guard cartridge (4 x 2.0 mm) at a flow rate of 300 µl/min at 50ºC. The column was equilibrated in Solvent A [water-acetonitrile-acetic acid (70:30:0.02; v/v/v)], and 40 µl of sample was injected using a 50 µl injection loop and eluted with 0% solvent B [acetonitrile-isopropyl alcohol (50:50; v/v)] between 0 and 1 min. Solvent B was increased in a linear gradient to 25% solvent B until 3 min, to 45% until 11 min, to 60% until 13 min, to 75% until 18 min, and to 90% until 18.5 min. Solvent B was held at 90% until min 20, dropped to 0% by 21 min and held until 25 min.

Were every potential eicosanoid to be present in a sample, it would not be possible to quantify them all. In some cases, two eicosanoids can produce the same MRM pair and, while partially separated by LC, cannot be fully baseline resolved. Thus, a quantitative curve containing all 104 metabolites in a single injection would not be useful. To identify eicosanoids less likely to be present in a sample (and confirm their absence), seven eicosanoid solution groups were prepared and injected before and after sample analysis (Table 2-3). These retention time solutions contained 1 ng/µl of each eicosanoid in ethanol; dilute 2.5 ng into 98.5 µl of LC solvent A, and inject 40 µl (1 ng) on column. Should a compound not present in the standard curve solution be detected, a second quantitative solution was made and run following the experiment.

Consistent and reproducible retention times are critical for eluting eicosanoids within the appropriate analysis window. For this reason, the following procedures have been put in place. The guard cartridge was replaced before each experiment to reduce the potential of debris buildup affecting LC separation, and the column was equilibrated in the heating jacket for 20 min. The process of making Solvent A and Solvent B is noticeably exothermic, and this appears to cause small but noticeable affects on eicosanoid elution times. For this reason, solvents were either brought to room temperature using a water bath or allowed to equilibrate with the ambient temperature for one week.

While the relative elution order of a given set of eicosanoids can be readily reproduced from experiment to experiment, the exact retention times between any two experiments shift when using new solvents, columns and guard cartridges. For this reason, the method must be calibrated each time one of these factors is changed, so that

the MRM period breaks occur such that all eicosanoids elute during their allotted detection time. To do this, a calibration mixture containing eicosanoids that elute at the beginning and end of each period is analyzed to determine the appropriate time to switch periods (Figure 2-8). This is analyzed using the same LC protocol, but with a mass spectrometry method that contains a single period containing only the calibration mixture MRM pairs.

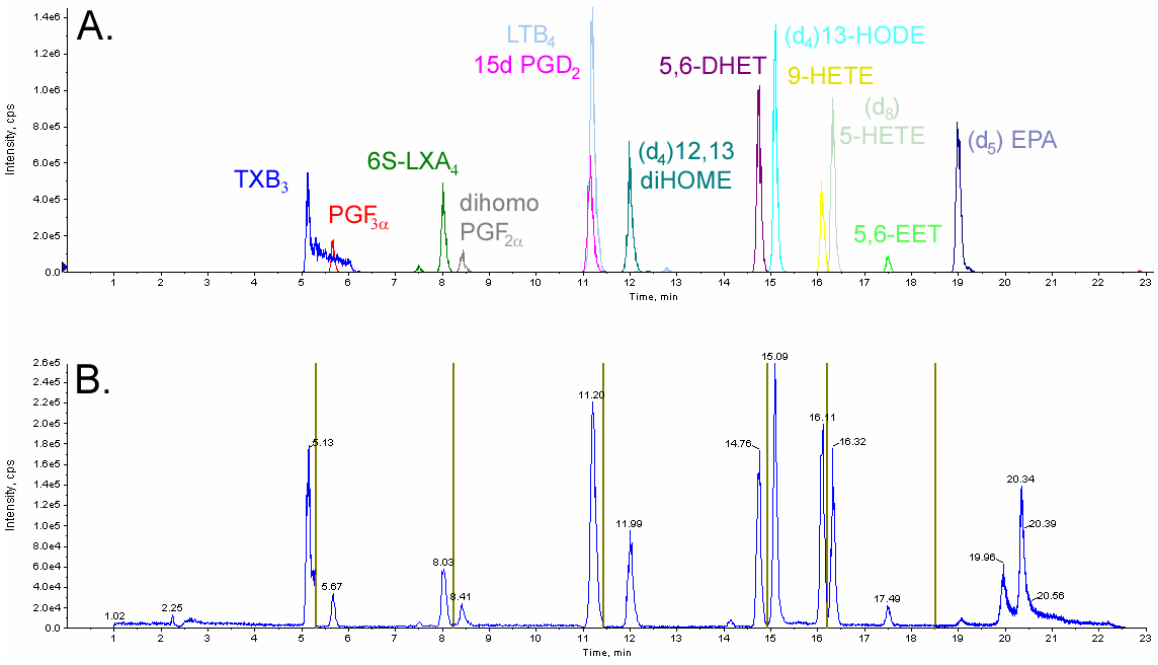

Figure 2-8. Calibration of "Method 2". A calibration standard mix, containing eicosanoids that elute immediately before or after a duty cycle period ends, was (A) analyzed using the calibration method and used to determine the duration of each MS analysis period in "Method 2". Following calibration, the same mixture was (B) analyzed by "Method 2", with duty cycle breaks indicated in gold.

2.D.4 Analysis of 3 eicosanoids in a 9 min run ("Method 3")

In addition to scaling up the "Method 1" to increase the number of eicosanoids analyzed, we scaled down the method to use it as a high-throughput inhibitor screening tool. Since a thorough analysis of the activation of RAW264 cells had been performed in Chapter 3, eicosanoids that were indicative of selective inhibitor action in these cells were monitored. This protocol was termed "Method 3", and used toward the development of selective metalloprotein inhibitors in Chapter 4.

In "Method 3", eicosanoids were separated by reverse-phase LC on a Hydrosil C18 column (2.1 mm×250 mm) at a flow rate of 300 μl/min at 50 °C. The column was equilibrated in 90% LC solvent A (water-acetonitrile-acetic acid (70:30:0.02; v/v/v)) and 10% LC solvent B (acetonitrile-isopropyl alcohol (50:50, v/v)). Samples were injected using a 50 μl injection loop and eluted with 10% solvent B from 0 to 2 min, followed by a gradual increase to 100% solvent B using a linear gradient from 2 to 7 min, held at 100% solvent B from 7 to 8.5 min, dropped back to 10% solvent B using a linear gradient from 8.5 to 9 min, and finally held at 10% solvent B until 11 min. The precursor→product MRM pairs were selected as follows: d_4-PGD_2 (355→275), d_5-LTC_4 (629.6→272), d_8-AA (311→267), PGD_2 (351→271), LTC_4 (624.6→272), and AA (303→259).

2.E Limit of detection

Table 2-1 contains an estimate of the lower limit of detection (LOD) for the eicosanoids when employing “Method 1". A set of standards was serially diluted such that 1 to 5000 pg would be loaded onto the column. A signal was judged to be significant if the peak area was three times the noise three standard deviation level. Most limits were between 1 and 50 pg loaded onto the column. Only PGE_2-EA had an LOD greater than 50 ng. The detection limits that we obtained were achieved with a 2.1 mm x 250 mm, Grace-Vydac reverse phase C18 column with 5μm particle size. Decreasing the column diameter, the particle size, and the flow rate can all increase sensitivity; as can changing the column packing. We have analyzed only one isomer of any isomeric analytes and only non-deuterated analytes. Therefore, we have listed the LOD and recovery values for the other isomers and for the deuterated standards as not determined (ND) in Table 2-1. However, their recoveries and LODs should be very similar to the corresponding isomer that was analyzed or the equivalent non-deuterated analyte.

Figure 2-9 shows an example of the analysis of a sample that was close to our lower limit of detection. It is the chromatogram showing the analysis of PGE_2 and PGD_2 in a sample of spinal fluid from a rat that had been subjected to the carrageenan model of inflammatory pain. This represents 52 pg of PGE_2 loaded onto the column and correlates with 150 pg of PGE_2 being present in the original 42 μl spinal fluid sample.

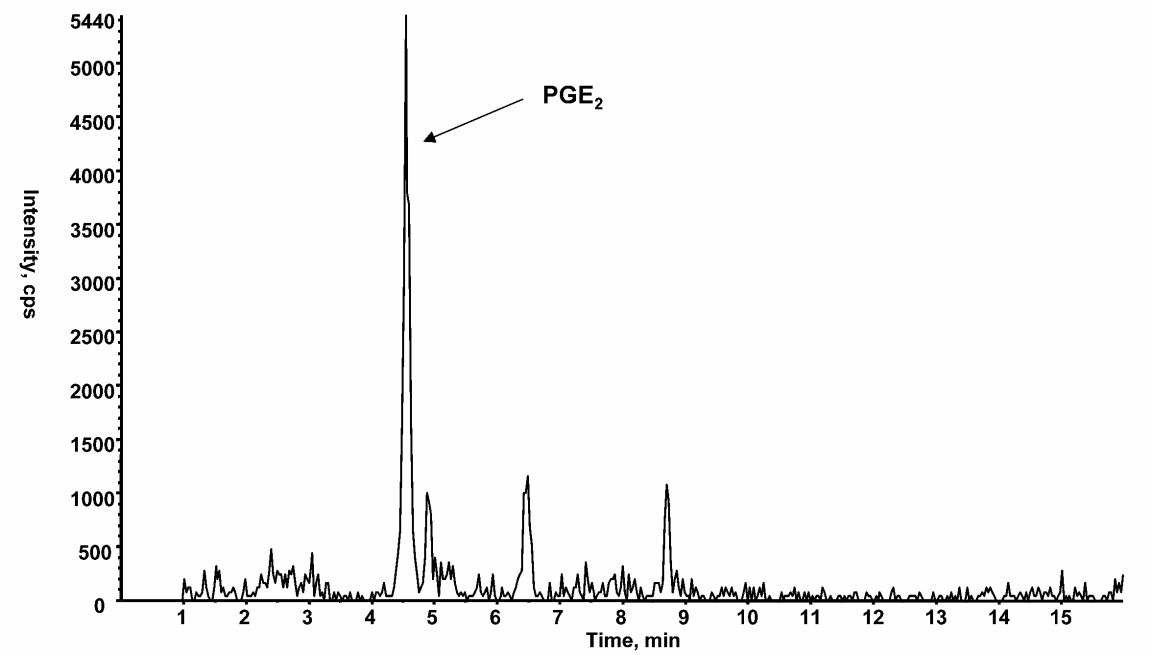

Figure 2-9. PGE_2 analysis of rat spinal fluid. Spinal fluid was collected from a rat whose paw had been injected with carrageenan to induce an inflammatory pain state. A sample of spinal fluid was removed (42 µl), purified by solid phase extraction and analyzed by "Method 1". Eighty percent of the sample was analyzed. The PGE_2 peak corresponds to 52 pg of PGE_2 being loaded onto the column. The signal-to-noise (S/N) ratio was 16-fold over a three-standard-deviation noise level.

2.F Eicosanoid isolation procedures

2.F.1 Macrophage cell culture

The following procedure was developed for the isolation of eicosanoids from 6 well cell culture plates containing 2.0 ml of media. We have also adapted this method to other sample types and sample volumes by scaling our procedure, as needed. The media was removed and 100 µl of a mixture of internal standards (containing 10 ng/100 µl of each standard, in EtOH) was added followed by 100 µl of EtOH to bring the total concentration of EtOH to 10% by volume. Samples were centrifuged for 5 minutes at 3000 rpm to remove cellular debris. The eicosanoids were then isolated by solid phase extraction.

When intracellular eicosanoids were analyzed, adherent cells were scraped into 500 µl MeOH, and then 1000 µl PBS and 100 µl of internal standards were added. Scraping cells in aqueous solutions was shown to activate eicosanoid production, whereas doing so in MeOH effectively stopped the reactions and lysed the cells. These samples were then isolated by solid phase extraction.

2.F.2 Mouse tibiotarsal (ankle) joints

Female C3H/HeJ (C3H) and DBA/2J (DBA) mice, 4-6 weeks of age, were purchased from The Jackson Laboratory (Bar Harbor, ME). Animals were housed in a specific pathogen-free facility and given sterile food and water *ad libitum*. Basal eicosanoid levels have been shown to be strongly influenced by diet, so it is important to use age and diet matched control animals for these experiments.

Following excision from the mouse, tissues were snap-frozen in liquid nitrogen and stored at -80ºC until extraction. Tibiotarsal joints were pulverized and the resulting powder placed in 3 ml of 50% ethanol in water and then weighed. 10 µl of antioxidant cocktail (0.2 mg/ml butylated hydroxytoluene, 0.2 mg/ml EDTA, 2 mg/ml triphenylphosphine, 2 mg/ml indomethacin in a solution of 2:1:1 methanol:ethanol:H_2O) was added to each sample before incubation at -20ºC for 72h. Samples were then centrifuged at 3500 x g for 30 minutes, the clear ethanolic supernatant removed to a new tube, and dried under nitrogen gas.

Samples were reconstituted with 2 ml of 10% MeOH and supplemented with 50 µl of a mixture of internal standard containing 50 pg/µl (2.5 ng total). Samples sonicated with a probe sonicator, and the eicosanoids were then isolated by solid phase extraction.

Prior to LC-MS/MS analysis, reconstituted samples were centrifuged at 10,000 rpm for 30 sec to remove debris.

2.F.3 Solid phase extraction

Eicosanoids were extracted using Strata-X SPE columns (Phenomenex). Columns were washed with 2 ml MeOH and then 2 ml H_2O. After applying the sample, the columns were washed with 10% MeOH, and the eicosanoids were then eluted with 1 ml MeOH. The eluant was dried under vacuum and redissolved in 50 – 100 µl of solvent A for LC-MS/MS analysis.

2.F.4 Extraction efficiency

Our primary goal was to analyze as many eicosanoids in a single run as possible. We chose to focus on maximizing the recovery of AA, prostaglandins and HETES. Table 2-1 shows the recoveries that "Method 1" achieved for most of the analytes that we detect. These recoveries were determined by adding a known amount of each analyte, contained in a standard mix, to 2.0 ml of water or DMEM and then isolating the eicosanoids via the standard sample preparation method outlined above. We also did an "add back" experiment where DMEM alone was extracted by the same method; however, instead of adding an aliquot of the standard eicosanoid mixture to the DMEM sample before extraction, the eicosanoids were added to the post-extraction methanol column effluent. Losses in the "add back" samples would indicate that materials in the media are being co-extracted with the eicosanoids, and that these contaminants affect the eicosanoid MS response. All three sets of samples were analyzed with our LC-MS/MS procedure.

The eicosanoid peak intensities of these samples were compared to those of standards that had not been through the isolation procedure, but instead were directly analyzed by LC-MS/MS.

Table 2-1 reports the relative recoveries of standards that were extracted from DMEM. The mono and di-hydroxy eicosanoids had excellent recoveries between 75 and 100%. The leukotrienes and prostaglandins had only moderate recoveries in the range of 50%. In most cases, the recoveries of these compounds from water were in the 80 to 100% range. The "add back" experiment showed that, for the prostaglandins, most of the losses occurred in the "add back" experiment, implying that some component from the media is being extracted that decreases the MS response to the prostaglandins. However, the "add back" levels for the cysteinyl leukotrienes were 100% within experimental error, suggesting that the losses occurred during the extraction process and that media components are not affecting leukotriene detection. Tetranor PGEM and PGFM yielded low recoveries and do not bind tightly to the Strata-X SPE columns under these conditions. The PGK_2 had very large errors, and its extraction recovery could not be interpreted in this experiment. Again, the yield of a given class of compounds could be improved by altering the conditions or column type, but often at the expense of other analytes.

2.G Miscellany

The process of culturing cells can affect the eicosanoid levels in other ways as well. For example, PGD_2 can undergo dehydration to form PGJ_2, 15d PGD_2, and 15d PGJ_2. This dehydration has been reported to be accelerated in serum albumin[279, 280]. This decomposition will not be compensated for by the internal standards since they are not added until after the cell incubations. We have also found that when 10% serum is present during the cell culture no LTC_4 could be detected but LTE_4, which is a breakdown product of LTC_4, was detected. When the same experiments are run in serum free media significant levels of the LTC_4 was detected but vary little LTE_4. Presumably, the serum is catalyzing the conversion of LTC_4 to LTE_4. Clearly, the types of recovery experiments outlined above must be conducted whenever applying this system to a new type of sample (e.g. media, serum, or tissues), or when changing the conditions of an already tested sample. Care must also be taken to determine the effects that the addition of any agents (e.g. inhibitors, activators, or drugs) have on the extractions and on the quantitation of any other analytes. LC-MS/MS should also be done on the agents being added to determine if they have any MRM transitions that could be mistaken for one of the standard analytes.

Traditionally, lipids solutions were routinely acidified before subjecting them to liquid extractions. We compared our recoveries with and with out acidifying the media before application to the SPE columns. We found that there were no significant differences; therefore, we do not routinely acidify the media. It is possible that eicosanoids other than those we employed in our testing, could benefit by acidification. In addition some eicosanoid species are susceptible to air oxidation and/or adhere to

vessels and should not be taken to dryness. To guard against these losses, 20 µl of a 50/50 solution of glycerol/ethanol can be added to the methanol column elution just before drying down the samples on the speed vac. The glycerol remains, and the eicosanoids are concentrated into the glycerol which can then be taken up in the LC equilibration buffer for LC-MS/MS analysis.

2.H Discussion

The three methods outlined above is a sensitive, accurate method of identifying and quantitating a large number of eicosanoids in a single LC-MS/MS run. This method can detect 1 pg (on column) of many eicosanoids which is similar to the sensitivity of EIA analysis. Its primary advantage is that a large number of different species can be measured in a single analysis, while EIA analysis requires specific antibodies which are often not commercially available. These methods were applied to the study of eicosanoid biosynthesis and signaling in Chapters 3 – 5.

2.I Acknowledgments

Raymond A. Deems, Rebecca Bowers-Gentry, and Richard Harkewicz co-authored work from this chapter in the journal Methods in Enzymology, titled “Detection and Quantitation of Eicosanoids via High Performance Liquid Chromatography-Electrospray Ionization-Mass Spectrometry. We would like to thank Dr. Robert C. Murphy (University of Colorado School of Medicine, Denver, CO) for his invaluable help and advice on the use of LC-MS/MS as a quantitative tool to analyze eicosanoids.

Table 2-1. Liquid Chromatography and Mass Spectrometry Parameters for "Method 1".

Eicosanoid	LIPID MAPS ID	Precursor Ion (*m/z*)	Product Ion (*m/z*)	Retention Time (min)	Internal Standard	Recovery (%)	LOD (pg)
AA	LMFA01030001	303	259	12.4	(d_8) AA	E	50
(d_8) AA	LMFA01030003	311	267	12.4		ND	ND
AA-EA	LMFA08040001	346	259	10.6		E	10
5,6R-diHETE	LMFA03060017	335	163	9.0		M	5
5,6-diHETE	LMFA03060018	335	163	9.0		E	1
5,15-diHETE	LMFA03060049	335	201	7.8		E	5
8,15-diHETE	LMFA03060050	335		ND[5]		ND	ND
5,6-DHET	LMFA03050004	337	145	9.0		E	1
8,9-DHET	LMFA03050006	337	127	8.8		E	1
11,12-DHET	LMFA03050008	337	167	8.7		E	1
14,15-DHET	LMFA03050010	337	207	8.6		E	1
5,6-EET	LMFA03080002	319	191	10.1		E	5
8,9-EET	LMFA03080003	319	127	10.0		E	5
11,12-EET	LMFA03080004	319	167	9.8		E	10
14,15-EET	LMFA03080005	319	139	9.7		E	50
5R-HETE	LMFA03060024	319	115	9.64	(d_8) 5-HETE	ND	ND
5-HETE	LMFA03060002	319	115	9.64	(d_8) 5-HETE	E	1
(d_8) 5-HETE	LMFA03060005	327	116	9.60		ND	ND
8R-HETE	LMFA03060021	319	155	9.43		ND	ND
8-HETE	LMFA03060006	319	155	9.43		E	1
9-HETE	LMFA03060089	319	151	9.49		E	1
11-HETE	LMFA03060028	319	167	9.31	(d_8) 5-HETE	ND	ND
11S-HETE	LMFA03060003	319	167	9.31	(d_8) 5-HETE	E	1
12R-HETE	LMFA03060008	319	179	9.38		ND	ND
12-HETE	LMFA03060088	319	179	9.38		E	1
15R-HETE	LMFA03060030	319	175	9.19	(d_8) 5-HETE	ND	ND
15-HETE	LMFA03060001	319	175	9.19	(d_8) 5-HETE	E	1
20-HETE	LMFA03060009	319	245	8.98		E	1
12-HHTrE	LMFA03050002	279	163	8.7		E	50
5-HpETE	LMFA03060012	335	155	9.7		E	5
12-HpETE	LMFA03060013	335	153	9.4		E	1
15-HpETE	LMFA03060014	335	113	9.2		E	1
LTB_4	LMFA03020001	335	195	8.2		M	5
12epi LTB_4	LMFA03020015	335	195	7.8		E	1
6t,12epi LTB_4	LMFA03020014	335	195	8.0		E	5
LTC_4	LMFA03020003	624	272	8.8		P	1
Δ11 LTC_4	LMFA03020020	624	272	9.2		M	1
LTE_4	LMFA03020002	438	235	10.1		M	5
Δ11 LTE_4	LMFA03020022	438	235	10.4		M	1
6R-LXA_4	LMFA03040001	351	115	5.2		M	1
6S-LXA_4	LMFA03040003	351		ND[5]		ND	ND
LXB_4	LMFA03040002	351		ND[5]		ND	ND
5-oxoETE	LMFA03060011	317	203	9.8		E	5
12-oxoETE	LMFA03060019	317	153	9.4		E	1
15-oxoETE	LMFA03060051	317		ND[5]		ND	ND

Table 2-1. *Continued.*

Eicosanoid	LIPID MAPS ID	Precursor Ion (*m/z*)	Product Ion (*m/z*)	Retention Time (min)	Internal Standard	Recovery (%)	LOD (pg)
PGA_2	LMFA03010035	333		ND[5]		ND	ND
dhk PGA_2	LMFA03010033	333		ND[5]		ND	ND
PGB_2	LMFA03010018	333	175	6.6		E	5
PGD_2	LMFA03010004	351	189	4.6	(d_4) PGD_2	M	5
(d_4) PGD_2	LMFA03010007	355	193	4.6		ND	ND
PGD_2-EA	LMFA03010152	394	271	3.3		E	10
15d PGD_2	LMFA03010051	333	271	8.2	(d_4) 15d PGJ_2	E	1
dhk PGD_2	LMFA03010022	351	207	5.9	(d_4) dhk PGD_2	P	1
(d_4) dhk PGD_2	LMFA03010178	355	211	5.9		ND	ND
6k PGE_1	LMFA03010012	367	143	3.1		P	5
PGE_2	LMFA03010003	351	189	4.3	(d_4) PGE_2	M	10
(d_4) PGE_2	LMFA03010008	355	193	4.3		ND	ND
PGE_2-EA	LMFA03010151	394	203	3.0		M	10000
bicyclo PGE_2	LMFA03010034	333	175	7.4		E	5
dhk PGE_2	LMFA03010031	351	207	5.3	(d_4) dhk PGD_2	M	1
19oh PGE_2	LMFA03010024	367	287	2.4		M	1
20oh PGE_2	LMFA03010014	367	287	2.4		M	5
15k PGE_2	LMFA03010031	349	161	4.7		M	1
tetranor PGE_2	LMFA03010032	327	291	2.3		P[4]	50
6,15 dk-,dh- $PGF_{1\alpha}$	LMFA03010013	369	267	3.6		P	50
6k $PGF_{1\alpha}$	LMFA03010001	369	207	2.9	(d_4) 6k $PGF_{1\alpha}$	E	10
(d_4) 6k $PGF_{1\alpha}$	LMFA03010037	373	211	2.9		ND	ND
$PGF_{2\alpha}$	LMFA03010002	353	193	4.0	(d_4) $PGF_{2\alpha}$	M	10
(d_4) $PGF_{2\alpha}$	LMFA03010006	357	197	4.0		ND	ND
$PGF_{2\alpha}$-EA	LMFA03010075	396	334	3.0		M	10
11β $PGF_{2\alpha}$	LMFA03010060	353	193	3.7		M	1
dhk $PGF_{2\alpha}$	LMFA03010027	353	209	5.2	(d_4) dhk $PGF_{2\alpha}$	M	5
(d_4) dhk $PGF_{2\alpha}$	LMFA03010179	357	213	5.2		ND	ND
2,3 dinor 11β $PGF_{2\alpha}$	LMFA03010011	325	145	3.0		M	1
20oh $PGF_{2\alpha}$	LMFA03010029	369	193	2.3		M	50
15k $PGF_{2\alpha}$	LMFA03010026	351	217	4.5		M	1
$PGF_{2\beta}$	LMFA03010025	353		ND[5]		ND	ND
tetranor $PGF_{2\alpha}$	LMFA03010139	329	293	2.1		P[4]	10
PGG_2	LMFA03010009	367		ND[5]		ND	ND
PGH_2	LMFA03010010	351		ND[5]		ND	ND
PGJ_2	LMFA03010019	333	189	6.5	(d_4) 15d PGJ_2	E	1
Δ12 PGJ_2	LMFA03010020	333		ND[5]		ND	ND
15d PGJ_2	LMFA03010021	315	271	8.8	(d_4) 15d PGJ_2	E	5
(d_4) 15d PGJ_2	LMFA03010177	319	275	8.8		ND	ND
PGK_2	LMFA03010023	349	205	4.4		ND	ND
TXB_2	LMFA03030002	369	169	3.6	(d_4) TXB_2	M	10
(d_4) TXB_2	LMFA03030010	373	173	3.6		ND	ND
11dh TXB_2	LMFA03030004	367	123	ND[5]		ND	ND
dinor TXB_2	LMFA03030003	341	167	ND[5]		ND	ND

[1] Gray boxes indicated internal standards.
[2] The retention times are given to indicate the relative elution position of the compounds with the understanding that the absolute values are not significant.
[3] Recoveries were grouped as P for poor (< 25%), M for moderate (25% to 75%), E for excellent (> 76%), and ND for not determined.
[4] Tetranor PGFM and tetranor PGEM did not bind to the Strata-X SPE column and thus could not be detected by this method
[5] These compounds were not analyzed quantitatively for this table but the MS/MS spectra and LC retention times are available in the LIPID MAPS Eicosanoid library at www.lipidmaps.org.

Table 2-2. Liquid Chromatography and Mass Spectrometry Parameters for "Method 2".

Period	Eicosanoid	LIPID MAPS ID	Precursor Ion	Product Ion	Retention Time	Internal Standard
1	tetranor $PGF_{2\alpha}$	LMFA03010139	329	293	3.10	(d_4) $PGF_{2\alpha}$
	tetranor PGE_2	LMFA03010032	327	291	3.11	(d_4) PGE_2
	20oh $PGF_{2\alpha}$	LMFA03010029	369	193	3.35	(d_4) $PGF_{2\alpha}$
	19oh $PGF_{2\alpha}$	LMFA03010042	369	193	3.48	(d_4) $PGF_{2\alpha}$
	20oh PGE_2	LMFA03010014	367	189	3.65	(d_4) PGE_2
	19oh PGE_2	LMFA03010024	367	189	3.66	(d_4) PGE_2
	Δ17 6k $PGF_{1\alpha}$	LMFA03010149	367	163	4.19	(d_4) 6k $PGF_{1\alpha}$
	20cooh LTB_4	LMFA03020016	365	195	4.79	(d_4) LTB_4
	6k $PGF_{1\alpha}$	LMFA03010001	369	163	4.87	(d_4) 6k $PGF_{1\alpha}$
	(d_4) 6k $PGF_{1\alpha}$	LMFA03010037	373	167	4.92	-
	Resolvin E_1	LMFA03070019	349	195	4.99	(d_4) LTB_4
	2,3 dinor 11β $PGF_{2\alpha}$	LMFA03010011	325	145	5.07	(d_4) $PGF_{2\alpha}$
	20oh LTB_4	LMFA03020018	351	195	5.10	(d_4) LTB_4
	6k PGE_1	LMFA03010012	367	143	5.20	(d_4) 6k $PGF_{1\alpha}$
	TXB_3	LMFA03030006	367	169	5.27	(d_4) TXB_2
2	TXB_1	LMFA03030008	371	171	5.93	(d_4) TXB_2
	$PGF_{3\alpha}$	LMFA03010138	351	193	5.96	(d_4) $PGF_{2\alpha}$
	(d_4) TXB_2	LMFA03030010	373	173	6.20	-
	TXB_2	LMFA03030002	369	169	6.22	(d_4) TXB_2
	6,15 dk-,dh- $PGF_{1\alpha}$	LMFA03010013	369	113	6.22	(d_4) $PGF_{2\alpha}$
	PGE_3	LMFA03010135	349	269	6.25	(d_4) PGE_2
	8-iso $PGF_{2\alpha}$ III	LMFA03110001	353	193	6.25	(d_{11}) 5-iso $PGF_{2\alpha}$ VI
	11β $PGF_{2\alpha}$	LMFA03010036	353	193	6.51	(d_4) $PGF_{2\alpha}$
	PGD_3	LMFA03010142	349	269	6.58	(d_4) PGD_2
	(d_{11}) 5-iso $PGF_{2\alpha}$ VI	LMFA03110012	364	115	6.73	-
	5-iso $PGF_{2\alpha}$ VI	LMFA03110011	353	115	6.87	(d_{11}) 5-iso $PGF_{2\alpha}$ VI
	(d_4) $PGF_{2\alpha}$	LMFA03010006	357	197	7.05	-
	$PGF_{2\alpha}$	LMFA03010002	353	193	7.11	(d_4) $PGF_{2\alpha}$
	$PGF_{1\alpha}$	LMFA03010137	355	293	7.13	(d_4) $PGF_{2\alpha}$
	(d_4) PGE_2	LMFA03010008	355	275	7.31	-
	PGE_2	LMFA03010003	351	271	7.33	(d_4) PGE_2
	PGK_2	LMFA03010023	349	205	7.48	(d_4) PGE_2
	11β PGE_2	LMFA03010060	351	271	7.56	(d_4) PGE_2
	LXB_4	LMFA03040002	351	221	7.56	(d_4) LTB_4
	PGE_1	LMFA03010134	353	273	7.60	(d_4) PGE_2
	14,15 LTC_4	LMFA03020031	624.6	272	7.61	(d_4) LTB_4
	15k $PGF_{2\alpha}$	LMFA03010026	351	113	7.67	(d_4) $PGF_{2\alpha}$
	(d_4) PGD_2	LMFA03010007	355	275	7.76	-
	PGD_2	LMFA03010004	351	271	7.77	(d_4) PGD_2
	PGD_1	LMFA03010049	353	273	7.77	(d_4) PGD_2
	15k PGE_2	LMFA03010031	349	113	7.83	(d_4) PGE_2
	15k $PGF_{1\alpha}$	LMFA03010150	353	113	7.96	(d_4) $PGF_{2\alpha}$
	dh $PGF_{2\alpha}$	LMFA03010079	355	275	8.25	(d_4) $PGF_{2\alpha}$
	14,15 LTD_4	LMFA03020032	495	177	8.26	(d_4) LTB_4
	11β dhk $PGF_{2\alpha}$	LMFA03010203	353	113	8.40	(d_4) $PGF_{2\alpha}$
	Resolvin D_1	LMFA04000006	375	141	8.50	(d_4) LTB_4
	6R-LXA_4	LMFA03040001	351	115	8.62	(d_4) LTB_4
	dhk PGE_2	LMFA03010031	351	207	8.64	(d_4) dhk PGD_2
	(d_4) dhk $PGF_{2\alpha}$	LMFA03010179	357	295	8.81	-
	dhk $PGF_{2\alpha}$	LMFA03010027	353	291	8.88	(d_4) dhk $PGF_{2\alpha}$
	6S-LXA_4	LMFA03040003	351	115	8.96	(d_4) LTB_4

Table 2-2. *Continued.*

Period	Eicosanoid	LIPID MAPS ID	Precursor Ion	Product Ion	Retention Time	Internal Standard
	14,15 LTE_4	LMFA03020033	438	333	9.30	(d_4) LTB_4
	dihomo $PGF_{2\alpha}$	LMFA03010157	381	221	9.43	(d_4) $PGF_{2\alpha}$
	(d_4) dhk PGD_2	LMFA03010178	355	211	9.46	-
	dhk PGD_2	LMFA03010022	351	207	9.49	(d_4) dhk PGD_2
	dihomo PGE_2	LMFA03010155	379	299	9.79	(d_4) PGE_2
	LTC_4	LMFA03020003	624.6	272	9.89	(d_4) LTB_4
	dihomo PGD_2	LMFA03010156	379	299	10.13	(d_4) PGD_2
	PGA_2	LMFA03010035	333	271	10.18	(d_4) 15d PGJ_2
	LTD_4	LMFA03020006	495	177	10.33	(d_4) LTB_4
	PGJ_2	LMFA03010019	333	271	10.35	(d_4) 15d PGJ_2
	PGB_2	LMFA03010018	333	271	10.51	(d_4) 15d PGJ_2
	Δ11 LTC_4	LMFA03020020	624.6	272	10.68	(d_4) LTB_4
	LTE_4	LMFA03020002	438	333	10.96	(d_4) LTB_4
	Δ11 LTD_4	LMFA03020021	495	177	10.99	(d_4) LTB_4
3	PD_1	LMFA04000011	359	153	11.23	(d_4) LTB_4[3]
	bicyclo PGE_2	LMFA03010034	333	113	11.36	(d_4) PGE_2
	Δ15t-PD_1	LMFA04000045	359	153	11.53	(d_4) LTB_4[3]
	Δ11 LTE_4	LMFA03020022	438	333	11.58	(d_4) LTB_4
	8,15-diHETE	LMFA03060050	335	127	11.61	(d_4) LTB_4
	10S,17S-DiHDoHE	LMFA04000047	359	153	11.83	(d_4) LTB_4
	5,15-diHETE	LMFA03060049	335	201	12.06	(d_4) LTB_4
	6t LTB_4	LMFA03020013	335	195	12.10	(d_4) LTB_4
	12epi LTB_4	LMFA03020015	335	195	12.10	(d_4) LTB_4
	6t,12epi LTB_4	LMFA03020014	335	195	12.20	(d_4) LTB_4
	(d_4) 12,13 diHOME	LMFA01050357	317	185	12.22	-
	12,13 diHOME	LMFA01050351	313	183	12.26	(d_4) 12,13-diHOME
	(d_4) LTB_4	LMFA03020030	339	197	12.46	-
	15d PGD_2	LMFA03010051	333	271	12.51	(d_4) 15d PGJ_2
	LTB_4	LMFA03020001	335	195	12.52	(d_4) LTB_4
	dihomo PGJ_2	LMFA03010158	361	299	13.08	(d_4) 15d PGJ_2
	(d_4) 9,10 diHOME	LMFA01050358	317	203	13.58	-
	9,10 diHOME	LMFA01050350	313	201	13.65	(d_4) 9,10-diHOME
	14,15-DHET	LMFA03050010	337	207	13.82	(d_8) 5-HETE
	12-HHTrE	LMFA03050002	279	163	13.87	(d_8) 5-HETE
	dihomo 15d PGD_2	LMFA03010159	361	299	14.20	(d_4) 15d PGJ_2
	11,12-DHET	LMFA03050008	337	167	14.28	(d_8) 5-HETE
	HXA_3	LMFA03090005	335	127	14.46	(d_8) 11,12-EET
4	HXB_3	LMFA03090003	335	183	14.60	(d_8) 11,12-EET
	(d_4) 15d PGJ_2	LMFA03010177	319	275	14.67	-
	15d PGJ_2	LMFA03010021	315	271	14.71	(d_4) 15d PGJ_2
	8,9-DHET	LMFA03050006	319	155	14.71	(d_8) 5-HETE
	(d_6) 20-HETE	LMFA03060082	325	295	14.97	-
	20-HETE	LMFA03060009	319	289	15.02	(d_6) 20-HETE
	15d PGA_2	LMFA03010172	315	271	15.17	(d_4) 15d PGJ_2
	5,6-diHETE	LMFA03060018	335	163	15.30	(d_4) LTB_4
	5,6-DHET	LMFA03050004	337	145	15.31	(d_8) 5-HETE

Table 2-2. *Continued.*

Period	Eicosanoid	LIPID MAPS ID	Precursor Ion	Product Ion	Retention Time	Internal Standard
	(d_4) 13-HODE	LMFA01050359	299	198	15.61	-
	13-HODE	LMFA01050349	295	195	15.68	(d_4) 13-HODE
	(d_4) 9-HODE	LMFA01050353	299	172	15.75	-
	(d_8) 15-HETE	LMFA03060080	327	226	15.75	-
	17-HDoHE	LMFA04000012	343	245	15.81	(d_8) 15-HETE
	9-HODE	LMFA01050278	295	171	15.82	(d_4) 9-HODE
	15-HETE	LMFA03060001	319	219	15.88	(d_8) 15-HETE
5	13-oxoODE	LMFA02000016	293	113	15.97	(d_7) 5-oxoETE
	15-oxoETE	LMFA03060051	317	113	16.07	(d_7) 5-oxoETE
	11-HETE	LMFA03060028	319	167	16.21	(d_8) 5-HETE
	9-oxoODE	LMFA01060177	293	185	16.25	(d_7) 5-oxoETE
	12-HETE	LMFA03060088	319	179	16.40	(d_8) 15-HETE
	8-HETE	LMFA03060006	319	155	16.50	(d_8) 5-HETE
	12-oxoETE	LMFA03060019	317	153	16.51	(d_7) 5-oxoETE
	9-HETE	LMFA03060089	319	151	16.65	(d_8) 5-HETE
	(d_8) 5-HETE	LMFA03060005	327	116	16.88	-
	5-HETE	LMFA03060002	319	115	16.98	(d_8) 5-HETE
	(d_8) 14,15-EET	LMFA03050020	327	226	17.10	-
	14,15-EET	LMFA03080005	319	219	17.22	(d_8) 14,15-EET
	12,13-EpOME	LMFA02000038	295	195	17.29	(d_8) 11,12-EET
	(d_7) 5-oxoETE	LMFA03060083	323	209	17.36	-
6	5-oxoETE	LMFA03060011	317	203	17.44	(d_7) 5-oxoETE
	9,10-EpOME	LMFA02000037	295	171	17.45	(d_8) 11,12-EET
	11,12-EET	LMFA03080004	319	167	17.66	(d_8) 11,12-EET
	(d_8) 8,9-EET	LMFA03050021	327	158	17.72	-
	(d_8) 11,12-EET	LMFA03080011	327	171	17.72	-
	8,9-EET	LMFA03080003	337	127	17.83	(d_8) 8,9-EET
	5,6-EET	LMFA03080002	319	191	18.03	(d_8) 11,12-EET

[1] Gray boxes indicated internal standards.

[2] The retention times are given to indicate the relative elution position of the compounds with the understanding that the absolute values are not significant.

[3] Protectin D_1 and Δ15-Protectin D_1 were a kind gift from Dr. Charles N. Serhan. To minimize their use, these compounds were used in the RT calibration groups (Table 3), but not included in the quantitative standard curve. The structural isomer 10S,17S-DiHDoHE was used as a surrogate primary standard.

Table 2-3. Eicosanoids Groups for LC-MS Identification with "Method 2".

Group	Eicosanoid	LIPID MAPS ID	Precursor Ion (*m/z*)	Product Ion (*m/z*)	Retention Time (min)
	9,10-EpOME	LMFA02000037	295	171	17.50
	12,13-EpOME	LMFA02000038	295	195	17.30
	12,13-diHOME	LMFA01050351	313	183	12.30
	9,10-diHOME	LMFA01050350	313	201	13.70
	15d PGJ_2	LMFA03010021	315	271	14.70
	11,12-EET	LMFA03080004	319	167	17.70
	5,6-EET	LMFA03080002	319	191	18.00
	14,15-EET	LMFA03080005	319	219	17.20
	PGJ_2	LMFA03010019	333	271	10.40
	15d PGD_2	LMFA03010051	333	271	12.50
1	LTB_4	LMFA03020001	335	195	12.50
	8,9-EET	LMFA03080003	337	127	17.80
	PGE_2	LMFA03010003	351	271	7.33
	PGD_2	LMFA03010004	351	271	7.77
	$PGF_{2\alpha}$	LMFA03010002	353	193	7.11
	20cooh LTB_4	LMFA03020016	365	195	4.79
	6k $PGF_{1\alpha}$	LMFA03010001	369	163	4.87
	TXB_2	LMFA03030002	369	169	6.22
	LTE_4	LMFA03020002	438	333	11.00
	LTD_4	LMFA03020006	495	177	10.30
	LTC_4	LMFA03020003	624.6	272	9.89
	13-oxoODE	LMFA02000016	293	113	15.97
	9-oxoODE	LMFA01060177	293	185	16.25
	9-HODE	LMFA01050278	295	171	15.82
	13-HODE	LMFA01050349	295	195	15.68
	15d PGA_2	LMFA03010172	315	271	15.17
	15-oxoETE	LMFA03060051	317	113	16.07
	12-oxoETE	LMFA03060019	317	153	16.51
	5-oxoETE	LMFA03060011	317	203	17.44
	5-HETE	LMFA03060002	319	115	16.98
	9-HETE	LMFA03060089	319	151	16.65
	8-HETE	LMFA03060006	319	155	16.50
	11-HETE	LMFA03060028	319	167	16.21
	12-HETE	LMFA03060088	319	179	16.40
2	15-HETE	LMFA03060001	319	219	15.88
	20-HETE	LMFA03060009	319	289	15.02
	PGA_2	LMFA03010035	333	271	10.18
	6t LTB_4	LMFA03020013	335	195	12.10
	6S-LXA_4	LMFA03040003	351	115	8.96
	5-iso $PGF_{2\alpha}$ VI	LMFA03110011	353	115	6.87
	8-iso $PGF_{2\alpha}$ III	LMFA03110001	353	193	6.25
	PGE_1	LMFA03010134	353	273	7.60
	PGD_1	LMFA03010049	353	273	7.77
	$PGF_{1\alpha}$	LMFA03010137	355	293	7.13
	TXB_1	LMFA03030008	371	171	5.93
	Δ11 LTE_4	LMFA03020022	438	333	11.58
	Δ11 LTD_4	LMFA03020021	495	177	10.99
	Δ11 LTC_4	LMFA03020020	624.6	272	10.68

Table 2-3. *Continued.*

Group	Eicosanoid	LIPID MAPS ID	Precursor Ion (*m/z*)	Product Ion (*m/z*)	Retention Time (min)
3	tetranor PGE_2	LMFA03010032	327	291	3.11
	PGB_2	LMFA03010018	333	271	10.51
	8,15-diHETE	LMFA03060050	335	127	11.61
	5,6-diHETE	LMFA03060018	335	163	15.30
	12epi LTB_4	LMFA03020015	335	195	12.10
	5,15-diHETE	LMFA03060049	335	201	12.06
	PGE_3	LMFA03010135	349	269	6.25
	PGD_3	LMFA03010142	349	269	6.58
	6R-LXA_4	LMFA03040001	351	115	8.62
	$PGF_{3\alpha}$	LMFA03010138	351	193	5.96
	20oh LTB_4	LMFA03020018	351	195	5.10
	11β PGE_2	LMFA03010060	351	271	7.56
	11β dhk $PGF_{2\alpha}$	LMFA03010203	353	113	8.40
	11β $PGF_{2\alpha}$	LMFA03010036	353	193	6.51
	6k PGE_1	LMFA03010012	367	143	5.20
	Δ17 6k $PGF_{1\alpha}$	LMFA03010149	367	163	4.19
	TXB_3	LMFA03030006	367	169	5.27
	20oh PGE_2	LMFA03010014	367	189	3.65
	6,15 dk-,dh- $PGF_{1\alpha}$	LMFA03010013	369	113	6.22
	20oh $PGF_{2\alpha}$	LMFA03010029	369	193	3.35
	dihomo $PGF_{2\alpha}$	LMFA03010157	381	221	9.43
	14,15 LTE_4	LMFA03020033	438	333	9.30
	14,15 LTD_4	LMFA03020032	495	177	8.26
	14,15 LTC_4	LMFA03020031	624.6	272	7.61
4	12-HHTrE	LMFA03050002	279	163	13.87
	8,9-DHET	LMFA03050006	319	155	14.71
	2,3 dinor 11β $PGF_{2\alpha}$	LMFA03010011	325	145	5.07
	tetranor $PGF_{2\alpha}$	LMFA03010139	329	293	3.10
	bicyclo PGE_2	LMFA03010034	333	113	11.36
	HXA_3	LMFA03090005	335	127	14.46
	HXB_3	LMFA03090003	335	183	14.60
	6t,12epi LTB_4	LMFA03020014	335	195	12.20
	5,6-DHET	LMFA03050004	337	145	15.31
	11,12-DHET	LMFA03050008	337	167	14.28
	14,15-DHET	LMFA03050010	337	207	13.82
	17-HDoHE	LMFA04000012	343	245	15.81
	15k PGE_2	LMFA03010031	349	113	7.83
	Resolvin E_1	LMFA03070019	349	195	4.99
	PGK_2	LMFA03010023	349	205	7.48
	15k $PGF_{2\alpha}$	LMFA03010026	351	113	7.67
	dhk PGE_2	LMFA03010031	351	207	8.64
	dhk PGD_2	LMFA03010022	351	207	9.49
	15k $PGF_{1\alpha}$	LMFA03010150	353	113	7.96
	dhk $PGF_{2\alpha}$	LMFA03010027	353	291	8.88
	dh $PGF_{2\alpha}$	LMFA03010079	355	275	8.25
	10S,17S-DiHDoHE	LMFA04000047	359	153	11.83
	19oh PGE_2	LMFA03010024	367	189	3.66
	19oh $PGF_{2\alpha}$	LMFA03010042	369	193	3.48

Table 2-3. *Continued.*

Group	Eicosanoid	LIPID MAPS ID	Precursor Ion (*m/z*)	Product Ion (*m/z*)	Retention Time (min)
5	dihomo PGJ_2	LMFA03010158	361	299	13.08
	dihomo 15d PGD_2	LMFA03010159	361	299	14.20
	dihomo PGE_2	LMFA03010155	379	299	9.79
	dihomo PGD_2	LMFA03010156	379	299	10.13
6	(d_4) 9-HODE	LMFA01050353	299	172	15.75
	(d_4) 13-HODE	LMFA01050359	299	198	15.61
	(d_4) 12,13-diHOME	LMFA01050357	317	185	12.22
	(d_4) 9,10-diHOME	LMFA01050358	317	203	13.58
	(d_4) 15d PGJ_2	LMFA03010177	319	275	14.67
	(d_7) 5-oxoETE	LMFA03060083	323	209	17.36
	(d_6) 20-HETE	LMFA03060082	325	295	14.97
	(d_8) 5-HETE	LMFA03060005	327	116	16.88
	(d_8) 8,9-EET	LMFA03050021	327	158	17.72
	(d_8) 11,12-EET	LMFA03080011	327	171	17.72
	(d_8) 15-HETE	LMFA03060080	327	226	15.75
	(d_8) 14,15-EET	LMFA03050020	327	226	17.10
	(d_4) LTB_4	LMFA03020030	339	197	12.46
	(d_4) dhk PGD_2	LMFA03010178	355	211	9.46
	(d_4) PGE_2	LMFA03010008	355	275	7.31
	(d_4) PGD_2	LMFA03010007	355	275	7.76
	(d_4) $PGF_{2\alpha}$	LMFA03010006	357	197	7.05
	(d_4) dhk $PGF_{2\alpha}$	LMFA03010179	357	295	8.81
	(d_{11}) 5-iso $PGF_{2\alpha}$ VI	LMFA03110012	364	115	6.73
	(d_4) 6k $PGF_{1\alpha}$	LMFA03010037	373	167	4.92
	(d_4) TXB_2	LMFA03030010	373	173	6.20
7	LXB_4	LMFA03040002	351	221	7.56
	PD_1	LMFA04000011	359	153	11.23
	Δ15t-PD_1	LMFA04000045	359	153	11.53
	Resolvin D_1	LMFA04000006	375	141	8.50

[1] Gray boxes indicated internal standards.
[2] The retention times are given to indicate the relative elution position of the compounds with the understanding that the absolute values are not significant.

Chapter 3.

TLR-4 and Sustained Calcium Agonists Synergistically Produce Eicosanoids Independent of Protein Synthesis in RAW264.7 cells

3.A Abstract

Arachidonic acid (AA) is released by phospholipase A_2 (PLA_2) and converted into hundreds of distinct bioactive mediators by a variety of cyclooxygenases (COX), lipoxygenases (LO) and cytochrome P450s. Due to the size and diversity of the eicosanoid class of signaling molecules produced, a thorough and systematic investigation of these biological processes requires the simultaneous quantitation of a large number of eicosanoids in a single analysis. We have developed a robust LC-MS/MS method that can identify and quantitate over 60 different eicosanoids in a single analysis, and applied it to agonist stimulated RAW264.7 murine macrophages. Fifteen different eicosanoids produced through COX and 5-LOX were detected either intracellularly or in the media following stimulation with 16 different agonists of Toll-like receptors (TLR), G protein-coupled receptors, and purinergic receptors. No significant differences in the COX metabolite profiles were detected using the different agonists; however, we determined that only agonists creating a sustained Ca^{2+} influx were capable of activating the 5-LOX pathway in these cells. Synergy between Ca^{2+} and TLR pathways was detected and discovered to be independent of NF-κB induced protein synthesis. This demonstrates that TLR induction of protein synthesis and priming for enhanced PLA_2 mediated eicosanoid production work through two distinct pathways.

3.B Introduction

Arachidonic acid (AA) and its eicosanoid metabolites are associated with a variety of different physiological systems including the central nervous, cardiovascular, gastrointestinal, genitourinary, respiratory, and immune systems. Eicosanoids are formed when phospholipase A_2 (PLA_2) action liberates AA from the sn-2 position of membrane phospholipids [8, 281]. Free AA is then converted into potent bioactive mediators by the action of the various cyclooxygenases (COX), lipoxygenases (LO) and cytochrome P450s. The eicosanoid production cascade often works in a non-linear fashion, with multiple enzymes creating a single product, and multiple products acting as a substrate for a single enzyme. COX activity produces prostaglandins (PG) and hydroxy-eicosatetraenoic acids (HETEs) [4, 5], whereas lipoxygenases can create leukotrienes (LT), HETEs and lipoxins [267, 268, 282, 283]. Cytochrome P450s catalyze the production of HETEs and epoxy-eicosatetraenoic acids, as well as ω-oxidation of various eicosanoids [284]. Other enzymes can further act on eicosanoids by catalyzing hydration, dehydration, and β-oxidation reactions [285]. Eicosanoid producing enzymes and their biological receptors are differentially expressed among various cell and tissue types, enhancing signaling specificity [3]. This is illustrated by Fitzgerald and coworkers [286], who demonstrated that decreased vascular PGE_2 release leads to increased endothelial PGI_2 production, impeding the development of atherogenesis.

Early studies of eicosanoid identification and quantification focused on enzyme-linked immunosorbent assays [269, 270]. This method is reliable for measuring relative changes in the level of an individual eicosanoid; however, specificity deficiencies and cost limitations reduce their usefulness for studying an array of eicosanoids. Gas

Chromatography/Mass Spectrometry (GC/MS) methods were developed that greatly improved upon these limitations [271] and allowed the simultaneous analysis of multiple eicosanoids. One drawback of the GC/MS method is the requirement that eicosanoids be chemically derivatized in order to be volatile for GC chromatography. While a wide variety of derivatization methods have been developed increasing the number of eicosanoids that can be effectively detected, a single derivatization method is not suitable to prepare all of the diverse eicosanoids for GC volatilization. Furthermore, some eicosanoids are ill-suited for any gas phase analysis [272], making GC/MS insufficient for analysis of the entire class.

The development of electrospray ionization (ESI) eliminated the requirement for derivatization by directly ionizing eicosanoids in biological samples. The carboxylate moiety, a prevalent eicosanoid structural feature, readily ionizes in mass spectrometric analysis using ESI. By coupling ESI with triple quadrupole mass spectrometry, eicosanoids can be ionized and their molecular precursor ion $[M - H]^-$ can be subjected to collision induced decomposition to produce a series of distinct product ion fragments. A set of precursor/product ion pairs can be analyzed in a single MS analysis using multiple reaction monitoring (MRM) which, when coupled with high performance liquid chromatography (LC) retention times, will uniquely identify a majority of the eicosanoids. ESI-MRM was first employed in this field by Issakson and coworkers in 1996 to quantitate 14 eicosanoids directly from a biological sample [273]. In 2002 the resolving power of LC was coupled with the sensitivity of ESI-MRM to study 5 eicosanoids from LPS stimulated synovial cells [274]. Recently, Shimizu and coworkers

have developed a high-throughput method that can detect and quantitate 18 different eicosanoids from biological samples [275].

These methods detected a limited subset of eicosanoids that was selected based on previous experiments with a given cell type or disease model. However, more than a hundred unique eicosanoids have been discovered to date, with many having unique biological activities. A thorough investigation of these biological processes requires one to simultaneously analyze a large number of eicosanoids in a single analysis. Analogous to gene array analyses in the genomics field, we have created a library of MS/MS spectra for a large number of eicosanoids and have defined a set of MRM precursor/product ion pairs and an LC system that allows for the identification and quantitation of a large number of these compounds in a single LC-MS/MS run. By using this less biased approach, it should be possible to identify novel eicosanoid signaling networks and efficiently translate this methodology across a diverse array of biological models.

This methodology has now been applied to the study of RAW264.7 macrophages. Macrophages express a number of Toll-like receptors (TLR) [287]. TLRs comprise a family of receptors that recognize specific structures of microbial pathogens, leading to the induction of numerous pro-inflammatory cytokines, COX-2 up-regulation and delayed eicosanoid release. Macrophages also express receptors that can induce rapid changes in intracellular Ca^{2+} levels. Ca^{2+} affects a number of processes within the macrophage, and specifically binds to Group IVA cytosolic PLA_2 ($cPLA_2$) and 5-LOX promoting their translocation to the membrane phospholipid surface [267, 281]. Platelet-activating factor (PAF) and uridine diphosphate (UDP) signal through specific G protein-coupled receptors (GPCR) that create a transient Ca^{2+} spike [288-290]. Non-receptor mediated

ionophores such as ionomycin, and purinergic receptor activation by high levels of adenosine triphosphate (ATP), can produce sustained changes in intracellular Ca^{2+} levels that induce eicosanoid production [288, 290, 291]. Furthermore, the response to Ca^{2+} agonists has been shown to be synergistically increased by priming cells with a 60 minute dose of a TLR activator [288, 292-296], producing more eicosanoid release than the additive amount of TLR and Ca^{2+} stimulation alone. Here, we employed LC-MS/MS methodology to specifically investigate these mechanisms of eicosanoid generation, identifying two distinct eicosanoid profiles. We further investigated the synergy between TLR and Ca^{2+} agonists, and have elucidated details of the mechanism for endotoxin priming and stimulation of eicosanoid production.

3.C Results

3.C.1 Eicosanoid production during long-term TLR activation

We examined two factors that modulate the release of eicosanoids in macrophages are TLR activation and changes in intracellular Ca^{2+} levels. TLR activation initiates many changes in the cell, including the induction of gene expression, changes in protein levels, and changes in protein phosphorylation levels. We have measured changes in eicosanoid release when RAW264.7 cells were activated by long-term exposure to 12 different TLR agonists, which leads to the induction of a number of pro-inflammatory proteins through the transcription factor NF-κB.

We began by qualitatively analyzing the eicosanoids released into the extracellular media of RAW264.7 macrophages when challenged with one of 12 TLR agonists (Table 3-1). A signal was judged to be significant, and the eicosanoid present (+ in shaded cell), if the signal area was three times the noise three standard deviation level. A minus sign indicates that the signal was below this level. In these experiments, we screened all 64 eicosanoids listed in Table 2-1. In all, eight different TLRs were examined. We began with Kdo_2-Lipid A, a nearly homogeneous LPS sub-structure

Table 3-1. Eicosanoids produced by RAW264.7 cells under 21 different conditions.

Agonist	Receptor	Physiological Response	$PGF_{2\alpha}$	PGE_2	PGD_2	PGJ_2	15d PGD_2	15d PGJ_2	dhk $PGF_{2\alpha}$	dhk PGE_2	dhk PGD_2	LTC_4	11t LTC_4	5-HETE	11-HETE	15-HETE	AA
KDO	TLR-4	Toll-like Receptor Agonist	+	+	+	+	+	+	+	+	+	-	-	-	+	+	+
Pam3SCK4	TLR-1/2		+	+	+	+	+	+	+	+	+	-	-	-	+	+	+
HKLM	TLR-2		+	+	+	+	+	+	+	+	+	-	-	-	+	+	+
LTA	TLR-2		+	+	+	+	+	+	+	+	+	-	-	-	+	+	+
Poly(I:C)	TLR-3		+	+	+	+	+	+	+	+	+	-	-	-	+	+	+
LPS	TLR-4		+	+	+	+	+	+	+	+	+	-	-	-	+	+	+
Flagellin	TLR-5		+	+	+	+	+	+	-	-	+	-	-	-	+	+	+
FSL-1	TLR-6/2		+	+	+	+	+	+	+	+	+	-	-	-	+	+	+
Zymosan	TLR-6/2		+	+	+	+	+	+	+	+	+	-	-	-	+	+	+
Imiquimod	TLR-7		+	+	+	+	+	+	+	+	+	-	-	-	+	+	+
Gardiquimod	TLR-7		+	+	+	+	+	+	+	+	+	-	-	-	+	+	+
ODN1826	TLR-9		+	+	+	+	+	+	+	+	+	-	-	-	+	+	+
KDO	TLR-4	TLR-priming	+	+	+	+	+	-	-	-	-	-	-	-	+	+	+
PAF	PAFr	Transient Ca^{2+} Spike	+	+	+	+	+	-	-	-	-	-	-	-	+	+	+
KDO, PAF	TLR-4, PAFr		+	+	+	+	+	-	-	-	-	-	-	-	+	+	+
UDP	P2Y6		+	+	+	+	+	-	-	-	-	-	-	-	+	+	+
KDO, UDP	TLR-4, P2Y6		+	+	+	+	+	-	-	-	-	-	-	-	+	+	+
Iono	Ionophore	Sustained Ca^{2+} Modulator	+	+	+	+	+	-	-	-	-	+	+	+	+	+	+
KDO, Iono	TLR-4,		+	+	+	+	+	-	-	-	-	+	+	+	+	+	+
ATP	General P2		+	+	+	+	+	-	-	-	-	+	+	+	+	+	+
KDO, ATP	TLR-4, P2		+	+	+	+	+	-	-	-	-	+	+	+	+	+	+

LPS, consisting of lipid A and an attached 3-keto-D-*manno*-octulosonic acid disaccharide. The highly variable carbohydrate chains that are present on natural LPS have been removed, and the Lipid A portion of the molecule has a fatty acid composition that is greater than 90% homogeneous. Kdo_2-Lipid A binds to and activates only the TLR-4 receptor [297]. While we looked for each of the 64 different eicosanoids, when RAW264.7 cells were challenged with Kdo_2-Lipid A for 12 hours, only compounds produced by the COX pathway were detected. COX derived $PGF_{2\alpha}$, PGE_2, and PGD_2 were released, and prostaglandin PGD_2 dehydration metabolites PGJ_2, 15d PGD_2, and 15d PGJ_2 were also detected. Additionally, oxidation metabolites 13,14-dihydro-15-keto $PGF_{2\alpha}$ (dhk $PGF_{2\square}$, 13,14-dihydro-15-keto PGE_2 (dhk PGE_2, and 13,14-dihydro-15-keto $PGD_{2\alpha}$ (dhk PGD_2 were identified. The potential side-products of COX action on AA, 11-HETE and 15-HETE, were also detected. Their formation was completely inhibited by the COX inhibitor indomethacin (data not shown), confirming that they are being generated by the COX enzymes.

The eicosanoid release profiles of TLRs-1 through -7 and TLR-9, when stimulated with the appropriate receptor specific agonists for 12 hrs, were the same as that seen with Kdo_2-Lipid A. The one exception was that in response to the TLR-5 agonist, flagellin, dhk $PGF_{2\square}$ or dhk PGE_2 were not detected. In these experiments, we employed levels of agonist within the range suggested by Invivogen, but did not attempt to maximize the response. Therefore, the absolute levels of the response do not necessarily represent maximal responses, and only the relative eicosanoid profiles should be compared.

We then narrowed our focus and repeated these experiments quantitating only those compounds detected in the screen. This examination of long-term Kdo_2-Lipid A stimulation of TLR-4 showed that PGD_2 was the most abundant eicosanoid released (Figure 3-1). Though not as substantial as PGD_2 levels, PGE_2 and $PGF_{2\alpha}$ levels were also significantly increased. Metabolites of PGD_2 resulting from a single dehydration (PGJ_2 and 15d PGD_2) were higher than the double dehydration product 15d PGJ_2. Activation of TLRs -1, -2, -4, -6, -7 and -9 all produced significant levels of PGs, releasing greater than 70 ng/1x10^6 cells of PGD_2 in 12 hrs, whereas TLR-3 activation by Poly (I:C) only induced a moderate activation (9 ng/1x10^6 cells PGD_2). While each of these TLR specific agonists produced different absolute levels of PGs, none altered the relative eicosanoid profile from the one induced by Kdo_2-Lipid A. Flagellin, the TLR-5 agonist, did not lead to an increase in eicosanoid production over control levels under the conditions employed in RAW264.7 cells.

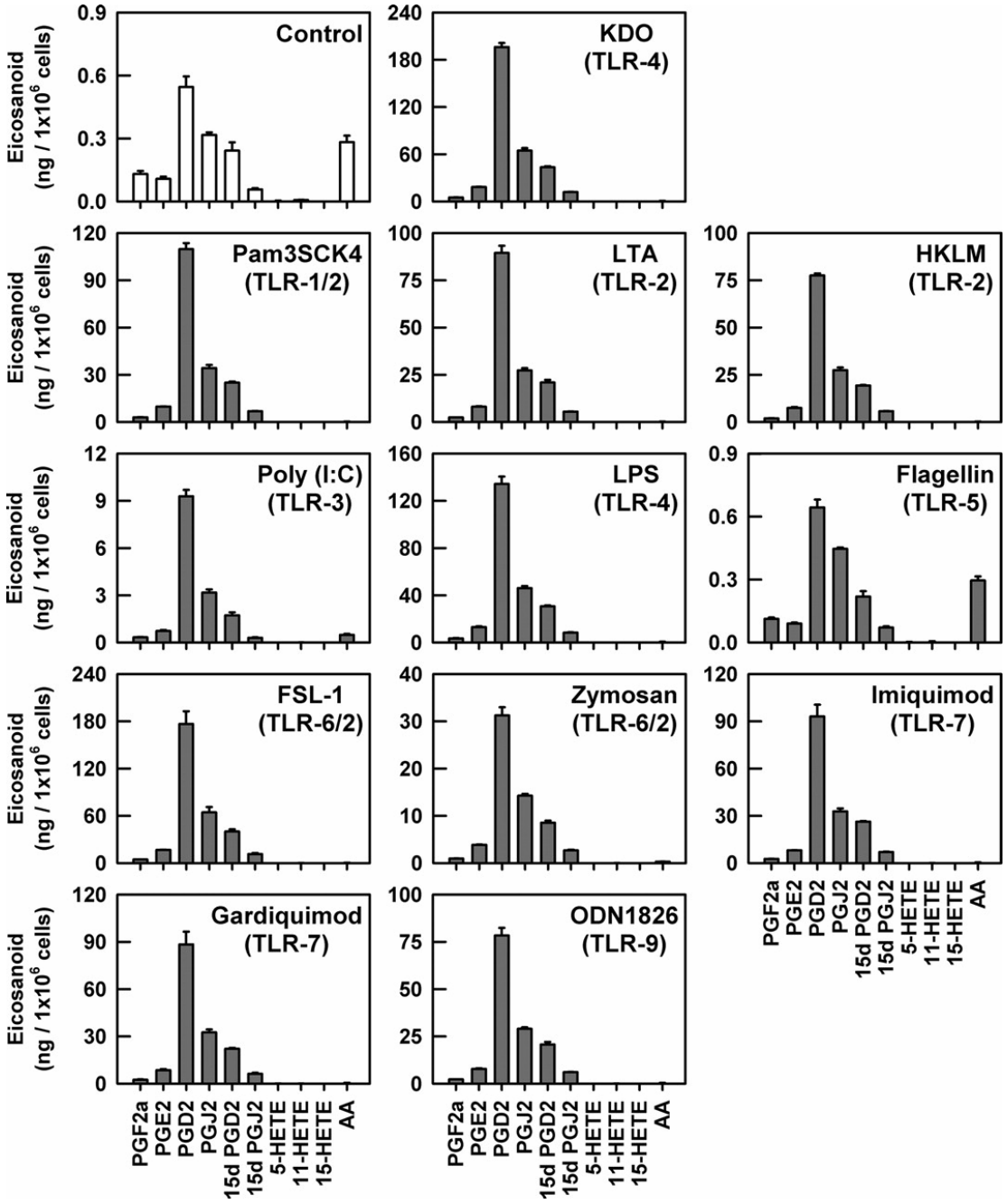

Figure 3-1. TLR agonist stimulated eicosanoid production profiles. RAW264.7 cells were stimulated with the following TLR receptor agonists: Kdo_2-Lipid A (KDO, TLR-4, 100 ng/ml), Pam3SCK4 (TLR-1/2, 1 µg/ml), LTA (TLR-2, 1 µg/ml), HKLM (TLR-2, 10^8 cells/ml), Poly(I:C) (TLR-3, 50 µg/ml), LPS (TLR-4, 100 ng/ml), Flagellin (TLR-5, 50 ng/ml), FSL-1 (TLR-6/2, 1 µg/ml), Zymosan (TLR-6/2, 500 ng/ml), Imiquimod (TLR-7, 5 µg/ml), Gardiquimod (TLR-7, 1 µg/ml), ODN1826 (TLR-9, 1 µM). Extracellular media was removed at 12 hours and analyzed for eicosanoid levels by mass spectrometry. A representative experiment is shown, and the data is expressed as mean values ± S.D. of three individual replicates.

3.C.2 Eicosanoid production during short-term Ca^{2+} agonist activation

Eicosanoid release is also regulated by increasing intracellular Ca^{2+} levels, which facilitate the translocation of eicosanoid producing enzymes, such as $cPLA_2$ and 5-LOX, to the phospholipid membrane [267, 281] where they can actively generate eicosanoid metabolites. Ca^{2+} fluxes can occur in two distinct modes [288, 290]. The release of intracellular Ca^{2+} stores causes a transient spike which quickly returns to near basal levels, whereas changes in the permeability of the plasma membrane create a sustained Ca^{2+} elevation from the influx of extracellular Ca^{2+}. Both of these Ca^{2+} changes occur within seconds of activation. In these studies, four short-term stimuli that modified Ca^{2+} levels were examined. PAF and UDP stimulate GPCRs and give rise to a transient Ca^{2+} spike [288, 290], while ionomycin and ATP produce sustained increases in Ca^{2+} levels.

The qualitative analysis of PAF and UDP stimulation are shown in Table 3-1. Following a 10 minute stimulation with PAF or UDP, COX derived $PGF_{2\alpha}$, PGE_2, PGD_2, 11-HETE and 15-HETE were released, and PGD_2 dehydration metabolites PGJ_2 and 15d PGD_2 were detected (Table 3-1). 15d PGJ_2 and the three dhk PGs were not detected. 15d PGJ_2 was presumably not detected because it requires two separate dehydration steps which require a longer period of time to occur; even after 60 minutes of Kdo_2-Lipid A stimulation 15d PGJ_2 was not detected. Likewise, PG breakdown into dhk $PGF_{2\alpha}$, dhk PGE_2, and dhk PGD_2 requires an oxidation and a reduction, and these products were not detected. Again, none of the other 64 eicosanoids were detected. The quantitative analysis demonstrated that the foremost eicosanoids released in these pathways were PGD_2 and AA (Figure 3-2). The PGD_2 levels were between 0.3 ng/1x10^6 cells for PAF

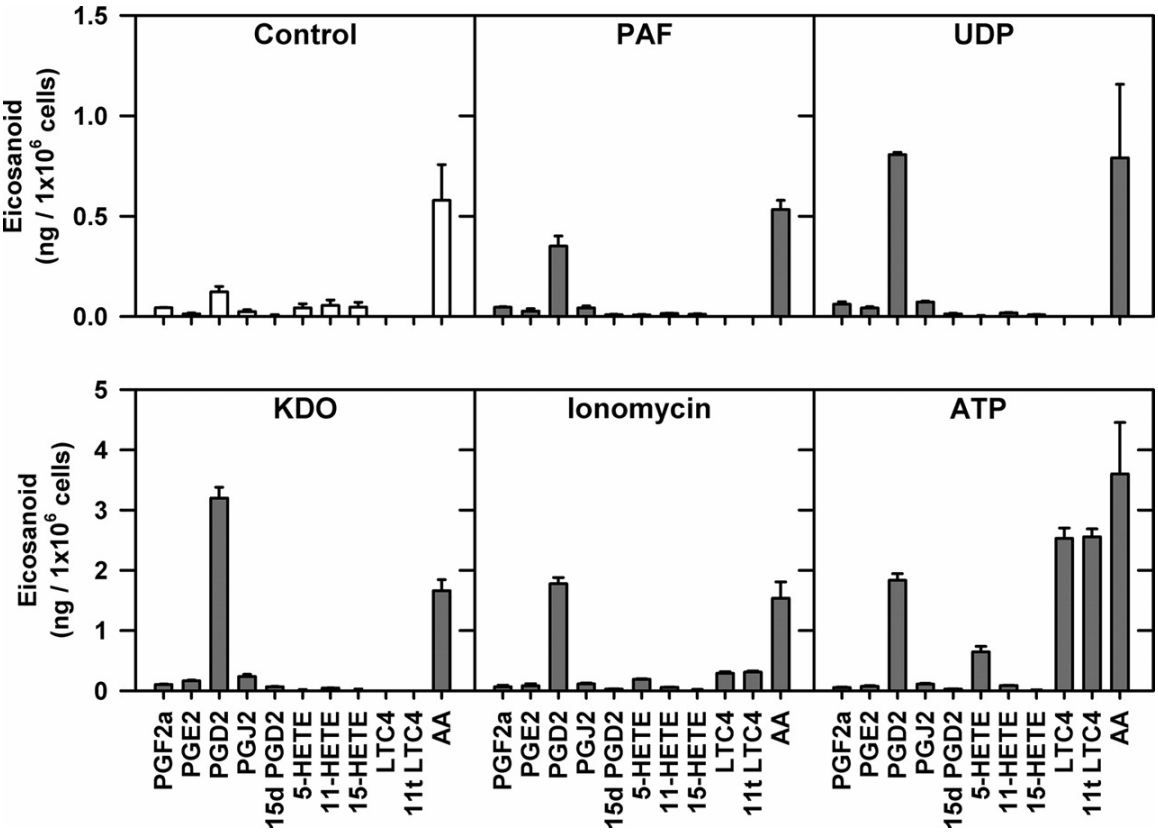

Figure 3-2. GPCR and sustained Ca^{2+} stimulated eicosanoid production profiles. RAW264.7 cells were stimulated for 10 minutes with GPCR agonists (100 nM PAF, 25 μM UDP) and sustained Ca^{2+} modulators (1 μM ionomycin, 2 mM ATP). Cells were also stimulated for 60 minutes with 100 ng/ml Kdo_2-Lipid A. Extracellular media was removed at the indicated time points, extracted and analyzed for eicosanoid levels by mass spectrometry. A representative experiment is shown, and the data is expressed as mean values ± S.D. of three individual replicates.

and UDP stimulated eicosanoid production, these experiments were performed in the presence of 2 mM EGTA (data not shown). The level of eicosanoid release was unaffected by the removal of extracellular calcium using EGTA, confirming that intracellular calcium stores play a primary role in activating eicosanoid production in response to these two agonists. This supports data by Asmis and coworkers [288], who demonstrated that the calcium spike generated by PAF in murine macrophages does not require extracellular Ca^{2+}.

Millimolar concentrations of ATP [290], which activate both P2Y and P2X purinergic receptors, and ionomycin [288], a Ca^{2+} ionophore, both produce sustained Ca^{2+} levels in the cell in addition to inducing a transient Ca^{2+} spike like PAF and UDP. The qualitative screen of RAW264.7 cells challenged by either 2 mM ATP or ionomycin showed that these agonists were capable of generating every eicosanoid produced by PAF or UDP stimulation, and in addition activated the 5-LOX pathway. Significant levels of 5-HETE, LTC_4 and its heat-induced isomer 11t LTC_4 were detected. While ionomycin produced 2 ng/1x10^6 cells of PGD_2 and less than 0.5 ng/1x10^6 cells of the LTC_4s, ATP stimulation produced 2.5 ng/1x10^6 cells of both LTC_4 and PGD_2. LTC_4, 11t-LTC4 and 5-HETE production was completely inhibited by the 5-LOX inhibitor zileuton (data not shown). Furthermore, when 2 mM EGTA was added extracellularly, it completely blocked the production of 5-LOX products without significantly affecting COX activity (data not shown), confirming the role of a sustained Ca^{2+} influx in the activation of this pathway. It also demonstrated that the transient spike of Ca^{2+} from the internal stores was insufficient for this activation.

This is significantly less than the levels of PGs seen in the long-term stimulations. Presumably, 12 hours of TLR activation allows for more time to release AA and up-regulate eicosanoid producing proteins such as COX-2. For comparison, a 60 minute stimulation of Kdo_2-Lipid A produced a similar profile to UDP and PAF, generating all of the eicosanoids produced by long-term Kdo_2-Lipid A except 15d PGJ_2, dhk $PGF_{2\alpha}$, dhk PGE_2, and dhk PGD_2. It should be noted that the PGD_2 level at 60 minutes represents a ten fold activation over control, and that while this is larger than any of the Ca^{2+}

agonists, it pails in comparison to the several hundred fold activation seen in long-term TLR stimulations.

3.C.3 Spatial and time dependence of eicosanoid production

The analysis of 16 agonists showed that only millimolar ATP or ionomycin exhibited significant differences in the eicosanoid profile, presumably due to the sustained elevation of Ca^{2+}. In order to explore the nature of these differences, we chose to compare the eicosanoid secretion and degradation over time between short-term purinergic activation with ATP and the long-term activation with the TLR-4 specific agonist Kdo_2-Lipid A. In doing so, we also compared the levels of secreted eicosanoids to their levels inside the cell.

Kdo_2-Lipid A stimulation caused intracellular AA levels to rise dramatically, peaking at 1 hour and returning to basal levels by 4 hours (Figure. 3-3); extracellular AA followed the same temporal release pattern. COX-derived 11-HETE, but not lipoxygenase derived 5-HETE, was produced in response to Kdo_2-Lipid A, peaking at 1 hour and slowly returned to basal levels by 12 hours. $PGF_{2\alpha}$ and PGE_2 were released into the extracellular media at a constant rate over 24 hours. Extracellular PGD_2, however, increases until 8 hours, then began to slowly decline. This decline appears to be due in large part to increases in PGD_2 metabolites PGJ_2, 15d PGD_2, and 15d PGJ_2. Significantly elevated levels of PGJ_2 were detected after 2 hours of stimulation, 15d PGD_2 after 4 hours, and 15d PGJ_2 after 8 hours. The sum of the levels of PGD_2 and its dehydration

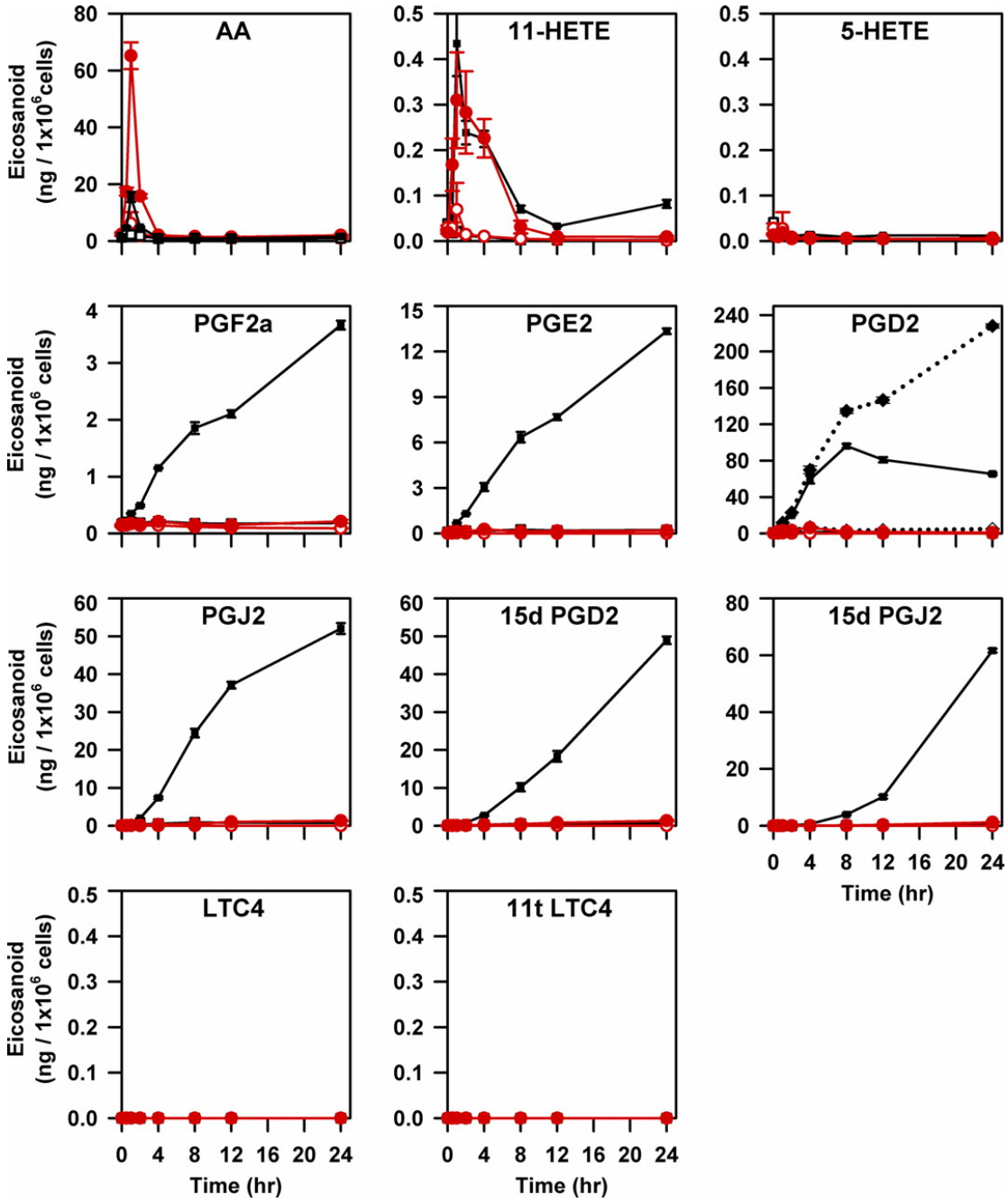

Figure 3-3. Kdo_2-Lipid A stimulated intracellular and extracellular eicosanoids production. RAW264.7 cells were incubated in the absence (open symbols) and presence (closed symbols) of 100 ng/ml Kdo_2-Lipid A, and then subsequently extracellular (black squares) and intracellular (red circles) eicosanoid levels were determined at the indicated times over a 24 hour period by mass spectrometry. For PGD_2 production, the dashed line represents the sum of PGD_2, PGJ_2, 15d PGD_2 and 15d PGJ_2 detected at the indicated time point. A representative experiment is shown, and the data is expressed as mean values ± S.D. of three individual replicates.

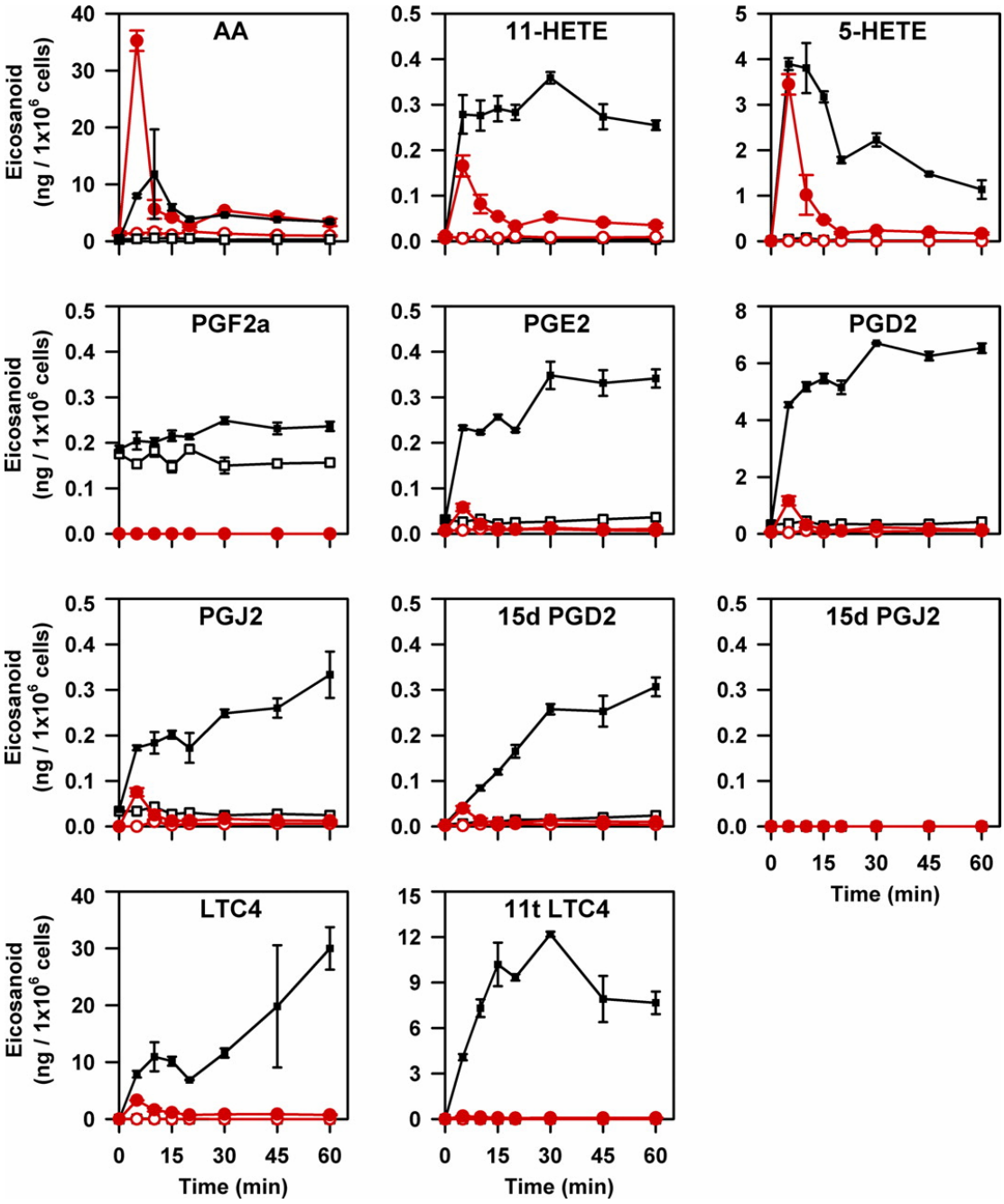

Figure 3-4. ATP stimulated intracellular and extracellular eicosanoids production. RAW264.7 cells were incubated in the absence (open symbols) and presence (closed symbols) of 2 mM ATP, and then subsequently extracellular (black squares) and intracellular (red circles) eicosanoid levels were determined at the indicated times over a 60 minute period by mass spectrometry. A representative experiment is shown, and the data is expressed as mean values ± S.D. of three individual replicates.

metabolites continue to increase similar to PGE_2 and $PGF_{2\alpha}$. PGs and their metabolites were not detected intracellularly during the 24 hour stimulation period.

ATP activation of purinergic receptors created a sustained Ca^{2+} influx and rapid production of eicosanoids by RAW264.7 cells (Figure 3-4). Intracellular AA levels peaked during the first 5 minutes of stimulation, and returned to near-basal levels by 10 minutes. AA was also released into the extracellular media during the initial 5 minutes, and remained elevated throughout the time-course. 11-HETE and 5-HETE, products of COX and 5-LOX respectively, were maximally released within minutes of activation. 11-HETE remained stable in the extracellular media, while 5-HETE levels slowly dropped over the 60 minute time-course.

PGE_2 and PGD_2 were released within minutes of ATP stimulation, and their levels remained constant for the remainder of the one hour time-course, whereas PGJ_2 and 15d PGD_2 continued to increase. LTC_4 showed a biphasic release, with a burst of LTC_4 released in the first 5 minutes, followed by a gradual release after 15 minutes. However, the second phase of this response was not reproducible. 11t LTC_4 increases during the first 15 minutes, and then remains constant for the remainder of the time-course. Small but detectable levels of PG and LT metabolites were detected inside the cell at 5 minutes, but by 10 minutes these metabolites were detected only in the extracellular media.

3.C.4 Synergy between TLR and Ca^{2+} activations

Individually, both Kdo_2-Lipid A and Ca^{2+} agonists can stimulate eicosanoid production in macrophage cells. Previous work has also demonstrated that the level of eicosanoid release can be modulated by adding these agonists together [288, 294-296]. Specifically, Aderem and coworkers showed that adding the TLR-4 agonist LPS for 60 minutes primed murine macrophages for enhanced eicosanoid release by Ca^{2+} agonists [292, 293].

We studied RAW264.7 cells stimulated with Kdo2-Lipid A and Ca^{2+} agonists to determine if these pathways were overlapping, additive or synergistic in activating eicosanoid production. To identify the nature of interaction between activation pathways, we calculated a synergistic activation ratio (Equation 1):

$$\text{Eq. 1} \qquad \text{Synergistic Activation} = \frac{[\text{KDO} + Ca^{2+}\ \text{Agonist}]}{[\text{KDO}] + [Ca^{2+}\ \text{Agonist}]}$$

where [KDO] is the quantity of eicosanoid produced by KDO alone, [Ca^{2+} Agonist] is the quantity of the eicosanoid produced by the Ca^{2+} agonist alone, and [KDO + Ca^{2+} Agonist] is the quantity of the eicosanoid produced by stimulation with both agonists. If the agonists act on separate independent pathways, the eicosanoid production would be additive and the synergistic activation ratio would be 1. If the two agonists activate the same pathway, their outputs would overlap and the maximum combined output would not be greater that that of either agonist alone. In this case, the ratio would be less than the sum of each pathways separately and would drop below 1. Lastly, if these agonists combine to synergistically generate more eicosanoids than the sum of the individual

pathways, the activation ratio would be greater than 1 and indicate a synergistic activation.

To this end, RAW264.7 cells were stimulated with Kdo_2-Lipid A for 50 minutes followed with a 10 minute dose of one of four Ca^{2+} agonists: PAF, UDP, ionomycin or ATP. The synergistic activation ratios are presented in Figure 3-5. Within experimental error, the ratios for the PGs in PAF and UDP were 1. The only exception was that the 11-HETE was elevated with UDP. In contrast, Kdo_2-Lipid A enhanced ionomycin stimulated LTC_4 and AA release by about 8 fold, and ATP release of these metabolites by about 3 fold. PG release, however, was not enhanced by priming by either ATP or ionomycin. Again, 11-HETE was the exception, showing some enhanced release that was midway between the 5-LOX products and the PGs.

Activation of the TLR-4 receptor is known to activate NF-κB induced protein synthesis, particularly COX-2, and this has long been thought to be the mechanism which primes macrophages for enhanced eicosanoid production [11, 295, 296]. To examine this possibility, protein levels of $cPLA_2$ COX-1, COX-2, 5-LOX and 5-LOX activating protein (FLAP) were assessed by Western blot, and did not noticeably change during the first hour of Kdo_2-Lipid A stimulation (Figure 3-6A). The levels of $cPLA_2$ phosphorylated at serine 505 (p-$cPLA_2$ (S505)), which have been reported to modulate protein activity within the cell [11], also did not change significantly. Cell lysates were further analyzed for $cPLA_2$ activity with our *in vitro* assay (Figure.3-6B). This assay measures activity under controlled conditions suitable for $cPLA_2$. We did not detect a significant change in the level of $cPLA_2$ activity following either stimulation with

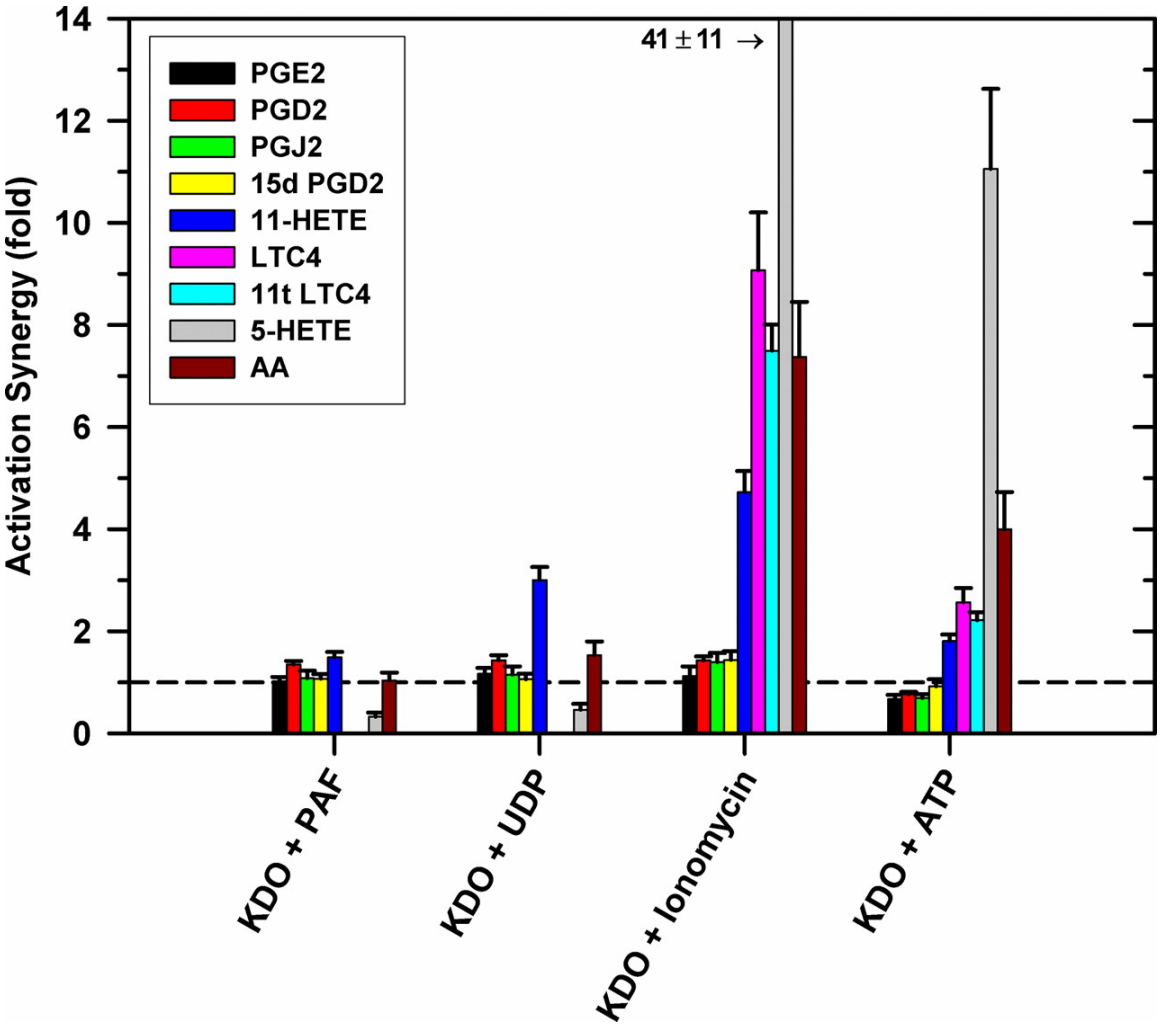

Figure 3-5. Synergistic activation of eicosanoid release between Kdo_2-Lipid A and Ca^{2+} Agonists. RAW264.7 cells were incubated with vehicle or 100 ng/ml Kdo_2-Lipid A for 60 minutes. During the last 10 minutes, cells from both conditions were incubated with vehicle, 100 nM PAF, 25 μM UDP, 1 μM ionomycin or 2 mM ATP. Extracellular media was removed and analyzed for eicosanoid levels by mass spectrometry. The synergistic activation ratios were calculated via Equation 1. A representative experiment is shown, and the data is expressed as mean values ± S.D. of three individual replicates.

Kdo_2-Lipid A or ATP. Since both the level of protein, detected by Western blot, and the level of $cPLA_2$ activity, analyzed by *in vitro* assay, did not change, it appears that both stimuli lead to activation of the preexisting $cPLA_2$, but do not increase the enzyme's level

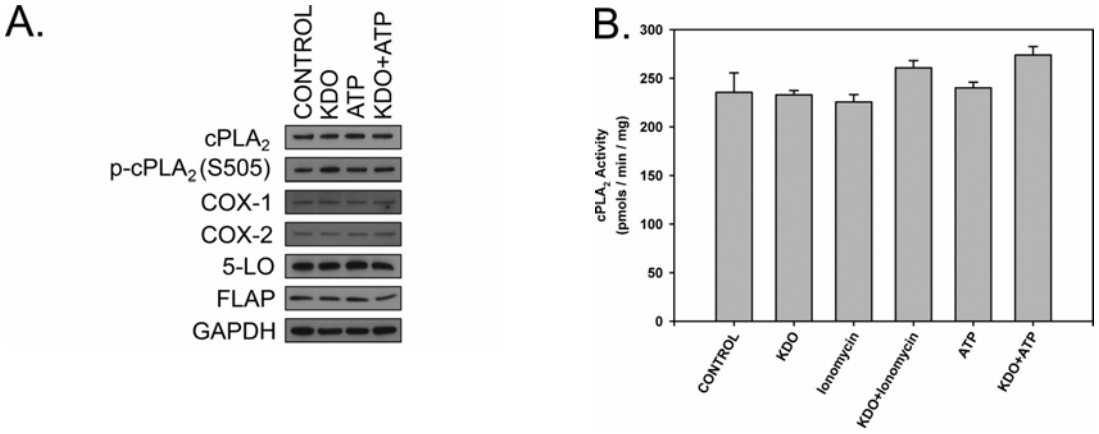

Figure 3-6. Selected protein levels in Kdo_2-Lipid A primed RAW264.7 cells. RAW264.7 cells were incubated with vehicle or 100 ng/ml Kdo_2-Lipid A for 60 minutes. During the last 10 minutes, cells from both conditions were incubated with vehicle or 2 mM ATP. (A) Cell lysates were analyzed by Western blot analysis using antibodies for p-$cPLA_2$ (S505), $cPLA_2$, COX-1, COX-2, 5-LOX, FLAP and GAPDH. (B) Cell lysates were analyzed for $cPLA_2$ enzyme activity using the group specific Dole assay.

nor its phosphorylation state. This does not eliminate protein synthesis as a mechanism for eicosanoid production by TLR activation during the first hour. In fact, Kdo_2-Lipid A activation of TLR-4 directly induced PG synthesis during the first hour was inhibited by ActD and CHX, which block the transcription and translation of cellular proteins, respectively (Figure 3-7A). Inhibition of NF-κB with BAY also reduced PG synthesis by 60 to 90 %, implicating this transcription factor in the production of protein required for eicosanoid release in the first hour of stimulation. On the other hand, ATP stimulation of the purinergic receptors was only slightly blunted (10-30% inhibition) by these inhibitors (Figure 3-7B), indicating that little or no *de novo* protein synthesis is required for the short-term ATP response and that the constitutive enzyme levels are sufficient to produce these eicosanoid levels.

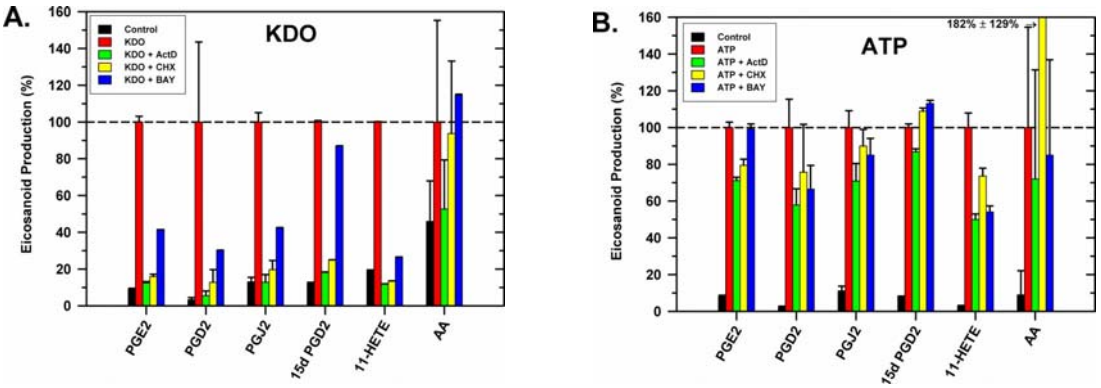

Figure 3-7. Protein synthesis in discrete Kdo_2-Lipid A and ATP stimulation. RAW264.7 cells were incubated with vehicle, 10 μM ActD, 10 μM CHX, or 10 μM BAY for 30 minutes prior to stimulation. Cells were stimulated with (A) 100 ng/ml Kdo_2-Lipid A for 60 minutes or (B) 2 mM ATP for 10 minutes. Extracellular media was removed at the indicated time points, extracted and analyzed for eicosanoid levels by mass spectrometry. Eicosanoids were expressed as relative amounts to stimulation in the absence of inhibitor. A representative experiment is shown, and the data is expressed as mean values ± S.D. of three individual replicates.

To determine if protein synthesis was required for the synergistic enhancement of ATP induced eicosanoid synthesis, RAW264.7 cells were stimulated with Kdo_2-Lipid A for 50 minutes and followed with a 10 minute dose of ATP in the presence of 3 inhibitors: ActD, CHX, and BAY (Figure 3-8). As expected, these inhibitors reduced the absolute eicosanoid levels produced by combined Kdo_2-Lipid A and ATP stimulation. Interestingly, the inhibition of protein synthesis did not appear to inhibit Kdo_2-Lipid A synergistic activation of leukotriene or AA release. Furthermore, direct inhibition of NF-κB activity by BAY also did not affect the synergy between these pathways. To help confirm this finding, a second inhibitor of NF-κB activation, 6-Amino-4-(4-phenoxyphenylethylamino) quinazoline, was tested. At a 50 nM dose, this compound

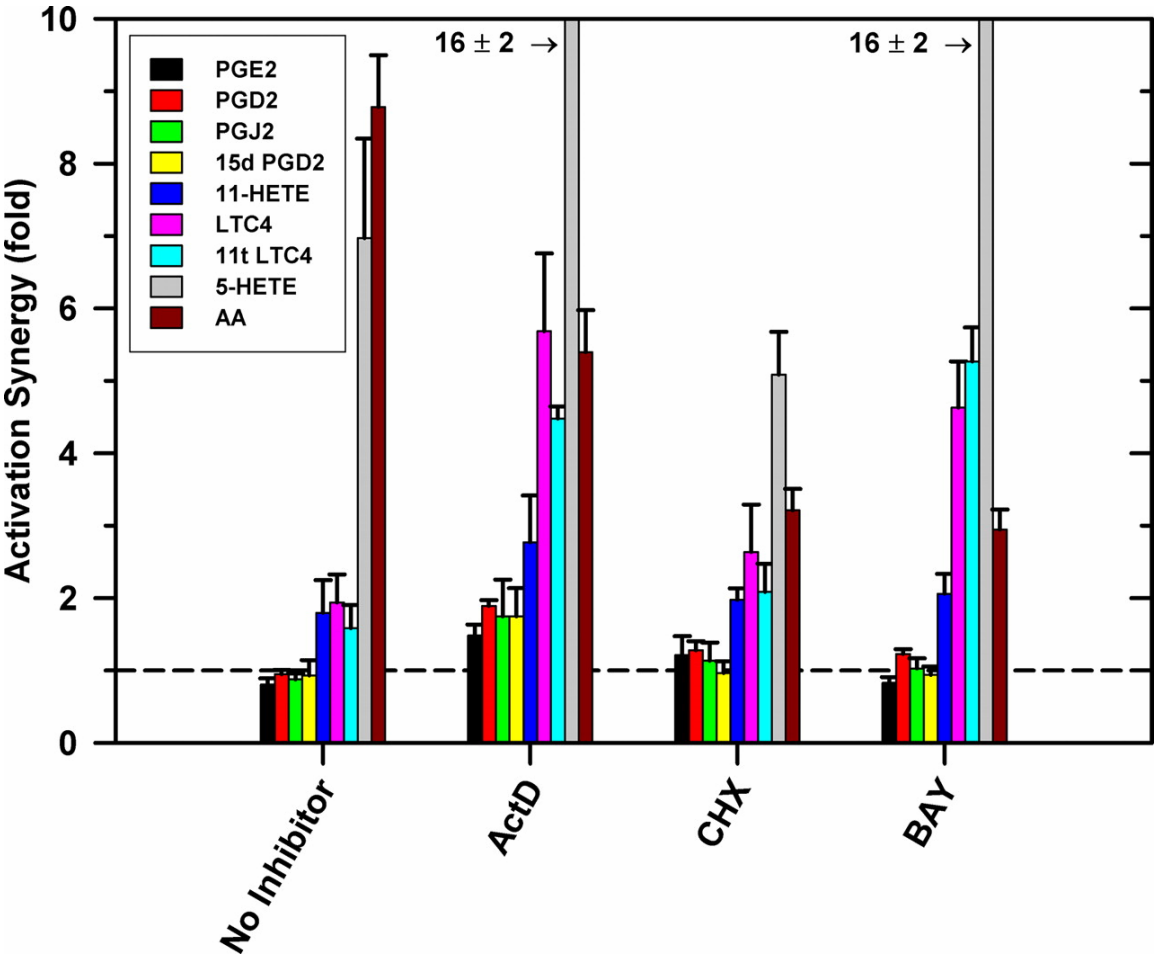

Figure 3-8. Protein synthesis in Kdo_2-Lipid A and ATP synergistic activation. The synergistic activation ratios for Kdo_2-Lipid A and ATP were analyzed in the presence of vehicle, 10 μM ActD, 10 μM CHX, or 10 μM BAY, incubated for 30 minutes prior to stimulation. RAW264.7 cells were incubated with either. vehicle or 100 ng/ml Kdo_2-Lipid A for 60 minutes; during the last 10 minutes, cells from both conditions were incubated with either. vehicle or 2 mM ATP. Extracellular media was removed and analyzed for eicosanoid levels by mass spectrometry, and the synergistic activation ratios were calculated via Equation 1. A representative experiment is shown, and the data is expressed as mean values ± S.D. of three individual replicates.

did not affect Kdo_2-Lipid A and ATP synergy (data not shown). Taken together, this demonstrates that, although inhibitors of protein synthesis blocked Kdo_2-Lipid A stimulated eicosanoid release and blunted ATP stimulated release, they did not prevent Kdo_2-Lipid A from priming for enhanced ATP stimulated eicosanoid release.

3.D Discussion

3.D.1 Eicosanoid profiles in RAW264.7 cells

Macrophages express a large number of distinct TLRs, G protein-coupled receptors, and purinergic receptors. When stimulated, these receptors activate $cPLA_2$ to liberate AA from membrane phospholipids and generate an eicosanoid response by distinctly different pathways. It was anticipated that by using a diverse array of macrophage stimuli a number of different eicosanoid profiles would be generated which could indicate the presence of agonist specific responses. To test this hypothesis, we examined the eicosanoid profiles of RAW264.7 cells stimulated with 16 different agonists.

We found that 14 of the 16 agonists produced the same eicosanoid profile. This profile was dominated by COX products, and by far the largest eicosanoid produced was PGD_2 and its dehydration products PGJ_2, 15d PGJ_2, and 15d PGD_2. For long-term TLR-4 stimulation, this result is consistent with the observations that the levels of COX-2 dramatically increase over this time period, whereas at the same time 5-LOX activity is impaired by subsequent nitric oxide production

It was surprising that the GPCR agonists UDP and PAF exhibited the same profile as TLR agonists since they induce a transient Ca^{2+} spike which activates eicosanoid synthesis within 10 minutes, well before gene expression and protein synthesis could significantly alter protein levels. Thus, in contrast GPCR agonists should induce eicosanoid synthesis via basally expressed enzymes, which include 5-LOX and relatively small amounts of COX. Yet, these two agonists induced similar COX-dependent PGD_2 dominated profiles as the TLRs.

The uniformity of the eicosanoid profile in response to these agonists was particularly striking in light of the fact that macrophages obtained from *in vivo* sources do yield different eicosanoid profiles, as shown by studies that modulate diet [286, 298] and studies in which different methods of macrophage elicitation are employed [275]. Furthermore, a comparative study of human atherosclerotic plaques [299] showed that macrophages in unstable plaques have a significantly higher ratio of PGE_2 to PGD_2 synthase than stable plaque macrophages. In this study, plaque stability was attributed to changes in the PGE_2 and PGD_2 synthase levels. The obvious difference between *in vivo* macrophages and the RAW264.7 cells is that the differentiation process occurs in different environments. Thus, it is possible that the eicosanoid profile was set during monocyte to macrophage differentiation when the RAW264.7 cell line was first generated.

Only one of the receptor mediated responses investigated, purinergic activation by millimolar levels of ATP, produced a different eicosanoid profile in RAW264.7 cells. In addition to producing COX-derived eicosanoids previously detected from other short-term agonists, ATP activated the 5-LOX pathway leading to the production of LTC_4. ATP can activate both the P2Y GPCRs to produce a transient Ca^{2+} spike, and P2X cation channels to generate sustained elevated Ca^{2+} levels [290]. However, of all the purinergic receptors, only the $P2X_7$ requires millimolar levels of ATP for activation [300, 301]. This receptor is expressed and functional in RAW264.7 cells, and Balboa and coworkers have shown that this receptor is responsible for the majority of AA-derived metabolite release in response to 2 mM ATP stimulation in murine macrophages [291]. Peripheral tissue cells

contain millimolar levels of ATP in the cytosol, and release cytosolic ATP during cellular stress and non-physiological necrosis [302, 303].

The eicosanoid profile generated by ATP stimulation was also seen with ionomycin stimulation. Ionomycin is a Ca^{2+} ionophore which also creates a sustained Ca^{2+} mobilization in murine macrophage cells [288]. In both cases, the emergence of 5-LOX products was accompanied by higher (3 to 4 fold) levels of PG release when compared to PAF and UDP. In the case of ATP, the 5-LOX products were produced in equivalent amounts to the PGs. Thus, ATP stimulation not only turns on the 5-LOX pathway but also enhances the total eicosanoid production. This response is presumably due to the extended elevated Ca^{2+} levels, which are required for 5-LOX activity in this model. These levels would keep $cPLA_2$ at the membrane longer and would last long enough to see the activation of the 5-LOX.

3.D.2 Intracellular eicosanoid levels

During these studies, we have also examined the eicosanoid levels inside the cell. Kdo_2-Lipid A induced an intracellular AA release, which peaked at 60 minutes and receded as extracellular prostaglandin levels began to rise. The AA inside the cell was approximately 4 times greater than the amount detected outside. Given the large difference between the volume of the cell and volume of extracellular media, the intracellular concentration of AA would be significant. 11-HETE was also detected inside the cell at a level roughly equal to the extracellular level. These findings confirm the observations of Balsinde and coworkers [304], who also saw increases in intracellular AA-derived compounds following [^{3}H]AA labeling of phospholipids and stimulation of

$P388D_1$ murine macrophages. Significant levels of prostaglandins and their metabolites were not detected intracellularly during long-term Kdo_2-Lipid A stimulation.

Similar results were observed for the short-term Ca^{2+} based stimulation. Within 5 minutes of stimulation, ATP generated a spike of free AA which dissipated by 10 minutes. The AA peak coincided with the burst of PGs, LTs and HETEs that were also released in the first 5 minutes of ATP stimulation. Similar to Kdo_2-Lipid A, AA spiked inside the cell approximately 4 times higher than secreted levels. In addition to AA, small but detectable levels of PGs and LT could be detected intracellularly at 5 minutes after stimulation with ATP. By 10 minutes, eicosanoid levels returned to those found in the controls. Taken together, this suggests that the eicosanoids do not build up in RAW264.7 cells, but instead are rapidly secreted.

It has been reported that the PGD_2 metabolite 15d PGJ_2 could be detected intracellularly using a monoclonal antibody [285], and suggested that it initiates an anti-inflammatory response through the transcription factor PPAR-λ. We were unable to detect significant levels of 15d PGJ_2 in the cells at any time during our studies, indicating that at least 98% of this metabolite remained outside the cell. If 15d PGJ_2 is binding to PPAR-□in RAW264.7 cells, it is either being reabsorbed or the levels needed to activate PPAR-□ are so low that they are below our 5 pg detection limit.

3.D.3 TLR and Ca^{2+} synergy

We have previously shown that incubating macrophages with LPS acts to prime them for enhanced eicosanoid production in response to the Ca^{2+} agonist PAF [288, 295, 296]. In that work, $P388D_1$ cells were primed with LPS prior to activation with PAF, creating enhanced release of [^{3}H]AA metabolites that was decreased in the presence of protein synthesis inhibitors ActD and CHX. This led to the hypothesis that TLR-4 induced protein synthesis, presumably COX-2, was responsible for priming the cells for a Ca^{2+} burst, which would activate $cPLA_2$ to synthesize PGs.

In the present study, we investigated TLR priming in RAW264.7 cells. While the previous studies investigated either PGE_2 or total radiolabel release, we have now examined the complete eicosanoid spectrum. When primed with Kdo_2-Lipid A, GPCR agonists PAF and UDP stimulated eicosanoid production that was not enhanced. The transient Ca^{2+} spike was sufficient to activate eicosanoid production, presumably through COX-1, but this pathway was additive with the TLR-4 pathway. On the other hand, Kdo_2-Lipid A appears to synergistically enhance the release of specific eicosanoids produced by ATP and ionomycin. While the majority of PGs showed no significant change, the release of AA, COX-derived 11-HETE, and 5-LOX products increased dramatically. The 5-LOX product 5-HETE was enhanced by 20 to 40 fold while the total AA released, i.e. the sum of all AA and eicosanoids, was enhanced 3 to 5 fold. This indicates that both $cPLA_2$ mediated AA release and 5-LOX mediated products were enhanced.

Our results differ from the previous published work in that here we found no enhancement of PG production. This difference from $P388D_1$ cells is due in part to the

fact that in the previous studies the enhancement was calculated under the assumption that TLR activation did not generate significant levels of PGE_2 within one hour of activation. However, our results clearly demonstrate that in RAW264.7 cells TLR-4 activation leads to eicosanoid generation within this timeframe and if this is taken into account there is no significant enhancement of the PGs.

Furthermore, when ActD and CHX were used to inhibit protein synthesis, or BAY was used to inhibit NF-κB specifically, eicosanoid production via Kdo_2-Lipid A was completely shut down during the first hour. However, the levels of AA were not affected. This confirms that eicosanoid production during this period is dependent upon new protein synthesis, presumably COX-2, and that this enzyme production requires NF-κB. Apparently the AA produced in response to Kdo_2-Lipid A activation cannot reach the existing pools of COX, but can be used by newly synthesized COX. This could be do to the fact that without a Ca^{2+} spike, $cPLA_2$ is brought to the membrane via PIP_2 [305, 306] or ceramide 1 phosphate (C1P) [307, 308] that are located in specific subcellular organelles, whereas a Ca^{2+} spike allows $cPLA_2$ to bind non-specifically or to a different set of membranes.

In contrast to 60 minutes of Kdo_2-Lipid A, stimulation with ATP alone in the presence of protein synthesis inhibitors had only a small effect on eicosanoid release. Inhibition of NF-κB also had no significant effect on eicosanoid synthesis. Since ATP-induced eicosanoid production was complete within 10 minutes, it is not expected that protein synthesis would play a significant role in this pathway.

The total eicosanoid release of ATP-activated cells that were primed with Kdo_2-Lipid A was also diminished by the presence of ActD, CHX, and BAY. This was not

surprising, in light of the fact that these inhibitors blunted ATP stimulated eicosanoid release and completely inhibited Kdo_2-Lipid A eicosanoid production. However, the synergistic activation ratio was unchanged by these inhibitors, as well as by the NF-κB activation inhibitor 6-Amino-4-(4-phenoxyphenylethylamino) quinazoline. This indicates that TLR-4 priming does not require the NF-κB induced protein synthesis triggered by TLR-4 activation.

The separation of eicosanoid release enhancement from protein synthesis is bolstered by the results shown in Figure 3-6. The levels of $cPLA_2$, COXs, 5-LOX, and FLAP do not change significantly during this timeframe. The enhancement effect appears to be due to synergistic activation of $cPLA_2$ and the subsequent release of AA and LTs, whereas protein synthesis only affects COX metabolites. Since the phosphorylation levels and *in vitro* activity of $cPLA_2$ aren't noticeably altered, changes in the components that translocate $cPLA_2$ to its membrane substrate are likely to play a significant role.

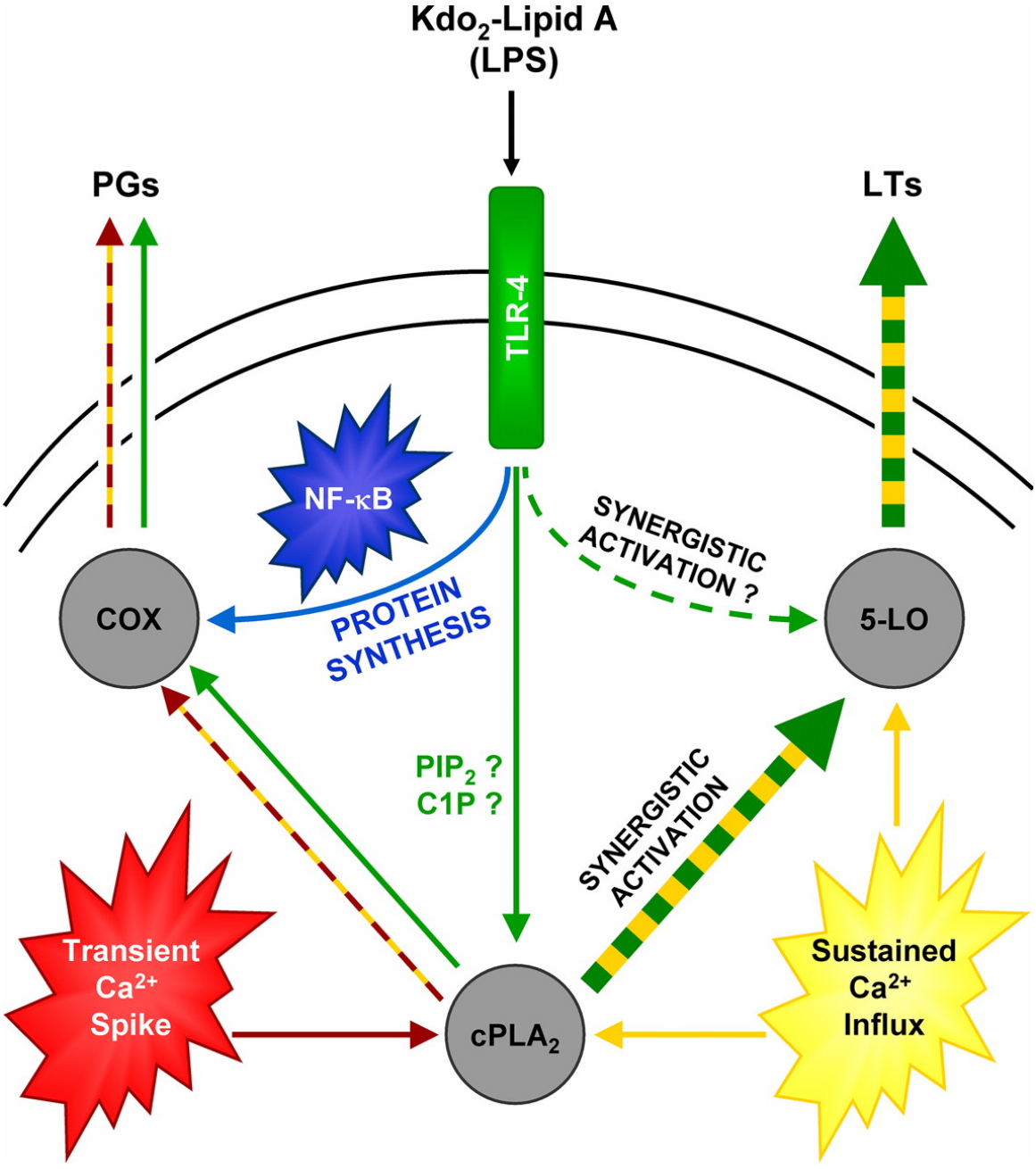

Figure 3-9. Model for TLR and Ca^{2+} activation of eicosanoid production. Eicosanoid production pathways stimulated by transient Ca^{2+} agonists (red), sustained Ca^{2+} agonists (yellow) and TLR agonists (green) are indicated by color.

3.D.4 Current model of eicosanoid activation

We have developed a working model that explains the eicosanoid profiles and priming characteristics demonstrated in RAW264.7 cells (Figure 3-9). This model accounts for the data through the differential regulation of $cPLA_2$, COX, and 5-LOX.

The activity of $cPLA_2$ can be controlled by three possible mechanisms. First, the enzyme levels in the cell could be increased by gene up-regulation. There is evidence that this does not occur for $cPLA_2$ in macrophages [309, 310], and in our hands the level of this enzyme does not appear to change in response to various agonists. Second, the activity could be increased by phosphorylation of the enzyme. Phosphorylation of Ser505 has been shown to increase $cPLA_2$ activity when studied *in vitro* [311]; however, there is some question whether this mechanism is utilized *in vivo* to regulate activity, since in resting cells the enzyme exhibits some basal phosphorylation [309, 312]. In this regard, our data demonstrates that Ser505 is highly phosphorylated on $cPLA_2$ in basal RAW264.7 cells, and neither Kdo_2-Lipid A, ionomycin nor ATP affects the *in vitro* activity. The third and most likely mechanism for macrophage regulation of $cPLA_2$ is through control of its translocation to membranes.

Under resting conditions, $cPLA_2$ is a soluble enzyme and must translocate to the membrane to reach its substrate and to produce AA. To date, translocation has been shown to be increased by both changes in Ca^{2+} and phospholipids. Increases in cytosolic Ca^{2+} facilitate $cPLA_2$ binding to phospholipids in membranes via its C-2 domain. Translocation can also be accomplished in a Ca^{2+} independent fashion through an increase in specific membrane phospholipids. Six and coworkers have shown that PIP_2 increases $cPLA_2$ membrane affinity and activity [305, 306]. In addition to membrane binding

affects, they also identified a potential PIP_2 conformational change that increases specific activity of the enzyme. PIP_2 generation has recently been linked with TLR activation [313, 314]. Murayama and coworkers have recently demonstrated a similar *in vitro* activation effect with C1P [307]. Additionally, ceramide [315, 316] and diacylglycerol [317] have also been shown to increase $cPLA_2$ membrane affinity. Localized concentrations of a number of specific phospholipid species could realistically facilitate translocation, and thus increase the activity of the $cPLA_2$ enzyme.

The activities of the COX enzymes appear to be primarily controlled by expression. COX-1 is usually expressed constitutively, whereas COX-2 is typically found at low levels in resting cells but can be up-regulated by several hundred fold in response to certain agonists. Once expressed, both enzymes do not require Ca^{2+} or phosphorylation for activity. However, the enzymatic mechanism requires a tyrosine radical for activity which is easily quenched [4, 5], leading to it's inactivation after a relatively small number of turnovers. This rapid inactivation naturally limits PG production in the absence of continual expression.

Similar to $cPLA_2$, 5-LOX appears to be controlled by a complex set of mechanisms. It contains a similar C-2 domain to $cPLA_2$ that requires significant levels of Ca^{2+} for translocation to the membrane. This enzyme can also be activated by phosphorylation [281, 311]. Additionally, the presence of 5-LOX activating protein (FLAP) is essential for productive *in vivo* activity, although its exact role remains unclear [267]. The catalytic activity of 5-LOX can be inhibited by nitric oxide produced by long-term TLR activation [318]. Using this information regarding $cPLA_2$, COX and 5-LOX regulation, we

shall describe our results parting terms of an integrated model for regulating eicosanoid production.

In response to PAF or UDP, a burst of Ca^{2+}, but no sustained change, is generated. This leads to a transient release of AA, as $cPLA_2$ temporarily moves to the membrane in response to Ca^{2+}. Since this occurs within minutes, little or no protein synthesis occurs. Thus, released AA must be converted to eicosanoids by basally expressed enzymes. PG production may be further limited by the lack of COX-2 expression, as constitutive COX enzyme becomes rapidly suicide-inactivated. The transient Ca^{2+} changes are insufficient to activate 5-LOX, thus leading to very low levels of predominately PG production.

Ionomycin and ATP produce a significant, sustained Ca^{2+} elevation that leads to a more robust, longer lasting translocation of $cPLA_2$ to the membrane. This is reflected by a 2-4 fold higher release of total AA derived metabolites by ionomycin and ATP when compared to GPCR receptor agonists. In addition to increased $cPLA_2$ activity, a sustained Ca^{2+} flux is sufficient to additionally activate 5-LOX. In this case, the COX and 5-LOX pathways are both active and generate PGs and LTs, respectively.

Short-term Kdo_2-Lipid A stimulation activates protein synthesis that begins to increase COX levels in 60 minutes. Since Kdo_2-Lipid A does not induce Ca^{2+} release, it must activate $cPLA_2$ by an alternative mechanism. Presumably this occurs by increasing the levels of PIP_2 or C1P that sequester the enzyme to the membrane. Again, the 5-LOX arm is not active since there is no Ca^{2+} change. This stimulation pathway produces a moderate level of primarily PG production.

The level of total eicosanoid production by either transient or sustained Ca^{2+} activation pales in comparison to long-term Kdo_2-Lipid A stimulation. Long-term stimulation with Kdo_2-Lipid A leads to significant protein synthesis, in particular COX-2; it would also allow for the significant changes in the levels of PIP_2 or C1P, which could explain the increase in $cPLA_2$ activity. Both of these factors would also explain the significant increase in the levels of PG released. Again, the lack of a Ca^{2+} increase means that only the PG arm of the pathway is active and thus the PG dominated eicosanoid profile.

Kdo_2-Lipid A priming causes two dramatic changes in the RAW264.7 cell response to ATP. First, the total level of AA released, i.e. the sum of AA and all of the eicosanoids detected, increase considerably. Second, PG levels are not enhanced while leukotrienes are significantly enhanced. An increase in total eicosanoid production, including arachidonic acid, implies a corresponding change in $cPLA_2$ activity. We have shown that the levels of $cPLA_2$ and its *in vitro* activity do not seem to change during priming. TLR-4 activation also increases the MAP kinase pathways. However, we could not detect an increase in $cPLA_2$ phosphorylation. Of course, some other mechanism for $cPLA_2$ activation may be involved. It is possible that the Ca^{2+} could be acting synergistically with PIP_2 or C1P to increase the levels of $cPLA_2$ at the surface. *In vitro* studies have shown that PIP_2 increases the specific activity of $cPLA_2$, which could indicate a potential mechanism for synergy.

The activation ratio of the 5-HETE is significantly greater than that for total AA production. This implies that the 5-LOX activity is synergistically enhanced as well. However, while 5-LOX has a Ca^{2+} requirement and similar C-2 binding domain as

$cPLA_2$, we have no evidence indicating the precise mechanism for synergistic activation of 5-LOX. Enhanced 5-LOX activity could pull the bulk of the increased AA release through the 5-LOX pathway. This would account for the lack of enhancement in the PG levels; it is also possible that the levels of COX are limiting over the 60 minute incubation.

The fact that the UDP and PAF agonists did not show enhancement with Kdo_2-Lipid A priming reinforces the idea that synergy requires a sustained increase in Ca^{2+} coupled to the non-protein synthesis portions of the Kdo_2-Lipid A priming. The lack of synergy with UDP and PAF could also be explained if the COX levels are limited.

In summary, we have found that it is critical to track all eicosanoid products when characterizing agonist induced cellular responses. This has allowed us to refine our understanding of the Kdo_2-Lipid A priming of RAW264.7 cells and to discover that TLR-4 priming involves a synergistic activation of $cPLA_2$, and possibly 5-LOX, that does not requires protein synthesis. Further studies are required to identify the precise mechanism of this synergy.

3.E Experimental procedures

Materials – RAW264.7 murine macrophage cells were purchased from American Type Culture Collection (Manassas, VA). LC-grade solvents were purchased from EMD Biosciences. Strata-X solid phase extraction columns were purchased from Phenomenex (Torrance, CA). Phosphate buffer saline (PBS) was purchased from VWR. Dulbecco's modified Eagles's medium, fetal bovine serum and broad range DNA Quant-Kit were purchased from Invitrogen. Lipopolysaccharide (LPS), zymosan, ionomycin, adenosine triphosphate (ATP), uridine diphosphate (UDP), ethylene glycol tetraacetic acid (EGTA) and bovine serum albumin were purchased from Sigma. The TLR agonists N-palmitoyl-S-[2,3-bis(palmitoyloxy)-(2RS)-propyl]-[R]-Cys-[S]-Ser-[S]-Lys(4) trihydrochloride (Pam3SCK4), heat killed *Listeria Monocytogenes* (HKLM), lipoteichoic acid from *Staphylococcus aureus* (LTA), polyinosine-polycytidylic acid (Poly(I:C)), flagellin from *Salmonella typhimurium* (flagellin), S-(2,3-bispalmitoyloxypropyl)-Cys-Gly-Asp-Pro-Lys-His-Pro-Ser-Phe (FSL-1), imiquimod, gardiquimod and synthetic oligodeoxynucleotide 1826: 5'-TCCATGACGTTCCTGACGTT-3' (ODN1826) were purchased from Invivogen (San Diego, CA). Kdo_2-Lipid A and 1-palmitoyl-2-arachidonyl phoshatidylcholine was obtained from Avanti Polar Lipids (Alabaster, AL). L-1-palmitoyl, 2-[^{14}C]-arachidonyl phosphatidylcholine was purchased from Perkin-Elmer (Shelton, CT). All eicosanoids, PAF, and indomethacin were purchased from Cayman Chemicals (Ann Arbor, MI). The $cPLA_2$, p-$cPLA_2$ (S505), anti-rabbit IgG-HRP and anti-mouse IgG-HRP antibodies were purchased from Cell Signaling (Beverly, MA). The 5-LOX, COX-1, COX-2 antibodies and 5-LOX blocking peptide were purchased from AbCam (Cambridge, MA). The GAPDH antibody was purchased from HyTest

(Turku, Finland). The anti-goat IgG-HRP antibody was purchased from Sigma. Actinomycin D (ActD), cyclohexamide (CHX), and BAY 11-7082 (BAY) were purchased from Biomol (Plymoth Meeting, PA). 6-Amino-4-(4-phenoxyphenylethylamino) quinazoline was purchased from Calbiochem (La Jolla, CA). Pyrrophenone was a kind gift from Dr. Kohji Hanasaki (Shionogi Research Laboratories). Zileuton was a kind gift from Prof. Robert C. Murphy (University of Colorado). All other reagents were reagent grade or better.

Cell Culture and Stimulation Protocol – The RAW264.7 mouse murine macrophage cells were cultured in Dulbecco's modified Eagles's medium with 10% fetal bovine serum and 100 units/ml penicillin/streptomycin at 37ºC in a humidified 5% CO_2 atmosphere. Cells were plated in 6-well culture plates with 2 ml media (2 x 10^6 cells for short-term studies, 1 x 10^6 cells for long-term studies), allowed to adhere for 24 hours, the media was replaced with 1.8 ml of serum free media, and after 1 hour were stimulated. Short-term stimuli were added for 10 minutes at the following doses: PAF (100 nM), UDP (25 μM), ionomycin (1 μM), ATP (2 mM). Long-term stimuli were added for 12 hours at the following doses: Pam3SCK4 (1 μg/ml), HKLM (10^8 cells/ml), LTA (1 μg/ml), Poly(I:C) (50 μg/ml), LPS (100 ng/ml), Kdo_2-Lipid A (100 ng/ml), flagellin (50 ng/ml), FSL-1 (1 μg/ml), zymosan (500 ng/ml), imiquimod (5 μg/ml), gardiquimod (1 μg/ml), ODN1826 (1 μM). In priming experiments, cells were incubated with Kdo_2-Lipid A (100 ng/ml) for 50 minutes, followed by the addition of vehicle or short-term agonist (PAF, UDP, ionomycin, ATP) for 10 minutes.

Sample Preparation – The media was analyzed for extracellular eicosanoid release. After stimulation, the entire 1.8 ml of media was removed and each sample was supplemented with 100 µl of internal standards (100 pg/µl, EtOH) and 100 µl of EtOH to bring the total volume of EtOH to 10% by volume. Samples were centrifuged for 5 minutes at 3000 rpm to remove cellular debris, and then purified. Intracellular eicosanoids were analyzed in the remaining adherent cells by scraping them into 500 µl MeOH and then adding 1000 µl PBS and 100 µl of internal standards.

Eicosanoids were extracted using Strata-X SPE columns. Columns were washed with 3 ml MeOH and then 3 ml H_2O. After applying the sample, the columns were washed with 10% MeOH and the eicosanoids were then eluted with 1 ml MeOH. The eluant was dried under vacuum and redissolved in 100 µl of LC solvent A [water-acetonitrile-formic acid (63:37:0.02; v/v/v)] for LC-MS/MS analysis. It was experimentally determined that intracellular samples contained 1-2% of the extracellular media. The remaining 2% of extracellular eicosanoids were not removed with a wash step because it was determined that the process of washing the cells stimulated eicosanoid release. Measurements approaching 2% of the extracellular eicosanoid level were assumed to be due to media carryover.

Cell Quantitation – Eicosanoid levels were normalized to cell number using DNA quantitation. After the extracellular media was removed, the cells were scraped in 500 µl PBS and stored at 4ºC for DNA quantitation using the Broad Range DNA Quant-Kit according to the manufacturer instructions. Intracellular experiments required scraping cells into pure MeOH for eicosanoid analysis. Since MeOH significantly affected the

DNA quantitation assay, we determined DNA levels from a separate well in these experiments. A conversion factor of 664 cells per ng of DNA was experimentally determined by comparison to hemacytometer cell counting.

LC and Mass Spectrometry – The analysis of eicosanoids was performed by LC-MS/MS using "Method 1", as described in Chapter 2. Eicosanoids were separated by reverse-phase LC on a C18 column (2.1 mm x 250 mm, Grace-Vydac) at a flow rate of 300 µl/min at 25ºC. The column was equilibrated in Solvent A [water-acetonitrile-formic acid (63:37:0.02; v/v/v)], and samples were injected using a 50 µl injection loop and eluted with a linear gradient from 0%-20% solvent B [acetonitrile-isopropyl alcohol (50:50; v/v)] between 0 to 6 min; solvent B was increased to 55% from 6 to 6.5 min and held until 10 min. Solvent B was increased to 100% from 10 to 12 min and held until 13 min; solvent B was dropped to 0% by 13.5 min and held until 16 min.

Eicosanoids were analyzed using a tandem quadrupole mass spectrometer (ABI 4000 Q Trap®, Applied Biosystems) via multiple-reaction monitoring in negative-ion mode. The electrospray voltage was -4.5 kV, the turbo ion spray source temperature was 525ºC. Collisional activation of eicosanoid precursor ions used nitrogen as a collision gas. Table 2-1 lists the Precursor→Product MRM pairs used for each analyte, as well as the limit of detection.

Quantitative eicosanoid determination was performed by the stable isotope dilution method, previously described by Hail and Murphy [278]. PGs and AA were obtained as precisely weighed quantitative standards from Cayman Chemicals, whereas the concentrations of HETEs and LTs were determined by UV spectroscopy. A standard

curve was prepared by adding 10 ng of each internal (deuterated) eicosanoid standard to the following amounts of eicosanoid (non-deuterated) primary standard: 0.3, 1, 3, 10, 30 and 100 ng. Results are reported as ng of eicosanoid per million cells (mean ± standard deviation).

Immunoblotting – Cells were washed twice with cold PBS and scraped into 200 μL of Complete Mini protease cocktail solution (Roche, Mannheim, Germany). Protein concentrations were determined and normalized using the BioRad Protein Assay (BioRad, Hercules, CA). 15 μg of total protein was loaded onto 4-12% Bis-Tris SDS-PAGE gels, electrophoresed and transferred onto a nitrocellulose membrane.

For COX-1 or COX-2, the membrane was blocked with (3% bovine serum albumin/1% Casein) in Tris buffered saline (TBS) buffer containing 0.05% Tween 20 for 1 hour, incubated with either 1:100 COX-1 (Cayman Chemicals, Ann Arbor, MI) or 1:100 COX-2 (Cayman Chemicals, Ann Arbor, MI) specific antibody overnight, washed three times in TBS containing 0.05% Tween 20, incubated with 1:2000 anti-rabbit biotinylated IgG secondary antibody (Vector Laboratories, Burlingame, CA) for 30 minutes, washed three times, and incubated with 1:5000 streptavidin-HRP conjugated antibody (Vector Laboratories, Burlingame, CA) for 30 minutes.

For all other proteins, the membrane was blocked with 5% milk protein in PBS buffer containing 0.1% Tween 20 for 1 hour, incubated with 1:1000 of the appropriate specific antibody overnight, washed three times in PBS containing 0.1% Tween 20, and incubated with 1:1000 of the appropriate secondary antibody for one hour. All membranes were

washed three times before development using the Western Lightning ECL kit (Amersham Biosciences).

Group IVA PLA_2 Assay – Group IVA $cPLA_2$ activity was determined by measuring the release of free [^{14}C]-arachidonic acid. Final assay conditions were: 100 mM HEPES pH 7.5, 80 μM $CaCl_2$, 0.1 mg/ml bovine serum albumin, 2 mM Dithiothreitol, 400 μM Triton X-100, 3 μM phosphatidylinositol 4,5-bisphosphate (PIP_2), and 97 μM 1-palmitoyl-2-arachidonyl phoshatidylcholine with 100,000 cpm L-1-palmitoyl, 2-[^{14}C]-arachidonyl phosphatidylcholine. Radiolabeled free fatty acid was separated from the phospholipid substrate via our dole fatty acid extraction procedure [319, 320] and counted in a Packard 1600TR (Packard Instruments).

3.F. Acknowledgments

Daren L. Stephens, Rebecca Bowers-Gentry, Andrej Grkovich and Raymond A. Deems co-authored work from this chapter in the Journal of Biological Chemistry, titled "TLR-4 and Sustained Calcium Agonists Synergistically Produce Eicosanoids Independent oof Protein Synthesis in RAW264.7 Cells". We would like to thank Dr. Richard Harkewicz for discussions regarding mass spectrometry, and Faith E. Jacobsen for assistance preparing the manuscript. This work was supported by grant GM64611 and the LIPID MAPS Large Scale Collaborative Grant GM069338 from the National Institute of Health.

Chapter 4.

A Macrophage Cell Model for Selective Metalloprotein Inhibitor Design

4.A Abstract

The desire to inhibit zinc-dependent matrix metalloproteinases (MMPs) has lead to the development of a plethora of MMP inhibitors over the course of the last 30 years that bind directly to the active site metal. With the exception of one inhibitor, all of these drugs have failed in clinical trials due to many factors, including an apparent lack of specificity for MMPs. To address the question of whether these inhibitors are selective for MMPs in a biological setting, a cell-based screening method is presented to compare the relative activities of zinc, heme iron, and non-heme iron enzymes in the presence of these compounds using the RAW264.7 macrophage cell-line. We screened nine different zinc-binding groups (ZBGs), four established MMP inhibitors (MMPi) and two novel MMP inhibitors developed in our laboratory to determine their selectivity against five different metalloenzymes. Using this model, we identified DPA and TACN as the most promising ZBGs for zinc metalloenzyme inhibitor development. We also demonstrated that the model could predict known non-specific interactions of some of the most commonly used MMP inhibitors, as well as give cross-reactivity information for newly developed MMPi. This work demonstrates the utility of cell-based assays in both the design and screening of novel metalloenzyme inhibitors.

4.B Introduction

One of the main targets for metalloenzyme inhibition over the last thirty years has been matrix metalloproteinases (MMPs).[321-326] MMPs comprise a family of calcium(II)- and zinc(II)-dependant hydrolytic enzymes involved in the maintenance of the extracellular matrix components.[327-330] Constitutively active MMPs facilitate nerve and

bone growth, endometrial cycling, wound healing, and angiogenesis;[327, 328] however, MMPs are also associated with chronic inflammatory diseases, cardiomyopathy, and cancer metastasis.[323, 331-333] Thus, the development of potent and selective MMP inhibitors (MMPi) has therapeutic potential in the treatment of a number of human diseases.[321-326] Presently, the FDA has only approved one compound that inhibits MMP activity, the broad spectrum inhibitor doxycycline[334] (under the commercial name Periostat) used for the treatment of periodontal disease.[334] However, the mechanism of MMP inhibition by doxycycline has not been fully elucidated,[335] and it is known to have numerous interactions with other metalloenzymes.[336-338] Furthermore, hundreds of other MMPi have been developed over the past thirty years that show excellent potency in vitro, only to exhibit several problematic side-effects in clinical trials.[325, 339-341] A significant number of these effects have been attributed to a lack of selectivity. In particular, the hydroxamic acid zinc-binding group (ZBG) that is most often utilized in MMPi, and other metalloprotein inhibitors, is not selective for the zinc(II) ion over other biologically relevant metal ions, such as iron.[342] To this end, several efforts have been made to identify more zinc-selective ZBGs.[343-345]

Too often, potential therapeutics are tested in vitro and in cellular assays against MMPs, only to discover a lack of efficacy and side-effects in animal models or in clinical trials caused by their lack of selectivity. A number of studies have reported screening techniques which identify cross-reactivity between MMP isoforms[346-348]; however, they do not systematically test whether MMP inhibitors can have an effect on non-MMP off-target enzymes. To overcome the limitations of previous in vitro screening approaches, a robust assay system using the macrophage as a model is presented that can determine the

efficacy of inhibitors against MMPs alongside a number of other relevant metalloenzymes, which serve as markers of cross-reactivity. For these studies, we selected the RAW264.7 murine macrophage cell-line, which has been used extensively as a model of inflammation,[349-353] has a wealth of publicly accessible information available from the LIPID MAPS consortium at www.lipidmaps.org, and in contrast to human monocyte cells lines such as U937 and THP-1 does not require differentiation into adherent macrophages[354, 355].

Acute inflammation serves as an important component of the innate immune system defense against bacterial infection and entails the activity of a number of important metalloenzymes (Figure 4-1). In response to pathogenic stimuli, macrophage cells upregulate and release pro-MMPs into the extracellular space. In addition, arachidonic acid (AA) released by activated macrophage cells is converted into bioactive mediators by a variety of cyclooxgenase (COX) and lipoxygenase (LO) enzymes.[349] The pro-inflammatory cytokine tumor necrosis factor α (TNF_α) is transformed from its upregulated pro-form to its activated state by TNF_α converting enzyme (TACE), also known as ADAM17.[356, 357] Finally, macrophages upregulate inducible nitric oxide synthase (iNOS), which produces reactive oxygen species that kill bacteria.[358] Each of the aforementioned processes is metal-dependent: COX and iNOS are heme iron enzymes, LOs are non-heme iron enzymes, and TACE and MMPs are zinc-dependent metalloenzymes. The RAW264.7 cell-line can recapitulate each of these hallmarks of acute inflammatory processes, and provides a relevant model system for examining the effects of MMPi on each metal-dependent pathway.

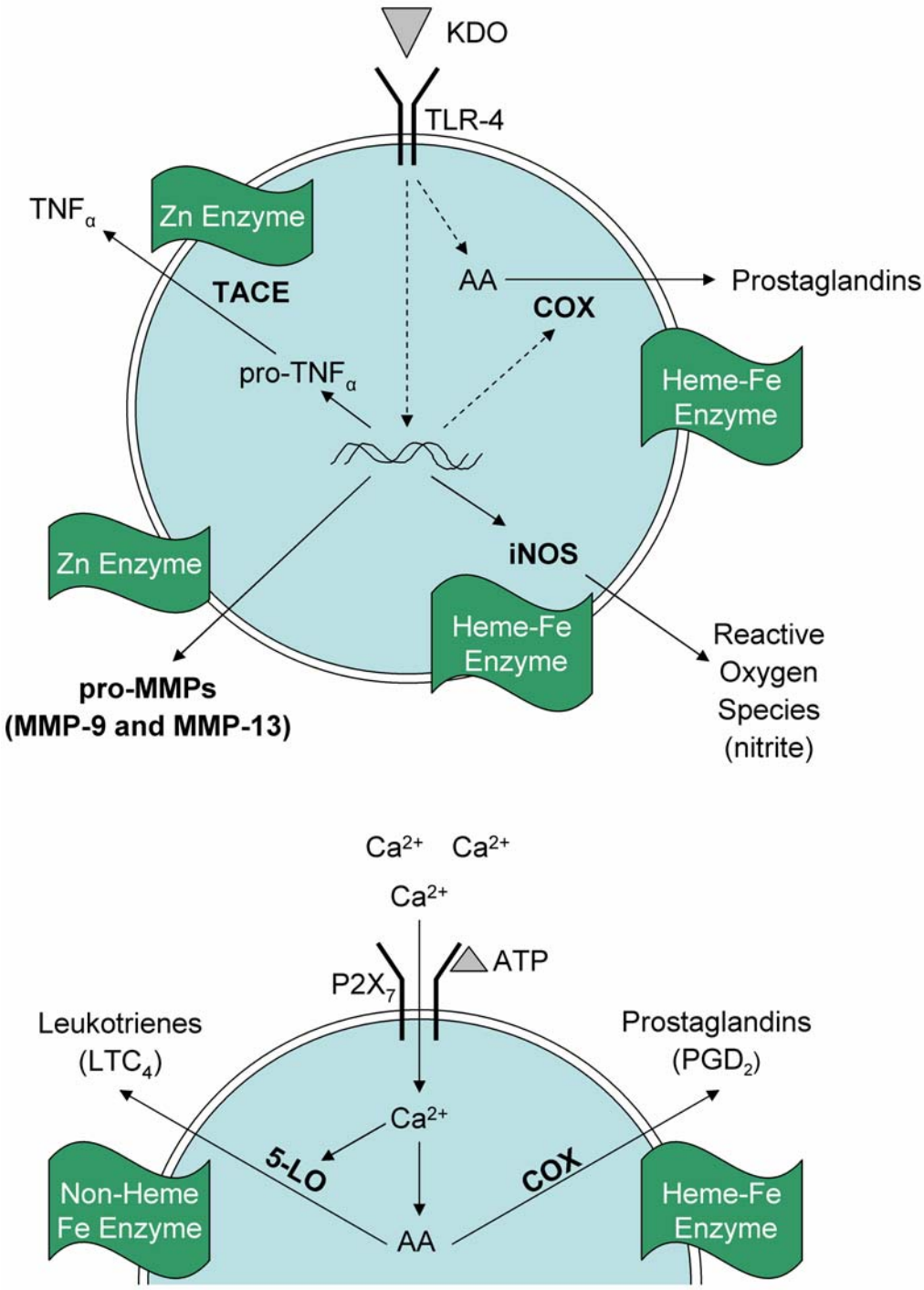

Figure 4-1. Overview of RAW264.7 macrophage activation. KDO (Kdo_2-Lipid A) is recognized by TLR-4 (toll-like receptor 4), resulting in upregulation of COX, TNF□, iNOS, and pro-MMPs. ATP is recognized by purinergic receptors, including $P2X_7$, causing an influx of extracellular Ca^{2+} which results in AA release and 5-lipoxygenase (5-LOX) activation. The outcome is an increase of LTC_4 (leukotriene C_4) by 5-LOX and PGD_2 (prostaglandin D_2) by COX. Metalloenzymes are flagged in green, describing the type of metalloenzyme; the specific metabolites measured in this study are shown in parenthesis.

Using the RAW264.7 cell-line, the metalloenzyme selectivity of nine different ZBGs has been examined. o-Phenanthroline (OP) is a common metal chelator that is known to remove the catalytic zinc(II) ion from the MMP active site (Figure 4-2).[359] 3-Hydroxy-2-methyl-4*H*-pyran-4-one (maltol), 3-hydroxy-2-methyl-4*H*-pyran-4-thione (thiomaltol), 1-hydroxypyridin-2(1*H*)-one (1,2-HOPO), and 1-hydroxypyridin-2(1*H*)-thione (1,2-HOPTO) are chelators that have demonstrated greater MMP inhibition than simple hydroxamates, such as acetohydroxamic acid (AHA).[345] Picolinic acid (PA), 2,2'-dipyridylamine (DPA), and triazocyclonane (TACN) also inhibit MMPs better when compared to AHA and are expected to be more selective for binding zinc(II) relative to the aforementioned chelating groups (Figure 4-2).[344]

In addition, the RAW264.7 cell-line model has been used to identify off-target interactions of a variety of known MMPi. For example, GM6001 (Figure 4-2) is a potent inhibitor of MMPs, but has also been shown to inhibit the zinc(II) enzyme TACE.[360, 361] Doxycycline and minocycline (Figure 4-2), which are broad-spectrum MMP inhibitors, are also known to blunt the activity of iNOS.[362] Overall, six MMPi were evaluated in the macrophage model, including four commercially available MMPi (Figure 4-2) and two potent MMPi (Figure 4-2) developed in our laboratory[363] whose interactions with other metalloenzymes have not be previously characterized. The results show that the macrophage cell model is predictive of the off-target interactions that have been reported in the literature. The findings presented here show that a cell-based model can be used to examine the activity of compounds on a variety of metalloenzymes simultaneously. While we have applied this model towards the design of selective MMPi, this screening method provides a useful tool for determining the specificity of a molecular fragment or

complete inhibitor for any of the metalloenzymes assayed in this model. Thus, the screening method developed here represents a powerful tool to analyze the specificity of not only MMPi, but also TACE inhibitors, COX inhibitors, iNOS inhibitors, 5-lipoxygenase (5-LOX) inhibitors, as well as dual COX and 5-LOX inhibitors.[364]

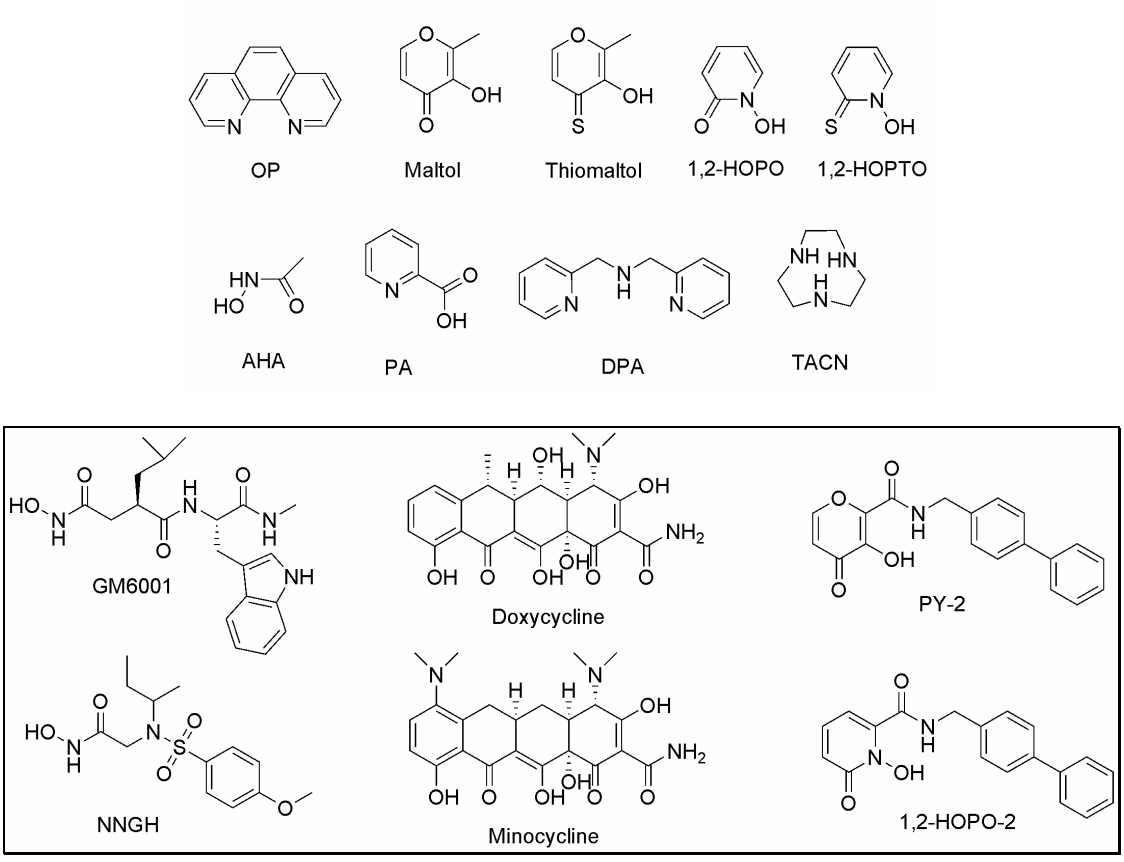

Figure 4-2. Metal chelator and MMPi structures. Chelators (top) and MMPi (bottom, in box) evaluated in a macrophage-based model of metalloenzyme activity.

4.C Results

4.C.1 Cell viability in the presence of ZBGs

Prior to examining metalloprotein activity, the toxicity of the different ZBGs was determined. Cell viability was assessed by the release of lactate dehydrogenase (LDH) from Kdo_2-Lipid A (KDO) stimulated macrophage cells in the presence of 100 μM of each ZBG for 24 hours. LDH is a stable, cytosolic enzyme that is released upon cell death, and the concentration of LDH in the extracellular media correlates with cell death. The results are shown in Figure 4-3 and were confirmed visually using Trypan Blue Dye. RAW264.7 cells proved to be greater than 90% viable in the presence of all the ZBGs tested except OP, which killed approximately 50% of the cells at 100 μM. The results

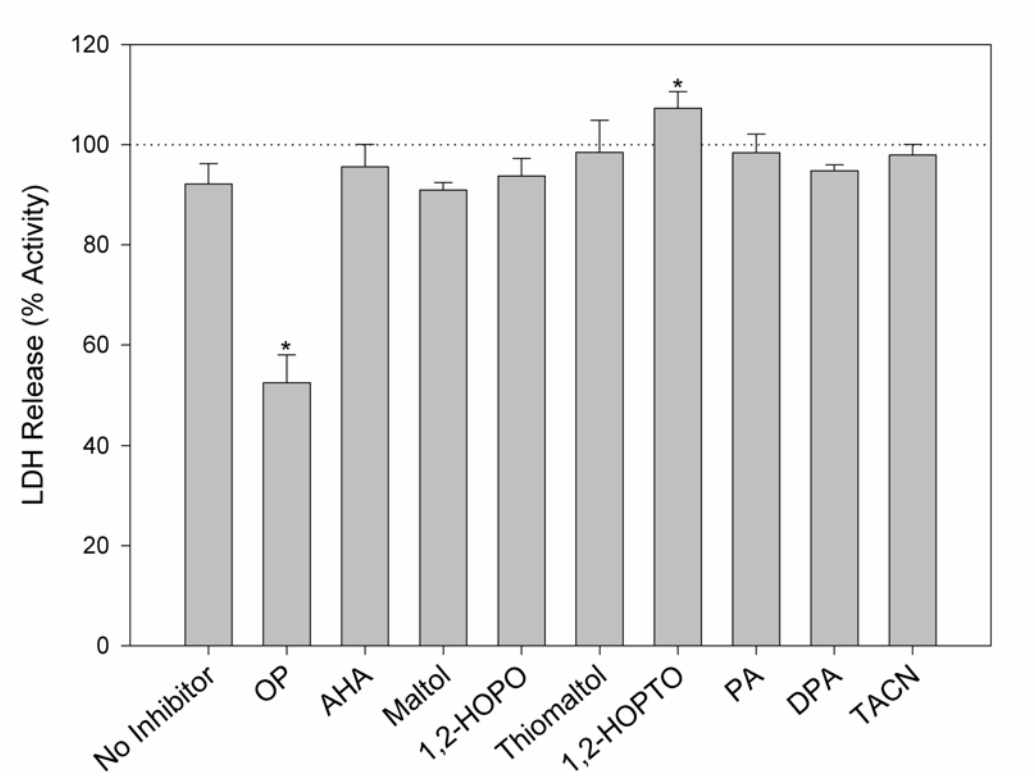

Figure 4-3. Viability of RAW264.7 cells in the presence of 100 **μ**M of each ZBG. Only OP showed any significant toxicity.

were consistent with previous toxicity studies on cardiac fibroblasts,[365] which showed that maltol, thiomaltol, 1,2-HOPO, and 1,2-HOPTO demonstrated low toxicity at 100 μM. The high toxicity of OP at 100 μM makes it difficult to determine whether a decrease in enzymatic activity (as measured in the assays described below) is due to inhibition by OP or simply results from an overall increase in cell death. Because of this complication the data obtained from OP (vide supra) are not interpreted in detail.

4.C.2 Metalloenzyme selectivity in RAW264.7 cells

Knowing that metal chelators have different thermodynamic affinities for metal ions in vitro,[344] we sought to evaluate the inhibition of several metalloproteins by various ZBGs in a biological setting using a RAW264.7 macrophage cell model. As shown in Figure 4-1, two stimulation scenarios, using either ATP or KDO, were examined in order to probe the activity of different metalloenzymes. Stimulating the $P2X_7$ purinergic receptor with ATP generates an influx of extracellular Ca^{2+}. Within minutes, this Ca^{2+} influx transiently activates both the cytosolic phospholipase A_2 ($cPLA_2$) to release AA from membrane phospholipids and the non-heme iron enzyme 5-LOX to process AA to form bioactive leukotriene C_4 (LTC_4).[349] AA can also be acted upon by the constitutively expressed heme iron enzyme COX to make prostaglandin D_2 (PGD_2). Additionally, the bacterial membrane component KDO, a specific lipopolysaccharide, was used to stimulate the toll-like receptor 4 (TLR-4) on the macrophages, which induces sustained $cPLA_2$ activity over a 24 hour period.[349] Over this period, KDO activates the transcription factor NF-κB, allowing for the upregulation of COX, iNOS, pro-TNF_α, pro-MMP-9, and pro-MMP-13 (Figure 4-4, www.lipidmaps.org).[366] Pro-TNF_α is cleaved by

membrane associated TACE[367] to the soluble signaling protein TNF_{α}. Using these two stimulation pathways, the activity of five different metalloenzymes could be examined in the presence of different ZBGs. In the sections below, the activity of different ZBGs against zinc-dependent enzymes is described, followed by the results against iron-dependent enzymes.

4.C.3 Inhibition of zinc metalloenzymes

Previous work has shown that TLR-4 stimulated RAW264.7 cells primarily induce pro-MMP-9 and pro-MMP-13 expression (Figure 4-4, www.lipidmaps.org).[366] In this study, cells were stimulated with KDO in the presence of 100 μM ZBG. As macrophages in culture have not been shown to activate their own pro-MMP[368-370] and thus have no basal level of MMP activity in the extra-cellular media, the pro-MMP was activated with *p*-aminophenylmercuric acetate (AMPA)[371]. While the MMP fluorescent

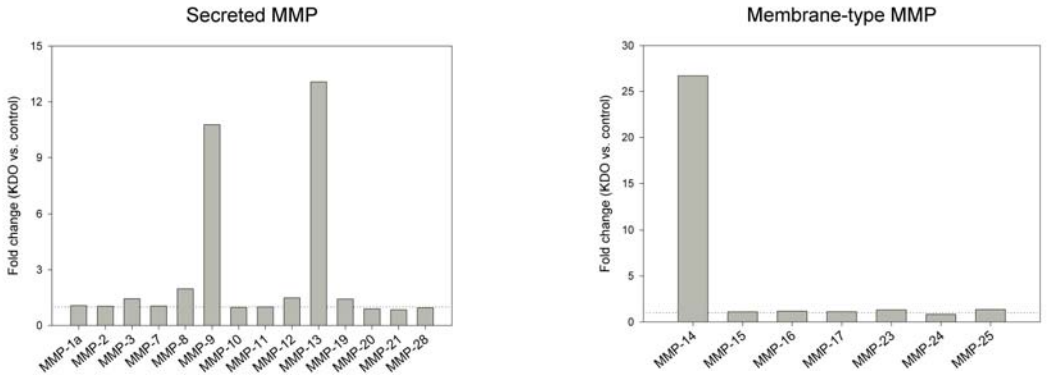

Figure 4-4. MMP expression by KDO stimulated RAW264.7 macrophages. LIPID MAPS investigated changes in gene expression by KDO stimulated RAW264.7 cells using an Agilent microarray analysis, and made the data publically available at www.lipidmaps.org. From this data, the profile of MMP expression by KDO stimulated RAW264.7 cells was extracted. MMPs were designated as either secreted (above) or membrane bound (below), and their expression at 24 hours is expressed as a fold-change compared with unstimulated cells. For more experimental details, see www.lipidmaps.org.

substrate can also be cleaved by TACE, this protein is cell-membrane associated[367] and would not be present in an assay of the extra-cellular media. This is confirmed by experiments showing no activity in the extra-cellular media when AMPA is excluded from the assay (data not shown).

At 100 μM, DPA and TACN inhibited MMP activity greater than 90%. The sulfur-containing ligands, 1,2-HOPTO and thiomaltol also inhibited the MMP activity, but to a lesser extent (80% and 45%, respectively). The model hydroxamic acid, AHA, inhibited 35% of the expressed MMP activity in the cells, while the other ZBGs (maltol, 1,2-HOPO, PA) inhibited less than 20% of the MMP activity. The MMP assay results are summarized in Figure 4-5.

TACE activity was measured by the relative amount of TNF_{α} in the extracellular media following KDO stimulation. Because TACE is a zinc-dependent enzyme, it was anticipated that some ZBGs would inhibit TNF_{α} release. Indeed, DPA and TACN are both inhibitors of activity (Figure 4-5), with 100 μM DPA inhibiting TNF_{α} release by 60%. Other ZBGs including PA, maltol, and thiomaltol inhibited release by approximately 25%, 30%, and 40%, respectively. All other ZBGs inhibited TNF_{α} production by less than 20%, including 1,2-HOPTO. The low inhibition by 1,2-HOPTO was surprising, as this chelator is a potent ZBG against MMP-3 in vitro,[345, 365] but does not appear to inhibit the zinc-dependent TACE in this model.

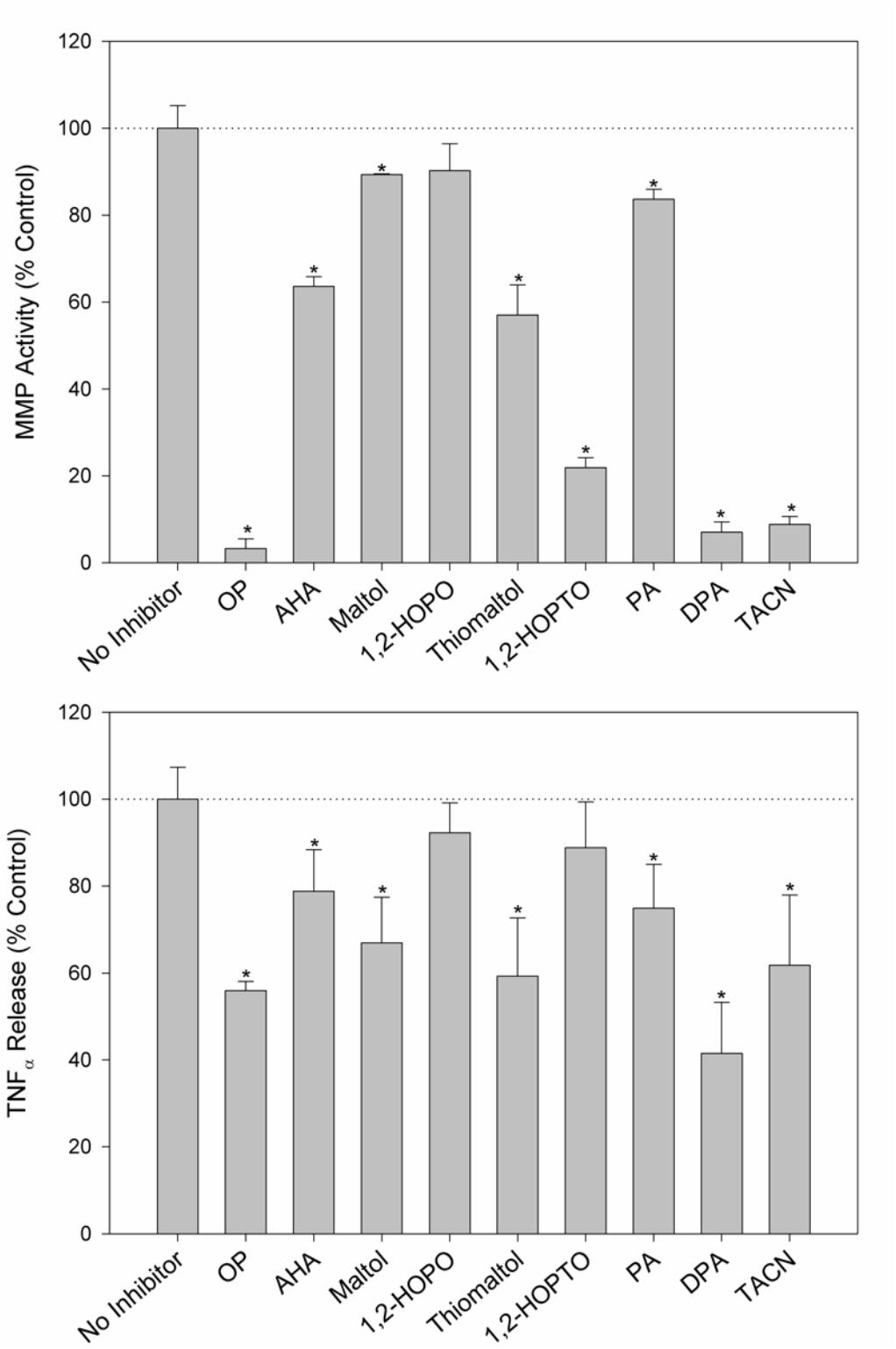

Figure 4-5. Inhibition of zinc-dependent enzymes MMPs and TACE by different ZBGs. MMP activity (top) and release of TNF□ (bottom) from KDO stimulated RAW264.7 cells in the presence of 100 **μ**M of each ZBG.

4.C.4 Inhibition of heme-iron and non-heme-iron enzymes by ZBGs

To determine the activity of 5-LOX and COX, the presence of their AA products were analyzed following stimulation with ATP. The activity of 5-LOX was measured by the production of LTC_4; the activity of COX was monitored by the production of PGD_2. Both metabolites were monitored simultaneously using LC-MS/MS methodology that has been previously described.[349] Zileuton[372, 373] and indomethacin[374] were used as a positive control for 5-LOX and COX inhibition, respectively (data not shown). The levels of AA, the substrate for both 5-LOX and COX, were also examined and determined to be independent of the presence/absence of the ZBGs (data not shown). This confirms that the ZBGs did not affect the availability of AA in the assay.

At 100 μM, none of the ZBGs examined showed any significant inhibition of 5-LOX (Figure-6). A potential explanation for this finding is that the concentration of these chelators was simply too low to effect lipoxygenase activity. In addition, 5-LOX is localized in the nuclear envelope,[375, 376] potentially making it more difficult for the ZBGs to gain access to this enzyme. In contrast, the activity of COX decreased noticeably in the presence of the sulfur-containing ZBGs, thiomaltol and 1,2-HOPTO, by 75% and 50%, respectively (Figure4-6). None of the other ZBGs showed greater than 20% inhibition of COX.

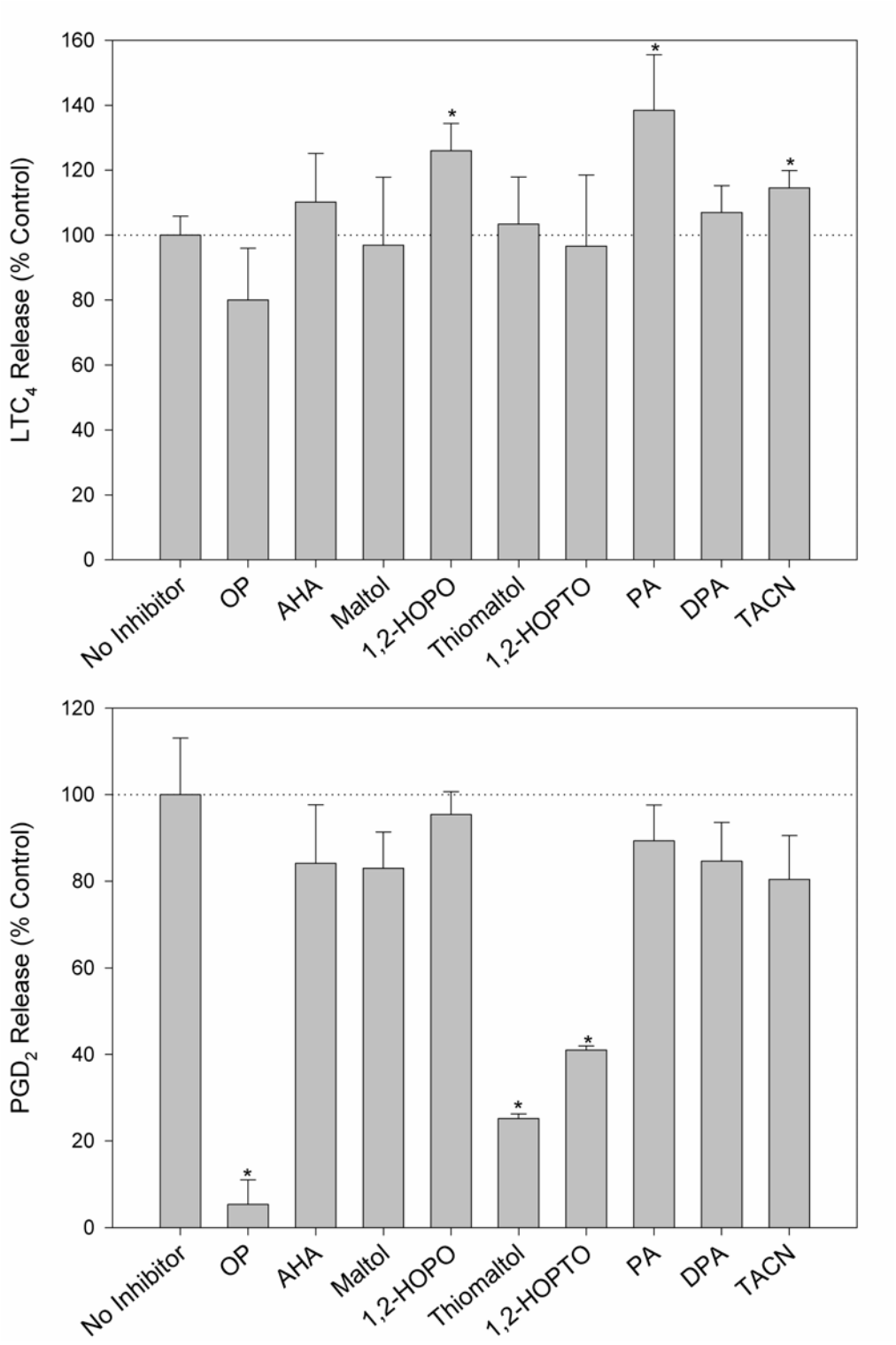

Figure 4-6. Inhibition of 5-LOX and COX by different ZBGs. Production of the LTC_4 (top) and PGD_2 (bottom) from ATP stimulated RAW264.7 cells in the presence of 100 μM of each ZBG.

The activity of iNOS was monitored by measuring one of its reactive oxygen products, nitrite, using the Griess reagent assay.[377] In a control experiment, all ZBGs were tested and shown to have no significant reactivity with the nitrite ion under standard assay conditions (data not shown). Similar to COX, the ZBGs that caused the most significant decrease in nitrite product were sulfur-containing ligands (Figure 4-74-7). Thiomaltol inhibited 80% and 1,2-HOPTO inhibited 75% of nitrite production. The only other ZBG to significantly affect nitrite concentration was DPA, which inhibited iNOS activity by 40%.

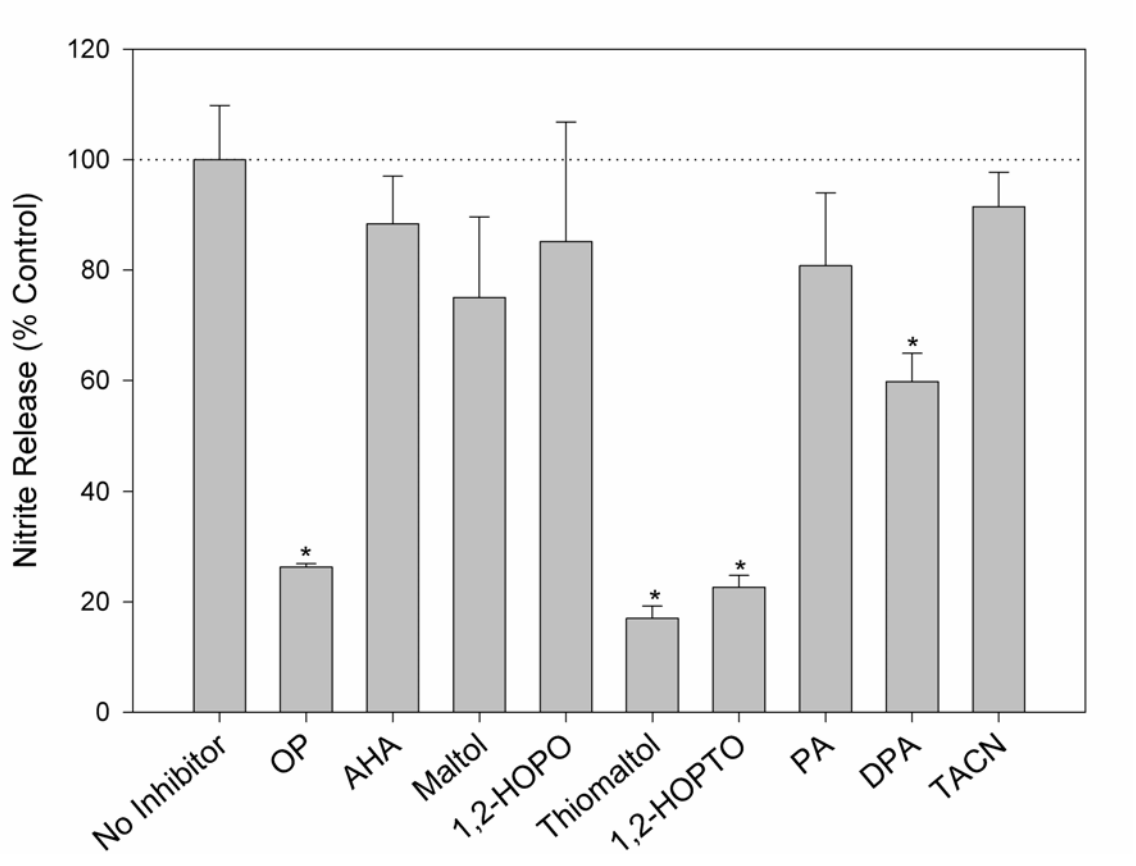

Figure 4-7. Inhibition of iNOS by different ZBGs. Production of nitrite from KDO stimulated RAW264.7 cells in the presence of 100 μM of each ZBG.

4.C.5 Metalloenzyme inhibition by complete MMPi

In addition to testing ZBGs, the macrophage model system was used to determine the activity of several full length inhibitors. Six known MMPi were examined: GM6001, NNGH, doxycycline, minocycline, PY-2, and 1,2-HOPO-2 (Figure 4-2). GM6001 and NNGH are commercially available, broad spectrum, nanomolar MMPi.[326] Doxycycline and minocycline are tetracycline-based, broad spectrum MMP inhibitors,[335, 378] which exhibit rather weak potency in vitro (150 μM and 3500 μM for MMP-3, respectively);[379] however, doxycycline is the only FDA approved drug for MMP inhibition.[334] PY-2 and 1,2-HOPO-2 are MMPi that have been shown to be semi-selective, with submicromolar inhibition of MMP-3, MMP-8, and MMP-12.[363] 1,2-HOPO-2 also possesses submicromolar inhibition of MMP-2 as well.[363] RAW264.7 macrophage cells were incubated with each MMPi at concentrations near or greater than their most potent reported IC_{50} values (GM6001, NNGH, PY-2 and 1,2-HOPO-2 were applied at 5 μM; doxycycline and minocycline at 100 μM) and enzymatic assays were performed as described above. The summary of the data is shown in Figure 8.

Both NNGH and GM6001 showed potent inhibition of MMPs. GM6001 also caused a reduction in TNF_{α}, indicating inhibition of zinc-dependent TACE. The presence of NNGH leads to a decrease in LTC_4, the metabolite of 5-LOX. Doxycycline shows minimal inhibition of MMPs at 100 μM, but there is a marked increase in LTC_4 and PGD_2 metabolites, with a concomitant decrease in nitrite production. Minocycline does not affect LTC_4 and PGD_2 levels as strongly, but does show a decrease in nitrite similar to that observed with doxycycline. PY-2 does not appear to effect any of the

enzymes examined in this assay, while 1,2-HOPO-2 appears to cross-inhibit the iron enzymes, slightly blunting the production of 5-LOX, COX, and iNOS products.

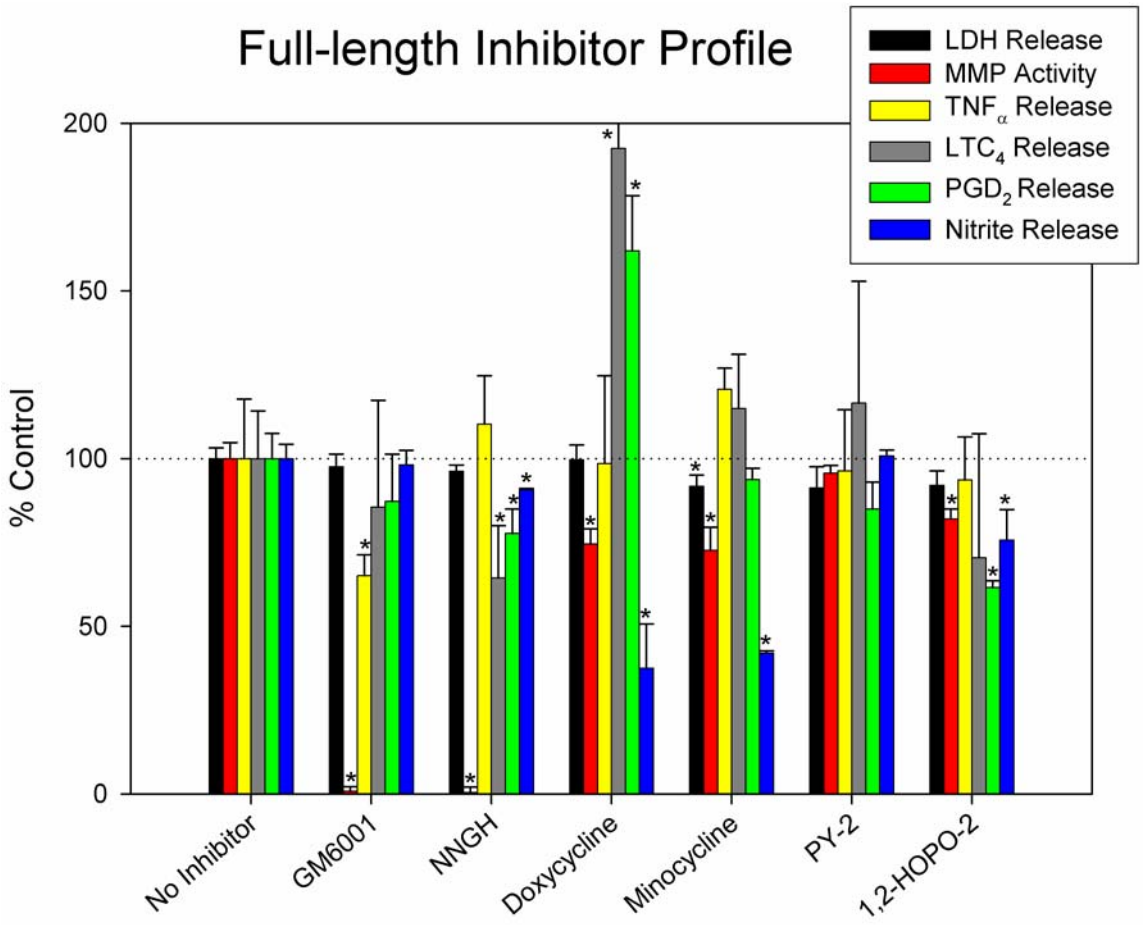

Figure 4-8. Metalloenzyme inhibition profile of RAW264.7 cells. Effects of the presence of GM6001 (5 μM), NNGH (5 μM), PY-2 (5 μM), and 1,2-HOPO-2 (5 μM), doxycycline (100 μM), and minocycline (100 μM) on RAW264.7 cells.

4.D Discussion

Many inhibitors that target metalloenzymes use chelating moieties that are not selective for the metal contained in the target protein, potentially leading to undesirable side effects in animal model and in clinical evaluations.[323] The findings described here show that a series of straightforward assays in a macrophage cell model can be used to rapidly screen metal chelating fragments or complete enzyme inhibitors against many metalloenzymes simultaneously, to determine the metalloenzyme selectivity of a compound in a biological setting. To this end, the ZBGs and MMPi shown in Figure 4-2 were examined.

A number of new ZBGs have been developed in recent years[380-384] to address some of the in vivo problems associated with hydroxamic acids. Many have been shown in vitro to have improved potency against MMPs when compared to a simple hydroxamic acid such as AHA (Figure 4-2).[345] Some of these ZBGs have been developed into complete MMPi that show semi-selective inhibition against several MMP isoforms.[363] One drawback of many of these new ZBGs is that they do not selectively bind zinc(II) over other biologically relevant metal ions. In fact, hydroxypyrone inhibitors have been shown to inhibit iron-dependent soybean lipoxygenase in vitro.[344, 385] In the macrophage model presented here, 100 μM of maltol, 1,2-HOPO, or PA showed little inhibition of MMP activity in RAW264.7 cells. Similarly, none of these ZBGs inhibited iNOS, COX, or 5-LOX at 100 μM in the cell based assay. In the case of MMPs, the lack of inhibition is likely due to the relatively low affinity of these compounds for the enzymes, as these ZBGs have IC_{50} values of >100 μM in vitro,[344, 345]. Maltol and PA showed minimal in vivo inhibition of TACE, while 1,2-HOPO showed no significant inhibition (Figure 4-

54-5). Thus, under the present assay conditions, maltol, 1,2-HOPO, and PA did not stand out as particularly potent zinc(II) chelators.

The sulfur-containing ligands, thiomaltol and 1,2-HOPTO demonstrate a stronger affinity for zinc(II) than their oxygen-only analogues (maltol and 1,2-HOPO, respectively, Figure 4-2).[345, 365] 1,2-HOPTO has a lower IC_{50} value than thiomaltol against MMP-3 in vitro,[345, 365] and similarly was also more effective than thiomaltol at inhibiting MMP activity in RAW264.7 cells (Figure 4-5). In contrast, these chelators only weakly inhibited the zinc-dependent enzyme TACE in the cellular assay, to a degree similar to their oxygen-only counterparts (Figure 4-54-5). Interestingly, thiomaltol and 1,2-HOPTO were extremely potent inhibitors of heme-iron enzymes. Both compounds inhibited COX activity by 70% (Figure4-6), and iNOS activity by more than 80% (Figure 4-74-7). This strongly suggests that MMPi using these moieties could show cross reactivity with heme enzymes. Without appropriately designed substituents (i.e. a selective backbone moiety),[325, 326] the use of thiomaltol and 1,2-HOPTO as binding groups for either zinc- or heme-iron enzymes should be approached with caution, as these chelators may act promiscuously in vivo.

Nitrogenous ligands such as DPA and TACN demonstrated the greatest promise as platforms for zinc(II)-dependent enzyme inhibitors. Consistent with in vitro results,[344] TACN and DPA were potent inhibitors of MMP and TACE in RAW264.7 cells, inhibiting ~90% of MMP activity (Figure 4-5) and 50% of TACE activity (Figure 4-54-5). This makes these two chelators the most potent ZBGs against the zinc(II) metalloenzymes based on the results of the macrophage screening presented in this study. In contrast, neither DPA nor TACN significantly inhibited any of the iron enzymes

examined. DPA showed some inhibition of iNOS (Figure 4-7), but had no effect on COX or 5-LOX. TACN demonstrated no significant inhibition of any of these metalloenzymes. Given that both of these ZBGs inhibit zinc(II) enzymes in vitro[344] and show selective inhibition over other metalloenzymes in the macrophage model, these ZBGs stand out as excellent candidates to develop selective MMP and/or TACE inhibitors. With an appropriate backbone to further increase the potency and specificity for these targets, DPA and TACN provide an excellent starting point for creating potent and selective zinc(II)-dependent metalloenzyme inhibitors.

In addition to screening simple ZBGs, the macrophage model was used to identify potential off target activity for four known MMPi: GM6001, NNGH, doxycycline, and minocycline. GM6001 completely inhibited MMP activity in RAW264.7 cells, while also blunting TNF_{α} production. This is not surprising, as GM6001 is known to also inhibit TACE.[360, 361] NNGH also showed complete inhibition of MMPs, had no effect on TNF_{α} production, but blunted the activity of 5-LOX, COX, and iNOS (Figure), indicating some degree of promiscuity of this compound between zinc- and iron-dependent enzymes. The hydroxamate ZBG employed by NNGH has a strong thermodynamic preference for binding iron(III) over zinc(II),[325, 342] and this type of broad, albeit weak, inhibition of several metalloenzymes could contribute to potential side effects in the clinical setting. However, to the best of our knowledge, NNGH has not yet undergone clinical trials.

The tetracycline compounds, doxycycline and minocycline, both showed a modest decrease in MMP activity, but did not effect levels of TNF_{α}. Both tetracyclines decreased nitrite production, which is likely caused or exacerbated by a decrease in iNOS

expression, a known off-target interaction of doxycycline.[362] Interestingly, doxycycline increased the production of the 5-LOX metabolite LTC_4 and the COX metabolite PGD_2; furthermore, AA levels were found to be increased by 5-fold (data not shown). This is consistent with work done by Attur et al., who showed that doxycycline increased PGE_2 production by lipopolysaccharide stimulated RAW264.7 cells.[386] Our data further demonstrates an increase in levels of AA, suggesting that doxycycline may hyperactivate cPLA2 and exacerbate the inflammatory response.[349] In general, our findings in the macrophage model support the known pleiotropic nature of these compounds in vivo and confirm that this model can accurately predict in a simple assay known off-target interactions for a variety of MMPi.

Two recently developed MMPi based on hydroxypyrone (maltol) and hydroxypyridinone (1,2-HOPO) ZBGs, PY-2 and 1,2-HOPO-2, were analyzed to determine how MMPi using non-hydroxamate ZBGs interacted with the different metalloenzymes. At 5 μM, neither compound was found to significantly reduce MMP activity in the macrophage model (Figure 4-8). However, RAW264.7 cells primarily express MMP-9 and MMP-13 (Figure 4-4, www.lipidmaps.org), and while PY-2 and 1,2-HOPO-2 inhibit MMP-2, -3, -8, and -12 effectively, they do not significantly inhibit MMP-1, -7, -9, or -13.[363] Thus the observation that PY-2 and 1,2-HOPO-2 do not exhibit significant MMP inhibition in this assay confirms the isoform specificity of these MMPi as determined by in vitro experiments. PY-2 did not significantly inhibit TACE, 5-LOX, COX, or iNOS at 5 μM, demonstrating good selectivity against these enzymes. In contrast, 1,2-HOPO-2 did show some inhibition of COX and iNOS, indicating it may have significant off-target activity in vivo. The difference between PY-2 and 1,2-HOPO-

2 with respect to the heme-iron enzymes is quite striking considering the similar overall structure of the two MMPi and this difference in activity was not recapitulated by the ZBGs alone (Figure4-6 and Figure 4-74-7). This finding points to the significance of the ZBG in designing MMPi, and supports the hypothesis that small changes in the ZBG may have profound effects on the behavior of these compounds in vivo.[363, 365] The results of these facile screening experiments may be useful to avoid such pitfalls prior to more advanced development (i.e. clinical) of these or other metalloenzyme inhibitors.

A general, cell-based method to screen the effect of compounds against a broad range of zinc- and iron-dependent enzymes has been presented. Two ZBGs, DPA and TACN, showed good selectivity, inhibiting the zinc(II) metalloenzymes MMP and TACE, while sparing the iron enzymes 5-LOX, COX, and iNOS. Mixed oxygen/sulfur-based ZBGs, such as thiomaltol and 1,2-HOPTO, inhibited not only MMPs, but also the heme-iron enzymes COX and iNOS. In addition to isolated ZBGs, full length MMPi were examined, including: the hydroxamate inhibitors GM6001 and NNGH, the tetracycline inhibitors doxycycline and minocycline, and the hydroxypyrone and hydroxypyridinone inhibitors PY-2 and 1,2-HOPO-2. The macrophage screen correctly predicted the off-target inhibition that is known for the hydroxamate and tetracycline MMPi. The hydroxypyridione MMPi 1,2-HOPO-2 reduced heme-iron dependant COX and iNOS activity, whereas its hydroxypyrone analogue, PY-2, did not cause any non-specific inhibition. Overall, we identified TACN and DPA as excellent ZBGs for the development of potent, selective zinc(II) metalloenzyme inhibitors, and show that through a simple, cell-based experiment the potential limitations of new full length inhibitors can be evaluated.

4.E Experimental procedures

Materials. Maltol, PA, 1,2-HOPO, 1,2-HOPTO, OP, TACN, DPA, doxycycline, minocycline, and ATP were obtained from Sigma-Aldrich (St. Louis, MO). GM6001 (Illomastat), NNGH (N-Isobutyl-N-(4-methoxyphenylsulfonyl)-glycyl hydroxamic acid), the Griess assay, and fluorogenic MMP Substrate III were purchased from Calbiochem (San Diego, CA). OmniMMP fluorogenic substrate was purchased from Biomol (Plymouth, PA). Thiomaltol, PY-2, and 1,2-HOPO-2 were prepared according to literature methods.[363, 387] RAW264.7 murine macrophages were purchased from American Type Culture Collection (ATCC, Manassas, VA). LC grade solvents were purchased from EMD Biosciences. Synergy C18 reverse phase HPLC column and Strata-X solid phase extraction columns were purchased from Phenomenex (Torrance, CA). Phosphate buffered saline (PBS) was purchased from VWR. Dulbecco's modified Eagle's medium and fetal bovine serum were purchased from Invitrogen (Carlsbad, CA). Kdo_2-Lipid A (KDO) was purchased from Avanti Polar Lipids (Alabaster, AL). All eicosanoids and indomethacin were purchased from Cayman Chemicals (Ann Arbor, MI). The TNF_α assay kit was purchased from R&D Systems (Minneapolis, MN). The CytoTox 96 Non-Radioactive Cytotoxicity Assay for measuring lactate dehydrogenase (LDH) activity was purchased from Promega (Madison, WI). All other reagents were reagent grade or better. UV-Visible spectra were recorded using a Perkin-Elmer Lambda 25 spectrophotometer.

Data Analysis. The data has been normalized to value measure in uninhibited cells or media, unless explicitly described otherwise. Results were reported as mean ± standard deviation, and statistical analysis was performed using the Student's *t*-test. The critical values for statistical significance were set at $\alpha = 0.05$, and *p*-values meeting this threshold were denoted in the figures with an asterisk (*).

Cell Culture and Stimulation. The RAW264.7 murine macrophage cells were cultured in Dulbecco's modified Eagle's medium with 10% fetal bovine serum and 100 units/mL penicillin/streptomycin at 37 °C in a humidified 5% CO_2 atmosphere. 5×10^5 cells were plated in 24-well culture plates in 0.5 mL of media and allowed to adhere for 24 h. The media was replaced with 0.5 mL of serum free media, incubated for 1 h, and stimulated with either 2 mM ATP for 10 min, or with 100 ng/mL KDO for 24 h. Following stimulation, the media was removed and utilized in subsequent assays. All ZBGs and inhibitors were added 30 min prior to stimulation.

Sample Preparation for Short-term (ATP) Stimulation. Following ATP stimulation, the entire 0.5 mL of media was removed and supplemented with 50 μL of internal standards (200 pg/μL of d_4-PGD_2, d_5-LTC_4, and d_8-AA in EtOH) and extracted for PGD_2 and LTC_4 analysis by SPE as previously described.[349, 350] The samples were reconstituted in 50 μL of LC solvent A (water-acetonitrile-acetic acid (70:30:0.02; v/v/v)) for LC-MS/MS analysis.

Sample Preparation for Long-term (KDO) Stimulation. Following KDO stimulation, the entire 0.5 mL of media was removed and supplemented with 50 μL of internal standards (200 pg/μL of d_4-PGD_2, d_5-LTC_4, and d_8-AA in EtOH). The sample was then divided as follows: 100 μL was extracted for PGD_2 analysis as previously described,[349, 350] 50 μL was analyzed for TNF_α, 50 μL was analyzed for nitrite levels, 80 μL was analyzed for MMP activity, and 50 μL was analyzed for LDH activity to determine cell viability. Samples were stored at -20°C until analysis.

Lactate Dehydrogenase Release Assay. Cell viability was assessed using the LDH release assay according to the manufacturer's protocol. Typically, 50 μL of macrophage cell supernatant was incubated for 30 min with a tetrazolium substrate that is converted by LDH activity (via NADH) into a red formazan product that was measured by absorbance at 490 nm on a Bio-Tek ELX808 absorbance microplate reader. To determine the amount of LDH released at 0% viability, cells were frozen at –80 °C for 1 h, thawed, and media was removed. To determine the amount of LDH released at 100% viability, media was removed from unfrozen cells. The viability of cells incubated with inhibitors was determined relative to these two endpoints.

MMP Activity Assay. MMP activity of KDO stimulated cell media was analyzed using a fluorescence substrate assay on a Bio-Tek FLX 800. 80 μL of cell media was incubated at 37 °C with 20 μL of assay buffer (50 mM MES, 10 mM $CaCl_2$, 0.05% Brij-35, pH 6.0) containing MMP Substrate III (final concentration in each well 400 μM) and *p*-aminophenylmercuric acetate (AMPA, final concentration in each well 1 mM). Upon

substrate cleavage, the fluorescence (λ_{ex} = 340 nm, λ_{em} = 485 nm) of each well was measured after 24 h at 37˚C and expressed as relative activity to cells without inhibitors.[345, 365]

TNF_α Release Assay. TACE activity was determined by measuring the amount of TNF_α secretion using a fluorometric assay. Typically, 50 μL of KDO-stimulated cell media was diluted 1:50 in PBS, and 50 μL of the diluted solution was analyzed according to the manufacturer's protocol. The concentration of TNF_α was measured by absorbance at 450 nm on a Bio-Tek ELX808 absorbance microplate reader and compared to a standard curve established using 23 pg/mL to 1500 pg/mL mouse TNF_α standard. Results are reported as relative release to cells without inhibitors.

PGD_2 and LTC_4 Eicosanoid Production Assay. The activity of COX and 5-LOX were determined by measuring the levels of PGD_2 and LTC_4, respectively, by LC-MS/MS[349, 350] using "Method 3" as described in Chapter 3. Briefly, eicosanoids were separated by reverse-phase LC on a Hydrosil C18 column (2.1 mm×250 mm) at a flow rate of 300 μL/min at 50 °C. The column was equilibrated in 90% LC solvent A (water-acetonitrile-acetic acid (70:30:0.02; v/v/v)) and 10% LC solvent B (acetonitrile-isopropyl alcohol (50:50, v/v)). Samples were injected using a 50 μL injection loop and eluted with 10% solvent B from 0 to 2 min, followed by a gradual increase to 100% solvent B using a linear gradient from 2 to 7 min, held at 100% solvent B from 7 to 8.5 min, dropped back to 10% solvent B using a linear gradient from 8.5 to 9 min, and finally held at 10% solvent B until 11 min. Eicosanoids were analyzed using a tandem quadrupole mass

spectrometer (ABI 4000 Q-Trap®, Applied Biosystems) via multiple-reaction monitoring (MRM) in negative-ion mode. The electrospray voltage was -4.5 kV, the turbo ion spray source temperature was 525 °C. Collisional activation of eicosanoid precursor ions used nitrogen as a collision gas. The precursor→product MRM pairs were selected as follows: d_4-PGD_2 (355→275), d_5-LTC_4 (629.6→272), d_8-AA (311→267), PGD_2 (351→271), LTC_4 (624.6→272), and AA (303→259). Quantitative eicosanoid analysis was performed by using a stable isotope dilution method, previously described by Hall and Murphy[278]. A standard curve was prepared by adding 10 ng of each internal (deuterated) eicosanoid standard to the following amounts of primary (non-deuterated) eicosanoid standard: 0.3, 1, 3, 10, 30, and 100 ng. Results are reported as relative release to cells without inhibitors.

Nitrite Production Assay. The activity of iNOS was determined by the measuring the amount of nitrite in KDO stimulated cell media. Nitric oxide is readily oxidized into nitrite, which can be measured using the Griess assay.[377] Following the manufacturer's protocol, 50 μL of KDO stimulated media was analyzed using a colorimetric assay. Briefly, to the cell media was added sulfanilamide, which reacts with nitrite to form a diazonium salt. *N*-1-Napthylethylenediamine dihydrochloride was then added, which reacts with the diazonium salt to form a colored azo compound that was detected by absorbance at 550 nm on a Bio-Tek ELX808 absorbance microplate reader. Results are reported as relative release to cells without inhibitors.

4.F. Acknowledgements

Faith E. Jacobsen and Seth M. Cohen co-authored work from this chapter in the journal ChemBioChem, titled “A Macrophage Cell Model for Selective Metalloprotein Inhibitor Design”. The authors thank Arpita Agrawal (U.C. San Diego) for providing PY-2 and 1,2-HOPO-2, Dr. Jana Lewis (Vanderbilt University) for assistance with protein purification, Prof. Robert C. Murphy (University of Colorado) for providing Zileuton, Daren Stephens for maintaining the RAW264.7 cell line, and Prof. Hideaki Nagase and Dr. Robert Visse (Imperial College of London) for the generous gift of the plasmid vector pET3A containing the human proMMP-3(ΔC) DNA. This work has been supported by grants from the National Institutes of Health (HL080049-01, S.M.C.), the LIPID MAPS Large Scale Collaborative Grant from the National Institutes of Health (GM069338, E.A.D.), and the American Heart Association (0430009N, S.M.C.). F.E.J. was supported in part by a GAANN fellowship (GM-602020-03). M.W.B. was supported in part by a Gastroenterology training grant (T32 DK07202). S.M.C. is a Cottrell Scholar of the Research Corporation.

Chapter 5.

Eicosanoid Dynamics During the Development and Resolution of Lyme Disease-induced Arthritis

5.A Abstract

Eicosanoids and other lipid mediators are indispensable regulators of biological processes as demonstrated by the numerous inflammatory diseases which result from their dysregulation, such as cancer, atherosclerosis and arthritis. Using a murine model of Lyme disease, we utilize the LIPID MAPS lipidomics approach for the quantification of over 100 eicosanoids by LC-MS/MS. Here, we determine for the first time the temporal production of eicosanoids *in vivo*, from the induction of inflammation to its resolution. We propose a model for Lyme arthritis that integrates all the major eicosanoid biosynthetic pathways (cyclooxygenase, lipoxygenase, cytochrome P450), and demonstrate that a lipidomic approach can identify potential contributors to pathology and provide insight into novel diagnosis and treatment strategies.

5.B Introduction

Systems biology has advanced exponentially during the past decade, producing a wealth of data regarding disease susceptibility and pathology. Metabolomics has lagged behind its counterparts, genomics and proteomics, hampering the advancement of sequential systems biology as a cohesive approach to disease investigation and drug discovery. The Lipid Metabolites and Pathway Strategy (LIPID MAPS) consortium was created to address the unique challenges faced by metabolomics researchers in the emerging field of lipidomics[2]. Eicosanoids comprise a diverse class of hundreds of bioactive lipid mediators derived from the metabolism of polyunsaturated fatty acids by cyclooxygenase (COX)[3], lipoxygenase (LOX)[3, 6], cytochrome P450 (CYP)[170] and other, non-enzymatic pathways. Because of their contributions to inflammatory diseases[6, 388],

eicosanoids have been intensely studied, yet *in vivo* research has been primarily focused on a few select metabolites[7]. A quantitative metabolomics approach is essential to our understanding of inflammation as many enzymes can synthesize both pro-inflammatory and pro-resolution mediators[389, 390]. We have developed LC-MS/MS methodology to identify and quantify 104 unique lipid species and utilized this method to determine the temporal eicosanoid profile in the tibiotarsal (ankle) joints of mice infected with *Borrelia burgdorferi,* the causative agent of Lyme disease.

5.C Murine model of Lyme infection and arthritis

Lyme disease is the most common vector-borne illness in the United States and Europe and presents diverse pathologies, the most common of which is arthritis[391]. If not treated with antibiotics, about 60% of individuals will develop severe arthritis, the pathology of which is recapitulated in the murine model[392]. Upon infection with *B. burgdorferi,* arthritis-susceptible C3H/HeJ (C3H) mice developed a severe inflammatory response, which peaked at two weeks post-infection and then spontaneously resolved, whereas DBA/2J (DBA) mice developed a very mild inflammation and are considered arthritis resistant (Figure 5-1A). Bacterial loads in the joints tended to mirror the course of pathology (Figure 5-1B); however, infectious dose does not affect susceptibility or resistance to arthritis development in most mouse strains[393]. The difference in pathology was most evident at the peak of arthritis, the development of which is dependent upon neutrophil recruitment into the infected joint (Figure 5-1C, day 10)[394], whereas macrophages predominated during the resolution phase (Figure 5-1C, day 35)[392].

Resolution of arthritis is attributed to *Borrelia*-specific IgM- and IgG–mediated (Figure 5-1, D and E) clearance of bacteria from infected joints[395].

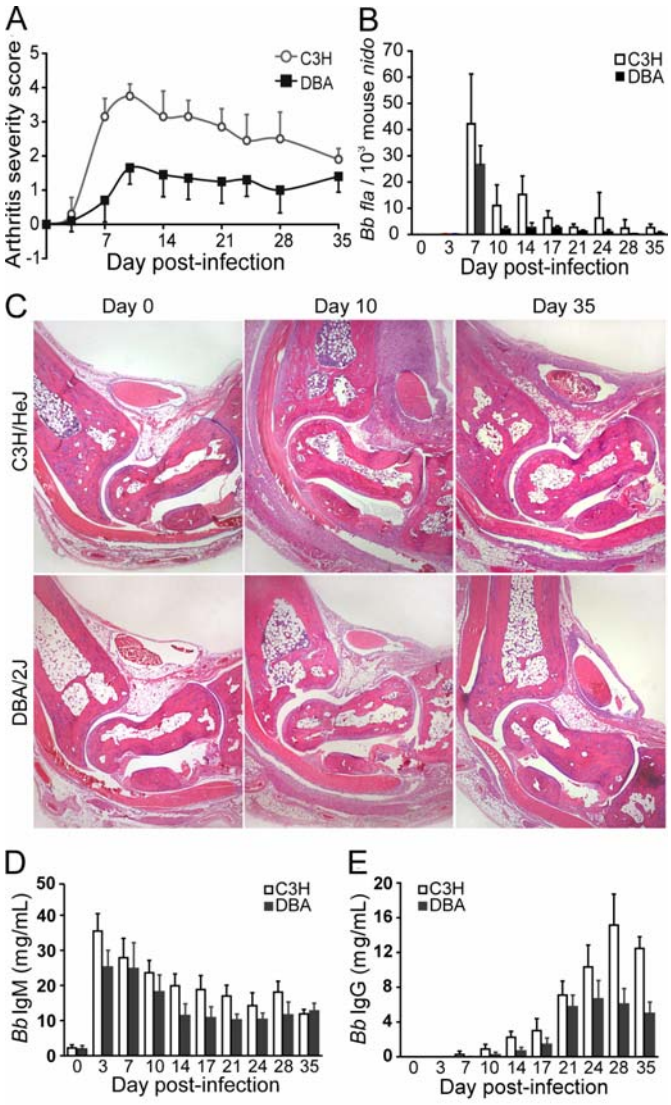

Figure 5-1. Differential development of experimental Lyme disease in resistant DBA and susceptible C3H mice. C3H/HeJ and DBA/2J mice were infected with 1 x 10^5 *Borrelia burgdorferi* and sacrificed at the indicated time points, day 0 through day 35 post-infection. (**A**) Arthritis severity scores were determined by histological examination of H&E stained sections of tibiotarsal joints. (**B**) *Borrelia* loads in the knee joint as determined by real-time PCR. (**C**) Representative sections of ankle joints from C3H (top panels) and DBA (bottom panels) mice before infection and during the peak and resolution phases of the inflammatory response to *Borrelia* infection (day 10 and day 35 post-infection, respectively). (**D** and **E**) Production of *B. burgdorferi*-specific IgM and IgG throughout infection. All results are expressed as the mean ± s.e.m. and are representative of two experiments. (*n* = 5).

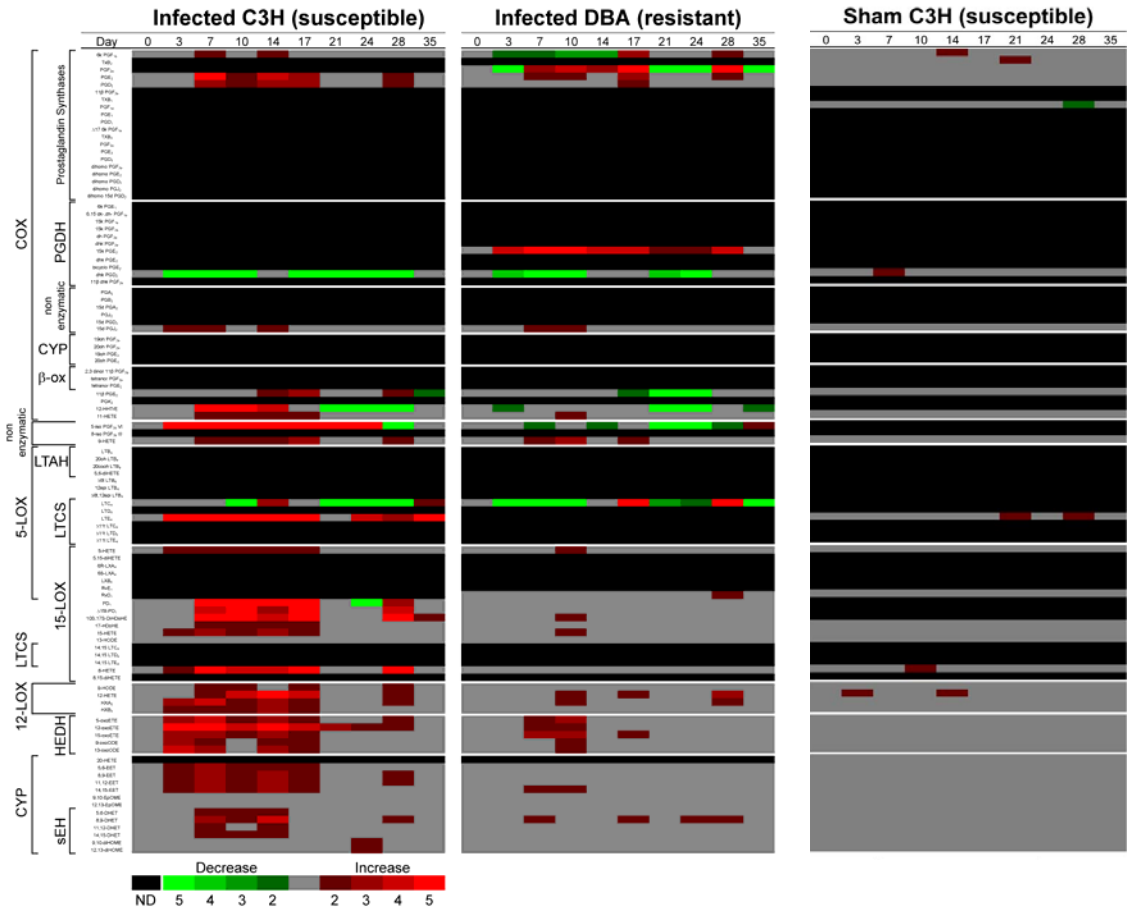

Figure 5-2. Lipidomic profiling reveals temporal changes in major enzymatic and non-enzymatic pathways. Heat map representing changes relative to day 0 (uninfected) of 104 eicosanoid species analyzed in *B. burgdorferi*-infected Lyme arthritis-susceptible (C3H) and -resistant (DBA) mouse strains. Increases in metabolite levels are indicated by red, decreases by green, and detectable but unchanged levels by grey. Metabolites below the level of detection at day 0 are indicated by black.

5.D Lipidomic analysis of infected ankle (tibiotarsal) joints

B. burgdorferi-infected joints were analyzed for eicosanoid production during the progression of arthritis (Figure 5- 2). In total, 42 unique molecular species were detected in C3H or DBA mice, including metabolites derived from cyclooxygenases, lipoxygenases, cytochrome P450s, and non-enzymatic and degradative pathways. In C3H mice, the majority of these were generally elevated between days 3 and 17 post-infection.

Arthritis-resistant DBA mice generated a similar but muted metabolic profile, concentrated in days 7 and 10. Isoprostane levels increased dramatically in C3H mice but not DBA, indicating that massive changes in oxidative stress correlate with the severity of arthritis in C3H mice. Sham-infected C3H mice showed no significant changes in eicosanoid production in the ankle joint. Selected metabolites are described herein; the complete data set has been made available (Tables 5-1 through 5-3).

Prostaglandin (PG) E_2 and D_2 are classic pro-inflammatory cyclooxygenase products that induce and regulate inflammatory responses, as well as some aspects of adaptive immunity[3]. PGE_2 and PGD_2 levels increased in C3H mice beginning at day 3, and returned to basal levels by day 17 (Figure 5-3A), preceding both the rise and fall of bacterial levels in the joint and the production of *Borrelia*-specific antibodies. Prostaglandin D_2 can be hydrolyzed to 15d PGJ_2, which exerts anti-inflammatory effects by inhibiting NF-κB and activating PPARγ *in vitro*[396]; however, its role *in vivo* remains equivocal[59]. C3H joints contained significant amounts of 15d PGJ_2 at days 3, 7 and 14 post-infection. PGE_2 is enzymatically oxidized to form the less bioactive 15k PGE_2, which was detected at days 3 through 21. Arthritis-resistant DBA mice produced these same prostaglandins, but had higher basal levels of PGE_2 and 15k PGE_2 (Figure 5-3B), potentially facilitating a more rapid response to infection. While PGD_2 was not increased during peak bacterial levels on days 7 and 10 in DBA mice, 15d PGJ_2 was significantly elevated (Figure 5-4A). Taken together, these data suggest that PGE_2 and PGD_2 promote the onset of inflammation and allow for the subsequent recruitment of neutrophils early during infection, and prime the subsequent adaptive immune response.

Table 5-1. Eicosanoid fold changes in C3H mice infected with *B. burgdorferi.*

Eicosanoid	Day 0	Day 3	Day 7	Day 10	Day 14	Day 17	Day 21	Day 24	Day 28	Day 35
6k $PGF_{1\alpha}$	1.0	0.7	2.0	1.0	2.5	1.4	0.7	0.9	1.3	1.6
TXB_2	-	-	-	-	-	-	-	-	-	-
$PGF_{2\alpha}$	-	-	-	-	-	-	-	-	-	-
PGE_2	1.0	1.9	5.2	2.8	4.2	3.7	1.2	1.7	2.4	1.7
PGD_2	1.0	1.9	3.7	2.1	3.5	3.1	1.5	1.3	2.2	1.0
11β $PGF_{2\alpha}$	-	-	-	-	-	-	-	-	-	-
TXB_1	-	-	-	-	-	-	-	-	-	-
$PGF_{1\alpha}$	-	-	-	-	-	-	-	-	-	-
PGE_1	-	-	-	-	-	-	-	-	-	-
PGD_1	-	-	-	-	-	-	-	-	-	-
Δ17 6k $PGF_{1\alpha}$	-	-	-	-	-	-	-	-	-	-
TXB_3	-	-	-	-	-	-	-	-	-	-
$PGF_{3\alpha}$	-	-	-	-	-	-	-	-	-	-
PGE_3	-	-	-	-	-	-	-	-	-	-
PGD_3	-	-	-	-	-	-	-	-	-	-
dihomo $PGF_{2\alpha}$	-	-	-	-	-	-	-	-	-	-
dihomo PGE_2	-	-	-	-	-	-	-	-	-	-
dihomo PGD_2	-	-	-	-	-	-	-	-	-	-
dihomo PGJ_2	-	-	-	-	-	-	-	-	-	-
dihomo 15d PGD_2	-	-	-	-	-	-	-	-	-	-
6k PGE_1	-	-	-	-	-	-	-	-	-	-
6,15 dk-,dh- $PGF_{1\alpha}$	-	-	-	-	-	-	-	-	-	-
15k $PGF_{1\alpha}$	-	-	-	-	-	-	-	-	-	-
15k $PGF_{2\alpha}$	-	-	-	-	-	-	-	-	-	-
dh $PGF_{2\alpha}$	-	-	-	-	-	-	-	-	-	-
dhk $PGF_{2\alpha}$	-	-	-	-	-	-	-	-	-	-
15k PGE_2	-	-	-	-	-	-	-	-	-	-
dhk PGE_2	-	-	-	-	-	-	-	-	-	-
bicyclo PGE_2	-	-	-	-	-	-	-	-	-	-
dhk PGD_2	1.0	0.0	0.1	0.0	0.7	0.0	0.0	0.0	0.0	0.5
11β dhk $PGF_{2\alpha}$	-	-	-	-	-	-	-	-	-	-
PGA_2	-	-	-	-	-	-	-	-	-	-
PGB_2	-	-	-	-	-	-	-	-	-	-
15d PGA_2	-	-	-	-	-	-	-	-	-	-
PGJ_2	-	-	-	-	-	-	-	-	-	-
15d PGD_2	-	-	-	-	-	-	-	-	-	-
15d PGJ_2	1.0	2.7	2.7	1.4	2.2	1.5	1.3	1.3	1.2	1.1
19oh $PGF_{2\alpha}$	-	-	-	-	-	-	-	-	-	-
20oh $PGF_{2\alpha}$	-	-	-	-	-	-	-	-	-	-
19oh PGE_2	-	-	-	-	-	-	-	-	-	-
20oh PGE_2	-	-	-	-	-	-	-	-	-	-
2,3 dinor 11β $PGF_{2\alpha}$	-	-	-	-	-	-	-	-	-	-
tetranor $PGF_{2\alpha}$	-	-	-	-	-	-	-	-	-	-
tetranor PGE_2	-	-	-	-	-	-	-	-	-	-
11β PGE_2	1.0	1.8	1.8	0.9	2.4	3.5	1.1	0.7	2.9	0.4
PGK_2	-	-	-	-	-	-	-	-	-	-
12-HHTrE	1.0	1.4	8.8	5.6	4.0	1.0	0.0	0.0	0.0	1.5
11-HETE	1.0	1.6	2.3	2.1	2.5	2.5	1.6	1.2	1.7	1.1
5-iso $PGF_{2\alpha}$ VI	1.0	6.1	8.7	8.9	10.3	8.9	6.4	5.9	0.0	1.4
8-iso $PGF_{2\alpha}$ III	-	-	-	-	-	-	-	-	-	-
9-HETE	1.0	2.0	2.8	2.7	2.9	3.5	1.6	1.6	2.1	1.2

Table 5-1. *Continued.*

Eicosanoid	Day 0	Day 3	Day 7	Day 10	Day 14	Day 17	Day 21	Day 24	Day 28	Day 35
LTB_4	-	-	-	-	-	-	-	-	-	-
20oh LTB_4	-	-	-	-	-	-	-	-	-	-
20cooh LTB_4	-	-	-	-	-	-	-	-	-	-
5,6-diHETE	-	-	-	-	-	-	-	-	-	-
Δ6t LTB_4	-	-	-	-	-	-	-	-	-	-
12epi LTB_4	-	-	-	-	-	-	-	-	-	-
Δ6t,12epi LTB_4	-	-	-	-	-	-	-	-	-	-
LTC_4	1.0	0.5	1.9	0.0	3.4	1.4	0.0	0.0	0.0	2.4
LTD_4	-	-	-	-	-	-	-	-	-	-
LTE_4	1.0	5.1	13.8	6.6	13.0	6.4	0.7	5.0	3.2	5.6
Δ11t LTC_4	-	-	-	-	-	-	-	-	-	-
Δ11t LTD_4	-	-	-	-	-	-	-	-	-	-
Δ11t LTE_4	-	-	-	-	-	-	-	-	-	-
5-HETE	1.0	2.0	2.7	2.2	2.6	2.4	1.6	1.2	1.7	1.0
5,15-diHETE	-	-	-	-	-	-	-	-	-	-
6R-LXA_4	-	-	-	-	-	-	-	-	-	-
6S-LXA_4	-	-	-	-	-	-	-	-	-	-
LXB_4	-	-	-	-	-	-	-	-	-	-
RvE_1	-	-	-	-	-	-	-	-	-	-
RvD_1	-	-	-	-	-	-	-	-	-	-
PD_1	1.0	1.9	11.5	10.6	10.0	18.4	0.8	0.0	3.7	1.4
Δ15t-PD_1	1.0	1.3	4.3	6.4	3.8	5.3	1.1	1.0	4.4	1.7
10S,17S-DiHDoHE	1.0	1.5	6.2	9.8	4.5	10.1	0.9	0.8	8.6	2.2
17-HDoHE	1.0	1.5	2.4	2.0	2.7	2.5	1.0	0.7	1.6	0.9
15-HETE	1.0	2.3	3.0	2.5	3.2	2.8	1.5	1.1	1.9	1.0
13-HODE	1.0	1.7	1.7	1.5	1.9	1.8	1.1	1.1	1.3	1.0
14,15 LTC_4	-	-	-	-	-	-	-	-	-	-
14,15 LTD_4	-	-	-	-	-	-	-	-	-	-
14,15 LTE_4	-	-	-	-	-	-	-	-	-	-
8-HETE	1.0	2.6	5.0	4.9	4.2	9.3	1.6	1.4	6.0	1.8
8,15-diHETE	-	-	-	-	-	-	-	-	-	-
9-HODE	1.0	1.7	2.2	2.0	1.9	2.2	1.0	1.2	2.3	1.4
12-HETE	1.0	1.5	2.7	4.1	6.6	4.8	1.4	1.1	2.5	1.2
HXA_3	1.0	3.2	4.1	2.4	3.3	2.2	1.6	1.0	2.2	0.7
HXB_3	1.0	2.0	2.7	2.0	3.0	2.1	1.2	0.8	1.8	0.9
5-oxoETE	1.0	3.2	4.3	2.7	3.4	2.7	1.8	1.3	2.0	1.1
12-oxoETE	1.0	5.8	5.8	4.8	5.0	4.4	3.2	2.1	2.4	1.5
15-oxoETE	1.0	3.7	3.9	2.6	3.3	2.7	1.9	1.2	1.9	1.1
9-oxoODE	1.0	3.2	2.7	1.6	2.6	2.2	1.2	0.9	1.7	1.1
13-oxoODE	1.0	4.1	3.0	1.9	3.2	2.6	1.3	0.9	1.6	1.0
20-HETE	-	-	-	-	-	-	-	-	-	-
5,6-EET	1.0	2.2	3.2	2.4	2.9	2.4	1.6	1.2	1.9	1.1
8,9-EET	1.0	2.6	3.5	2.8	3.3	2.7	1.8	1.6	2.5	1.1
11,12-EET	1.0	2.0	3.2	2.8	3.3	2.7	1.8	1.5	2.0	1.2
14,15-EET	1.0	2.0	3.1	2.6	3.2	2.5	1.7	1.4	2.0	1.1
9,10-EpOME	1.0	1.7	1.5	1.2	1.7	1.3	1.1	1.5	1.3	1.0
12,13-EpOME	1.0	1.5	1.4	1.3	1.7	1.5	1.1	1.7	1.3	1.1
5,6-DHET	1.0	1.5	2.2	2.1	2.5	2.0	1.1	1.3	1.7	1.2
8,9-DHET	1.0	1.0	3.5	2.1	4.1	1.5	1.8	0.6	2.1	1.7
11,12-DHET	1.0	1.2	2.2	2.0	2.1	2.0	1.4	1.2	1.7	1.2
14,15-DHET	1.0	1.2	2.3	2.0	2.1	2.0	1.3	1.4	1.6	1.4
9,10-diHOME	1.0	1.0	1.1	1.4	1.8	1.6	1.0	2.9	1.2	1.7
12,13-diHOME	1.0	1.0	1.6	1.5	1.6	1.6	1.1	2.6	1.3	1.7

Table 5-2. Eicosanoid fold changes in DBA mice infected with *B. burgdorferi.*

Eicosanoid	Day 0	Day 3	Day 7	Day 10	Day 14	Day 17	Day 21	Day 24	Day 28	Day 35
6k $PGF_{1\alpha}$	1.0	0.4	0.4	0.3	0.3	3.2	0.6	0.6	2.3	0.8
TXB_2	-	-	-	-	-	-	-	-	-	-
$PGF_{2\alpha}$	1.0	0.0	3.0	4.7	3.2	8.9	0.0	0.0	22.4	0.0
PGE_2	1.0	1.3	2.8	2.9	1.4	3.8	1.3	1.5	2.2	1.2
PGD_2	1.0	0.9	1.4	1.4	0.8	2.7	0.8	0.7	1.6	0.9
11β $PGF_{2\alpha}$	-	-	-	-	-	-	-	-	-	-
TXB_1	-	-	-	-	-	-	-	-	-	-
$PGF_{1\alpha}$	-	-	-	-	-	-	-	-	-	-
PGE_1	-	-	-	-	-	-	-	-	-	-
PGD_1	-	-	-	-	-	-	-	-	-	-
Δ17 6k $PGF_{1\alpha}$	-	-	-	-	-	-	-	-	-	-
TXB_3	-	-	-	-	-	-	-	-	-	-
$PGF_{3\alpha}$	-	-	-	-	-	-	-	-	-	-
PGE_3	-	-	-	-	-	-	-	-	-	-
PGD_3	-	-	-	-	-	-	-	-	-	-
dihomo $PGF_{2\alpha}$	-	-	-	-	-	-	-	-	-	-
dihomo PGE_2	-	-	-	-	-	-	-	-	-	-
dihomo PGD_2	-	-	-	-	-	-	-	-	-	-
dihomo PGJ_2	-	-	-	-	-	-	-	-	-	-
dihomo 15d PGD_2	-	-	-	-	-	-	-	-	-	-
6k PGE_1	-	-	-	-	-	-	-	-	-	-
6,15 dk-,dh- $PGF_{1\alpha}$	-	-	-	-	-	-	-	-	-	-
15k $PGF_{1\alpha}$	-	-	-	-	-	-	-	-	-	-
15k $PGF_{2\alpha}$	-	-	-	-	-	-	-	-	-	-
dh $PGF_{2\alpha}$	-	-	-	-	-	-	-	-	-	-
dhk $PGF_{2\alpha}$	-	-	-	-	-	-	-	-	-	-
15k PGE_2	1.0	4.9	9.3	12.1	4.6	4.5	2.4	2.6	4.3	1.4
dhk PGE_2	-	-	-	-	-	-	-	-	-	-
bicyclo PGE_2	-	-	-	-	-	-	-	-	-	-
dhk PGD_2	1.0	0.2	0.0	0.1	0.6	0.6	0.2	0.0	0.8	0.6
11β dhk $PGF_{2\alpha}$	-	-	-	-	-	-	-	-	-	-
PGA_2	-	-	-	-	-	-	-	-	-	-
PGB_2	-	-	-	-	-	-	-	-	-	-
15d PGA_2	-	-	-	-	-	-	-	-	-	-
PGJ_2	-	-	-	-	-	-	-	-	-	-
15d PGD_2	-	-	-	-	-	-	-	-	-	-
15d PGJ_2	1.0	1.7	2.9	2.3	1.1	1.9	1.6	1.2	0.9	0.9
19oh $PGF_{2\alpha}$	-	-	-	-	-	-	-	-	-	-
20oh $PGF_{2\alpha}$	-	-	-	-	-	-	-	-	-	-
19oh PGE_2	-	-	-	-	-	-	-	-	-	-
20oh PGE_2	-	-	-	-	-	-	-	-	-	-
2,3 dinor 11β $PGF_{2\alpha}$	-	-	-	-	-	-	-	-	-	-
tetranor $PGF_{2\alpha}$	-	-	-	-	-	-	-	-	-	-
tetranor PGE_2	-	-	-	-	-	-	-	-	-	-
11β PGE_2	1.0	0.6	0.5	1.2	0.8	0.4	0.0	0.1	0.7	0.6
PGK_2	-	-	-	-	-	-	-	-	-	-
12-HHTrE	1.0	0.3	0.7	2.0	0.7	1.6	0.1	0.2	1.2	0.4
11-HETE	1.0	1.1	2.0	2.2	1.1	1.8	0.9	1.0	1.3	0.9
5-iso $PGF_{2\alpha}$ VI	1.0	0.7	0.4	0.6	0.5	0.5	0.0	0.1	0.5	2.2
8-iso $PGF_{2\alpha}$ III	-	-	-	-	-	-	-	-	-	-
9-HETE	1.0	1.4	2.5	3.0	1.4	2.0	1.1	1.4	0.6	1.0

Table 5-2. *Continued.*

Eicosanoid	Day 0	Day 3	Day 7	Day 10	Day 14	Day 17	Day 21	Day 24	Day 28	Day 35
LTB_4	-	-	-	-	-	-	-	-	-	-
20oh LTB_4	-	-	-	-	-	-	-	-	-	-
20cooh LTB_4	-	-	-	-	-	-	-	-	-	-
5,6-diHETE	-	-	-	-	-	-	-	-	-	-
Δ6t LTB_4	-	-	-	-	-	-	-	-	-	-
12epi LTB_4	-	-	-	-	-	-	-	-	-	-
Δ6t,12epi LTB_4	-	-	-	-	-	-	-	-	-	-
LTC_4	1.0	0.0	0.0	0.0	0.5	12.3	0.3	0.5	6.0	0.0
LTD_4	-	-	-	-	-	-	-	-	-	-
LTE_4	-	-	-	-	-	-	-	-	-	-
Δ11t LTC_4	-	-	-	-	-	-	-	-	-	-
Δ11t LTD_4	-	-	-	-	-	-	-	-	-	-
Δ11t LTE_4	-	-	-	-	-	-	-	-	-	-
5-HETE	1.0	1.1	1.8	2.4	1.1	1.5	0.6	0.8	1.2	0.8
5,15-diHETE	-	-	-	-	-	-	-	-	-	-
6R-LXA_4	-	-	-	-	-	-	-	-	-	-
6S-LXA_4	-	-	-	-	-	-	-	-	-	-
LXB_4	-	-	-	-	-	-	-	-	-	-
RvE_1	-	-	-	-	-	-	-	-	-	-
RvD_1	1.0	1.3	1.1	1.0	0.9	1.1	1.1	0.7	3.0	0.6
PD_1	1.0	1.3	1.4	1.8	0.7	1.5	0.8	0.8	1.1	0.9
Δ15t-PD_1	1.0	0.9	1.5	1.9	0.7	1.4	0.7	0.8	0.9	0.8
10S,17S-DiHDoHE	1.0	0.6	1.5	2.9	0.5	1.4	0.6	0.9	0.6	0.7
17-HDoHE	1.0	1.1	1.3	1.9	0.8	1.0	0.7	0.7	1.9	0.7
15-HETE	1.0	1.1	1.8	2.7	1.1	1.9	0.8	0.8	1.6	0.8
13-HODE	1.0	0.8	1.1	1.4	0.7	1.2	0.6	0.6	1.0	0.7
14,15 LTC_4	-	-	-	-	-	-	-	-	-	-
14,15 LTD_4	-	-	-	-	-	-	-	-	-	-
14,15 LTE_4	-	-	-	-	-	-	-	-	-	-
8-HETE	1.0	0.6	1.9	1.8	0.7	1.3	0.7	0.8	0.8	0.7
8,15-diHETE	-	-	-	-	-	-	-	-	-	-
9-HODE	1.0	0.6	1.1	1.5	0.6	1.1	0.6	0.7	0.8	0.6
12-HETE	1.0	1.1	1.5	2.8	1.0	2.4	0.9	0.8	3.1	0.7
HXA_3	1.0	1.0	1.6	2.1	0.9	1.5	1.2	1.1	2.6	1.1
HXB_3	1.0	0.9	1.1	1.8	0.8	1.6	0.8	0.7	2.5	0.8
5-oxoETE	1.0	1.4	2.7	3.4	1.5	2.0	1.3	1.3	1.7	1.0
12-oxoETE	1.0	1.6	2.5	2.5	1.2	1.5	1.6	1.4	1.9	1.0
15-oxoETE	1.0	1.5	3.4	3.9	1.8	2.2	1.4	1.4	1.8	1.0
9-oxoODE	1.0	1.2	2.0	2.0	1.0	1.7	1.0	0.9	1.0	0.7
13-oxoODE	1.0	1.2	2.0	2.1	1.1	1.5	1.0	0.8	1.2	0.7
20-HETE	-	-	-	-	-	-	-	-	-	-
5,6-EET	1.0	0.9	1.5	1.7	0.9	1.2	1.1	1.0	1.1	1.0
8,9-EET	1.0	0.9	1.4	1.4	0.8	1.0	0.7	0.7	1.1	0.8
11,12-EET	1.0	0.9	1.4	1.5	0.8	1.1	0.8	0.8	1.0	0.8
14,15-EET	1.0	1.2	2.2	2.5	1.2	1.6	1.0	1.0	1.1	1.0
9,10-EpOME	1.0	1.0	1.1	1.1	0.7	1.0	0.8	0.7	0.8	0.7
12,13-EpOME	1.0	0.9	1.0	1.0	0.6	1.0	0.8	0.7	0.9	0.7
5,6-DHET	1.0	1.0	1.4	2.0	0.7	1.4	0.6	0.7	1.1	0.8
8,9-DHET	1.0	1.3	2.2	1.6	1.5	2.1	1.8	2.0	2.0	1.6
11,12-DHET	1.0	0.8	1.3	1.6	0.9	1.4	1.1	1.1	1.1	1.1
14,15-DHET	1.0	0.7	1.2	1.3	0.9	1.2	1.0	1.0	1.1	1.0
9,10-diHOME	1.0	0.7	0.6	0.7	0.7	1.0	0.7	0.8	1.2	1.0
12,13-diHOME	1.0	0.6	0.6	0.8	0.7	0.9	0.7	0.9	1.2	1.1

Table 5-3. Eicosanoid fold changes in sham-infected C3H mice.

Eicosanoid	Day 0	Day 3	Day 7	Day 10	Day 14	Day 17	Day 21	Day 24	Day 28	Day 35
6k $PGF_{1\alpha}$	1.0	2.0	1.1	1.3	2.8	0.9	1.2	1.0	1.3	0.6
TXB_2	1.0	1.0	0.8	1.0	1.1	1.4	2.1	1.7	1.9	0.9
$PGF_{2\alpha}$	1.0	0.9	0.7	1.3	0.7	0.7	0.6	0.6	0.8	0.7
PGE_2	1.0	1.4	1.3	1.4	1.1	1.7	1.4	1.6	1.4	0.8
PGD_2	1.0	1.2	1.2	1.4	1.4	1.2	0.9	1.0	1.0	0.9
11β $PGF_{2\alpha}$	-	-	-	-	-	-	-	-	-	-
TXB_1	-	-	-	-	-	-	-	-	-	-
$PGF_{1\alpha}$	1.0	1.1	1.1	0.9	1.2	0.8	0.9	0.6	0.3	0.8
PGE_1	-	-	-	-	-	-	-	-	-	-
PGD_1	-	-	-	-	-	-	-	-	-	-
Δ17 6k $PGF_{1\alpha}$	-	-	-	-	-	-	-	-	-	-
TXB_3	-	-	-	-	-	-	-	-	-	-
$PGF_{3\alpha}$	-	-	-	-	-	-	-	-	-	-
PGE_3	-	-	-	-	-	-	-	-	-	-
PGD_3	-	-	-	-	-	-	-	-	-	-
dihomo $PGF_{2\alpha}$	-	-	-	-	-	-	-	-	-	-
dihomo PGE_2	-	-	-	-	-	-	-	-	-	-
dihomo PGD_2	-	-	-	-	-	-	-	-	-	-
dihomo PGJ_2	-	-	-	-	-	-	-	-	-	-
dihomo 15d PGD_2	-	-	-	-	-	-	-	-	-	-
6k PGE_1	-	-	-	-	-	-	-	-	-	-
6,15 dk-,dh- $PGF_{1\alpha}$	-	-	-	-	-	-	-	-	-	-
15k $PGF_{1\alpha}$	-	-	-	-	-	-	-	-	-	-
15k $PGF_{2\alpha}$	-	-	-	-	-	-	-	-	-	-
dh $PGF_{2\alpha}$	-	-	-	-	-	-	-	-	-	-
dhk $PGF_{2\alpha}$	-	-	-	-	-	-	-	-	-	-
15k PGE_2	-	-	-	-	-	-	-	-	-	-
dhk PGE_2	-	-	-	-	-	-	-	-	-	-
bicyclo PGE_2	-	-	-	-	-	-	-	-	-	-
dhk PGD_2	1.0	1.6	2.3	1.1	1.0	1.0	0.7	0.8	1.0	1.2
11β dhk $PGF_{2\alpha}$	-	-	-	-	-	-	-	-	-	-
PGA_2	-	-	-	-	-	-	-	-	-	-
PGB_2	-	-	-	-	-	-	-	-	-	-
15d PGA_2	-	-	-	-	-	-	-	-	-	-
PGJ_2	-	-	-	-	-	-	-	-	-	-
15d PGD_2	-	-	-	-	-	-	-	-	-	-
15d PGJ_2	1.0	1.0	1.4	1.1	0.7	0.8	0.8	0.7	1.0	1.1
19oh $PGF_{2\alpha}$	-	-	-	-	-	-	-	-	-	-
20oh $PGF_{2\alpha}$	-	-	-	-	-	-	-	-	-	-
19oh PGE_2	-	-	-	-	-	-	-	-	-	-
20oh PGE_2	-	-	-	-	-	-	-	-	-	-
2,3 dinor 11β $PGF_{2\alpha}$	-	-	-	-	-	-	-	-	-	-
tetranor $PGF_{2\alpha}$	-	-	-	-	-	-	-	-	-	-
tetranor PGE_2	-	-	-	-	-	-	-	-	-	-
11β PGE_2	1.0	1.3	1.2	1.2	0.7	0.5	1.1	0.7	1.1	1.1
PGK_2	-	-	-	-	-	-	-	-	-	-
12-HHTrE	-	-	-	-	-	-	-	-	-	-
11-HETE	1.0	1.4	1.3	1.4	1.0	0.9	0.8	0.9	1.1	0.8
5-iso $PGF_{2\alpha}$ VI	-	-	-	-	-	-	-	-	-	-
8-iso $PGF_{2\alpha}$ III	-	-	-	-	-	-	-	-	-	-
9-HETE	1.0	1.2	1.3	1.2	0.9	0.9	0.8	0.8	1.0	1.0

Table 5-3. *Continued.*

Eicosanoid	Day 0	Day 3	Day 7	Day 10	Day 14	Day 17	Day 21	Day 24	Day 28	Day 35
LTB_4	-	-	-	-	-	-	-	-	-	-
20oh LTB_4	-	-	-	-	-	-	-	-	-	-
20cooh LTB_4	-	-	-	-	-	-	-	-	-	-
5,6-diHETE	-	-	-	-	-	-	-	-	-	-
Δ6t LTB_4	-	-	-	-	-	-	-	-	-	-
12epi LTB_4	-	-	-	-	-	-	-	-	-	-
Δ6t,12epi LTB_4	-	-	-	-	-	-	-	-	-	-
LTC_4	-	-	-	-	-	-	-	-	-	-
LTD_4	-	-	-	-	-	-	-	-	-	-
LTE_4	1.0	1.0	0.6	0.9	0.5	1.0	2.2	1.4	2.1	1.3
Δ11t LTC_4	-	-	-	-	-	-	-	-	-	-
Δ11t LTD_4	-	-	-	-	-	-	-	-	-	-
Δ11t LTE_4	-	-	-	-	-	-	-	-	-	-
5-HETE	1.0	1.2	1.3	1.3	0.9	0.9	0.8	0.9	1.0	1.2
5,15-diHETE	-	-	-	-	-	-	-	-	-	-
6R-LXA_4	-	-	-	-	-	-	-	-	-	-
6S-LXA_4	-	-	-	-	-	-	-	-	-	-
LXB_4	-	-	-	-	-	-	-	-	-	-
RvE_1	-	-	-	-	-	-	-	-	-	-
RvD_1	1.0	1.1	0.8	1.1	1.1	0.7	0.9	0.9	0.8	0.6
PD_1	-	-	-	-	-	-	-	-	-	-
Δ15t-PD_1	-	-	-	-	-	-	-	-	-	-
10S,17S-DiHDoHE	-	-	-	-	-	-	-	-	-	-
17-HDoHE	1.0	1.7	1.2	1.3	1.5	1.0	0.8	0.9	1.0	0.8
15-HETE	1.0	1.5	1.3	1.4	1.1	0.9	0.8	0.9	1.0	1.0
13-HODE	1.0	1.3	1.2	1.3	1.4	1.1	1.0	1.1	1.2	1.2
14,15 LTC_4	-	-	-	-	-	-	-	-	-	-
14,15 LTD_4	-	-	-	-	-	-	-	-	-	-
14,15 LTE_4	-	-	-	-	-	-	-	-	-	-
8-HETE	1.0	1.9	1.4	2.0	1.4	1.0	0.8	1.3	1.9	1.0
8,15-diHETE	-	-	-	-	-	-	-	-	-	-
9-HODE	1.0	1.6	1.3	1.5	1.4	1.0	1.0	1.1	1.4	1.2
12-HETE	1.0	3.0	1.6	1.5	2.0	0.8	0.8	0.8	0.9	0.6
HXA_3	1.0	1.5	1.4	1.4	1.0	0.9	0.9	1.0	1.1	1.2
HXB_3	1.0	1.7	1.3	1.6	1.5	0.9	0.9	1.0	1.1	0.9
5-oxoETE	1.0	1.2	1.5	1.3	0.8	0.9	0.6	0.7	0.8	1.0
12-oxoETE	1.0	1.1	1.3	1.1	0.8	0.7	0.6	0.5	0.7	0.7
15-oxoETE	1.0	1.3	1.5	1.4	0.9	0.9	0.7	0.7	0.9	0.9
9-oxoODE	1.0	1.3	1.4	1.5	0.8	1.1	0.8	0.8	1.1	1.1
13-oxoODE	1.0	1.2	1.3	1.3	0.8	1.1	0.8	0.7	1.0	1.0
20-HETE	1.0	0.6	0.8	0.6	0.7	1.0	0.6	0.7	0.9	0.8
5,6-EET	1.0	1.3	1.2	1.3	0.9	0.8	0.7	0.7	0.8	0.6
8,9-EET	1.0	1.3	1.2	1.2	0.9	0.7	0.6	0.6	0.7	0.7
11,12-EET	1.0	1.3	1.3	1.2	1.0	0.7	0.7	0.6	0.7	0.7
14,15-EET	1.0	1.3	1.1	1.1	0.9	0.6	0.7	0.7	0.7	0.6
9,10-EpOME	1.0	1.6	1.2	1.1	0.9	1.1	1.2	1.2	1.1	1.1
12,13-EpOME	1.0	1.3	1.0	1.1	1.0	1.1	1.2	1.1	1.2	1.2
5,6-DHET	1.0	1.0	1.1	1.1	0.9	0.9	0.8	0.8	0.8	1.0
8,9-DHET	1.0	0.6	0.9	0.9	0.8	0.7	0.5	0.6	0.6	0.6
11,12-DHET	1.0	0.6	1.0	0.9	0.7	0.7	0.6	0.6	0.6	0.7
14,15-DHET	1.0	0.6	1.0	0.9	0.7	0.6	0.5	0.5	0.5	0.7
9,10-diHOME	1.0	0.9	0.9	0.8	0.9	1.1	1.1	1.0	0.8	1.0
12,13-diHOME	1.0	0.7	0.8	0.7	0.8	0.9	0.8	0.8	0.6	0.7

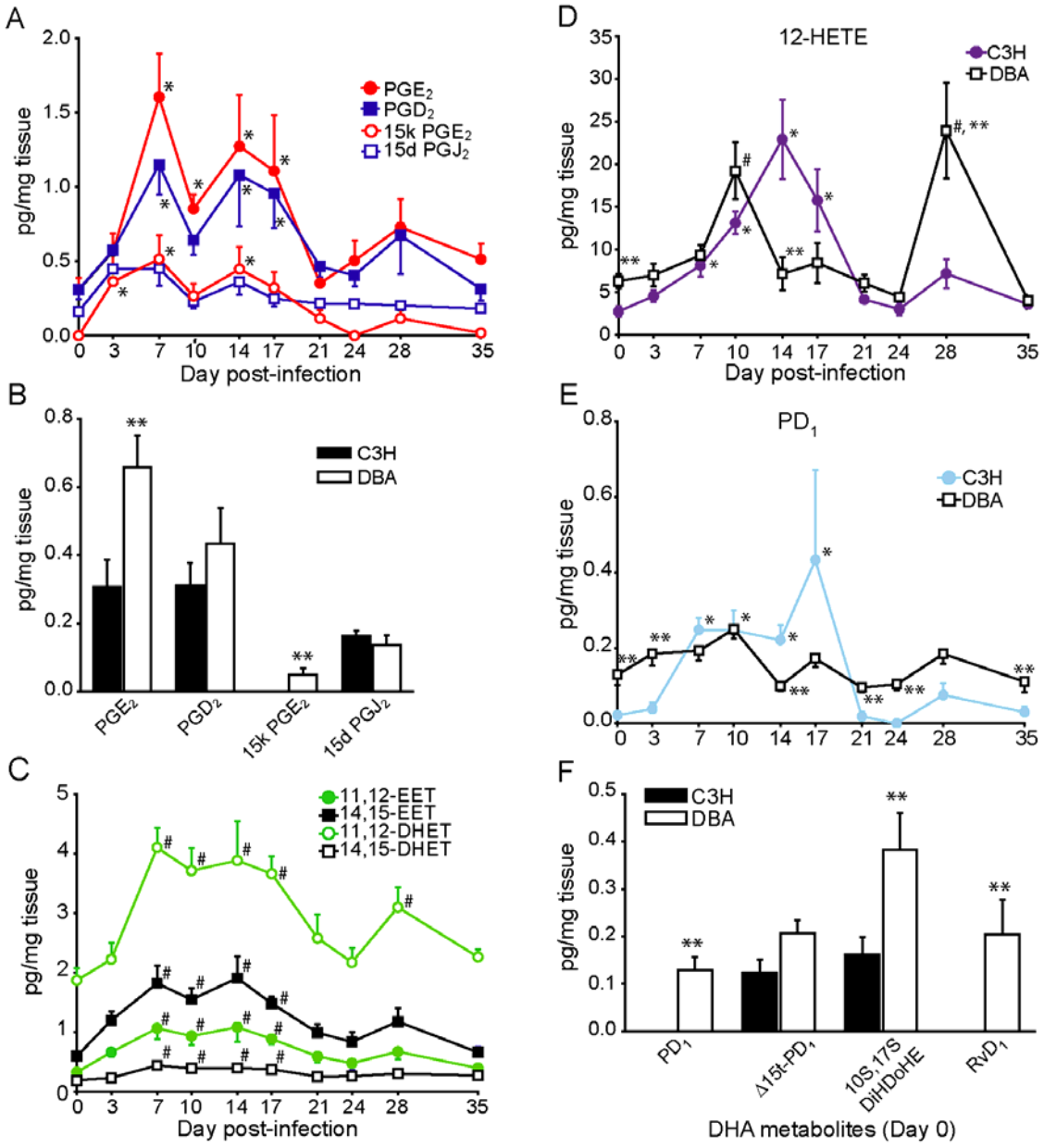

Figure 5-3. Temporal production of COX, CYP, 12-LOX, and DHA metabolites in ankle joints of C3H and DBA mice during *B. burgdorferi* infection. (**A**) Time course of PGE_2 and PGD_2, and their metabolites 15k PGE_2 and 15d PGJ_2, respectively, in *B. burgdorferi* infected C3H mice. (**B**) Differential basal production of PGE_2, PGD_2, 15d PGJ_2, and 15k PGE_2 in C3H and DBA mice. (**C**) Temporal production of 11,12-EET and 14,15-EET, and their metabolites 11,12-DHET and 14,15-DHET, in *B. burgdorferi* infected C3H mice. (**D** and **E**) Temporal production of (D) 12-HETE and (E) pro-resolution protectin D_1 in C3H and DBA mice from day 0 through day 35 post-infection. (**F**) Basal production of DHA metabolites PD_1, Δ15t-PD_1, 10S,17S-DiHDoHE, and resolvin D_1 (RvD_1) in C3H and DBA mice. Results are the mean ± s.e.m. (n = 8-10), except DBA day 28 (n=5). *P < 0.05 versus uninfected ankle joints (C3H). **P ≤ 0.05, DBA compared to C3H values at the same time point. #P< 0.05 versus uninfected values (DBA).

Epoxyeicosatrienoic acids (EETs), which are produced primarily by the CYP2C and CYP2J epoxygenases, modulate inflammation by promoting vasodilation, angiogenesis, and cellular proliferation,[397] as well as inhibiting NF-κB activity[214, 215]. Soluble epoxide hydrolase (sEH) terminates EET signaling by hydrolyzing EETs into biologically inactive dihydroxyeicosatrienoic acids (DHET)[235]. C3H mice demonstrated significant increases in EETs, as well as DHETs, from day 7 to day 17, and day 28 (Figure 5-3C). EETs increased in DBA mice at days 7 and 10, returning to basal levels following bacterial clearance. The ratio of any given EET/DHET pair remained unchanged (Figure 5-4, B and C), suggesting that sEH activity was unaffected in this model. However, while 5,6-EET, 8,9-EET and 14,15-EET were 6-, 12- and 4-fold, respectively, more prevalent than their corresponding DHET, 11,12-EET was 4-fold *less* abundant than 11,12-DHET. Node *et. al.* showed that 11,12-EET specifically prevents leukocyte recruitment by decreasing VCAM expression by inactivating NF-κB in a model of vascular inflammation[214], whereas Lui *et. al.* demonstrate similar effects with all four EETs using a model of laminar flow[215]. It is unlikely that sEH selectively metabolizes 11,12-EET, because the rank order of degradation rate is 14,15-EET > 11,12-EET = 8,9-EET[235, 398]. This suggests that EETs could counterbalance pro-inflammatory signals *in vivo*, and that 11,12-EET plays a unique role during nonvascular inflammation.

Mammalian LOX can be classified according to enzymatic activity (5-LOX, 8-LOX, 12-LOX, 15-LOX) or phylogenetic relatedness[94]. The murine isoforms of the 12-LOX and 15-LOX mediate the formation of 12-hydroperoxyeicosatetraenoic acid (12-HpETE) and then cellular peroxide tone determines its further metabolism. 12-HpETE

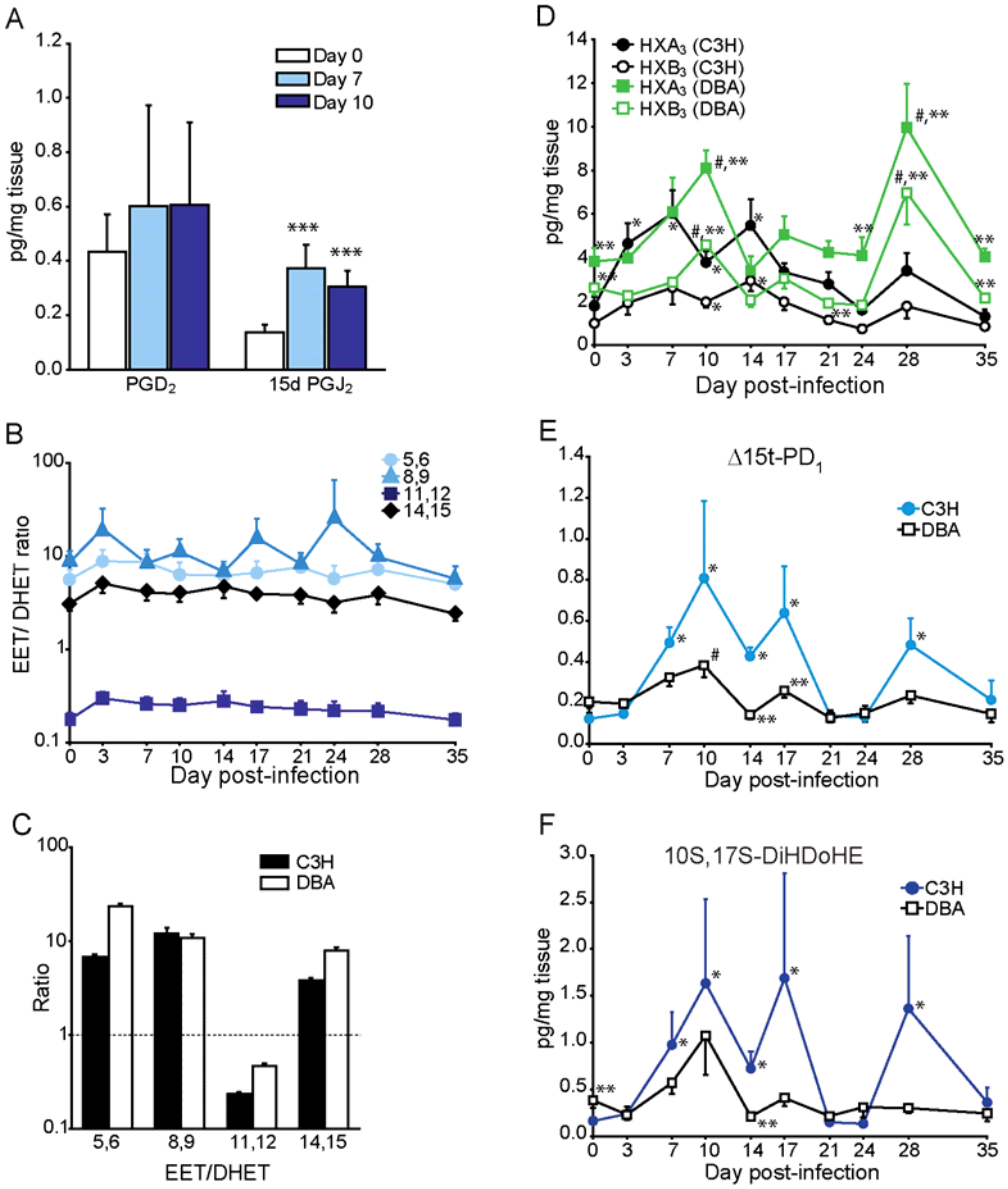

Figure 5-4. C3H and DBA mice differentially produce COX, CYP, 12-LOX and DHA metabolites during *B. burgdorferi* infection. (**A**) Metabolism of PGD_2 in DBA ankle joints at d0, 7, and 10 post-infection. ****p* = 0.02 versus d0 value. (**B**) Ratio of EET to DHET production. 5,6-EET/DHET, 8,9-EET/DHET, 11,12-EET/DHET, and 14,15-EET/DHET values during the course of *B. burgdorferi* infection in ankle joints of C3H mice. (**C**) Overall ratio of EET/DHET production during *B. burgdorferi* infection. The average [5,6], [8,9], [11,12], or [14,15] EET production across all time points was divided by the average of the respective DHET across all time points to determine the cumulative EET/DHET ratios for C3H or DBA ankle joints. (**D**) HXA_3 and HXB_3 in ankle joints of C3H and DBA mice from day 0 through day 35 post-infection. (**E** and **F**) Temporal production of the pro-resolution protectins (E) Δ15t-PD_1, and (F) 10S,17S-DiHDoHE, during *B. burgdorferi* infection in ankle joints of C3H and DBA mice from day 0 through day 35 post-infection. **P* < 0.05, C3H compared to day 0. *P* # < 0.05 DBA compared to day 0. *P*** < 0.05 DBA compared to C3H at the same time point. All results are expressed as the mean ± s.e.m. (*n* = 8-10), except DBA day 28 (n=5).

can be reduced to 12-HETE, which promotes monocyte recruitment by inducing macrophage chemoattractant protein-1 (MCP-1) expression[103], and induces monocyte adhesion through epithelial ICAM upregulation[399]. Alternatively, 12-HpETE can be oxidized to form hepoxilin A_3 (HXA_3), which elicits neutrophil chemotaxis without superoxide production or granule release, and biologically inert hepoxilin B_3 (HXB_3). *Borrelia*-infected C3H mice produced HXA_3 at significantly increased levels between days 3 and 14 (Figure 5-4D), whereas DBA mice produced spikes at day 10 and day 28. Hepoxilin B_3 was detected at lower levels in both strains. 12-HETE levels steadily rose during the induction phase of inflammation, peaking at day 14 in C3H mice and day 10 in DBA mice (Figure 5-3D). This preceded *Borrelia* clearance from the joints, implicating 12-HETE in macrophage recruitment for antibody-mediated bacterial clearance.

Lipoxins, resolvins and protectins comprise a class of lipid mediators produced from poly-unsaturated fatty acids by the action of a transcellular enzyme cascade of LOXs and epoxygenases[6] that are differentially expressed between heterogeneous combinations of neutrophils, macrophages, platelets or endothelial cells[6, 400]. Therapeutically administered protectins have anti-inflammatory and pro-resolution properties, including the prevention of neutrophil influx and the subsequent recruitment of anti-inflammatory macrophages[6, 401]. Protectins (PD) were identified in *B. burgdorferi* infected joints from both mouse strains (Figure 5-3E). PD_1 increased 5- to 10-fold from days 7 to 14 in DBA and C3H joints, respectively. The less biologically active isomers Δ15t-PD_1 and 10S,17S-DiHDoHE were also generated (Figure 5-4, E and F). The relative concentration of 10S,17S-DiHDoHE was greater than either PD_1 or Δ15t-PD_1 and peak production of 10S,17S-DiHDoHE was similar to pro-inflammatory PGE_2 levels. PD_1

was 4-fold less abundant than 10S,17S-DiHDoHE; however, its greater potency in blocking neutrophil influx *in vivo*[402] suggested a physiologically important role in the response to *Borrelia* infection. Overall, the temporal generation of protectins was commensurate with the production of 12-HETE and recruitment of macrophages to the site of infection. This suggests that protectins may dampen pro-inflammatory prostaglandin production, promote non-inflammatory monocyte migration and phagocytosis of apoptotic neutrophils, thus facilitating a return to homeostasis.

5.E Current model of inflammation caused by Lyme disease

Based upon our lipidomic analysis and using *in vitro* knowledge of eicosanoid function, we propose the following model to describe the possible progression of Lyme arthritis (Figure 5-5). Early during infection, pro-inflammatory PGE_2, PGD_2, and HXA_3 induce the release of additional pro-inflammatory factors, thus facilitating the recruitment

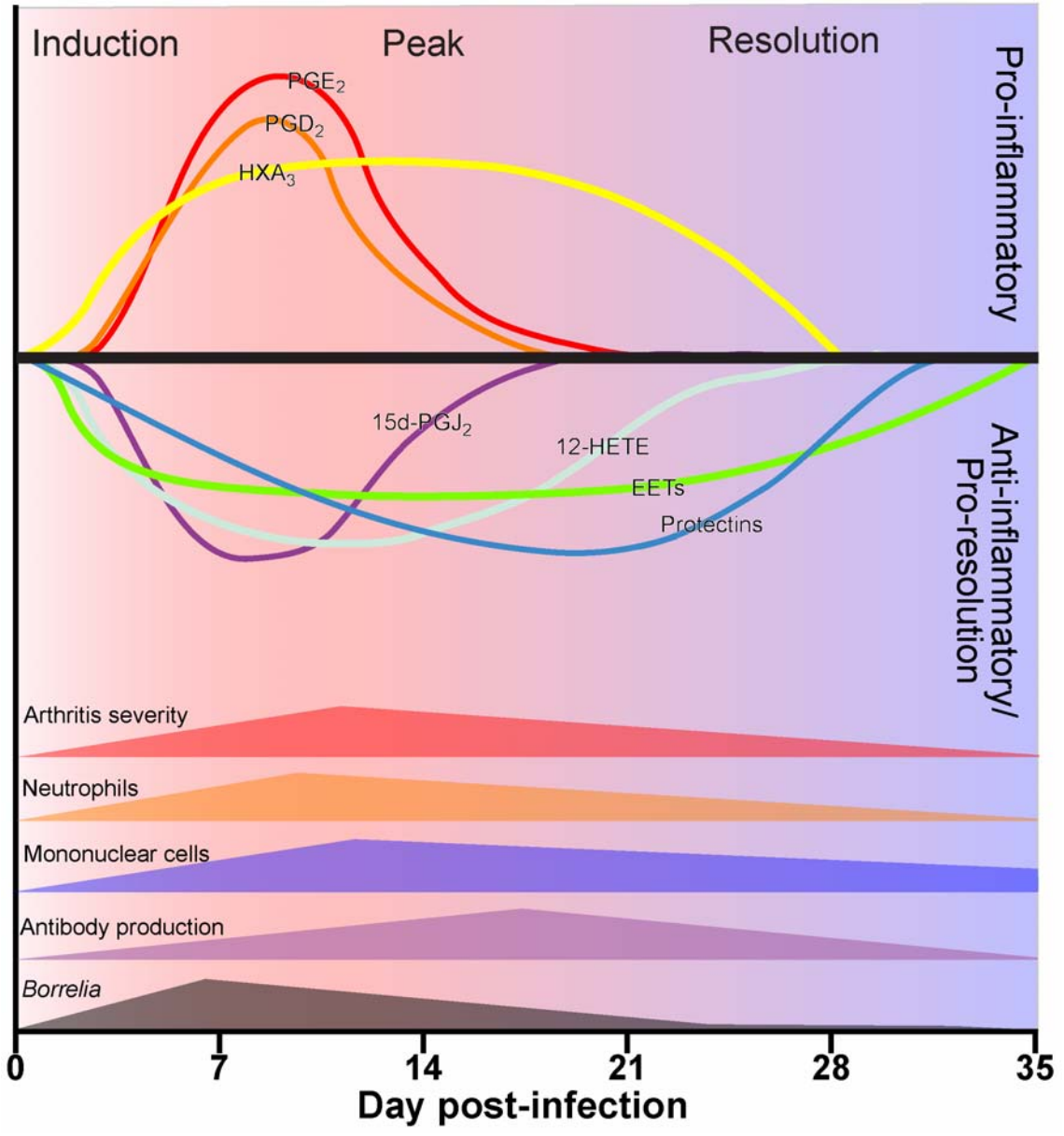

Figure 5-5. Model of the inflammatory response to *B. burgdorferi* infection.

of neutrophils into the joint and the generation of antibodies to combat *B. burgdorferi*. Concomitantly, 15d PGJ_2 and EETs counterbalance this response by activating PPARγ and inactivating NF-κB, aided by DHA-derived, pro-resolution protectins. Around the peak of bacterial levels, 12-HETE induces the recruitment of anti-inflammatory macrophages. Once bacteria and neutrophils have been cleared from the site of infection, EETs return to basal levels indicating a return to homeostasis. Undoubtedly, future studies will refine this model; however, it serves as a starting point for probing the complex manner in which eicosanoids collaborate to coordinate an inflammatory response.

By using two strains of mice, we have attempted to identify metabolic differences that may increase susceptibility to Lyme arthritis. For instance, DBA mice demonstrated 6-fold higher basal levels of protectins and resolvin D_1 (RvD_1) than did C3H mice (Figure 5-3F), although RvD_1 did not change significantly in either strain. Such differences in basal pro-resolution metabolite levels could alter the inflammatory tone, priming DBA mice toward a weaker arthritis. Increased basal levels of several eicosanoids were observed in DBA mice, suggesting a more controlled response to *Borrelia* infection in DBA versus C3H mice. In the broader sense, this type of metabolomic analysis of a naturally progressing inflammation demonstrates the power of a comprehensive lipidomic approach in the diagnosis and treatment of disease.

5.F Experimental procedures

Materials – LC grade solvents were purchased from EMD Biosciences. Synergy C18 reverse phase HPLC column and Strata-X solid phase extraction columns were purchased from Phenomenex (Torrance, CA). Eicosanoids were purchased from Cayman Chemicals (Ann Arbor, MI) and Biomol (Plymouth Meeting, PA).

Animals – Female C3H/HeJ (C3H) and DBA/2J (DBA) mice, 4-6 weeks of age, were purchased from The Jackson Laboratory (Bar Harbor, ME). Animals were housed in a specific pathogen-free facility and given sterile food and water *ad libitum*. All studies were conducted in accordance with the Animal Care and Use Committee of the University of Missouri.

Bacteria and infection – A virulent, low-passage, clonal isolate of the *B. burgdorferi* N40 strain was used for all infections. Frozen stocks were placed in 7.5 mL of Barbour, Stoenner, Kelly (BSK) II medium (Sigma-Aldrich, St. Louis, MO) with 6% rabbit serum (Sigma-Aldrich) and grown to log phase by incubation for 5-6 days at 32˚C. Spirochetes were enumerated using dark field microscopy and a Petroff-Hausser counting chamber (Hausser Scientific, Horsham, PA). Spirochete dilutions were made in sterile BSK II medium and mice were inoculated in both hind footpads with 2.5×10^5 *B. burgdorferi* organisms in 50 µl of medium, for a final inoculum of 5×10^5, a concentration which reliably produces arthritis in susceptible animals[394].

Arthritis severity score – To determine arthritis severity scores, a histologic analysis of the left tibiotarsal joint from each mouse was performed following sacrifice. The tibiotarsal joint was excised, fixed in 10% buffered zinc-formalin, and embedded in paraffin, and 5-µm sections were stained with hematoxylin and eosin (H&E). The sections were evaluated in a blinded manner by two independent observers and were assessed for arthritis severity on a scale of 0 to 4. A score of 0 indicated normal tissue, 1, 2, and 3 indicated minimal, mild, and moderate inflammation, respectively, and 4 indicated severe arthritis. The pathology present in histologic sections was characterized by neutrophil and monocyte infiltration into the joints, tendons, and ligament sheaths; hypertrophy and hyperplasia of the synovium; and fibrin exudates. The extent of the observed inflammatory changes formed the basis for the arthritis severity scores.

Determination of antibody level – B. burgdorferi-specific IgM and IgG levels in the sera of infected animals were determined by enzyme-linked immunosorbent assay (ELISA) as described previously[7].

Determination of B. burgdorferi loads – All tissues were snap-frozen in liquid nitrogen immediately after collection, then stored at -80ºC until extraction. Tissues were homogenized in TRIzol (Invitrogen Corp., Carlsbad, CA) and DNA was extracted according to manufacturer's instructions. Multiplex qPCR for determination of *B. burgdorferi* loads was performed using the TaqMan Universal PCR Master Mix (Applied Biosystems, Foster City, CA) as described previously[394]. Bacterial loads are expressed as copies of *B. burgdorferi Flagellin* per 1000 copies of mouse *Nidogen*.

Eicosanoid Extraction from Tibiotarsal Tissue – Tissues were snap-frozen in liquid nitrogen and stored at -80ºC until extraction. Tibiotarsal joints were pulverized and the resulting powder placed in 3 mL of 50% ethanol in water and then weighed. 10 µl of antioxidant cocktail (0.2 mg/mL butylated hydroxytoluene, 0.2 mg/mL EDTA, 2 mg/mL triphenylphosphine, 2 mg/mL indomethacin in a solution of 2:1:1 methanol:ethanol:H_2O) was added to each sample before incubation at -20ºC for 72h. Samples were then centrifuged at 3500 x g for 30 minutes, the clear ethanolic supernatant removed to a new tube, and dried under nitrogen gas. Samples were reconstituted with 2 ml of 10% MeOH and supplemented with 50 µL of internal standard containing 50 pg/µL (2.5 ng total) of the following deuterated eicosanoids: (d_4) 6k $PGF_{1\alpha}$, (d_4) TXB_2, (d_4) $PGF_{2\alpha}$, (d_4) PGE_2, (d_4) PGD_2, (d_4) 15d PGJ_2, (d_{11}) 5-iso $PGF_{2\alpha}$ VI, (d_4) dhk $PGF_{2\alpha}$, (d_4) dhk PGD_2, (d_4) LTB_4, (d_8) 5-HETE, (d_8) 15-HETE, (d_6) 20-HETE, (d_4) 9-HODE, (d_4) 13-HODE, (d_7) 5-oxoETE, (d_8) 8,9-EET, (d_8) 11,12-EET, (d_8) 14,15-EET, (d_4) 9,10-diHOME and (d_4) 12,13-diHOME Samples were sonicated for 30 seconds with a probe sonicator, and purified by solid phase extraction as previously described[389, 390]. Prior to LC-MS/MS analysis, samples were evaporated using a SpeedVac and reconstituted in 50 µL of LC Solvent A (water-acetonitrile-acetic acid (70:30:0.02; v/v/v)).

Liquid Chromatography and Mass Spectrometry – Eicosanoids were separated by reverse-phase LC on a Synergy C18 column (2.1 mm x 250 mm, 4u) at a flow rate of 300 µl/min at 50ºC. The column was equilibrated in Solvent A [water-acetonitrile-acetic acid (70:30:0.02; v/v/v)], and 40 µl of sample was injected using a 50 µl injection loop and eluted with 0% solvent B [acetonitrile-isopropyl alcohol (50:50; v/v)] between 0 and 1

min. Solvent B was increased in a linear gradient to 25% solvent B until 3 min, to 45% until 11 min, to 60% until 13 min, to 75% until 18 min, and to 90% until 18.5 min. Solvent B was held at 90% until min 20, dropped to 0% by 21 min and held until 25 min. Eicosanoids were analyzed using a tandem quadrupole mass spectrometer (ABI 4000 Q-Trap®, Applied Biosystems) via multiple-reaction monitoring in negative-ion mode. The electrospray voltage was -4.5 kV, the turbo ion spray source temperature was 525ºC. Collisional activation of eicosanoid precursor ions used nitrogen as a collision gas. Eicosanoids were measured using precursor→product multiple-reaction monitoring (MRM) pairs, and the MS analysis was divided into six periods (Table 2-2). The duty cycle for each period ranged between 390 and 840 ms, with an average time of 565 ms. The declustering potential and collision energy for each eicosanoid was optimized for maximal signal using flow injection mass spectrometry. Eicosanoids were identified in samples by matching their MRM signal and LC retention time with those of a pure standard.

Quantitative Eicosanoid Analysis – Quantitative eicosanoid determination was performed by the stable isotope dilution[278] using "Method 2" as described in Chapter 2. Deuterated internal standards (2.5 ng) were added to each sample to account for extraction efficiency and mass spectrometry ion suppression. To calculate the amount of eicosanoid in a sample, the ratio of the natural eicosanoid peak area to the deuterated eicosanoid peak area (termed "eicosanoid ratio") was determined for each sample. The eicosanoid ratio is proportional to the ng of eicosanoid, and was converted using the following standard curve: 2.5 ng of each internal (deuterated) eicosanoid standard mixed with the following

amounts of natural eicosanoid (non-deuterated) primary standard: 0.1, 0.3, 1, 3, 10, 30 and 100 ng. For PD_1 and Δ15t-PD_1, the isomer 10S,17S-DiHDoHE was used as the quantitative primary standard. Performing linear regression using Y = mX, where (Y = eicosanoid ratio, X = ng of eicosanoid, m = slope), the eicosanoid ratio was multiplied by (1/m) to determine the ng eicosanoid in a sample. The deuterated internal standards contained a small but detectable level of natural, undeuterated eicosanoid; to account for this, extraction controls were performed in quadruplicate and the ng of eicosanoid subtracted from each sample. The final values were normalized to the original weight of the tissue, and expressed as ng of eicosanoid per mg of tibiotarsal tissue.

Array Analysis of Lipid Fold Change – In addition to quantitative analysis, data was expressed as a heat map to identify relative increases and decreases in metabolites over time. Similar to the quantitative analysis, the extraction eicosanoid ratio was subtracted from the sample ratio, and normalized to the original weight of the tissue; this value was then normalized to the corresponding value at day 0. The (1/m) value determined from the quantitative curve cancels out of relative fold calculations; one advantage to eliminating (1/m) is that, for eicosanoids with a limited availability, analysis can be performed in the absence of full quantitation.

Statistics – Results are expressed as the mean ± stardard error of mean (s.e.m.). Comparisons were made using one way analysis of variance followed by a multiple comparison procedure, or *t*-test, with P values ≤ 0.05 considered significant.

5.G. Ackowledgements

Victoria A. Blaho and Charles R. Brown co-authored work currently in submission under the title “Eicosanoid Dynamics During the Development and Resolution of Lyme-Disease-induced Arthritis”. We would like to thank Dr. Richard Harkewicz and Daren L. Stephens for discussions regarding mass spectrometry, and Dr. Darren Dumlao and Dr. Linda A. Landon for assistance in preparing the manuscript. Protectin D1, Δ15t-Protectin D1, Resolvin D1, and Lipoxin B4 were a kind gift from Professor Charles N. Serhan (Harvard University). This work was supported by the LIPID MAPS Large Scale Collaborative Grant from the National Institutes of Health (GM069338, E.A.D.) and by a grant from the National Institute of Arthritis and Musculoskeletal and Skin Diseases (R01-AR052748, C.R.B.). M.W.B. was supported in part by a National Institutes of Health Gastroenterology training grant (T32 DK07202).

References

1. Fahy, E. et al. A comprehensive classification system for lipids. J Lipid Res 46, 839-61 (2005).

2. Schmelzer, K., Fahy, E., Subramaniam, S. & Dennis, E. A. The lipid maps initiative in lipidomics. Methods Enzymol 432, 171-83 (2007).

3. Funk, C. D. Prostaglandins and leukotrienes: advances in eicosanoid biology. Science 294, 1871-5 (2001).

4. Simmons, D. L., Botting, R. M. & Hla, T. Cyclooxygenase isozymes: the biology of prostaglandin synthesis and inhibition. Pharmacol Rev 56, 387-437 (2004).

5. Smith, W. L., DeWitt, D. L. & Garavito, R. M. Cyclooxygenases: structural, cellular, and molecular biology. Annu Rev Biochem 69, 145-82 (2000).

6. Serhan, C. N., Chiang, N. & Van Dyke, T. E. Resolving inflammation: dual anti-inflammatory and pro-resolution lipid mediators. Nat Rev Immunol 8, 349-61 (2008).

7. Blaho, V. A., Mitchell, W. J. & Brown, C. R. Arthritis develops but fails to resolve during inhibition of cyclooxygenase 2 in a murine model of Lyme disease. Arthritis Rheum 58, 1485-95 (2008).

8. Schaloske, R. H. & Dennis, E. A. The phospholipase A2 superfamily and its group numbering system. Biochim Biophys Acta 1761, 1246-59 (2006).

9. Six, D. A. & Dennis, E. A. The expanding superfamily of phospholipase A(2) enzymes: classification and characterization. Biochim Biophys Acta 1488, 1-19 (2000).

10. Uozumi, N. & Shimizu, T. Roles for cytosolic phospholipase A2alpha as revealed by gene-targeted mice. Prostaglandins Other Lipid Mediat 68-69, 59-69 (2002).

11. Gijon, M. A., Spencer, D. M., Siddiqi, A. R., Bonventre, J. V. & Leslie, C. C. Cytosolic phospholipase A2 is required for macrophage arachidonic acid release by agonists that Do and Do not mobilize calcium. Novel role of mitogen-activated protein kinase pathways in cytosolic phospholipase A2 regulation. J Biol Chem 275, 20146-56 (2000).

12. Adler, D. H. et al. Inherited human cPLA(2alpha) deficiency is associated with impaired eicosanoid biosynthesis, small intestinal ulceration, and platelet dysfunction. J Clin Invest 118, 2121-2131 (2008).

13. Chiba, H. et al. Cloning of a gene for a novel epithelium-specific cytosolic phospholipase A2, cPLA2delta, induced in psoriatic skin. J Biol Chem 279, 12890-7 (2004).

14. Ohto, T., Uozumi, N., Hirabayashi, T. & Shimizu, T. Identification of novel cytosolic phospholipase A(2)s, murine cPLA(2){delta}, {epsilon}, and {zeta}, which form a gene cluster with cPLA(2){beta}. J Biol Chem 280, 24576-83 (2005).

15. Song, C. et al. Molecular characterization of cytosolic phospholipase A2-beta. J Biol Chem 274, 17063-7 (1999).

16. Stewart, A., Ghosh, M., Spencer, D. M. & Leslie, C. C. Enzymatic properties of human cytosolic phospholipase A(2)gamma. J Biol Chem 277, 29526-36 (2002).

17. Nelson, N. A. Prostaglandin nomenclature. J Med Chem 17, 911-8 (1974).

18. Whittaker, N. et al. The chemical structure of prostaglandin X (prostacyclin). Prostaglandins 12, 915-28 (1976).

19. Wu, K. K. & Liou, J. Y. Cellular and molecular biology of prostacyclin synthase. Biochem Biophys Res Commun 338, 45-52 (2005).

20. Hecker, M. & Ullrich, V. On the mechanism of prostacyclin and thromboxane A2 biosynthesis. J Biol Chem 264, 141-50 (1989).

21. Katsuyama, M. et al. Cloning and expression of a cDNA for the human prostacyclin receptor. FEBS Lett 344, 74-8 (1994).

22. Boie, Y. et al. Cloning and expression of a cDNA for the human prostanoid IP receptor. J Biol Chem 269, 12173-8 (1994).

23. Aubert, J., Ailhaud, G. & Negrel, R. Evidence for a novel regulatory pathway activated by (carba)prostacyclin in preadipose and adipose cells. FEBS Lett 397, 117-21 (1996).

24. Hamberg, M., Svensson, J. & Samuelsson, B. Thromboxanes: a new group of biologically active compounds derived from prostaglandin endoperoxides. Proc Natl Acad Sci U S A 72, 2994-8 (1975).

25. Kinsella, B. T., O'Mahony, D. J. & Fitzgerald, G. A. The human thromboxane A2 receptor alpha isoform (TP alpha) functionally couples to the G proteins Gq and G11 in vivo and is activated by the isoprostane 8-epi prostaglandin F2 alpha. J Pharmacol Exp Ther 281, 957-64 (1997).

26. Samuelsson, B. Isolation And Identification Of Prostaglandins From Human Seminal Plasma. 18. Prostaglandins And Related Factors. J Biol Chem 238, 3229-34 (1963).

27. Park, J. Y., Pillinger, M. H. & Abramson, S. B. Prostaglandin E2 synthesis and secretion: the role of PGE2 synthases. Clin Immunol 119, 229-40 (2006).

28. Tanioka, T., Nakatani, Y., Semmyo, N., Murakami, M. & Kudo, I. Molecular identification of cytosolic prostaglandin E2 synthase that is functionally coupled with cyclooxygenase-1 in immediate prostaglandin E2 biosynthesis. J Biol Chem 275, 32775-82 (2000).

29. Murakami, M., Nakatani, Y., Tanioka, T. & Kudo, I. Prostaglandin E synthase. Prostaglandins Other Lipid Mediat 68-69, 383-99 (2002).

30. Jakobsson, P. J., Thoren, S., Morgenstern, R. & Samuelsson, B. Identification of human prostaglandin E synthase: a microsomal, glutathione-dependent, inducible enzyme, constituting a potential novel drug target. Proc Natl Acad Sci U S A 96, 7220-5 (1999).

31. Huang, X. et al. Structural and functional characterization of human microsomal prostaglandin E synthase-1 by computational modeling and site-directed mutagenesis. Bioorg Med Chem 14, 3553-62 (2006).

32. Naraba, H. et al. Segregated coupling of phospholipases A2, cyclooxygenases, and terminal prostanoid synthases in different phases of prostanoid biosynthesis in rat peritoneal macrophages. J Immunol 160, 2974-82 (1998).

33. Samuelsson, B., Morgenstern, R. & Jakobsson, P. J. Membrane prostaglandin E synthase-1: a novel therapeutic target. Pharmacol Rev 59, 207-24 (2007).

34. Watanabe, K., Kurihara, K., Tokunaga, Y. & Hayaishi, O. Two types of microsomal prostaglandin E synthase: glutathione-dependent and -independent prostaglandin E synthases. Biochem Biophys Res Commun 235, 148-52 (1997).

35. Tanikawa, N. et al. Identification and characterization of a novel type of membrane-associated prostaglandin E synthase. Biochem Biophys Res Commun 291, 884-9 (2002).

36. Yamada, T., Komoto, J., Watanabe, K., Ohmiya, Y. & Takusagawa, F. Crystal structure and possible catalytic mechanism of microsomal prostaglandin E synthase type 2 (mPGES-2). J Mol Biol 348, 1163-76 (2005).

37. Ito, S., Narumiya, S. & Hayaishi, O. Prostaglandin D2: a biochemical perspective. Prostaglandins Leukot Essent Fatty Acids 37, 219-34 (1989).

38. Abdel-Halim, M. S., Hamberg, M., Sjoquist, B. & Anggard, E. Identification of prostaglandin D2 as a major prostaglandin in homogenates of rat brain. Prostaglandins 14, 633-43 (1977).

39. Roberts, L. J., 2nd, Lewis, R. A., Oates, J. A. & Austen, K. F. Prostaglandin thromboxane, and 12-hydroxy-5,8,10,14-eicosatetraenoic acid production by ionophore-stimulated rat serosal mast cells. Biochim Biophys Acta 575, 185-92 (1979).

40. Urade, Y. et al. Structural and functional significance of cysteine residues of glutathione-independent prostaglandin D synthase. Identification of Cys65 as an essential thiol. J Biol Chem 270, 1422-8 (1995).

41. Shimamoto, S. et al. NMR solution structure of lipocalin-type prostaglandin D synthase: evidence for partial overlapping of catalytic pocket and retinoic acid-binding pocket within the central cavity. J Biol Chem 282, 31373-9 (2007).

42. Kanaoka, Y. et al. Cloning and crystal structure of hematopoietic prostaglandin D synthase. Cell 90, 1085-95 (1997).

43. Pettipher, R. The roles of the prostaglandin D(2) receptors DP(1) and CRTH2 in promoting allergic responses. Br J Pharmacol 153 Suppl 1, S191-9 (2008).

44. Sawyer, N. et al. Molecular pharmacology of the human prostaglandin D2 receptor, CRTH2. Br J Pharmacol 137, 1163-72 (2002).

45. Daiyasu, H., Watanabe, K. & Toh, H. Recruitment of thioredoxin-like domains into prostaglandin synthases. Biochem Biophys Res Commun 369, 281-6 (2008).

46. Suzuki-Yamamoto, T. et al. cDNA cloning, expression and characterization of human prostaglandin F synthase. FEBS Lett 462, 335-40 (1999).

47. Moriuchi, H. et al. Molecular characterization of a novel type of prostamide/prostaglandin F synthase, belonging to the thioredoxin-like superfamily. J Biol Chem 283, 792-801 (2008).

48. Basu, S. Novel cyclooxygenase-catalyzed bioactive prostaglandin F2alpha from physiology to new principles in inflammation. Med Res Rev 27, 435-68 (2007).

49. Abramovitz, M. et al. Cloning and expression of a cDNA for the human prostanoid FP receptor. J Biol Chem 269, 2632-6 (1994).

50. Komoto, J., Yamada, T., Watanabe, K. & Takusagawa, F. Crystal structure of human prostaglandin F synthase (AKR1C3). Biochemistry 43, 2188-98 (2004).

51. Komoto, J., Yamada, T., Watanabe, K., Woodward, D. F. & Takusagawa, F. Prostaglandin F2alpha formation from prostaglandin H2 by prostaglandin F synthase (PGFS): crystal structure of PGFS containing bimatoprost. Biochemistry 45, 1987-96 (2006).

52. Penning, T. M. et al. Aldo-keto reductase (AKR) 1C3: role in prostate disease and the development of specific inhibitors. Mol Cell Endocrinol 248, 182-91 (2006).

53. Levine, L., Wu, K. Y. & Pong, S. S. Stereospecificity of enzymatic reduction of prostaglandin E2 to F2alpha. Prostaglandins 9, 531-44 (1975).

54. Wermuth, B. Purification and properties of an NADPH-dependent carbonyl reductase from human brain. Relationship to prostaglandin 9-ketoreductase and xenobiotic ketone reductase. J Biol Chem 256, 1206-13 (1981).

55. Miura, T., Nishinaka, T. & Terada, T. Different functions between human monomeric carbonyl reductase 3 and carbonyl reductase 1. Mol Cell Biochem (2008).

56. Yokoyama, Y. et al. Clofibric acid, a peroxisome proliferator-activated receptor alpha ligand, inhibits growth of human ovarian cancer. Mol Cancer Ther 6, 1379-86 (2007).

57. Waclawik, A. & Ziecik, A. J. Differential expression of prostaglandin (PG) synthesis enzymes in conceptus during peri-implantation period and endometrial expression of carbonyl reductase/PG 9-ketoreductase in the pig. J Endocrinol 194, 499-510 (2007).

58. Straus, D. S. & Glass, C. K. Cyclopentenone prostaglandins: new insights on biological activities and cellular targets. Med Res Rev 21, 185-210 (2001).

59. Powell, W. S. 15-Deoxy-delta12,14-PGJ2: endogenous PPARgamma ligand or minor eicosanoid degradation product? J Clin Invest 112, 828-30 (2003).

60. Murphy, R. C., Hammarstrom, S. & Samuelsson, B. Leukotriene C: a slow-reacting substance from murine mastocytoma cells. Proc Natl Acad Sci U S A 76, 4275-9 (1979).

61. Matsumoto, T. et al. Molecular cloning and amino acid sequence of human 5-lipoxygenase. Proc Natl Acad Sci U S A 85, 26-30 (1988).

62. Ferguson, A. D. et al. Crystal structure of inhibitor-bound human 5-lipoxygenase-activating protein. Science 317, 510-2 (2007).

63. Murphy, R. C. & Gijon, M. A. Biosynthesis and metabolism of leukotrienes. Biochem J 405, 379-95 (2007).

64. Powell, W. S. & Rokach, J. Biochemistry, biology and chemistry of the 5-lipoxygenase product 5-oxo-ETE. Prog Lipid Res 44, 154-83 (2005).

65. Jones, C. E. et al. Expression and characterization of a 5-oxo-6E,8Z,11Z,14Z-eicosatetraenoic acid receptor highly expressed on human eosinophils and neutrophils. Mol Pharmacol 63, 471-7 (2003).

66. Borgeat, P. & Samuelsson, B. Metabolism of arachidonic acid in polymorphonuclear leukocytes. Structural analysis of novel hydroxylated compounds. J Biol Chem 254, 7865-9 (1979).

67. Ford-Hutchinson, A. W., Bray, M. A., Doig, M. V., Shipley, M. E. & Smith, M. J. Leukotriene B, a potent chemokinetic and aggregating substance released from polymorphonuclear leukocytes. Nature 286, 264-5 (1980).

68. Tager, A. M. & Luster, A. D. BLT1 and BLT2: the leukotriene B(4) receptors. Prostaglandins Leukot Essent Fatty Acids 69, 123-34 (2003).

69. Tager, A. M. et al. BLTR mediates leukotriene B(4)-induced chemotaxis and adhesion and plays a dominant role in eosinophil accumulation in a murine model of peritonitis. J Exp Med 192, 439-46 (2000).

70. Haribabu, B. et al. Targeted disruption of the leukotriene B(4) receptor in mice reveals its role in inflammation and platelet-activating factor-induced anaphylaxis. J Exp Med 192, 433-8 (2000).

71. Okuno, T. et al. 12(S)-Hydroxyheptadeca-5Z, 8E, 10E-trienoic acid is a natural ligand for leukotriene B4 receptor 2. J Exp Med 205, 759-66 (2008).

72. Haeggstrom, J. Z. Leukotriene A4 hydrolase/aminopeptidase, the gatekeeper of chemotactic leukotriene B4 biosynthesis. J Biol Chem 279, 50639-42 (2004).

73. Tholander, F. et al. Leukotriene A4 hydrolase, insights into the molecular evolution by homology modeling and mutational analysis of enzyme from Saccharomyces cerevisiae. J Biol Chem 280, 33477-86 (2005).

74. Fitzpatrick, F., Haeggstrom, J., Granstrom, E. & Samuelsson, B. Metabolism of leukotriene A4 by an enzyme in blood plasma: a possible leukotactic mechanism. Proc Natl Acad Sci U S A 80, 5425-9 (1983).

75. Funk, C. D. et al. Molecular cloning and amino acid sequence of leukotriene A4 hydrolase. Proc Natl Acad Sci U S A 84, 6677-81 (1987).

76. Thunnissen, M. M., Nordlund, P. & Haeggstrom, J. Z. Crystal structure of human leukotriene A(4) hydrolase, a bifunctional enzyme in inflammation. Nat Struct Biol 8, 131-5 (2001).

77. Peters-Golden, M., Gleason, M. M. & Togias, A. Cysteinyl leukotrienes: multi-functional mediators in allergic rhinitis. Clin Exp Allergy 36, 689-703 (2006).

78. Rovati, G. E. & Capra, V. Cysteinyl-leukotriene receptors and cellular signals. ScientificWorldJournal 7, 1375-92 (2007).

79. Lam, B. K., Penrose, J. F., Freeman, G. J. & Austen, K. F. Expression cloning of a cDNA for human leukotriene C4 synthase, an integral membrane protein conjugating reduced glutathione to leukotriene A4. Proc Natl Acad Sci U S A 91, 7663-7 (1994).

80. Welsch, D. J. et al. Molecular cloning and expression of human leukotriene-C4 synthase. Proc Natl Acad Sci U S A 91, 9745-9 (1994).

81. Scoggan, K. A., Jakobsson, P. J. & Ford-Hutchinson, A. W. Production of leukotriene C4 in different human tissues is attributable to distinct membrane bound biosynthetic enzymes. J Biol Chem 272, 10182-7 (1997).

82. Kanaoka, Y., Maekawa, A., Penrose, J. F., Austen, K. F. & Lam, B. K. Attenuated zymosan-induced peritoneal vascular permeability and IgE-dependent passive cutaneous anaphylaxis in mice lacking leukotriene C4 synthase. J Biol Chem 276, 22608-13 (2001).

83. Ago, H. et al. Crystal structure of a human membrane protein involved in cysteinyl leukotriene biosynthesis. Nature 448, 609-12 (2007).

84. Martinez Molina, D. et al. Structural basis for synthesis of inflammatory mediators by human leukotriene C4 synthase. Nature 448, 613-6 (2007).

85. Anderson, M. E., Allison, R. D. & Meister, A. Interconversion of leukotrienes catalyzed by purified gamma-glutamyl transpeptidase: concomitant formation of leukotriene D4 and gamma-glutamyl amino acids. Proc Natl Acad Sci U S A 79, 1088-91 (1982).

86. Keillor, J. W., Castonguay, R. & Lherbet, C. Gamma-glutamyl transpeptidase substrate specificity and catalytic mechanism. Methods Enzymol 401, 449-67 (2005).

87. Carter, B. Z. et al. Metabolism of leukotriene C4 in gamma-glutamyl transpeptidase-deficient mice. J Biol Chem 272, 12305-10 (1997).

88. Heisterkamp, N., Rajpert-De Meyts, E., Uribe, L., Forman, H. J. & Groffen, J. Identification of a human gamma-glutamyl cleaving enzyme related to, but distinct from, gamma-glutamyl transpeptidase. Proc Natl Acad Sci U S A 88, 6303-7 (1991).

89. Carter, B. Z., Shi, Z. Z., Barrios, R. & Lieberman, M. W. gamma-glutamyl leukotrienase, a gamma-glutamyl transpeptidase gene family member, is expressed primarily in spleen. J Biol Chem 273, 28277-85 (1998).

90. Shi, Z. Z., Han, B., Habib, G. M., Matzuk, M. M. & Lieberman, M. W. Disruption of gamma-glutamyl leukotrienase results in disruption of leukotriene D(4) synthesis in vivo and attenuation of the acute inflammatory response. Mol Cell Biol 21, 5389-95 (2001).

91. Adachi, H. et al. Purification and characterization of human microsomal dipeptidase. J Biochem 105, 957-61 (1989).

92. Habib, G. M. et al. Leukotriene D4 and cystinyl-bis-glycine metabolism in membrane-bound dipeptidase-deficient mice. Proc Natl Acad Sci U S A 95, 4859-63 (1998).

93. Habib, G. M., Shi, Z. Z., Cuevas, A. A. & Lieberman, M. W. Identification of two additional members of the membrane-bound dipeptidase family. Faseb J 17, 1313-5 (2003).

94. Kuhn, H. & O'Donnell, V. B. Inflammation and immune regulation by 12/15-lipoxygenases. Prog Lipid Res 45, 334-56 (2006).

95. Minor, W. et al. Crystal structure of soybean lipoxygenase L-1 at 1.4 A resolution. Biochemistry 35, 10687-701 (1996).

96. Skrzypczak-Jankun, E., Amzel, L. M., Kroa, B. A. & Funk, M. O., Jr. Structure of soybean lipoxygenase L3 and a comparison with its L1 isoenzyme. Proteins 29, 15-31 (1997).

97. Gillmor, S. A., Villasenor, A., Fletterick, R., Sigal, E. & Browner, M. F. The structure of mammalian 15-lipoxygenase reveals similarity to the lipases and the determinants of substrate specificity. Nat Struct Biol 4, 1003-9 (1997).

98. Coffa, G., Schneider, C. & Brash, A. R. A comprehensive model of positional and stereo control in lipoxygenases. Biochem Biophys Res Commun 338, 87-92 (2005).

99. Murakami, K., Ide, T., Suzuki, M., Mochizuki, T. & Kadowaki, T. Evidence for direct binding of fatty acids and eicosanoids to human peroxisome proliferators-activated receptor alpha. Biochem Biophys Res Commun 260, 609-13 (1999).

100. Huang, J. T. et al. Interleukin-4-dependent production of PPAR-gamma ligands in macrophages by 12/15-lipoxygenase. Nature 400, 378-82 (1999).

101. Muga, S. J. et al. 8S-lipoxygenase products activate peroxisome proliferator-activated receptor alpha and induce differentiation in murine keratinocytes. Cell Growth Differ 11, 447-54 (2000).

102. Hsi, L. C., Wilson, L. C. & Eling, T. E. Opposing effects of 15-lipoxygenase-1 and -2 metabolites on MAPK signaling in prostate. Alteration in peroxisome proliferator-activated receptor gamma. J Biol Chem 277, 40549-56 (2002).

103. Wen, Y., Gu, J., Vandenhoff, G. E., Liu, X. & Nadler, J. L. Role of 12/15-lipoxygenase in the expression of MCP-1 in mouse macrophages. Am J Physiol Heart Circ Physiol 294, H1933-8 (2008).

104. Zhang, B., Cao, H. & Rao, G. N. 15(S)-hydroxyeicosatetraenoic acid induces angiogenesis via activation of PI3K-Akt-mTOR-S6K1 signaling. Cancer Res 65, 7283-91 (2005).

105. Nie, D. et al. Mechanisms regulating tumor angiogenesis by 12-lipoxygenase in prostate cancer cells. J Biol Chem 281, 18601-9 (2006).

106. Kotha, A. et al. 15-(S)-HPETE and 15-(S)-HETE effects on acute lymphoblasticleukemia cell line-Jurkat: Activation of Fas mediated death pathway. Biotechnol Appl Biochem (2008).

107. Kwon, K. J., Jung, Y. S., Lee, S. H., Moon, C. H. & Baik, E. J. Arachidonic acid induces neuronal death through lipoxygenase and cytochrome P450 rather than cyclooxygenase. J Neurosci Res 81, 73-84 (2005).

108. Hwang, S. W. et al. Direct activation of capsaicin receptors by products of lipoxygenases: endogenous capsaicin-like substances. Proc Natl Acad Sci U S A 97, 6155-60 (2000).

109. Nigam, S., Zafiriou, M. P., Deva, R., Ciccoli, R. & Roux-Van der Merwe, R. Structure, biochemistry and biology of hepoxilins: an update. Febs J 274, 3503-12 (2007).

110. Pace-Asciak, C. R., Granstrom, E. & Samuelsson, B. Arachidonic acid epoxides. Isolation and structure of two hydroxy epoxide intermediates in the formation of

8,11,12- and 10,11,12-trihydroxyeicosatrienoic acids. J Biol Chem 258, 6835-40 (1983).

111. Pace-Asciak, C. R. & Lee, W. S. Purification of hepoxilin epoxide hydrolase from rat liver. J Biol Chem 264, 9310-3 (1989).

112. Dho, S., Grinstein, S., Corey, E. J., Su, W. G. & Pace-Asciak, C. R. Hepoxilin A3 induces changes in cytosolic calcium, intracellular pH and membrane potential in human neutrophils. Biochem J 266, 63-8 (1990).

113. Mrsny, R. J. et al. Identification of hepoxilin A3 in inflammatory events: a required role in neutrophil migration across intestinal epithelia. Proc Natl Acad Sci U S A 101, 7421-6 (2004).

114. Pace-Asciak, C. R., Martin, J. M. & Corey, E. J. Hepoxilins, potential endogenous mediators of insulin release. Prog Lipid Res 25, 625-8 (1986).

115. Nigam, S. et al. Hepoxilin A3 (HXA3) synthase deficiency is causative of a novel ichthyosis form. FEBS Lett 582, 279-85 (2008).

116. Carlen, P. L. et al. Formation and electrophysiological actions of the arachidonic acid metabolites, hepoxilins, at nanomolar concentrations in rat hippocampal slices. Neuroscience 58, 493-502 (1994).

117. Reynaud, D., Demin, P. & Pace-Asciak, C. R. Hepoxilin A3-specific binding in human neutrophils. Biochem J 313 (Pt 2), 537-41 (1996).

118. Serhan, C. N., Hamberg, M. & Samuelsson, B. Lipoxins: novel series of biologically active compounds formed from arachidonic acid in human leukocytes. Proc Natl Acad Sci U S A 81, 5335-9 (1984).

119. Serhan, C. N. Lipoxins and aspirin-triggered 15-epi-lipoxins are the first lipid mediators of endogenous anti-inflammation and resolution. Prostaglandins Leukot Essent Fatty Acids 73, 141-62 (2005).

120. Serhan, C. N. & Sheppard, K. A. Lipoxin formation during human neutrophil-platelet interactions. Evidence for the transformation of leukotriene A4 by platelet 12-lipoxygenase in vitro. J Clin Invest 85, 772-80 (1990).

121. Claria, J. & Serhan, C. N. Aspirin triggers previously undescribed bioactive eicosanoids by human endothelial cell-leukocyte interactions. Proc Natl Acad Sci U S A 92, 9475-9 (1995).

122. Chiang, N. et al. The lipoxin receptor ALX: potent ligand-specific and stereoselective actions in vivo. Pharmacol Rev 58, 463-87 (2006).

123. Gronert, K., Martinsson-Niskanen, T., Ravasi, S., Chiang, N. & Serhan, C. N. Selectivity of recombinant human leukotriene D(4), leukotriene B(4), and lipoxin A(4) receptors with aspirin-triggered 15-epi-LXA(4) and regulation of vascular and inflammatory responses. Am J Pathol 158, 3-9 (2001).

124. Schaldach, C. M., Riby, J. & Bjeldanes, L. F. Lipoxin A4: a new class of ligand for the Ah receptor. Biochemistry 38, 7594-600 (1999).

125. Machado, F. S. et al. Anti-inflammatory actions of lipoxin A4 and aspirin-triggered lipoxin are SOCS-2 dependent. Nat Med 12, 330-4 (2006).

126. Yokoyama, C. et al. Arachidonate 12-lipoxygenase purified from porcine leukocytes by immunoaffinity chromatography and its reactivity with hydroperoxyeicosatetraenoic acids. J Biol Chem 261, 16714-21 (1986).

127. Feltenmark, S. et al. Eoxins are proinflammatory arachidonic acid metabolites produced via the 15-lipoxygenase-1 pathway in human eosinophils and mast cells. Proc Natl Acad Sci U S A 105, 680-5 (2008).

128. Drazen, J. M. et al. Contractile activities of structural analogs of leukotrienes C and D: necessity of a hydrophobic region. Proc Natl Acad Sci U S A 78, 3195-8 (1981).

129. Sala, A. et al. Contractile and binding activities of structural analogues of LTC4 in the longitudinal muscle of guinea-pig ileum. Eicosanoids 3, 105-10 (1990).

130. Burger, F., Krieg, P., Marks, F. & Furstenberger, G. Positional- and stereo-selectivity of fatty acid oxygenation catalysed by mouse (12S)-lipoxygenase isoenzymes. Biochem J 348 Pt 2, 329-35 (2000).

131. Schweiger, D., Furstenberger, G. & Krieg, P. Inducible expression of 15-lipoxygenase-2 and 8-lipoxygenase inhibits cell growth via common signaling pathways. J Lipid Res 48, 553-64 (2007).

132. Hamberg, M. & Samuelsson, B. Prostaglandin endoperoxides. Novel transformations of arachidonic acid in human platelets. Proc Natl Acad Sci U S A 71, 3400-4 (1974).

133. Funk, C. D., Furci, L. & FitzGerald, G. A. Molecular cloning, primary structure, and expression of the human platelet/erythroleukemia cell 12-lipoxygenase. Proc Natl Acad Sci U S A 87, 5638-42 (1990).

134. Izumi, T., Hoshiko, S., Radmark, O. & Samuelsson, B. Cloning of the cDNA for human 12-lipoxygenase. Proc Natl Acad Sci U S A 87, 7477-81 (1990).

135. Virmani, J., Johnson, E. N., Klein-Szanto, A. J. & Funk, C. D. Role of 'platelet-type' 12-lipoxygenase in skin carcinogenesis. Cancer Lett 162, 161-5 (2001).

136. Pidgeon, G. P., Tang, K., Cai, Y. L., Piasentin, E. & Honn, K. V. Overexpression of platelet-type 12-lipoxygenase promotes tumor cell survival by enhancing alpha(v)beta(3) and alpha(v)beta(5) integrin expression. Cancer Res 63, 4258-67 (2003).

137. Raso, E. et al. Molecular identification, localization and function of platelet-type 12-lipoxygenase in human melanoma progression, under experimental and clinical conditions. Melanoma Res 14, 245-50 (2004).

138. Chen, X. S. & Funk, C. D. Structure-function properties of human platelet 12-lipoxygenase: chimeric enzyme and in vitro mutagenesis studies. Faseb J 7, 694-701 (1993).

139. Sloane, D. L., Leung, R., Barnett, J., Craik, C. S. & Sigal, E. Conversion of human 15-lipoxygenase to an efficient 12-lipoxygenase: the side-chain geometry of amino acids 417 and 418 determine positional specificity. Protein Eng 8, 275-82 (1995).

140. Borngraber, S. et al. Shape and specificity in mammalian 15-lipoxygenase active site. The functional interplay of sequence determinants for the reaction specificity. J Biol Chem 274, 37345-50 (1999).

141. Nigam, S. et al. The rat leukocyte-type 12-lipoxygenase exhibits an intrinsic hepoxilin A3 synthase activity. J Biol Chem 279, 29023-30 (2004).

142. Romano, M. et al. Lipoxin synthase activity of human platelet 12-lipoxygenase. Biochem J 296 (Pt 1), 127-33 (1993).

143. Funk, C. D., Keeney, D. S., Oliw, E. H., Boeglin, W. E. & Brash, A. R. Functional expression and cellular localization of a mouse epidermal lipoxygenase. J Biol Chem 271, 23338-44 (1996).

144. Kinzig, A. et al. Murine epidermal lipoxygenase (Aloxe) encodes a 12-lipoxygenase isoform. FEBS Lett 402, 162-6 (1997).

145. Sun, D., Elsea, S. H., Patel, P. I. & Funk, C. D. Cloning of a human "epidermal-type" 12-lipoxygenase-related gene and chromosomal localization to 17p13. Cytogenet Cell Genet 81, 79-82 (1998).

146. Hammarstrom, S. et al. Increased concentrations of nonesterified arachidonic acid, 12L-hydroxy-5,8,10,14-eicosatetraenoic acid, prostaglandin E2, and

prostaglandin F2alpha in epidermis of psoriasis. Proc Natl Acad Sci U S A 72, 5130-4 (1975).

147. Woollard, P. M. Stereochemical difference between 12-hydroxy-5,8,10,14-eicosatetraenoic acid in platelets and psoriatic lesions. Biochem Biophys Res Commun 136, 169-76 (1986).

148. Boeglin, W. E., Kim, R. B. & Brash, A. R. A 12R-lipoxygenase in human skin: mechanistic evidence, molecular cloning, and expression. Proc Natl Acad Sci U S A 95, 6744-9 (1998).

149. Coffa, G. & Brash, A. R. A single active site residue directs oxygenation stereospecificity in lipoxygenases: stereocontrol is linked to the position of oxygenation. Proc Natl Acad Sci U S A 101, 15579-84 (2004).

150. Meruvu, S. et al. Sequence determinants for the reaction specificity of murine (12R)-lipoxygenase: targeted substrate modification and site-directed mutagenesis. J Biol Chem 280, 36633-41 (2005).

151. Kinzig, A., Heidt, M., Furstenberger, G., Marks, F. & Krieg, P. cDNA cloning, genomic structure, and chromosomal localization of a novel murine epidermis-type lipoxygenase. Genomics 58, 158-64 (1999).

152. Krieg, P., Marks, F. & Furstenberger, G. A gene cluster encoding human epidermis-type lipoxygenases at chromosome 17p13.1: cloning, physical mapping, and expression. Genomics 73, 323-30 (2001).

153. Jobard, F. et al. Lipoxygenase-3 (ALOXE3) and 12(R)-lipoxygenase (ALOX12B) are mutated in non-bullous congenital ichthyosiform erythroderma (NCIE) linked to chromosome 17p13.1. Hum Mol Genet 11, 107-13 (2002).

154. Yu, Z., Schneider, C., Boeglin, W. E., Marnett, L. J. & Brash, A. R. The lipoxygenase gene ALOXE3 implicated in skin differentiation encodes a hydroperoxide isomerase. Proc Natl Acad Sci U S A 100, 9162-7 (2003).

155. Sigal, E. et al. Molecular cloning and primary structure of human 15-lipoxygenase. Biochem Biophys Res Commun 157, 457-64 (1988).

156. Fleming, J. et al. The complete sequence of the rabbit erythroid cell-specific 15-lipoxygenase mRNA: comparison of the predicted amino acid sequence of the erythrocyte lipoxygenase with other lipoxygenases. Gene 79, 181-8 (1989).

157. Watanabe, T., Medina, J. F., Haeggstrom, J. Z., Radmark, O. & Samuelsson, B. Molecular cloning of a 12-lipoxygenase cDNA from rat brain. Eur J Biochem 212, 605-12 (1993).

158. Chen, X. S., Kurre, U., Jenkins, N. A., Copeland, N. G. & Funk, C. D. cDNA cloning, expression, mutagenesis of C-terminal isoleucine, genomic structure, and chromosomal localizations of murine 12-lipoxygenases. J Biol Chem 269, 13979-87 (1994).

159. Bryant, R. W., Schewe, T., Rapoport, S. M. & Bailey, J. M. Leukotriene formation by a purified reticulocyte lipoxygenase enzyme. Conversion of arachidonic acid and 15-hydroperoxyeicosatetraenoic acid to 14, 15-leukotriene A4. J Biol Chem 260, 3548-55 (1985).

160. Sailesh, S., Kumar, Y. V., Prasad, M. & Reddanna, P. Sheep uterus dual lipoxygenase in the synthesis of 14,15-leukotrienes. Arch Biochem Biophys 315, 362-8 (1994).

161. Sigal, E. et al. Expression of cloned human reticulocyte 15-lipoxygenase and immunological evidence that 15-lipoxygenases of different cell types are related. J Biol Chem 265, 5113-20 (1990).

162. Glass, C. K. & Witztum, J. L. Atherosclerosis. the road ahead. Cell 104, 503-16 (2001).

163. Harkewicz, R. et al. Cholesteryl ester hydroperoxides are biologically active components of minimally oxidized low density lipoprotein. J Biol Chem 283, 10241-51 (2008).

164. Merched, A. J., Ko, K., Gotlinger, K. H., Serhan, C. N. & Chan, L. Atherosclerosis: evidence for impairment of resolution of vascular inflammation governed by specific lipid mediators. Faseb J (2008).

165. Brash, A. R., Boeglin, W. E. & Chang, M. S. Discovery of a second 15S-lipoxygenase in humans. Proc Natl Acad Sci U S A 94, 6148-52 (1997).

166. Jisaka, M., Kim, R. B., Boeglin, W. E., Nanney, L. B. & Brash, A. R. Molecular cloning and functional expression of a phorbol ester-inducible 8S-lipoxygenase from mouse skin. J Biol Chem 272, 24410-6 (1997).

167. Jisaka, M., Kim, R. B., Boeglin, W. E. & Brash, A. R. Identification of amino acid determinants of the positional specificity of mouse 8S-lipoxygenase and human 15S-lipoxygenase-2. J Biol Chem 275, 1287-93 (2000).

168. Jisaka, M. et al. Double dioxygenation by mouse 8S-lipoxygenase: specific formation of a potent peroxisome proliferator-activated receptor alpha agonist. Biochem Biophys Res Commun 338, 136-43 (2005).

169. Nelson, D. R. Cytochrome P450 nomenclature, 2004. Methods Mol Biol 320, 1-10 (2006).

170. Roman, R. J. P-450 metabolites of arachidonic acid in the control of cardiovascular function. Physiol Rev 82, 131-85 (2002).

171. Omura, T. Forty years of cytochrome P450. Biochem Biophys Res Commun 266, 690-8 (1999).

172. Schlichting, I. et al. The catalytic pathway of cytochrome p450cam at atomic resolution. Science 287, 1615-22 (2000).

173. Hirao, H., Kumar, D., Thiel, W. & Shaik, S. Two states and two more in the mechanisms of hydroxylation and epoxidation by cytochrome P450. J Am Chem Soc 127, 13007-18 (2005).

174. Nelson, D. R. Cytochrome P450 and the individuality of species. Arch Biochem Biophys 369, 1-10 (1999).

175. Nelson, D. R. et al. Comparison of cytochrome P450 (CYP) genes from the mouse and human genomes, including nomenclature recommendations for genes, pseudogenes and alternative-splice variants. Pharmacogenetics 14, 1-18 (2004).

176. Ramarao, M. & Kemper, B. Substitution at residue 473 confers progesterone 21-hydroxylase activity to cytochrome P450 2C2. Mol Pharmacol 48, 417-24 (1995).

177. Fleming, I. Cytochrome P-450 under pressure: more evidence for a link between 20-hydroxyeicosatetraenoic acid and hypertension. Circulation 111, 5-7 (2005).

178. Ma, Y. H. et al. 20-Hydroxyeicosatetraenoic acid is an endogenous vasoconstrictor of canine renal arcuate arteries. Circ Res 72, 126-36 (1993).

179. Croft, K. D., McGiff, J. C., Sanchez-Mendoza, A. & Carroll, M. A. Angiotensin II releases 20-HETE from rat renal microvessels. Am J Physiol Renal Physiol 279, F544-51 (2000).

180. Schwartzman, M., Ferreri, N. R., Carroll, M. A., Songu-Mize, E. & McGiff, J. C. Renal cytochrome P450-related arachidonate metabolite inhibits (Na+ + K+)ATPase. Nature 314, 620-2 (1985).

181. Choudhary, D., Jansson, I., Stoilov, I., Sarfarazi, M. & Schenkman, J. B. Metabolism of retinoids and arachidonic acid by human and mouse cytochrome P450 1b1. Drug Metab Dispos 32, 840-7 (2004).

182. Capdevila, J. H., Falck, J. R. & Harris, R. C. Cytochrome P450 and arachidonic acid bioactivation. Molecular and functional properties of the arachidonate monooxygenase. J Lipid Res 41, 163-81 (2000).

183. Bylund, J., Kunz, T., Valmsen, K. & Oliw, E. H. Cytochromes P450 with bisallylic hydroxylation activity on arachidonic and linoleic acids studied with human recombinant enzymes and with human and rat liver microsomes. J Pharmacol Exp Ther 284, 51-60 (1998).

184. Bylund, J., Ericsson, J. & Oliw, E. H. Analysis of cytochrome P450 metabolites of arachidonic and linoleic acids by liquid chromatography-mass spectrometry with ion trap MS. Anal Biochem 265, 55-68 (1998).

185. Rifkind, A. B., Lee, C., Chang, T. K. & Waxman, D. J. Arachidonic acid metabolism by human cytochrome P450s 2C8, 2C9, 2E1, and 1A2: regioselective oxygenation and evidence for a role for CYP2C enzymes in arachidonic acid epoxygenation in human liver microsomes. Arch Biochem Biophys 320, 380-9 (1995).

186. Chuang, S. S. et al. CYP2U1, a novel human thymus- and brain-specific cytochrome P450, catalyzes omega- and (omega-1)-hydroxylation of fatty acids. J Biol Chem 279, 6305-14 (2004).

187. Wu, Z. L., Sohl, C. D., Shimada, T. & Guengerich, F. P. Recombinant enzymes overexpressed in bacteria show broad catalytic specificity of human cytochrome P450 2W1 and limited activity of human cytochrome P450 2S1. Mol Pharmacol 69, 2007-14 (2006).

188. Kalsotra, A. & Strobel, H. W. Cytochrome P450 4F subfamily: at the crossroads of eicosanoid and drug metabolism. Pharmacol Ther 112, 589-611 (2006).

189. Hardwick, J. P. Cytochrome P450 omega hydroxylase (CYP4) function in fatty acid metabolism and metabolic diseases. Biochem Pharmacol 75, 2263-75 (2008).

190. Keeney, D. S. et al. Differentiating keratinocytes express a novel cytochrome P450 enzyme, CYP2B19, having arachidonate monooxygenase activity. J Biol Chem 273, 32071-9 (1998).

191. Zeldin, D. C., DuBois, R. N., Falck, J. R. & Capdevila, J. H. Molecular cloning, expression and characterization of an endogenous human cytochrome P450 arachidonic acid epoxygenase isoform. Arch Biochem Biophys 322, 76-86 (1995).

192. Luo, G., Zeldin, D. C., Blaisdell, J. A., Hodgson, E. & Goldstein, J. A. Cloning and expression of murine CYP2Cs and their ability to metabolize arachidonic acid. Arch Biochem Biophys 357, 45-57 (1998).

193. DeLozier, T. C. et al. CYP2C44, a new murine CYP2C that metabolizes arachidonic acid to unique stereospecific products. J Pharmacol Exp Ther 310, 845-54 (2004).

194. Wang, H. et al. Cloning, expression, and characterization of three new mouse cytochrome p450 enzymes and partial characterization of their fatty acid oxidation activities. Mol Pharmacol 65, 1148-58 (2004).

195. Qu, W. et al. Cytochrome P450 CYP2J9, a new mouse arachidonic acid omega-1 hydroxylase predominantly expressed in brain. J Biol Chem 276, 25467-79 (2001).

196. Muller, D. N. et al. Mouse Cyp4a isoforms: enzymatic properties, gender- and strain-specific expression, and role in renal 20-hydroxyeicosatetraenoic acid formation. Biochem J 403, 109-18 (2007).

197. Hsu, M. H., Savas, U., Griffin, K. J. & Johnson, E. F. Human cytochrome p450 family 4 enzymes: function, genetic variation and regulation. Drug Metab Rev 39, 515-38 (2007).

198. Wu, S. et al. Molecular cloning, expression, and functional significance of a cytochrome P450 highly expressed in rat heart myocytes. J Biol Chem 272, 12551-9 (1997).

199. Zhang, Q. Y., Ding, X. & Kaminsky, L. S. CDNA cloning, heterologous expression, and characterization of rat intestinal CYP2J4. Arch Biochem Biophys 340, 270-8 (1997).

200. Hoch, U., Zhang, Z., Kroetz, D. L. & Ortiz de Montellano, P. R. Structural determination of the substrate specificities and regioselectivities of the rat and human fatty acid omega-hydroxylases. Arch Biochem Biophys 373, 63-71 (2000).

201. Wang, M. H. et al. Cloning, sequencing, and cDNA-directed expression of the rat renal CYP4A2: arachidonic acid omega-hydroxylation and 11,12-epoxidation by CYP4A2 protein. Arch Biochem Biophys 336, 240-50 (1996).

202. Cowart, L. A. et al. The CYP4A isoforms hydroxylate epoxyeicosatrienoic acids to form high affinity peroxisome proliferator-activated receptor ligands. J Biol Chem 277, 35105-12 (2002).

203. Yamaguchi, Y. et al. Contribution of CYP4A8 to the formation of 20-hydroxyeicosatetraenoic acid from arachidonic acid in rat kidney. Drug Metab Pharmacokinet 17, 109-16 (2002).

204. Kikuta, Y., Kusunose, E., Ito, M. & Kusunose, M. Purification and characterization of recombinant rat hepatic CYP4F1. Arch Biochem Biophys 369, 193-6 (1999).

205. Carroll, M. A. et al. Cytochrome P-450-dependent HETEs: profile of biological activity and stimulation by vasoactive peptides. Am J Physiol 271, R863-9 (1996).

206. Bednar, M. M. et al. 16(R)-hydroxyeicosatetraenoic acid, a novel cytochrome P450 product of arachidonic acid, suppresses activation of human polymorphonuclear leukocyte and reduces intracranial pressure in a rabbit model of thromboembolic stroke. Neurosurgery 47, 1410-8; discussion 1418-9 (2000).

207. Keeney, D. S., Skinner, C., Wei, S., Friedberg, T. & Waterman, M. R. A keratinocyte-specific epoxygenase, CYP2B12, metabolizes arachidonic acid with unusual selectivity, producing a single major epoxyeicosatrienoic acid. J Biol Chem 273, 9279-84 (1998).

208. Lundblad, M. S., Stark, K., Eliasson, E., Oliw, E. & Rane, A. Biosynthesis of epoxyeicosatrienoic acids varies between polymorphic CYP2C enzymes. Biochem Biophys Res Commun 327, 1052-7 (2005).

209. Wu, S., Moomaw, C. R., Tomer, K. B., Falck, J. R. & Zeldin, D. C. Molecular cloning and expression of CYP2J2, a human cytochrome P450 arachidonic acid epoxygenase highly expressed in heart. J Biol Chem 271, 3460-8 (1996).

210. Ma, J. et al. Molecular cloning, enzymatic characterization, developmental expression, and cellular localization of a mouse cytochrome P450 highly expressed in kidney. J Biol Chem 274, 17777-88 (1999).

211. Capdevila, J. H. et al. Cytochrome P-450 enzyme-specific control of the regio- and enantiofacial selectivity of the microsomal arachidonic acid epoxygenase. J Biol Chem 265, 10865-71 (1990).

212. Seki, T., Wang, M. H., Miyata, N. & Laniado-Schwartzman, M. Cytochrome P450 4A isoform inhibitory profile of N-hydroxy-N'-(4-butyl-2-methylphenyl)-formamidine (HET0016), a selective inhibitor of 20-HETE synthesis. Biol Pharm Bull 28, 1651-4 (2005).

213. Thompson, C. M., Capdevila, J. H. & Strobel, H. W. Recombinant cytochrome P450 2D18 metabolism of dopamine and arachidonic acid. J Pharmacol Exp Ther 294, 1120-30 (2000).

214. Node, K. et al. Anti-inflammatory properties of cytochrome P450 epoxygenase-derived eicosanoids. Science 285, 1276-9 (1999).

215. Liu, Y. et al. The antiinflammatory effect of laminar flow: the role of PPARgamma, epoxyeicosatrienoic acids, and soluble epoxide hydrolase. Proc Natl Acad Sci U S A 102, 16747-52 (2005).

216. Wong, P. Y., Lai, P. S., Shen, S. Y., Belosludtsev, Y. Y. & Falck, J. R. Post-receptor signal transduction and regulation of 14(R),15(S)-epoxyeicosatrienoic acid (14,15-EET) binding in U-937 cells. J Lipid Mediat Cell Signal 16, 155-69 (1997).

217. Yang, W. et al. Characterization of epoxyeicosatrienoic acid binding site in U937 membranes using a novel radiolabeled agonist, 20-125i-14,15-epoxyeicosa-8(Z)-enoic acid. J Pharmacol Exp Ther 324, 1019-27 (2008).

218. Node, K. et al. Activation of Galpha s mediates induction of tissue-type plasminogen activator gene transcription by epoxyeicosatrienoic acids. J Biol Chem 276, 15983-9 (2001).

219. Li, P. L. & Campbell, W. B. Epoxyeicosatrienoic acids activate K+ channels in coronary smooth muscle through a guanine nucleotide binding protein. Circ Res 80, 877-84 (1997).

220. Falck, J. R. et al. 11,12-epoxyeicosatrienoic acid (11,12-EET): structural determinants for inhibition of TNF-alpha-induced VCAM-1 expression. Bioorg Med Chem Lett 13, 4011-4 (2003).

221. Gauthier, K. M., Falck, J. R., Reddy, L. M. & Campbell, W. B. 14,15-EET analogs: characterization of structural requirements for agonist and antagonist activity in bovine coronary arteries. Pharmacol Res 49, 515-24 (2004).

222. Watanabe, H. et al. Anandamide and arachidonic acid use epoxyeicosatrienoic acids to activate TRPV4 channels. Nature 424, 434-8 (2003).

223. Alessandri-Haber, N., Dina, O. A., Joseph, E. K., Reichling, D. & Levine, J. D. A transient receptor potential vanilloid 4-dependent mechanism of hyperalgesia is engaged by concerted action of inflammatory mediators. J Neurosci 26, 3864-74 (2006).

224. Alessandri-Haber, N., Dina, O. A., Joseph, E. K., Reichling, D. B. & Levine, J. D. Interaction of transient receptor potential vanilloid 4, integrin, and SRC tyrosine kinase in mechanical hyperalgesia. J Neurosci 28, 1046-57 (2008).

225. Sipe, W. E. et al. Transient receptor potential vanilloid 4 mediates protease activated receptor 2-induced sensitization of colonic afferent nerves and visceral hyperalgesia. Am J Physiol Gastrointest Liver Physiol 294, G1288-98 (2008).

226. Earley, S., Heppner, T. J., Nelson, M. T. & Brayden, J. E. TRPV4 forms a novel Ca2+ signaling complex with ryanodine receptors and BKCa channels. Circ Res 97, 1270-9 (2005).

227. Inceoglu, B., Schmelzer, K. R., Morisseau, C., Jinks, S. L. & Hammock, B. D. Soluble epoxide hydrolase inhibition reveals novel biological functions of epoxyeicosatrienoic acids (EETs). Prostaglandins Other Lipid Mediat 82, 42-9 (2007).

228. Lu, T., Hoshi, T., Weintraub, N. L., Spector, A. A. & Lee, H. C. Activation of ATP-sensitive K(+) channels by epoxyeicosatrienoic acids in rat cardiac ventricular myocytes. J Physiol 537, 811-27 (2001).

229. Ng, V. Y. et al. Cytochrome P450 eicosanoids are activators of peroxisome proliferator-activated receptor alpha. Drug Metab Dispos 35, 1126-34 (2007).

230. Kotlikoff, M. I. EDHF redux: EETs, TRPV4, and Ca2+ sparks. Circ Res 97, 1209-10 (2005).

231. Spector, A. A. & Norris, A. W. Action of epoxyeicosatrienoic acids on cellular function. Am J Physiol Cell Physiol 292, C996-1012 (2007).

232. Beetham, J. K., Tian, T. & Hammock, B. D. cDNA cloning and expression of a soluble epoxide hydrolase from human liver. Arch Biochem Biophys 305, 197-201 (1993).

233. Gomez, G. A., Morisseau, C., Hammock, B. D. & Christianson, D. W. Structure of human epoxide hydrolase reveals mechanistic inferences on bifunctional catalysis in epoxide and phosphate ester hydrolysis. Biochemistry 43, 4716-23 (2004).

234. Argiriadi, M. A., Morisseau, C., Hammock, B. D. & Christianson, D. W. Detoxification of environmental mutagens and carcinogens: structure, mechanism, and evolution of liver epoxide hydrolase. Proc Natl Acad Sci U S A 96, 10637-42 (1999).

235. Morisseau, C. & Hammock, B. D. Epoxide hydrolases: mechanisms, inhibitor designs, and biological roles. Annu Rev Pharmacol Toxicol 45, 311-33 (2005).

236. Draper, A. J. & Hammock, B. D. Inhibition of soluble and microsomal epoxide hydrolase by zinc and other metals. Toxicol Sci 52, 26-32 (1999).

237. Lu, T. et al. Dihydroxyeicosatrienoic acids are potent activators of Ca(2+)-activated K(+) channels in isolated rat coronary arterial myocytes. J Physiol 534, 651-67 (2001).

238. Fang, X. et al. 14,15-Dihydroxyeicosatrienoic acid activates peroxisome proliferator-activated receptor-alpha. Am J Physiol Heart Circ Physiol 290, H55-63 (2006).

239. Milne, G. L., Yin, H. & Morrow, J. D. Human biochemistry of the isoprostane pathway. J Biol Chem 283, 15533-7 (2008).

240. Morrow, J. D. et al. A series of prostaglandin F2-like compounds are produced in vivo in humans by a non-cyclooxygenase, free radical-catalyzed mechanism. Proc Natl Acad Sci U S A 87, 9383-7 (1990).

241. Kunapuli, P., Lawson, J. A., Rokach, J. & FitzGerald, G. A. Functional characterization of the ocular prostaglandin f2alpha (PGF2alpha) receptor. Activation by the isoprostane, 12-iso-PGF2alpha. J Biol Chem 272, 27147-54 (1997).

242. Takahashi, K. et al. Glomerular actions of a free radical-generated novel prostaglandin, 8-epi-prostaglandin F2 alpha, in the rat. Evidence for interaction with thromboxane A2 receptors. J Clin Invest 90, 136-41 (1992).

243. Guido, D. M., McKenna, R. & Mathews, W. R. Quantitation of hydroperoxy-eicosatetraenoic acids and hydroxy-eicosatetraenoic acids as indicators of lipid peroxidation using gas chromatography-mass spectrometry. Anal Biochem 209, 123-9 (1993).

244. Tai, H. H., Ensor, C. M., Tong, M., Zhou, H. & Yan, F. Prostaglandin catabolizing enzymes. Prostaglandins Other Lipid Mediat 68-69, 483-93 (2002).

245. Kumlin, M. & Granstrom, E. Radioimmunoassay for 11-dehydro-TXB2: a method for monitoring thromboxane production in vivo. Prostaglandins 32, 741-67 (1986).

246. Catella, F., Healy, D., Lawson, J. A. & FitzGerald, G. A. 11-Dehydrothromboxane B2: a quantitative index of thromboxane A2 formation in the human circulation. Proc Natl Acad Sci U S A 83, 5861-5 (1986).

247. Westlund, P., Fylling, A. C., Cederlund, E. & Jornvall, H. 11-Hydroxythromboxane B2 dehydrogenase is identical to cytosolic aldehyde dehydrogenase. FEBS Lett 345, 99-103 (1994).

248. Roberts, L. J., 2nd, Brash, A. R. & Oates, J. A. Metabolic fate of thromboxane A2 and prostacyclin. Adv Prostaglandin Thromboxane Leukot Res 10, 211-25 (1982).

249. Bohm, E. et al. 11-Dehydro-thromboxane B2, a stable thromboxane metabolite, is a full agonist of chemoattractant receptor-homologous molecule expressed on TH2 cells (CRTH2) in human eosinophils and basophils. J Biol Chem 279, 7663-70 (2004).

250. Ensor, C. M. & Tai, H. H. 15-Hydroxyprostaglandin dehydrogenase. J Lipid Mediat Cell Signal 12, 313-9 (1995).

251. Cho, H. et al. Role of glutamine 148 of human 15-hydroxyprostaglandin dehydrogenase in catalytic oxidation of prostaglandin E2. Bioorg Med Chem 14, 6486-91 (2006).

252. Myung, S. J. et al. 15-Hydroxyprostaglandin dehydrogenase is an in vivo suppressor of colon tumorigenesis. Proc Natl Acad Sci U S A 103, 12098-102 (2006).

253. Chou, W. L. et al. Identification of a novel prostaglandin reductase reveals the involvement of prostaglandin E2 catabolism in regulation of peroxisome proliferator-activated receptor gamma activation. J Biol Chem 282, 18162-72 (2007).

254. Yokomizo, T. et al. cDNA cloning, expression, and mutagenesis study of leukotriene B4 12-hydroxydehydrogenase. J Biol Chem 271, 2844-50 (1996).

255. Ensor, C. M., Zhang, H. & Tai, H. H. Purification, cDNA cloning and expression of 15-oxoprostaglandin 13-reductase from pig lung. Biochem J 330 (Pt 1), 103-8 (1998).

256. Clish, C. B., Levy, B. D., Chiang, N., Tai, H. H. & Serhan, C. N. Oxidoreductases in lipoxin A4 metabolic inactivation: a novel role for 15-onoprostaglandin 13-reductase/leukotriene B4 12-hydroxydehydrogenase in inflammation. J Biol Chem 275, 25372-80 (2000).

257. Gross, N. D. et al. Levels of prostaglandin E metabolite, the major urinary metabolite of prostaglandin E2, are increased in smokers. Clin Cancer Res 11, 6087-93 (2005).

258. Hori, T. et al. Structural basis of leukotriene B4 12-hydroxydehydrogenase/15-Oxo-prostaglandin 13-reductase catalytic mechanism and a possible Src homology 3 domain binding loop. J Biol Chem 279, 22615-23 (2004).

259. Berry, K. A., Borgeat, P., Gosselin, J., Flamand, L. & Murphy, R. C. Urinary metabolites of leukotriene B4 in the human subject. J Biol Chem 278, 24449-60 (2003).

260. Diczfalusy, U. Beta-oxidation of eicosanoids. Prog Lipid Res 33, 403-28 (1994).

261. Guilford, W. J. & Parkinson, J. F. Second-generation beta-oxidation resistant 3-oxa-lipoxin A4 analogs. Prostaglandins Leukot Essent Fatty Acids 73, 245-50 (2005).

262. Tukey, R. H. & Strassburg, C. P. Human UDP-glucuronosyltransferases: metabolism, expression, and disease. Annu Rev Pharmacol Toxicol 40, 581-616 (2000).

263. Turgeon, D. et al. Glucuronidation of arachidonic and linoleic acid metabolites by human UDP-glucuronosyltransferases. J Lipid Res 44, 1182-91 (2003).

264. Newman, J. W., Watanabe, T. & Hammock, B. D. The simultaneous quantification of cytochrome P450 dependent linoleate and arachidonate metabolites in urine by HPLC-MS/MS. J Lipid Res 43, 1563-78 (2002).

265. Cheng, Y. et al. Role of prostacyclin in the cardiovascular response to thromboxane A2. Science 296, 539-41 (2002).

266. Bresalier, R. S. et al. Cardiovascular events associated with rofecoxib in a colorectal adenoma chemoprevention trial. N Engl J Med 352, 1092-102 (2005).

267. Peters-Golden, M. & Brock, T. G. 5-lipoxygenase and FLAP. Prostaglandins Leukot Essent Fatty Acids 69, 99-109 (2003).

268. Spokas, E. G., Rokach, J. & Wong, P. Y. Leukotrienes, lipoxins, and hydroxyeicosatetraenoic acids. Methods Mol Biol 120, 213-47 (1999).

269. Reinke, M. Monitoring thromboxane in body fluids: a specific ELISA for 11-dehydrothromboxane B2 using a monoclonal antibody. Am J Physiol 262, E658-62 (1992).

270. Shono, F. et al. A heterologous enzyme immunoassay of prostaglandin E2 using a stable enzyme-labeled hapten mimic. Anal Biochem 168, 284-91 (1988).

271. Baranowski, R. & Pacha, K. Gas chromatographic determination of prostaglandins. Mini Rev Med Chem 2, 135-44 (2002).

272. Murphy, R. C. et al. Electrospray ionization and tandem mass spectrometry of eicosanoids. Anal Biochem 346, 1-42 (2005).

273. Margalit, A., Duffin, K. L. & Isakson, P. C. Rapid quantitation of a large scope of eicosanoids in two models of inflammation: development of an electrospray and tandem mass spectrometry method and application to biological studies. Anal Biochem 235, 73-81 (1996).

274. Takabatake, M. et al. Simultaneous quantification of prostaglandins in human synovial cell-cultured medium using liquid chromatography/tandem mass spectrometry. Prostaglandins Leukot Essent Fatty Acids 67, 51-6 (2002).

275. Kita, Y., Takahashi, T., Uozumi, N. & Shimizu, T. A multiplex quantitation method for eicosanoids and platelet-activating factor using column-switching reversed-phase liquid chromatography-tandem mass spectrometry. Anal Biochem 342, 134-43 (2005).

276. Kresge, N., Simoni, R. D. & Hill, R. L. The Prostaglandins, Sune Bergstrom and Bengt Samuelsson. J. Biol. Chem. 281, e9- (2006).

277. Harkewicz, R., Fahy, E., Andreyev, A. & Dennis, E. A. Arachidonate-derived dihomoprostaglandin production observed in endotoxin-stimulated macrophage-like cells. J Biol Chem 282, 2899-910 (2007).

278. Hall, L. M. & Murphy, R. C. Electrospray mass spectrometric analysis of 5-hydroperoxy and 5-hydroxyeicosatetraenoic acids generated by lipid peroxidation of red blood cell ghost phospholipids. J Am Soc Mass Spectrom 9, 527-32 (1998).

279. Fitzpatrick, F. A. & Wynalda, M. A. Albumin-catalyzed metabolism of prostaglandin D2. Identification of products formed in vitro. J Biol Chem 258, 11713-8 (1983).

280. Maxey, K. M., Hessler, E., MacDonald, J. & Hitchingham, L. The nature and composition of 15-deoxy-Delta(12,14)PGJ(2). Prostaglandins Other Lipid Mediat 62, 15-21 (2000).

281. Six, D. A. & Dennis, E. A. The expanding superfamily of phospholipase A(2) enzymes: classification and characterization. Biochim. Biophys. Acta 1488, 1-19 (2000).

282. Serhan, C. N. & Savill, J. Resolution of inflammation: the beginning programs the end. Nat Immunol 6, 1191-7 (2005).

283. Funk, C. D., Chen, X. S., Johnson, E. N. & Zhao, L. Lipoxygenase genes and their targeted disruption. Prostaglandins Other Lipid Mediat 68-69, 303-12 (2002).

284. Sacerdoti, D., Gatta, A. & McGiff, J. C. Role of cytochrome P450-dependent arachidonic acid metabolites in liver physiology and pathophysiology. Prostaglandins Other Lipid Mediat 72, 51-71 (2003).

285. Shibata, T. et al. 15-deoxy-delta 12,14-prostaglandin J2. A prostaglandin D2 metabolite generated during inflammatory processes. J Biol Chem 277, 10459-66 (2002).

286. Wang, M. et al. Deletion of microsomal prostaglandin E synthase-1 augments prostacyclin and retards atherogenesis. Proc Natl Acad Sci U S A 103, 14507-12 (2006).

287. Kawai, T. & Akira, S. Pathogen recognition with Toll-like receptors. Curr Opin Immunol 17, 338-44 (2005).

288. Asmis, R., Randriamampita, C., Tsien, R. Y. & Dennis, E. A. Intracellular Ca2+, inositol 1,4,5-trisphosphate and additional signalling in the stimulation by platelet-activating factor of prostaglandin E2 formation in P388D1 macrophage-like cells. Biochem J 298 Pt 3, 543-51 (1994).

289. Natarajan, M., Lin, K. M., Hsueh, R. C., Sternweis, P. C. & Ranganathan, R. A global analysis of cross-talk in a mammalian cellular signalling network. Nat Cell Biol 8, 571-80 (2006).

290. Greenberg, S., Di Virgilio, F., Steinberg, T. H. & Silverstein, S. C. Extracellular nucleotides mediate Ca2+ fluxes in J774 macrophages by two distinct mechanisms. J Biol Chem 263, 10337-43 (1988).

291. Balboa, M. A., Balsinde, J., Johnson, C. A. & Dennis, E. A. Regulation of arachidonic acid mobilization in lipopolysaccharide-activated P388D(1) macrophages by adenosine triphosphate. J Biol Chem 274, 36764-8 (1999).

292. Aderem, A. A., Cohen, D. S., Wright, S. D. & Cohn, Z. A. Bacterial lipopolysaccharides prime macrophages for enhanced release of arachidonic acid metabolites. J Exp Med 164, 165-79 (1986).

293. Aderem, A. A. & Cohn, Z. A. Bacterial lipopolysaccharides modify signal transduction in the arachidonic acid cascade in macrophages. Ciba Found Symp 118, 196-210 (1986).

294. Balsinde, J., Balboa, M. A., Insel, P. A. & Dennis, E. A. Differential regulation of phospholipase D and phospholipase A2 by protein kinase C in P388D1 macrophages. Biochem J 321 (Pt 3), 805-9 (1997).

295. Glaser, K. B., Asmis, R. & Dennis, E. A. Bacterial lipopolysaccharide priming of P388D1 macrophage-like cells for enhanced arachidonic acid metabolism. Platelet-activating factor receptor activation and regulation of phospholipase A2. J Biol Chem 265, 8658-64 (1990).

296. Schaloske, R. H., Provins, J. W., Kessen, U. A. & Dennis, E. A. Molecular characterization of the lipopolysaccharide/platelet activating factor- and zymosan-induced pathways leading to prostaglandin production in P388D1 macrophages. Biochim Biophys Acta 1687, 64-75 (2005).

297. Raetz, C. R. et al. Kdo2-Lipid A of Escherichia coli, a defined endotoxin that activates macrophages via TLR-4. J Lipid Res 47, 1097-111 (2006).

298. Trebino, C. E. et al. Redirection of eicosanoid metabolism in mPGES-1-deficient macrophages. J Biol Chem 280, 16579-85 (2005).

299. Cipollone, F. et al. Balance between PGD synthase and PGE synthase is a major determinant of atherosclerotic plaque instability in humans. Arterioscler Thromb Vasc Biol 24, 1259-65 (2004).

300. Di Virgilio, F. et al. Nucleotide receptors: an emerging family of regulatory molecules in blood cells. Blood 97, 587-600 (2001).

301. Khakh, B. S. Molecular physiology of P2X receptors and ATP signalling at synapses. Nat Rev Neurosci 2, 165-74 (2001).

302. Bours, M. J., Swennen, E. L., Di Virgilio, F., Cronstein, B. N. & Dagnelie, P. C. Adenosine 5'-triphosphate and adenosine as endogenous signaling molecules in immunity and inflammation. Pharmacol Ther 112, 358-404 (2006).

303. Ferrari, D. et al. The P2X7 receptor: a key player in IL-1 processing and release. J Immunol 176, 3877-83 (2006).

304. Balsinde, J., Bianco, I. D., Ackermann, E. J., Conde-Frieboes, K. & Dennis, E. A. Inhibition of calcium-independent phospholipase A2 prevents arachidonic acid incorporation and phospholipid remodeling in P388D1 macrophages. Proc Natl Acad Sci U S A 92, 8527-31 (1995).

305. Mosior, M., Six, D. A. & Dennis, E. A. Group IV cytosolic phospholipase A2 binds with high affinity and specificity to phosphatidylinositol 4,5-bisphosphate resulting in dramatic increases in activity. J Biol Chem 273, 2184-91 (1998).

306. Six, D. A. & Dennis, E. A. Essential Ca(2+)-independent role of the group IVA cytosolic phospholipase A(2) C2 domain for interfacial activity. J Biol Chem 278, 23842-50 (2003).

307. Nakamura, H., Hirabayashi, T., Shimizu, M. & Murayama, T. Ceramide-1-phosphate activates cytosolic phospholipase A2alpha directly and by PKC pathway. Biochem Pharmacol 71, 850-7 (2006).

308. Pettus, B. J. et al. Ceramide 1-phosphate is a direct activator of cytosolic phospholipase A2. J Biol Chem 279, 11320-6 (2004).

309. Qi, H. Y. & Shelhamer, J. H. Toll-like receptor 4 signaling regulates cytosolic phospholipase A2 activation and lipid generation in lipopolysaccharide-stimulated macrophages. J Biol Chem 280, 38969-75 (2005).

310. Murakami, M. & Kudo, I. Phospholipase A2. J Biochem (Tokyo) 131, 285-92 (2002).

311. Lin, L. L. et al. cPLA2 is phosphorylated and activated by MAP kinase. Cell 72, 269-78 (1993).

312. Balboa, M. A., Balsinde, J. & Dennis, E. A. Phosphorylation of cytosolic group IV phospholipase A(2) is necessary but not sufficient for Arachidonic acid release in P388D(1) macrophages. Biochem Biophys Res Commun 267, 145-8 (2000).

313. Grkovich, A., Johnson, C. A., Buczynski, M. W. & Dennis, E. A. Lipopolysaccharide-induced cyclooxygenase-2 expression in human U937 macrophages is phosphatidic acid phosphohydrolase-1-dependent. J Biol Chem 281, 32978-87 (2006).

314. Kagan, J. C. & Medzhitov, R. Phosphoinositide-mediated adaptor recruitment controls Toll-like receptor signaling. Cell 125, 943-55 (2006).

315. Huwiler, A., Johansen, B., Skarstad, A. & Pfeilschifter, J. Ceramide binds to the CaLB domain of cytosolic phospholipase A2 and facilitates its membrane docking and arachidonic acid release. Faseb J 15, 7-9 (2001).

316. Klapisz, E., Masliah, J., Bereziat, G., Wolf, C. & Koumanov, K. S. Sphingolipids and cholesterol modulate membrane susceptibility to cytosolic phospholipase A(2). J Lipid Res 41, 1680-8 (2000).

317. Seeds, M. C., Nixon, A. B., Wykle, R. L. & Bass, D. A. Differential activation of human neutrophil cytosolic phospholipase A2 and secretory phospholipase A2 during priming by 1,2-diacyl- and 1-O-alkyl-2-acylglycerols. Biochim Biophys Acta 1394, 224-34 (1998).

318. Coffey, M. J., Phare, S. M. & Peters-Golden, M. Prolonged exposure to lipopolysaccharide inhibits macrophage 5-lipoxygenase metabolism via induction of nitric oxide synthesis. J Immunol 165, 3592-8 (2000).

319. Lucas, K. K. & Dennis, E. A. Distinguishing phospholipase A2 types in biological samples by employing group-specific assays in the presence of inhibitors. Prostaglandins Other Lipid Mediat 77, 235-48 (2005).

320. Yang, H. C., Mosior, M., Johnson, C. A., Chen, Y. & Dennis, E. A. Group-specific assays that distinguish between the four major types of mammalian phospholipase A2. Anal Biochem 269, 278-88 (1999).

321. Alcaraz, L. A. et al. Matrix metalloproteinase-inhibitor interaction: the solution structure of the catalytic domain of human matrix metalloproteinase-3 with different inhibitors. J. Biol. Inorg. Chem. 12, 1197-1206 (2007).

322. Bertini, I. et al. Exploring the subtleties of drug-receptor interactions: The case of matrix metalloproteinases. J. Am. Chem. Soc. 129, 2466-2475 (2007).

323. Jacobsen, F. E., Lewis, J. A. & Cohen, S. M. The Design of Inhibitors for Medicinally Relavent Metalloenzymes. ChemMedChem 2, 152-171 (2007).

324. Lauer-Fields, J. et al. Triple-helical transition state analogues: A new class of selective matrix metalloproteinase inhibitors. J. Am. Chem. Soc. 129, 10408-10417 (2007).

325. Puerta, D. T. & Cohen, S. M. A Bioinorganic Perspective on Matrix Metalloproteinase Inhibition. Curr. Top. Med. Chem. 4, 1551-1573 (2004).

326. Whittaker, M., Floyd, C. D., Brown, P. & Gearing, A. J. H. Design and Therapeutic Application of Matrix Metalloproteinase Inhibitors. Chem. Rev. 99, 2735-2776 (1999).

327. Nagase, H., Visse, R. & Murphy, G. Structure and Function of Matrix Metalloproteinases and TIMPs. Cardiovasc. Res. 69, 562-573 (2006).

328. Nelson, A. R., Fingleton, B., Rathenberg, M. L. & Matrisian, L. M. Matrix metalloproteinaseses: biological actiity and clinical implications. J. Clin. Oncol. 18, 1135-1149 (2000).

329. Rosenblum, G. et al. Molecular Structures and Dynamics of the Stepwise Activation Mechanism of a Matrix Metalloproteinase Zymogen: Challenging the Cysteine Switch Dogma. J. Am. Chem. Soc. 129, 13566-13574 (2007).

330. Sternlicht, M. D. & Werb, Z. How Matrix Metalloproteinases Regulate Cell Behavior. Annu. Rev. Cell. Dev. Biol. 17, 463-516 (2001).

331. Elliott, S. & Cawston, T. The clinical potential of matrix metalloproteinase inhibitors in the rheumatic disorders. Drugs Aging 18, 87-99 (2001).

332. Hu, J., Van den Steen, P. E., Sang, Q.-X. A. & Opendanakker, G. Matrix metalloproteinase inhibitors as therapy for inflammatory and vascular diseases. Nature Rev. Drug Disc. 6, 480-498 (2007).

333. Kieseier, B., Seifert, T., Giovannoni, G. & Hartung, H. Matrix metalloproteinases in inflammatory demyelination: targets for treatment. Neurology 13, 20-25 (1999).

334. Golub, L. M. et al. Tetracyclines inhibit connective tissue breakdown by multiple non-antimicrobial mechanisms. Adv. Dent. Res. 12, 12-26 (1998).

335. García, R. A. et al. Molecular interactions between matrilysin and the matrix metalloproteinase inhibitor doxycycline investigated by deuterium exchange mass spectrometry. Mol. Pharmacol. 67, 1128-1136 (2005).

336. Brown, S., Meroueh, S. O., Fridman, R. & Mobashery, S. Quest for Selectivity in Inhibition of Matrix Metalloproteinases. Curr. Top. Med. Chem. 4, 1227-1238 (2004).

337. Martinot, M. Microbiological and pharmacological data useful for the treatment of Lyme disease. Treatment and follow up of early Lyme disease (erythema migrans). Medecine Et Maladies Infectieuses 37, 394-409 (2007).

338. Sapadin, A. N. & Fleischmajer, R. Tetracyclines: Nonantibiotic properties and their clinical implications. Journal of the American Academy of Dermatology 54, 258-265 (2006).

339. Coussens, L. M., Fingleton, B. & Matrisian, L. M. Matrix Metalloproteinase Inhibitors and Cancer: Trials and Tribulations. Science 295, 2387 - 2392 (2002).

340. Rao, B. G. Recent Developments in the Design of Specific Matrix Metalloproteinase Inhibitors Aided by Structural and Computational Studies. Curr. Pharm. Des. 11, 295-232 (2005).

341. Skiles, J. W., Gonnella, N. C. & Jeng, A. Y. The design, structure, and clinical update of small molecular weight matrix metalloproteinase inhibitors. Curr. Med. Chem. 11, 2911-2977 (2004).

342. Breuer, E., Frant, J. & Reich, R. Recent non-hydroxamate matrix metalloproteinase inhibitors. Expert Opin. Ther. Patents 15, 253-269 (2005).

343. Hajduk, P. J. et al. NMR-based modification of matrix metalloproteinase inhibitors with improved bioavailability. J. Med. Chem. 45, 5628-5639 (2002).

344. Jacobsen, F. E., Lewis, J. A. & Cohen, S. M. A New Role for Old Ligands: Discerning Chelators for Zinc Metalloproteinases. J. Am. Chem. Soc. 128, 3156-3157 (2006).

345. Puerta, D. T., Lewis, J. A. & Cohen, S. M. New Beginnings for Matrix Metalloproteinase Inhibitors: Identification of High-Affinity Zinc-Binding Groups. J. Am. Chem. Soc. 126, 8388-8389 (2004).

346. Cho, H. J. et al. Disulfiram suppresses invasive ability of osteosarcoma cells via the inhibition of MMP-2 and MMP-9 expression. J Biochem Mol Biol 40, 1069-76 (2007).

347. Roomi, M. W., Ivanov, V., Kalinovsky, T., Niedzwiecki, A. & Rath, M. Inhibitory effects of a nutrient mixture on human testicular cancer cell line NT 2/DT matrigel invasion and MMP activity. Med Oncol 24, 183-8 (2007).

348. Roomi, M. W., Ivanov, V., Kalinovsky, T., Niedzwiecki, A. & Rath, M. Inhibition of cell invasion and MMP production by a nutrient mixture in malignant liposarcoma cell line SW-872. Med Oncol 24, 394-401 (2007).

349. Buczynski, M. W. et al. TLR-4 and sustained calcium agonists synergistically produce eicosanoids independent of protein synthesis in RAW264.7 cells. J. Biol. Chem. 282, 22834-22847 (2007).

350. Deems, R., Buczynski, M. W., Bowers-Gentry, R., Harkewicz, R. & Dennis, E. A. Detection and Quantitation of Eicosanoids via High Performance Liquid Chromatography-Electrospray Ionization-Mass Spectrometry. Methods Enzymol. 432, 59-82 (2007).

351. Peng, H. B., Spiecker, M. & Liao, J. K. Inducible nitric oxide: An autoregulatory feedback inhibitor of vascular inflammation. Journal of Immunology 161, 1970-1976 (1998).

352. Rhule, A., Navarro, S., Smith, J. R. & Shepherd, D. A. Panax notoginseng attenuates LPS-induced pro-inflammatory mediators in RAW264.7 cells. Journal of Ethnopharmacology 106, 121-128 (2006).

353. Rouzer, C. A. et al. RAW264.7 cells lack prostaglandin-dependent autoregulation of tumor necrosis factor-alpha secretion. Journal of Lipid Research 46, 1027-1037 (2005).

354. Hass, R. et al. TPA-induced differentiation and adhesion of U937 cells: changes in ultrastructure, cytoskeletal organization and expression of cell surface antigens. Eur J Cell Biol 48, 282-93 (1989).

355. Tsuchiya, S. et al. Induction of maturation in cultured human monocytic leukemia cells by a phorbol diester. Cancer Res 42, 1530-6 (1982).

356. Black, R. Tumor necrosis fastor-alpha converting enzyme. Int. J. Biochem. Cell Biol. 34, 1-5 (2002).

357. Moss, M. et al. Structural features and biochemical properties of TNF-alpha converting enzyme (TACE). J. Neuroimmunol. 72, 127-129 (1997).

358. Nomura, Y. & Kitamura, Y. Inducible nitric oxide synthase in glial cells. Neurosci. Res. 18, 103-107 (1993).

359. Salowe, S. P. et al. Characterization of Zinc-Binding Sites in Human Stromelysin-1 - Stoichiometry of the Catalytic Domain and Identification of a Cysteine Ligand in the Proenzyme. Biochemistry 31, 4535-4540 (1992).

360. Mirastchijsku, U., Johannesson, K., Jeppsson, B. & Agren, M. S. Effect of a matrix metalloproteinase activity and TNF-alpha converting enzyme inhibitor on intra-abdominal adhesions. Eur. Surg. Res. 37, 68-75 (2005).

361. Ramesh, G. & Reeves, W. B. TNF-alpha mediates chemokine and cytokine expression and renal injury in cisplatin nephrotoxicity. J. Clin. Invest. 110, 835-842 (2002).

362. Amin, A. R. et al. Post-transcriptional regulation of inducible nitric oxide synthase mRNA in murine macrophages by doxycycline and chemically modified tetracyclines. FEBS Lett. 410, 259-264 (1997).

363. Agrawal, A., Romero-Perez, D., Jacobsen, J. A., Villarreal, F. J. & Cohen, S. M. Zinc-Binding Groups Modeulate Selective Inhibition of MMPs. ChemMedChem, in press (2008).

364. Charlier, C. & Michaux, C. Dual inhibition of cyclooxygenase-2 (COX-2) and 5-lipoxygenase (5-LOX) as a new strategy to provide safer non-steroidal anti-inflammatory drugs. European Journal of Medicinal Chemistry 38, 645-659 (2003).

365. Puerta, D. T. et al. Heterocyclic Zinc-Binding Groups for Use in Next-Generation Matrix Metalloproteinase Inhibitors: Potency, Toxicity, and Reactivity. J. Biol. Inorg. Chem. 11, 131-138 (2006).

366. Rhee, J. W. et al. NF-kappaB-dependent regulation of matrix metalloproteinase-9 gene expression by lipopolysaccharide in a macrophage cell line RAW 264.7. J. Biochem. Mol. Biol. 40, 88-94 (2007).

367. Black, R. A. Tumor necrosis factor-alpha converting enzyme. Int J Biochem Cell Biol 34, 1-5 (2002).

368. Dreier, R., Grassel, S., Fuchs, S., Schaumburger, J. & Bruckner, P. Pro-MMP-9 is a specific macrophage product and is activated by osteoarthritic chondrocytes via MMP-3 or a MT1-MMP/MMP-13 cascade. Exp Cell Res 297, 303-12 (2004).

369. Gough, P. J., Gomez, I. G., Wille, P. T. & Raines, E. W. Macrophage expression of active MMP-9 induces acute plaque disruption in apoE-deficient mice. J Clin Invest 116, 59-69 (2006).

370. Yoo, H. G. et al. IL-1beta induces MMP-9 via reactive oxygen species and NF-kappaB in murine macrophage RAW 264.7 cells. Biochem Biophys Res Commun 298, 251-6 (2002).

371. Okada, Y. et al. Matrix metalloproteinase 9 (92-kDa gelatinase/type IV collagenase) from HT 1080 human fibrosarcoma cells. Purification and activation of the precursor and enzymic properties. J Biol Chem 267, 21712-9 (1992).

372. Bell, R. L. et al. The discovery and development of zileuton: an orally active 5-lipoxygenase inhibitor. Int. J. Immunopharmacol. 14, 505-510 (1992).

373. Carter, G. W. et al. 5-Lipoxygenase Inhibitory Activity of Zileuton. J. Pharmacol. Exp. Ther. 256, 929-937 (1991).

374. Mitchell, J. A., Akarasereenont, P., Thiemermann, C., Flower, R. J. & Vane, J. R. Proc. Natl. Acad. Sci. USA 90, 11693-11697 (1993).

375. Jala, V. R. & Haribabu, B. Leukotrienes and atherosclerosis: new roles for old mediators. Trends Immun. 25, 315-322 (2004).

376. Luo, M., Jones, S. M., Peters-Golden, M. & Brock, T. G. Nuclear localization of 5-lipoxygenase as a determinant of leukotriene B4 synthetic capacity. Proc. Natl. Acad. Sci. USA 100, 12165-12170 (2003).

377. Greiss, P. Bemerkungen zu der Abhandlung der HH. Weselsky und Benedikt Ueber einige Azoverbindungen. Chem. Ber. 12, 426-428 (1879).

378. Peterson, J. T. Matrix metalloproteinase inhibitor development and the remodeling of drug discovery. Heart Failure Rev. 9, 63-79 (2004).

379. Gilbertson-Beadling, S. et al. The Tetracycline Analogs Minocycline and Doxycycline Inhibit Angiogenesis in Vitro by a Non-Metalloproteinase-Dependent Mechanism. Cancer Chemother. Pharmacol. 36, 418-424 (1995).

380. Auge, F., Hornebeck, W., Decarme, M. & Laronze, J. Y. Improved gelatinase a selectivity by novel zinc binding groups containing galardin derivatives. Bioorg Med Chem Lett 13, 1783-6 (2003).

381. Breuer, E. et al. Carbamoylphosphonates, a new class of in vivo active matrix metalloproteinase inhibitors. 1. Alkyl- and cycloalkylcarbamoylphosphonic acids. J Med Chem 47, 2826-32 (2004).

382. He, H., Linder, D. P., Rodgers, K. R., Chakraborty, I. & Arif, A. M. A thiazole-containing tripodal ligand: synthesis, characterization, and interactions with metal ions and matrix metalloproteinases. Inorg Chem 43, 2392-401 (2004).

383. Nuti, E., Tuccinardi, T. & Rossello, A. Matrix metalloproteinase inhibitors: new challenges in the era of post broad-spectrum inhibitors. Curr Pharm Des 13, 2087-100 (2007).

384. Zhang, Y. M. et al. Syntheses and in vitro evaluation of arylsulfone-based MMP inhibitors with heterocycle-derived zinc-binding groups (ZBGs). Bioorg Med Chem Lett 18, 405-8 (2008).

385. Hider, R. C. & Liu, Z. D. Design of Iron Chelators with Therapeutic Application. Coord. Chem. Rev. 232, 151-171 (2002).

386. Attur, M. G., Patel, R. N., Patel, P. D., Abramson, S. B. & Amin, A. R. Tetracycline Up-Regulates COX-2 Expression and Prostaglandin E2 Production Independent of Its Effect on Nitric Oxide. J. Immunol. 162, 3160-3167 (1999).

387. Lewis, J. A., Puerta, D. T. & Cohen, S. M. Metal Complexes of the *trans*-influencing Ligand Thiomaltol. Inorg. Chem. 42, 7455-7459 (2003).

388. Lawrence, T., Willoughby, D. A. & Gilroy, D. W. Anti-inflammatory lipid mediators and insights into the resolution of inflammation. Nat Rev Immunol 2, 787-95 (2002).

389. Buczynski, M. W. et al. TLR-4 and sustained calcium agonists synergistically produce eicosanoids independent of protein synthesis in RAW264.7 cells. J Biol Chem 282, 22834-47 (2007).

390. Deems, R., Buczynski, M. W., Bowers-Gentry, R., Harkewicz, R. & Dennis, E. A. Detection and quantitation of eicosanoids via high performance liquid chromatography-electrospray ionization-mass spectrometry. Methods Enzymol 432, 59-82 (2007).

391. Steere, A. C. & Glickstein, L. Elucidation of Lyme arthritis. Nat Rev Immunol 4, 143-52 (2004).

392. Barthold, S. W., Beck, D. S., Hansen, G. M., Terwilliger, G. A. & Moody, K. D. Lyme borreliosis in selected strains and ages of laboratory mice. J Infect Dis 162, 133-8 (1990).

393. Brown, C. R. & Reiner, S. L. Clearance of Borrelia burgdorferi may not be required for resistance to experimental lyme arthritis. Infect Immun 66, 2065-71 (1998).

394. Brown, C. R., Blaho, V. A. & Loiacono, C. M. Susceptibility to experimental Lyme arthritis correlates with KC and monocyte chemoattractant protein-1 production in joints and requires neutrophil recruitment via CXCR2. J Immunol 171, 893-901 (2003).

395. McKisic, M. D. & Barthold, S. W. T-cell-independent responses to Borrelia burgdorferi are critical for protective immunity and resolution of lyme disease. Infect Immun 68, 5190-7 (2000).

396. Straus, D. S. et al. 15-deoxy-delta 12,14-prostaglandin J2 inhibits multiple steps in the NF-kappa B signaling pathway. Proc Natl Acad Sci U S A 97, 4844-9 (2000).

397. Michaelis, U. R. & Fleming, I. From endothelium-derived hyperpolarizing factor (EDHF) to angiogenesis: Epoxyeicosatrienoic acids (EETs) and cell signaling. Pharmacol Ther 111, 584-95 (2006).

398. Zeldin, D. C. et al. Metabolism of epoxyeicosatrienoic acids by cytosolic epoxide hydrolase: substrate structural determinants of asymmetric catalysis. Arch Biochem Biophys 316, 443-51 (1995).

399. Bolick, D. T. et al. 12/15-lipoxygenase regulates intercellular adhesion molecule-1 expression and monocyte adhesion to endothelium through activation of RhoA and nuclear factor-kappaB. Arterioscler Thromb Vasc Biol 25, 2301-7 (2005).

400. Folco, G. & Murphy, R. C. Eicosanoid transcellular biosynthesis: from cell-cell interactions to in vivo tissue responses. Pharmacol Rev 58, 375-88 (2006).

401. Schwab, J. M., Chiang, N., Arita, M. & Serhan, C. N. Resolvin E1 and protectin D1 activate inflammation-resolution programmes. Nature 447, 869-74 (2007).

402. Serhan, C. N. et al. Anti-inflammatory actions of neuroprotectin D1/protectin D1 and its natural stereoisomers: assignments of dihydroxy-containing docosatrienes. J Immunol 176, 1848-59 (2006).